

Zinc and iron cross-homeostasis in *Arabidopsis thaliana*

Camilla Rose Stanton



University of East Anglia

A thesis submitted for the degree of Doctor of Philosophy

February 2021

This copy of the thesis has been supplied on condition that anyone who consults it is understood to recognise that its copyright rests with the author and that use of any information derived there from must be in accordance with current UK Copyright law. In addition, any quotation or extract must include full attribution.

This page is intentionally left blank -
blank pages are used throughout to allow for
formatting in the printed version of this
document

Abstract

Zinc (Zn) and iron (Fe) are essential micronutrients in all biological systems, being utilised by thousands of enzymes and regulatory proteins as cofactors and structural components. In plants, nutrition is closely interlinked, with Zn excess causing secondary Fe deficiency. Highly coordinated homeostatic mechanisms have evolved to maintain optimal cellular Zn and Fe concentrations, although little is known about the regulatory proteins involved in cross-talk between these homeostasis networks. The aim of this thesis is to uncover novel components involved in Zn and Fe cross-homeostasis in *Arabidopsis thaliana* using forward and reverse genetic approaches.

Two reporter-based mutant screens were established to identify new genes and mutant alleles involved in the Zn deficiency and excess response. Transgenic lines expressing firefly luciferase (*LUC*) under the control of a Zn deficiency-responsive promoter, *Zrt-/Irt-Like Protein 5 (ZIP5)*, or a Zn excess and Fe deficiency-responsive promoter, *Ferric Reduction Oxidase 3 (FRO3)*, were generated. Initial screening of EMS-mutagenised populations failed to identify any candidate mutants but helped to establish screening populations and optimise screening protocols for future research.

Previously, BRUTUS-LIKE 1 (BTSL1) and BTSL2 were identified as partially functionally redundant E3 ubiquitin ligases that negatively regulate Fe uptake by targeting a central regulator of Fe deficiency, FER-like Fe deficiency Induced Transcription factor (FIT), for proteasomal degradation. Enhanced Fe uptake capacity in the *bts1* double mutant confers tolerance to Fe deficiency, and here it is shown that BTSL1 and BTSL2 also impact Zn uptake and distribution, conferring an Fe-mediated Zn tolerance phenotype. The *bts1* double mutant shows constitutive expression of FIT-dependent and FIT-independent metal homeostasis genes in roots, suggesting that BTSL proteins have additional transcription factor targets upstream of FIT as well. Furthermore, the *bts1* mutant is insensitive to systemic Fe signalling, showing that BTSL proteins are regulated by both local and systemic Fe signals, likely mediated by the cellular ratio of Zn and Fe. Together, the work presented in this thesis proposes a new role for BTSL proteins in regulating Zn and Fe cross-homeostasis in plants.

Access Condition and Agreement

Each deposit in UEA Digital Repository is protected by copyright and other intellectual property rights, and duplication or sale of all or part of any of the Data Collections is not permitted, except that material may be duplicated by you for your research use or for educational purposes in electronic or print form. You must obtain permission from the copyright holder, usually the author, for any other use. Exceptions only apply where a deposit may be explicitly provided under a stated licence, such as a Creative Commons licence or Open Government licence.

Electronic or print copies may not be offered, whether for sale or otherwise to anyone, unless explicitly stated under a Creative Commons or Open Government license. Unauthorised reproduction, editing or reformatting for resale purposes is explicitly prohibited (except where approved by the copyright holder themselves) and UEA reserves the right to take immediate 'take down' action on behalf of the copyright and/or rights holder if this Access condition of the UEA Digital Repository is breached. Any material in this database has been supplied on the understanding that it is copyright material and that no quotation from the material may be published without proper acknowledgement.

“Maybe working on the little things as dutifully and honestly as we can is how we stay sane when the world is falling apart.”

– Haruki Murakami

Desire by Haruki Murakami (ISBN: 1784872636)

Table of contents

Abstract	iii
Table of contents	v
Acknowledgements.....	xi
List of Figures	xiii
List of tables.....	xvii
List of common abbreviations	xviii
Chapter 1: Introduction.....	1
1.1 The agricultural importance of zinc (Zn) and iron (Fe).....	2
1.1.1 Biochemical properties of Zn and Fe	2
1.1.2 Zn and Fe in soil	3
1.1.3 Zn and Fe in plants.....	7
1.1.4 Zn and Fe in the human diet.....	8
1.1.5 Genetic approaches for Zn and Fe biofortification in crops	11
1.2 Overview of Zn and Fe homeostasis in <i>A. thaliana</i>	12
1.2.1 Uptake and radial transport in roots	13
1.2.2 Zn and Fe chelators.....	20
1.2.3 Long distance transport.....	24
1.2.4 Subcellular sequestration and mobilisation	29
1.2.5 Regulation of Zn and Fe homeostasis	36
1.3 Objectives.....	42
1.3.1 Aims of this project.....	42
1.3.2 Overview of thesis contents	43
1.3.3 Contributions to thesis	45
Chapter 2: Materials and Methods	47
2.1 Plant maintenance	49
2.1.1 Plant materials.....	49

2.1.2	<i>A. thaliana</i> agar plate growth conditions	49
2.1.3	Preparation of chelator-washed agar	50
2.1.4	Modified Hoagland medium.....	50
2.1.5	<i>A. thaliana</i> 96-well plate growth conditions	50
2.1.6	<i>A. thaliana</i> soil growth conditions.....	51
2.1.7	<i>A. thaliana</i> split root plates	52
2.2	<i>A. thaliana</i> growth phenotyping	52
2.2.1	Root length measurements.....	52
2.2.2	Leaf surface area measurements and growth stage phenotyping	53
2.3	Quantitative reverse transcription-PCR (qRT-PCR)	53
2.3.1	RNA extraction	53
2.3.2	cDNA synthesis	53
2.3.3	Quantitative real-time PCR (qRT-PCR).....	54
2.4	Generation of transgenic <i>A. thaliana</i> lines	56
2.4.1	Genomic DNA extraction.....	56
2.4.2	Promoter cloning.....	57
2.4.3	DNA sequencing	58
2.4.4	Gateway® cloning.....	59
2.4.5	Heat shock transformation of <i>Escherichia coli</i> (<i>E. coli</i>).....	60
2.4.6	Colony PCR	60
2.4.7	Electroporation of <i>Agrobacterium tumefaciens</i> (<i>A. tumefaciens</i>).....	61
2.4.8	Floral dipping transformation of <i>A. thaliana</i>	61
2.5	Generation of mutant screening populations	61
2.5.1	Selection of homozygous T ₃ lines	61
2.5.2	Copy number analysis.....	62
2.5.3	Ethyl methanesulfonate (EMS) mutagenesis.....	62
2.6	Bioluminescence imaging.....	62
2.6.1	Bioluminescence on agar plates	62
2.6.2	Bioluminescence imaging in 96-well plates.....	63
2.7	Biochemical and histochemical methods.....	63
2.7.1	Chlorophyll quantification	63
2.7.2	Inductively Coupled Plasma-Optical Emission Spectrometry (ICP-OES).....	63

2.7.3	Ferric chelate reductase (FCR) assay	64
2.7.4	Perls' stain and DAB intensification.....	64
2.8	RNA sequencing.....	65
2.8.1	Preparation of samples.....	65
2.8.2	RNA-sequencing (RNA-seq)	65
2.8.3	Read alignment and differential gene expression (DGE).....	65
2.8.4	Bioinformatic analysis of RNA-seq data.....	66
Chapter 3: Establishing luciferase-based mutant screens to identify novel genes in the Zn homeostasis network.....		67
3.1	Introduction.....	68
3.1.1	Forward genetic screens investigating nutrient homeostasis in <i>A. thaliana</i> ...	68
3.1.2	Mutagenesis techniques in <i>A. thaliana</i>	69
3.1.3	Luciferase as a reporter gene in mutant screens	70
3.1.4	Filling in the gaps of the Zn homeostasis network	72
3.1.5	Aims of this chapter	74
3.2	Results	74
3.2.1	Selection of candidate Zn deficiency and Zn excess-responsive promoters ...	74
3.2.2	qRT-PCR analysis of candidate Zn deficiency-responsive promoters	77
3.2.3	qRT-PCR analysis of candidate Zn excess-responsive promoters	79
3.2.4	Generation of pZIP5/DEFL206/FRO3:LUC primary transformants	81
3.2.5	Optimisation of Zn deficiency screening conditions.....	83
3.2.6	Optimisation of Zn excess screening conditions.....	85
3.2.7	Initial screening of M ₂ populations.....	86
3.3	Discussion	89
3.3.1	Expansion of screening conditions to identify candidate mutants.....	89
3.3.2	The pFRO3:LUC screen	90
3.3.3	Further screening of the M ₂ population to identify candidate mutants	91
3.3.4	Transgene silencing and wild-type seed contamination issues in screens.....	92
3.3.5	Outlook for future Zn homeostasis mutant screens.....	93
Chapter 4: The Fe-mediated Zn tolerance phenotype of the <i>bts1x2</i> mutant reveals a role for BTSL proteins in Fe and Zn cross-homeostasis.....		94

4.1 Introduction	95
4.1.1 BTSL1 and BTSL2 are closely related homologs of BTS.....	95
4.1.2 BTSL1 and BTSL2 regulate FIT protein turnover	97
4.1.3 <i>bts</i> and <i>btsl</i> mutants are tolerant to Fe deficiency.....	97
4.1.4 The <i>btsl2</i> mutant is tolerant to Zn excess.....	100
4.1.5 Fe and Zn nutrition affect flowering time.....	101
4.1.6 Aims of this chapter.....	102
4.2 Results	102
4.2.1 The <i>btsl1x2</i> double mutant Zn tolerance phenotype	102
4.2.2 The <i>btsl1x2</i> mutant Fe deficiency tolerance phenotype	105
4.2.3 The <i>btsl1x2</i> mutant phenotype on varying Mn growth conditions	107
4.2.4 Zn, Fe and Mn content of <i>btsl1x2</i> mutant under Zn excess	109
4.2.5 The <i>btsl1x2</i> mutant constitutive Fe deficiency root response	112
4.2.6 The <i>btsl1x2</i> mutant is late flowering and has increased growth rate	115
4.3 Discussion	119
4.3.1 BTSL1 and BTSL2 have partial functional redundancy.....	119
4.3.2 BTSL1 and BTSL2 proteins regulate Fe, Zn and Mn uptake	120
4.3.3. <i>btsl1x2</i> enhanced Fe uptake capacity confers Fe-mediated Zn tolerance	121
4.3.4 BTSL1 and BTSL2 attenuate FIT-dependent gene expression under Fe deficiency and Zn excess	122
4.3.5 Root Fe overaccumulation in wild-type under Zn excess.....	123
4.3.6 Soil phenotyping of <i>btsl1x2</i>	125
4.3.7 Proposed model for the <i>btsl1x2</i> Fe-mediated Zn tolerance phenotype	126
4.3.8 New advances in the understanding of BTSL1 and BTSL2 function.....	129
Chapter 5: Transcriptomic analysis reveals a novel role for BTSL proteins in FIT- independent gene regulation	131
5.1 Introduction.....	132
5.1.1 Investigating the Fe-mediated Zn tolerance phenotype of <i>btsl1x2</i> through transcriptomics.....	132
5.1.2 RNA-seq analysis as a tool for transcriptomic analysis in <i>A. thaliana</i>	133
5.1.3 The FIT-dependent transcriptional response network.....	133
5.1.4 The FIT-independent transcriptional response network.....	136

5.1.5	Antagonistic gene regulation by bHLH121/URI and PYE	138
5.1.6	Fe sensing and signalling and implications in Fe and Zn cross-homeostasis	139
5.1.7	Aims of this chapter	140
5.2	Results	141
5.2.1	RNA-sequencing experimental design and quality control	141
5.2.2	Principal component analysis (PCA) demonstrates divergent transcriptomic responses of Col-0 and <i>bts1x2</i> to Zn excess	145
5.2.3	Genotype-specific Differential Gene Expression (DGE) in wild-type and <i>bts1x2</i> under Zn excess	147
5.2.4	Hierarchical clustering of shoot Differentially Expressed Genes (DEGs)	152
5.2.5	Hierarchical clustering of root DEGs	160
5.2.6	qRT-PCR confirmation of overexpression of FIT-dependent and FIT-independent genes in <i>bts1</i> mutants	172
5.2.7	<i>bts1x2</i> mutant insensitivity to systemic Fe signalling in roots demonstrated by split-root assays	175
5.3	Discussion	178
5.3.1	BTSL proteins negatively regulate FIT-, IVc bHLH- and bHLH121/URI-dependent gene expression	178
5.3.2	Overexpression of Zn sequestration and Fe mobilisation genes contributes to the Fe-mediated Zn tolerance phenotype of <i>bts1x2</i> mutants	180
5.3.3	The expression pattern of shoot and select PYE-repressed genes is consistent with Fe sufficiency signalling in <i>bts1x2</i>	181
5.3.4	BTSL proteins are important for regulating root responses to local and systemic Fe signals	183
5.3.5	BTSL2 plays a more prominent role in regulating the root Fe deficiency response than BTSL1	184
5.3.6	New model for the role of BTSL proteins in the root transcriptional response to Zn excess	185
5.3.7	Future outlook for investigation of the BTSL proteins	188
Chapter 6: General Discussion		190
6.1	Summary of research findings	191
6.1.1	Mutant screens utilising <i>pZIP5:LUC</i> and <i>pFRO3:LUC</i> lines are a useful resource for future Zn homeostasis research	193

6.1.2	BTSL proteins regulate Zn and Fe cross-homeostasis.....	194
6.1.3	BTSL proteins regulate FIT-, IVc bHLH- and bHLH121/URI-dependent gene expression	196
6.2	Open questions.....	197
6.2.1	Identification of Zn homeostasis mutants from pZIP5:LUC and pFRO3:LUC screens	197
6.2.2	The Zn/Fe-sensing and regulatory mechanism of BTS and BTSL proteins.....	198
6.2.3	The interaction of BTSL proteins with IVc bHLH and bHLH21/URI	199
6.2.4	BTS and BTSL regulation of other homeostasis networks	200
6.3	Implications of research findings.....	201
Appendix A: Chapter 3 supplemental figures		203
Appendix B: Chapter 4 supplementary figures		207
Appendix C: Chapter 5 supplementary figures		211
Bibliography		227

Acknowledgements

Firstly, I must extend my deep gratitude to my supervisors, Dale Sanders and Tony Miller, for their exceptional guidance, kindness and patience over the past four years. I will never forget the support and compassion you showed during my hardest times. I am also extremely grateful to Janneke Balk and Jorge Rodriguez-Celma, who have been amazing collaborators and instrumental in shaping this thesis through their generous sharing of materials, ideas and knowledge. Likewise, the incredible guidance offered by Richard Morris has been very much appreciated.

The Sanders/Miller lab have been an immensely enjoyable group to work in, and I would like to thank all members past and present for their support. I'd especially like to thank Nicola for being a steadfast friend who never fails to make me laugh, even when I want to cry. I'm also extremely thankful for the professional and personal support from Yi, Tom V, Sigi, Marco, Thomas, Josh, Maria, Kalyani and Ben. A huge thank you also to the BBSRC DTP for my funding and training, as well as the JIC support staff who keep the institute running and make it such a lovely place to work.

I owe a vast amount of where I am today to Timothy Hearn and Alex Webb, who set me on my plant sciences journey many years ago, and I am always grateful for their encouragement and friendship. Julia Davies and Katie Wilkins were incredible sources of inspiration as an undergraduate, as were the researchers I met during the JIC summer school, and I'd like to thank all of them for their teaching and guidance.

A massive thanks of course to all my family and friends – I am fortunate to say there are far too many of you to name. To Cass for being my kindred goth sister. To Abi Bleach for always telling me I could when I thought I couldn't. To my brilliant and long-suffering housemate, Emma. To the collective strays of Dereham road for the laughs, dancing and continual chaos. And Matt, I could thank you every minute of the day and it wouldn't even be close to expressing my gratitude for the love, happiness and adventures (and our ridiculous cat, Basho) that you've brought into my life. To Adelle, Henry, Alison, Joe, David and Laura, thank you for always being there and believing in me. Finally, to Mum, Steve, Dad and Harriet. I could fill a whole thesis with my gratitude to you, but I'm hoping that just saying thank you and I love you will suffice for now.

Dedicated to my mum, Josie Hall,
for all the wonderful things she taught me

List of Figures

Figure 1.1: The global prevalence of Zn and Fe deficiency in agricultural soils.	6
Figure 1.2: The global prevalence of Zn and Fe deficiency in the human population.	10
Figure 1.3: Radial transport of nutrients in roots.....	14
Figure 1.4: Strategy I Fe uptake in <i>A. thaliana</i>	19
Figure 1.5: Chelation and xylem loading of Zn and Fe.	22
Figure 1.6: Long distance Zn and Fe transport in the xylem and phloem.	28
Figure 1.7: Subcellular transport of Zn and Fe.	30
Figure 1.8: Transcriptional regulation of Zn deficiency responses by bZIP19 and bZIP23.	38
Figure 1.9: Regulation of the Fe deficiency response.	42
Figure 3.1: The bioluminescent firefly luciferase reaction.....	71
Figure 3.2: Schematic showing possible gaps in the Zn homeostasis network that a forward genetic screen could fill.....	73
Figure 3.3: Quantitative reverse transcription-PCR (qRT-PCR) analysis of candidate Zn deficiency-responsive genes for promoter selection.	78
Figure 3.4: Quantitative reverse transcription-PCR (qRT-PCR) analysis of candidate Zn excess-responsive genes for promoter selection.....	80
Figure 3.5: Overview of selection of pZIP5/FRO3:LUC primary transformant lines. .	82
Figure 3.6: Optimisation of luminescence imaging of pZIP5:LUC lines for the Zn deficiency screen.....	84
Figure 3.7: Optimising luminescence imaging of pFRO3:LUC lines for the Zn excess screen.....	86
Figure 3.8: Screening of pZIP5:LUC M2 population.....	88
Figure 3.9: Screening of pFRO3:LUC M2 population.....	89

Figure 4.1: Domain organisation of BTS, BTSL and closely related hemerythrin domain-containing E3 ligases involved in Fe homeostasis.	96
Figure 4.2: Role of BTS and BTSL proteins in the Fe deficiency transcriptional cascade.	99
Figure 4.3: The growth phenotype of Col-0, <i>bts1</i> , <i>bts2</i> and <i>bts1x2</i> on varying Zn concentrations.	104
Figure 4.4: The growth phenotype of Col-0, <i>bts1</i> , <i>bts2</i> and <i>bts1x2</i> on varying Fe concentrations.	106
Figure 4.5: The growth phenotype of Col-0, <i>bts1</i> , <i>bts2</i> and <i>bts1x2</i> on different Mn concentrations.	108
Figure 4.6: Zn, Fe and Mn accumulation in Col-0 and <i>bts1x2</i> roots and shoots under Zn excess.	111
Figure 4.7: Perls' staining, <i>IRT1</i> and <i>FRO2</i> expression and ferric chelate reductase activity of Col-0 and <i>bts1x2</i> roots under Fe deficiency and Zn excess.	114
Figure 4.8: Stage-based growth phenotyping of Col-0 and <i>bts1x2</i> under Zn excess.	117
Figure 4.9: Rosette phenotyping of Col-0 and <i>bts1x2</i> grown on Zn excess soil.	118
Figure 4.10: Proposed model for the Fe-mediated Zn tolerance phenotype of <i>bts1x2</i>	128
Figure 5.1: The FIT-dependent Fe deficiency response network.	135
Figure 5.2: The FIT-independent Fe deficiency transcriptional response network.	137
Figure 5.3: Principal component analysis (PCA) of shoot sample transcripts.	146
Figure 5.4: Principal component analysis (PCA) of root sample transcripts.	147
Figure 5.5: Significantly differentially expressed genes (DEGs) in Col-0 and <i>bts1x2</i> shoots grown under control (1 μ M Zn) or Zn excess (100 μ M Zn) conditions.	150
Figure 5.6: Significantly differentially expressed genes (DEGs) in Col-0 and <i>bts1x2</i> roots grown under control (1 μ M Zn) or Zn excess (100 μ M Zn) conditions.	151

Figure 5.7: Hierarchical clustering analysis of Zn-responsive genes in Col-0 and <i>bts1x2</i> shoots.	153
Figure 5.8: Hierarchical clustering analysis of Zn-responsive genes in Col-0 and <i>bts1x2</i> roots.....	161
Figure 5.9: Quantitative reverse transcription PCR (qRT-PCR) analysis of selected Fe and Zn-responsive genes in Col-0 and <i>bts1</i> mutant roots in response to Fe deficiency and Zn excess.	174
Figure 5.10: Schematic of split-root experimental set up to test systemic Fe signalling in <i>bts1x2</i>	176
Figure 5.11: Expression of Fe deficiency-responsive genes in Col-0 and <i>bts1x2</i> seedlings grown in the split-root system.	177
Figure 5.12: Model of proposed new function of BTSL proteins in the root Fe deficiency transcriptional response under Fe deficiency or Zn excess.	187
Figure 6.1: Proposed function of BTSL proteins in Zn and Fe cross-homeostasis in <i>A. thaliana</i>	192
Supplementary Figure A1: Plasmid maps of vectors used in Gateway cloning.....	204
Supplementary Figure A2: Luminescence imaging of pDEFL206:LUC T ₃ lines.....	205
Supplementary Figure B1: Schematic of <i>BTSL1</i> and <i>BTSL2</i> genes with position of T-DNA insertion shown.	208
Supplementary Figure B2: Fe-mediated Zn tolerance phenotype of Col-0 and <i>bts1x2</i>	209
Supplementary Figure B3: Rosette surface area of Col-0 and <i>bts1x2</i> grown on Zn excess soil.....	210
Supplementary Figure C1: Gel of RNAseq samples ran on Bioanalyzer 2100.	214
Supplementary Figure C2: GO enrichment analysis of common and unique Zn-responsive DEGs in Col-0 and <i>bts1x2</i> shoots.....	221
Supplementary Figure C3: KEGG pathway enrichment analysis of common and unique Zn-responsive DEGs in Col-0 and <i>bts1x2</i> shoots.	222

Supplementary Figure C4: GO enrichment analysis of common and unique Zn-responsive DEGs in Col-0 and <i>bts/1x2</i> roots.....	223
Supplementary Figure C5: KEGG pathway enrichment analysis of common and unique Zn-responsive DEGs in Col-0 and <i>bts/1x2</i> roots.	224
Supplementary Figure C6: Set up of split root experiment to test local and systemic Fe deficiency signalling in Col-0 and <i>bts/1x2</i>	225
Supplementary Figure C7: Shoot phenotypes of Col-0 and <i>bts/1x2</i> seedlings grown in the split-root system.....	226

List of tables

Table 2.1: Nutrient composition of 0.25x modified Hoagland medium.....	51
Table 2.2: Primers used for qRT-PCR analysis.	56
Table 2.3: Primers used in the Gateway cloning of Zn-responsive promoters.	58
Table 2.4: Primers used in sequencing.....	59
Table 3.1: Zn deficiency and Zn excess-responsive genes selected as promoter candidates for the luciferase-based mutant screen.....	76
Table 5.1: Summary of RNA-seq samples pseudoalignment.....	144
Table 5.2: Selected Fe- and Zn-homeostasis genes that were significantly ($qval < 0.05$, $\log_2FC > 1$) DE in Col-0 or <i>bts1x2</i> shoots in response to Zn excess.	155
Table 5.3: Selected Fe- and Zn-homeostasis genes that were significantly ($qval < 0.05$, $\log_2FC > 1$) DE in Col-0 or <i>bts1x2</i> roots in response to Zn excess.	166
Supplementary Table A1: Comparison of factors effecting suitability of agar plates and 96-well plate liquid growth systems for high-throughput screening.	206
Supplementary Table C1: Summary of RNA quality check for RNAseq samples.....	213
Supplementary Table C2: Summary of quality check for RNA-seq raw sequence data.	216
Supplementary Table C3: Top ten loading transcripts of shoot principal component (PC) 1 and PC2.	217
Supplementary Table C4: Top ten loading transcripts of root principal component (PC) 1 and PC2.	218
Supplementary Table C5: Overlap of significantly DEGs up- and downregulated in shoots between all pairwise comparisons.	219
Supplementary Table C6: Overlap of significantly DEGs up- and downregulated in roots between all pairwise comparisons.	220

List of common abbreviations

bHLH	basic helix-loop-helix
BTS(L)	BRUTUS(-LIKE)
bZIP	basic leucine zipper
Cd	cadmium
CIPK	calcineurin B-Like (CBL)-interacting protein kinases
CK	cytokinin
Cys	cysteine
DEG	differentially expressed gene
DGE	differential gene expression
DNA	deoxyribonucleic acid
DW	dry weight
ER	endoplasmic reticulum
FBXL5	F-Box and Leucine Rich Repeat Protein 5
FC	fold change
Fe ²⁺	ferrous iron ion
Fe ³⁺	ferric iron ion
Fe	iron
FIT	FER-like Fe deficiency Induced Transcription factor
FRO	Ferric Reduction Oxidase
GA	gibberellin
GFP	green fluorescent protein
GO	gene ontology
H ₂ O ₂	hydrogen peroxide
HHE	hemerythrin
His	histidine
HMA	Heavy Metal Associated
HRZ1/2	Haemerythrin motif-containing Really Interesting New Gene (RING) and Zinc finger protein 1/2
ICP	ion-coupled plasma

IRT	Iron-Regulated Transporter
JA	jasmonic acid
KEGG	Kyoto Encyclopedia of Genes and Genomes
LUC	luciferase
Mn	manganese
MT	metallothionein
MTP	Metal Tolerance Protein
N	nitrogen
NA	nicotianamine
NAS	nicotianamine synthase
NO	nitric oxide
NRAMP	Natural Resistance-Associated Macrophage Protein
OPT	Oligopeptide Transporter
Pb	lead
PCA	principle components analysis
PCR	polymerase chain reaction
PYE	POPEYE
qRT-PCR	quantitative real-time PCR
RNA-seq	RNA-sequencing
ROS	reactive oxygen species
S	sulphur
SA	salicylic acid
SAM	S-adenosyl methionine
SEM	standard error of the mean
RNA	ribonucleic acid
T-DNA	transfer DNA
TPEN	N,N,N',N'-tetrakis(2-pyridylmethyl)ethane-1,2-diamine
YSL	Yellow Stripe-Like
ZIF	Zinc-Induced Facilitator
ZIP	Zinc-inducible(Zrt-)/Iron-inducible (Irt-) Protein
Zn ²⁺	zinc ion
Zn	zinc

This page is intentionally left blank -
blank pages are used throughout to allow for
formatting in the printed version of this
document

Chapter 1: Introduction

1.1 The agricultural importance of zinc (Zn) and iron (Fe)

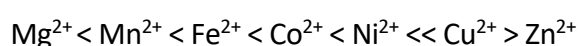
1.1.1 Biochemical properties of Zn and Fe

Zinc (Zn) and iron (Fe) are essential micronutrients in all biological systems, performing key functions in thousands of proteins across numerous biological processes [1-4]. Both Zn and Fe are found in the d-block of the periodic table, however only Fe is a true transition metal, and this gives Zn and Fe highly different chemical properties [5]. For instance, Zn is redox stable and in compounds is only found as a divalent cation (Zn^{2+}) [6]. In contrast, Fe can participate in oxidation-reduction reactions and is consequently found in multiple oxidative states, predominantly as Fe^{2+} and Fe^{3+} , with higher oxidation states transiently formed during catalysis [7].

As a result of their differing chemical characteristics, Zn and Fe have very different biochemical roles in enzymes and proteins. In prokaryotes ~6% of the proteome, and in eukaryotes ~9%, utilise Zn for catalytic, co-catalytic and structural purposes [4]. Acting as a Lewis acid, Zn is able to stabilise negative charges during enzymatic reactions, and is a versatile cofactor found in all six of the major classes of enzymes [8, 9]. Notable examples include carbonic anhydrases, carboxypeptidases and alcohol dehydrogenases [10-12]. As a structural component, Zn is able to coordinate with nitrogen (N), oxygen (O) and sulphur (S), and can form a number of different coordination geometries, although is most commonly found in tetrahedral complexes [13, 14]. In the context of its redox stability, these structural Zn-protein interactions are inert and highly suited to nucleotide-binding proteins, with Zn-finger protein motifs being commonly found in transcription factors, notably in eukaryotic systems [15]. The redox stability which makes Zn a useful cofactor also makes it difficult to study with traditional spectroscopic techniques, and thus, the majority of Zn-binding proteins have been identified using bioinformatics approaches [4, 16]. In mammalian systems, Zn also has an additional function as a signalling factor, with increasing cytosolic Zn concentrations and extracellular release of Zn mediating signals involved in processes such as insulin secretion, immune system function and neurotransmitter signalling [17-19].

During evolution, Fe was one of the earliest metal cofactors to be recruited for protein function and the number of Fe-binding proteins has remained relatively consistent, constituting 7% of the proteome in archaea, 4% in bacteria and 1% in eukaryotes [4, 20]. Fe proteins are classified as haem or non-haem depending upon the form of Fe they bind. Haemoproteins contain the metal-organic haem cofactor, which contains an Fe centre capable of reversibly binding oxygen. Haem proteins are found in all biological systems, although the best-known examples are the oxygen-transporting haemoglobin and oxygen-storage protein myoglobin from vertebrates [21]. Non-haem proteins either directly bind Fe ions or Fe-S clusters. Fe-S cluster proteins are commonly found involved in electron transfer chains and catalysis, and are key components of photosynthetic reactions in chloroplasts and respiration in mitochondria. Many Fe metalloproteins also function in ROS scavenging and cellular redox balance [22].

Despite their vastly different biochemical properties, the similar ionic radius and prevalence as divalent cations, means that protein mismetallation and sharing of transporters is common between Zn and Fe [23]. In fact, most metalloproteins do not preferably bind the metal cofactor they require for function, rather they show a ranked order of divalent cation binding preference based on the stability of the complexes they form. This is described in the Irving-Williams series:



and shows that in the absence of a specific metal delivery system, Fe proteins will preferentially bind cobalt (Co^{2+}), nickel (Ni^{2+}), copper (Cu^{2+}) and Zn^{2+} over Fe^{2+} [23, 24]. As a consequence, Zn and Fe compete for uptake, protein binding and transport within organisms, resulting in complicated homeostatic interactions, and ultimately excess of one often causing deficiency of the other [25-27].

1.1.2 Zn and Fe in soil

In the Earth's crust, Zn and Fe make up the 24th and 4th most abundant elements respectively, with the Zn content of unfertilised soil estimated to range between 10–300 mg/kg (50-55 mg/kg on average) and Fe 20–500 g/kg (20–40 g/kg on average)[28-32].

However, the heterogeneous distribution of micronutrients within soils, and the differing chemical, physical and biological processes which govern the balance of Zn and Fe species affects the availability of these nutrients for plant uptake. For instance, only solubilised Zn^{2+} and Fe^{2+} , or specific metal-chelate complexes, are available for uptake by roots, but a large portion of soil Zn and Fe is adsorbed to soil surfaces, associated with chelators or exists in organic complexes [33, 34].

Zn is one of the most geographically widespread soil micronutrient deficiencies, affecting ~50% of the world's agricultural soils, with regions in India, Pakistan, Turkey, China, sub-Saharan Africa and central and south America particularly affected (**Figure 1.1A**)[35, 36]. The prevalence of soil Zn deficiency is due to the susceptibility of a range of soil types to both low total Zn content ('primary deficiency'), as well as reduced accessibility of Zn for plant uptake ('secondary deficiency'). For instance, primary deficiency occurs in sandy soils formed from sandstone and highly leached tropical soils which show poor nutrient content and retention [37]. Secondary deficiencies can arise in calcareous limestone-based soils with high pH (>7), where Zn solubility is greatly reduced due to the adsorptive properties of calcium carbonate and precipitation with Fe oxides [32, 37]. Conditions and farming practices which reduce soil organic matter and the rate of microbial decomposition, such as flooding and topsoil levelling, also increase the risk of Zn deficiency in soils [38, 39]. Excessive use of fertilisers also inhibits symbiotic interactions between plants and arbuscular mycorrhizal fungi (AMF). Mycorrhizal pathways contribute significantly towards Zn and Fe uptake from the soil, and have also been demonstrated to play a key role in determining grain micronutrient content [40-42].

Despite the high abundance of Fe in the lithosphere, the majority is inaccessible for plant uptake, and consequently between one-fifth to one-third of the world's agricultural soils are considered Fe deficient [39, 43]. Arid soils in China, sub-Saharan and northern Africa, Mexico and the middle East are especially vulnerable to Fe deficiency [35, 44, 45]. Fe availability in soils is reduced by many of the same factors as Zn, such as high pH, calcareous soils, the presence of phosphate fertilisers and reduced organic matter decomposition [34]. Soil Fe availability is also strongly influenced by the redox environment in the soil, with neutral and alkaline well-aerated soils promoting the formation of inaccessible Fe^{3+} and the precipitation of Fe-hydroxide species, which can

be further complexed with organic matter [34, 46]. Some estimates suggest that these unfavourable conditions dramatically reduce solubilised Fe concentrations to 10^4 – 10^5 fold below the limit of what is required for adequate plant growth [47]. Excessive concentrations of other micronutrients which compete with Fe for plant uptake, such as Zn, Cu, manganese (Mn), cobalt (Co) and Ni, can also impact Fe accessibility [48]. Insufficient data are available to map the global distribution of soil Fe deficiency, but **Figure 1.1B** shows a map of soil pH with areas of known deficiency highlighted.

Some agricultural management practices have proven successful in counteracting soil Zn and Fe deficiency and improving crop yield, such as the application of Zn and Fe fertilisers, soil acidification and foliar micronutrient application [38, 49]. However, fertilisers can often be expensive, with Zn fertilisers costing 10-fold more than alternative Zn-fortifying interventions, such as foliar spray and flour fortification [50, 51]. This further highlights the need for alternative affordable and sustainable approaches to Zn and Fe biofortification in crops.

Excess Zn and Fe in soils can also impact crop growth. Heavy metal pollution in soils is often linked to anthropogenic activity, with Zn toxicity common in soils close to old mining and smelting sites, as well as in areas where sewage sludge has been applied as fertiliser [52]. Industrialised areas in Europe, India, China and Japan have all reported the toxic effect of heavy metal pollution from effluent run-off [33, 53-55]. Additionally, Fe toxicity is often linked to environmental conditions which increase the availability of naturally present Fe, such as in acidic and sulphate-rich soils as a result of flooding [56, 57]. Rice-growing areas in southeast-Asia, China and India, as well acidic soil regions in south America and sub-Saharan Africa are especially affected by Fe toxicity [58, 59]. Thus, there is great interest in the production of crops that can better tolerate these toxic soils, as well as the use of plants for phytoremediation strategies [60-62]. Phytoremediation involves the use of plants to reduce the concentration or bioavailability of toxic contaminants, such as heavy metals, in soil through hyperaccumulation, detoxification and sequestration processes [63]. Many phytoremediation efforts look at improving the efficiency of species that are found naturally growing on contaminated soils, such as *Neyraudia reynaudiana* for Zn and lead (Pb)[64], silver birch (*Betula pendula*) and *Brassica napus* for Zn [65, 66], and poplar hybrids for a variety of heavy metals including, Zn, Pb and cadmium (Cd)[67, 68]. A recent

study in *Arabidopsis thaliana* (*A. thaliana*) demonstrated that Fe overaccumulating plants are also able to take up high levels of Cd, and as such shows that metal cross-homeostasis can be exploited for phytoremediation approaches [69].

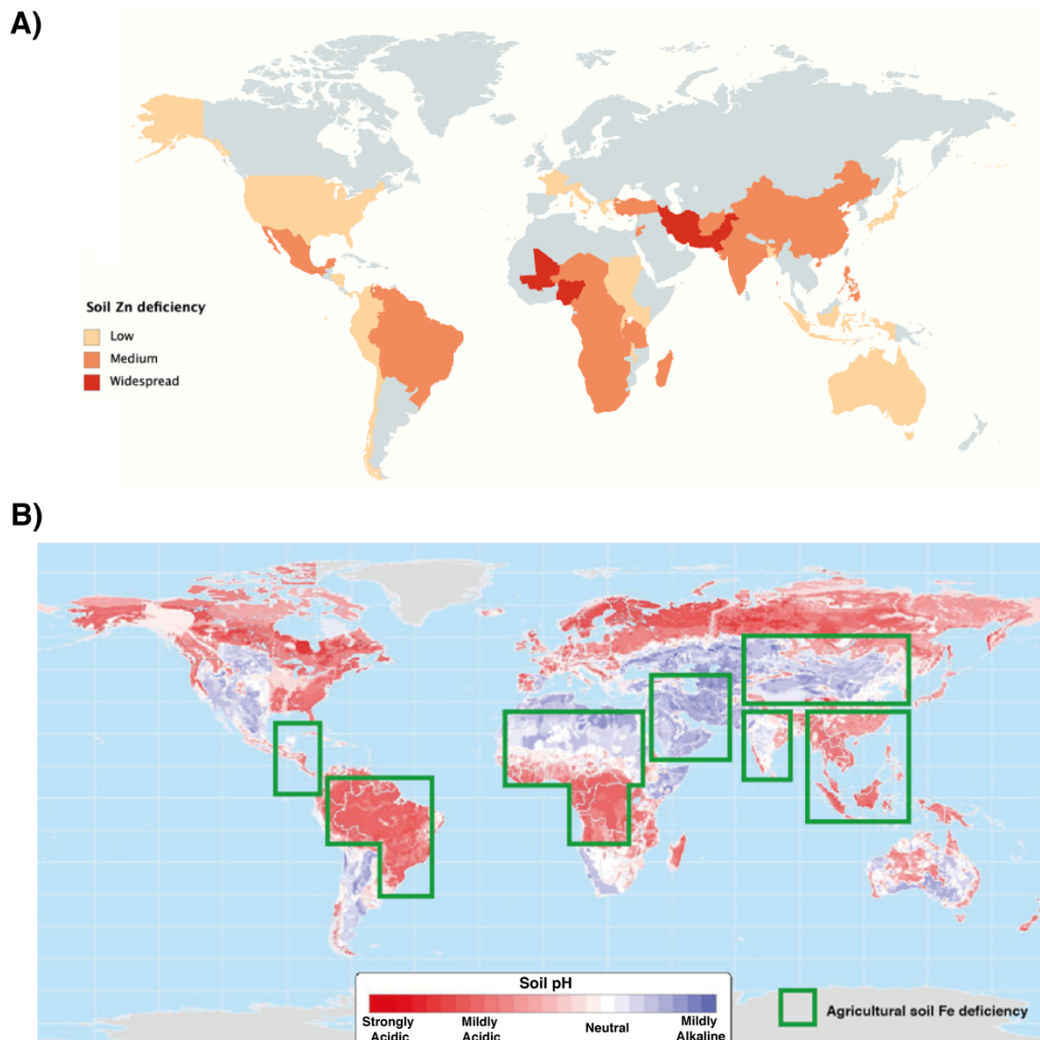


Figure 1.1: The global prevalence of Zn and Fe deficiency in agricultural soils.

A) Map showing countries and areas particularly affected by Zn deficiency in agricultural soils. Map created using Mapchart.net. B) Map showing the global soil pH with areas of known agricultural soil Fe deficiency highlighted. Soil pH map from [70]. Data from [37, 38, 71].

1.1.3 Zn and Fe in plants

Zn and Fe play essential roles in plant growth, development and disease resistance. Zn and Fe are also critically important for photosynthesis, with as much as 80% of cellular leaf Fe found in chloroplasts, and Zn an essential cofactor for carbonic anhydrase activity in photosystem II [72]. As such, defects in nutrition of these micronutrients can have a severe impact on crop health and yield [73].

Optimal leaf Zn concentrations in plants generally fall between 30–100 mg/kg DW (dry weight), with deficiency occurring at <15 mg/kg DW and toxicity symptoms occurring at >100 mg/kg DW, although these figures can differ depending upon the inherent Zn sensitivity of species and cultivars [74, 75]. Zn deficiency is thought to be the most common crop micronutrient deficiency, with severe cases resulting in root apex necrosis, growth stunting and infertility and milder symptoms visible as interveinal chlorosis, leaf bronzing and curling [73, 76]. At the other extreme, Zn toxicity, often seen in plants growing on polluted soils, results in protein mismetallation and the activation of Fe deficiency responses (chlorosis, growth stunting) as well as altered phosphate and Mn uptake [73]. Some metallophyte species, which are able to tolerate high levels of heavy metals, show Zn hypertolerance, and consequently can grow healthily on high Zn soil conditions that would otherwise be toxic [73]. Twenty-eight of these hypertolerant species have also been identified as Zn hyperaccumulators, reaching leaf Zn concentrations of >1000 mg/kg [77]. This hyperaccumulation phenotype has evolved independently several times, and generally involves the duplication or changes in cis-regulatory features of Zn-homeostasis genes to enhance Zn uptake, distribution and compartmentalisation [78]. As such, the study of Zn hyperaccumulation in species such as *Noccaea caerulescens* and *Arabidopsis halleri* can provide mechanistic approaches for biofortification and phytoremediation strategies.

Optimal leaf Fe concentrations fall between 50-300 mg/kg DW, with Fe deficiency occurring <30 mg/kg DW and toxicity >400 mg/kg DW [79]. Similar to Zn excess, Fe deficiency causes growth stunting and yield losses, and manifests as severe chlorosis and reduced photosynthetic capacity [80, 81]. Fe toxicity can initially look similar to deficiency, but is characterised by necrotic leaf spots, or bronzing, which appear in response to reactive oxygen species (ROS) produced during the Fenton

reaction [82]. Rice especially is vulnerable to Fe toxicity [58]. Both Zn and Fe deficiency have been linked with increased susceptibility to disease and pests as a result of the role of Zn and Fe in defence protein function and signalling [83, 84].

1.1.4 Zn and Fe in the human diet

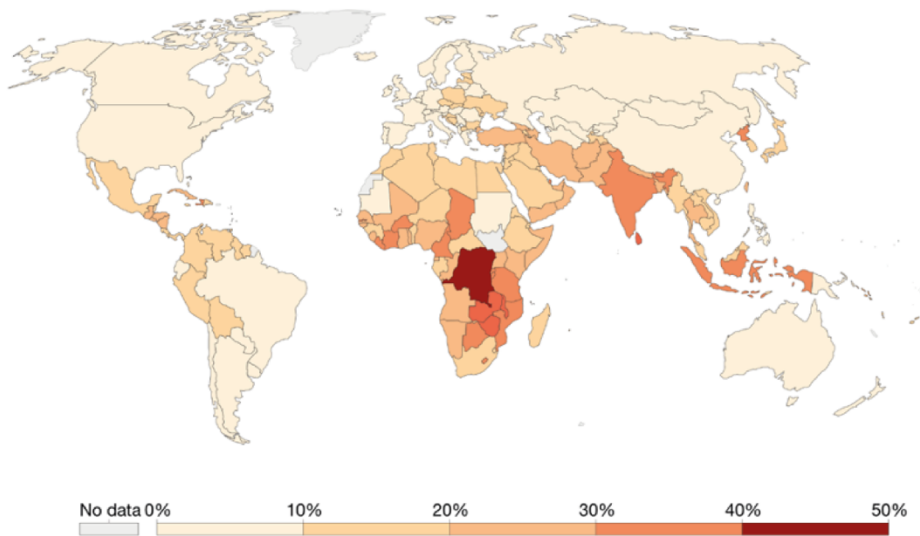
It is estimated that the average adult human body contains 1.5-2.5 g Zn and 3-4 g Fe, making Zn and Fe two of the most abundant and essential micronutrients in humans [85, 86]. Zn and Fe are important for a range of biological functions within the human body. Notably, Zn is required for immune system function, wound healing and development, while Fe is required for respiratory processes within mitochondria, oxygen delivery and muscle function, with over 60% of the body's Fe associated with haemoglobin and 25% with myoglobin [87]. The significance of these micronutrients for human health is highlighted by the range of disorders and health complications linked with Zn and Fe malnutrition when dietary intake falls below the recommended 5.5 mg/day for Zn and 5 mg/day for Fe [88]. Around one-third of the global population is affected by Zn deficiency, with 1.4% of deaths worldwide and 2.9% of Disability Adjusted Life Years (DALYs), which estimates the loss of healthy years of life due to disease burden, attributed to low dietary Zn intake [89]. Mild cases result in poor skin and hair health, diarrhoea and appetite loss, with chronic Zn malnutrition impacting immune system function, development and growth [90]. Fe deficiency affects upwards of 2 billion people in the global population, and is attributed to 1.5% of deaths worldwide and 2.4% of global DALYs [89]. A major indicator of Fe deficiency is anaemia, with severe anaemia shown to limit aerobic capacity, cognitive ability, as well as impair development in children [87]. The non-specific nature of symptoms and an inability to measure micronutrient levels reliably in the body means that these projections of the pervasiveness of micronutrient deficiencies within the human population are likely gross underestimates [91]. The major health and socio-economic impacts of micronutrient deficiencies on the human population make it one of the leading global issues in developing sustainable agriculture. Zn and Fe toxicity in humans is less common, but does occur in western countries where heavy, and largely unregulated, fortification of

food with Fe and Zn can lead to dietary overload, resulting in heart and liver problems and impaired Cu nutrition [88, 92, 93].

Zn and Fe deficiency disorders often occur simultaneously and have been shown to particularly affect women and children in low and middle-income countries whose populations are reliant upon low-meat cereal and legume-based diets [88, 89, 94]. Countries and regions especially affected by both Zn and Fe deficiency include sub-Saharan Africa, India, Pakistan, Afghanistan and south-east Asia (**Figure 1.2A**), with Fe deficiency affecting at least 10% of women in most countries (**Figure 1.2B**)[95]. The increased risk of micronutrient malnutrition in these populations can be linked to micronutrient deficiency in agricultural soils in these areas (**Figure 1.1**), as well as to the differential micronutrient bioavailability and content between meat and plant-based diets [88]. For instance, red meats contain large amounts of haem Fe and organically-complexed Zn which are readily solubilised and absorbed in the intestine [96, 97]. In comparison, non-haem Fe and inorganic Zn salts found in plant-based products are a less reliable source for dietary trace elements, largely due to low Zn and Fe content in grains and the presence of molecules that inhibit intestinal absorption [97].

A number of small molecules found in plant-based diets have been shown to suppress Zn and Fe bioavailability, the most well-known example of these being phytate. Phytic acid (IP₆) and its phytate salt forms are the main phosphate store in grains, and are capable of chelating metals into insoluble complexes. For this reason, phytate is commonly referred to as an antinutrient [98, 99]. Phytate-chelated Zn and Fe is unavailable for intestinal absorption because humans lack the phytases necessary to digest these complexes: just 250 mg of phytate has been shown to inhibit Fe absorption by 82% [100, 101]. Thus, consumption of phytate-rich cereals and legumes can increase susceptibility to Zn and Fe malnutrition, leading to growing interest in biofortification strategies that not only enhance grain Fe and Zn content, but also alter phytate levels. Other inhibitors are found in a diversity of foods, including polyphenols from tea and coffee [102-104], as well as soy proteins [105, 106], and highlights the need to consider the whole dietary matrix when developing nutritional interventions for vulnerable populations.

A) Zinc deficiency in the global population



B) Iron deficiency in women

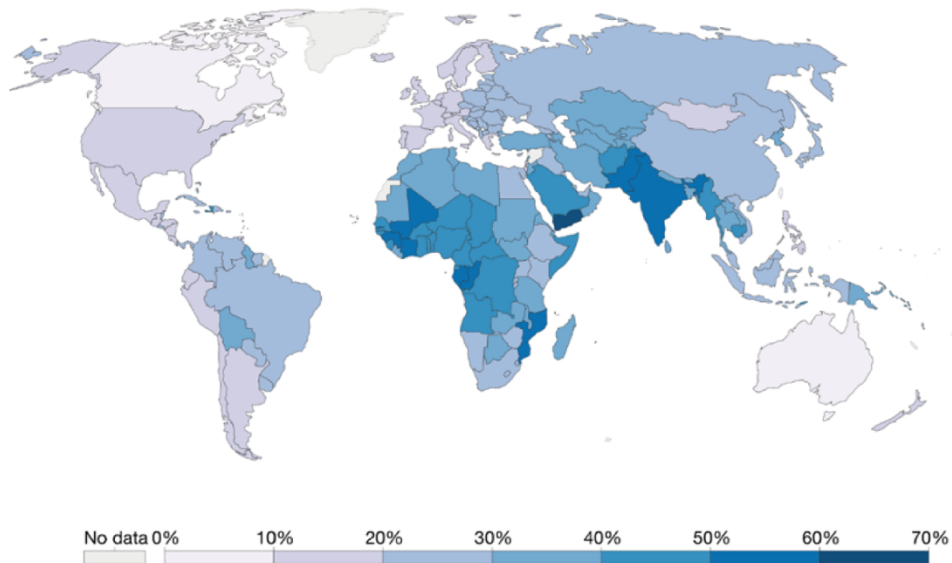


Figure 1.2: The global prevalence of Zn and Fe deficiency in the human population.

A) Map showing the prevalence of global Zn deficiency as percentage of each country's total population with intakes below physiological requirements. Daily requirements were calculated based on daily per capita caloric Zn availability (mg Zn/100 kcal). Data from [107].

B) Map showing the prevalence of global Fe deficiency in women (aged 15-49) as a percentage of women suffering from anaemia based on a haemoglobin level below 110 g/L. Data from [108]. Both maps from [109](CC BY).

1.1.5 Genetic approaches for Zn and Fe biofortification in crops

In order to counteract the impacts of nutrient and vitamin malnutrition in human populations (also referred to as 'hidden hunger'), numerous strategies have been deployed to increase the Zn, Fe, iodine and vitamin A bioavailability in plants and dietary systems [110]. For example, nutrition programmes for malnourished populations often use supplements, focus on improving the quality and diversity of diets, as well as the use of post-harvest food fortification (mass-fortification)[111]. However, these approaches require substantial and sustained investment and infrastructure, and especially for mass-fortification, are unlikely to be effective in communities that grow and produce the majority of their own food. Biofortification, which is the process of improving micronutrient content and bioavailability in the edible parts of crops during growth, is a more sustainable approach that has proven to be highly effective, especially when used alongside nutrition programmes in the most affected populations [112, 113]. Agronomic and genetic techniques are both utilised for biofortification, but as previously mentioned agronomic approaches such as the use of fertilisers or foliar sprays can be expensive and inaccessible, and their effectiveness is somewhat dependent upon the crop species and cultivar [114]. Genetic approaches to biofortification have become an increasingly promising avenue, with advances in genomic resources and biotechnology enabling the use of transgenics and genetic engineering alongside traditional breeding techniques [112, 115, 116]. Increased accessibility to sequencing technologies has also improved our understanding of the genetic variability available for use in breeding approaches through screening natural and mutagenised TILLING populations [117-120].

Most genetic biofortification efforts focussing on Zn and Fe have been carried out in staple crops such as maize (*Zea mays*), wheat (*Triticum aestivum*), rice (*Oryza sativa*) and barley (*Hordeum vulgare*)[116, 121]. Wheat is of particular interest as many modern cultivars are high-yielding but micronutrient-low, with Zn and Fe content further reduced during milling and post-harvest processing techniques [50, 122]. Compared to transgenic approaches, traditional breeding is generally the more accepted method and is not constrained by genetic modification (GM) regulations. However, traditional breeding techniques can be time-consuming and are limited by the genetic variation within species [121]. For instance, breeding program targets for increasing the Fe

content in rice grain look to achieve at least 30% of the estimated average requirement of women and children (>13 µg Fe/g in polished rice), but previous screening of over 20,000 different rice accessions has only found a maximum of 8 µg Fe/g naturally occurring [121, 123, 124]. Thus, a mixture of traditional breeding and biotechnology, is likely required to achieve biofortification goals.

Genetic targets for biofortification include transporters involved in Zn and Fe uptake and distribution within plants, proteins involved in synthesis of metal chelators, as well as genes that regulate the levels of phytic acid in the grain. Some of the most successful examples in wheat and rice to date include the overexpression of Fe storage *FERRITIN* genes in the endosperm [125-127], utilisation of the *NAC transcription factor NAM-B1* (*NAM-B1*) transcription factor in wheat [128], overexpression of *NICOTIANAMINE SYNTHASE* (*NAS*) and mugineic acid (MA) synthesis genes, which synthesise the Zn and Fe transport chelators [129-132]. Overexpression of Zn and Fe transporters involved in uptake and grain distribution, such as *OsYSL15* [133], *OsYSL2* [134], *OsIRT1* [135] in rice and *TaVIT2* [136] in wheat, and in barley the overexpression of *HvMTP1* [137], have also proven successful. Grain phytic acid content has been reduced through increasing the expression of phytases, such as *phyA* [138], and silencing the expression of grain phytic acid transporters, such as *ABCC13* [139]. Further understanding of the genes involved in Zn and Fe homeostasis is important in informing future micronutrient biofortification strategies.

1.2 Overview of Zn and Fe homeostasis in *A. thaliana*

To maintain cellular Zn and Fe concentrations within an optimal range, plants have evolved highly coordinated homeostasis networks of transporters, metal chelators and regulatory proteins. The activity of these proteins adjusts Zn and Fe uptake, cellular distribution and subcellular compartmentalisation in response to a variety of environmental and internal signals. The homeostasis of Zn and Fe are closely interlinked, with a number of transporters, chelators and regulatory proteins acting as important points of cross-talk between Zn and Fe nutrition. As a consequence, defective Zn

nutrition directly impacts Fe uptake and distribution, and vice versa. The genes in the following sections refer to *A. thaliana* genes unless otherwise stated.

1.2.1 Uptake and radial transport in roots

Zn and Fe are mainly taken up from the rhizosphere as divalent cations, and then undergo radial transport across the root through the epidermis, cortex, endodermis and pericycle towards the root vasculature for shoot translocation (**Figure 1.3**)[140].

During radial transport, ions are transported in both the symplast and apoplast (**Figure 1.3**)[141, 142]. The transmembrane pathway, formed of transmembrane nutrient transport proteins, regulates movement of ions across the plasma membrane and endomembranes. The symplastic pathway is formed from the cytoplasm of adjacent cells connected through plasmodesmata, while the apoplastic pathway consists of movement through the cell wall [143]. The apoplastic pathway is intercepted between the cortex and the stele by the Casparian strip, formed by the deposition of lignin in the endodermal cell walls, which results in connection and sealing of adjacent endodermal cells [144, 145]. The Casparian strip acts as a bi-directional diffusion barrier surrounding the root central vasculature, regulating the flow of water and nutrients both in and out of the root. The central role and bi-directionality of the Casparian strip in regulating nutrient movement in roots has been demonstrated by ionomic analysis of mutants with impaired Casparian strip development. For example, the knockout mutant of the leucine-rich repeat receptor-like kinase SCHENGEN3, *sgn3*, shows an interrupted Casparian strip and fails to form an apoplastic barrier, resulting in increased Mg accumulation and decreased Zn and K in leaves, as a result of nutrients freely following their diffusion gradient across the root endodermis [146]. After Casparian strip formation, suberin lamellae develop in endodermal cell walls, although suberinisation is not necessary for the apoplastic barrier [145, 147]. Suberin lamellae have been suggested to inhibit water and nutrient uptake from the apoplast into the endodermal cytoplasm, while also being associated with salt tolerance [148-150]. Suberinisation of the endodermis is highly responsive to environmental conditions, including salt and nutrient stresses. For instance, Zn, Fe and Mn result in reduced suberin deposition, while S and K deficiency result in enhanced deposition, demonstrating that plasticity of the endodermal barrier is an important nutrient regulation strategy in plants [148]

At this point, ions must pass into the symplastic pathway via the much more selective process of membrane transport. As such, the Casparian strip acts as an impermeable protective barrier against uncontrolled water and nutrient movement into the inner apoplast, which includes the xylem. Zn and Fe loading into the xylem is discussed in **1.2.3**

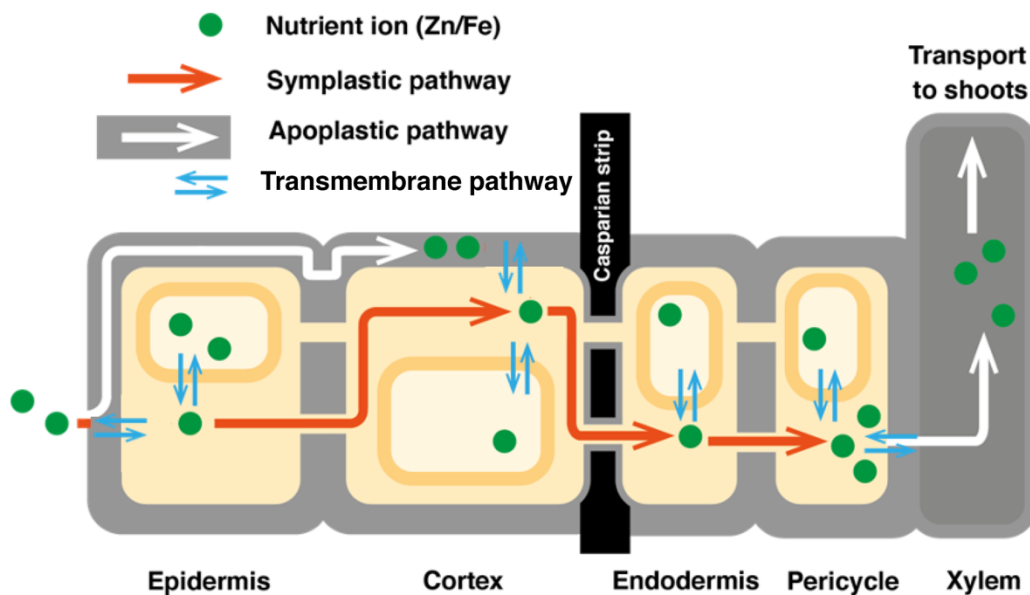


Figure 1.3: Radial transport of nutrients in roots.

Nutrients, such as Zn and Fe, are transported radially through the epidermis, cortex, endodermis and pericycle towards the xylem for root-to-shoot transport. Transport occurs in the symplast (orange arrows) through plasmodesmata that join adjacent cells, the apoplast (white arrows) through the extracellular space of the cell wall and the transmembrane transport pathway (blue arrows) via influx and efflux ion transport proteins (see **Figure 1.5** for Zn and Fe loading into the xylem). The Casparian strip blocks the apoplastic pathway at the endodermis. Movement through the symplastic pathway is regulated by sequestration and mobilisation of nutrients at the vacuole, and transport across the plasma membrane.

Zn uptake and radial transport: ZIP transporters and MTP2

Under replete or high environmental Zn concentrations, a low-affinity ($K_m = 2-5$ nM) uptake system is active, but as environmental Zn availability drops, a different suite of transporters involved in high-affinity ($K_m = 0.6-2$ μ M) uptake predominates at the

plasma membrane [151, 152]. A number of transporters involved in both high- and low-affinity uptake of Zn are members of the Zn-regulated/Iron-regulated-like Protein (ZIP) transporter family. ZIPs are an important family of metal transporters involved in the uptake and intracellular distribution of Zn^{2+} , Fe^{2+} , Mn^{2+} , Cu^{2+} and Cd^{2+} [152-154]. The *A. thaliana* genome encodes 15 ZIP transporters, named ZIP1-12 and Iron-Regulated Transporters 1-3 (IRT1-3) [152]. ZIP1-12 and IRT3 have been implicated in Zn^{2+} transport and homeostasis, while IRT1 and IRT2 are involved predominantly in Fe^{2+} uptake [152, 155, 156]. However, the vast majority of ZIP transporters has not yet been fully characterised *in planta* and their exact contribution to metal homeostasis is yet to be shown.

IRT3 is upregulated in response to Zn deficiency and localises to the plasma membrane where it mediates Zn^{2+} and Fe^{2+} uptake [157]. Expression is seen in both leaves and roots, notably in the root stele where it is thought to contribute to long-distance Zn transport through xylem unloading [157]. Overexpression of IRT3 increases accumulation of Zn in shoots and Fe in roots, although it is thought that Zn^{2+} is the primary IRT3 transport substrate, a notion that is further supported by the association of high IRT3 expression in the Zn hyperaccumulator *A. halleri* [157]. ZIP4 is also upregulated in Zn deficiency conditions and has been suggested to play a similar role to IRT3 in Zn^{2+} uptake at epidermal cells and xylem unloading [158]. ZIP1 and ZIP2 are downregulated and upregulated respectively in response to Zn deficiency and have been shown to function in Zn^{2+} and Mn^{2+} uptake and transport in roots [152]. ZIP1 is proposed to function in vacuolar remobilisation in roots, but the *zip1* mutant does not appear to have any obvious phenotype in varying Zn growth conditions, and as such may play a minor or functionally redundant role [156]. ZIP2 localises to the plasma membrane and is thought to act in Mn^{2+} and Zn^{2+} partitioning to the shoot through mediating movement in the stele towards the xylem [156]. The *zip2* loss-of-function mutant is more tolerant to low Zn growth conditions but is sensitive to excess Zn, due to root Zn overaccumulation [156].

ZIP3, ZIP7 and ZIP11 have additionally been shown to complement Zn^{2+} uptake in yeast mutants, with ZIP7 also able to transport Mn^{2+} and Fe^{2+} , but their role in metal homeostasis has yet to be fully investigated [156]. ZIP5, ZIP9 and ZIP12 are all upregulated under low Zn conditions, but little is known about their exact role in Zn

homeostasis, with single mutants only showing mild phenotypes under varying Zn growth conditions [156, 159].

Metal Tolerance Protein (MTP) transporters, also known as members of the cation diffusion facilitator (CDF) family, are cation/H⁺ antiporters primarily involved in Zn homeostasis, although they are also able to transport Fe²⁺, Mn²⁺, Cd²⁺, Co²⁺ and Ni²⁺ [160]. The *A. thaliana* genome encodes 12 MTP transporters, divided into three major groups, the Zn-CDFs, the Zn/Fe-CDFs and the Mn-CDFs [161]. MTP1, MTP2 and MTP3 all have important roles in Zn homeostasis, but MTP1 and MTP3 function in vacuolar storage so are discussed in **1.2.4**. However, MTP2 localises to the endoplasmic reticulum (ER) and functions under Zn deficiency to aid radial symplastic transport towards the vasculature through desmotubules [162]. The *hma2 mtp2* double mutant, which also contains a mutation in the Zn xylem-loading *HMA2* transport gene, is severely impaired in root-to-shoot transport, suggesting that HMA2 and MTP2 act together to regulate Zn flow towards the xylem and subsequent apoplastic loading [162].

Strategy I Fe uptake: IRT1, FRO2 and coumarins

Non-graminaceous species, such as *A. thaliana*, employ a reduction-based, or Strategy I, approach to Fe uptake (**Figure 1.4**). This involves acidification of the rhizosphere to solubilise Fe³⁺, reduction of Fe³⁺ to Fe²⁺ at the root surface, and finally Fe²⁺ uptake into the cytoplasm by transporters [163]. Fe uptake capacity is further increased through the secretion of Fe solubilising compounds into the rhizosphere [164, 165]. This differs from the chelation-based Strategy II used by graminaceous species, which involves the transport of Fe³⁺-phytosiderophore complexes across the plasma membrane [166]. Fe deficiency-responsive uptake strategies are also activated under Zn excess growth conditions.

IRT1 is the best-characterised of the ZIP transporters and is the major Fe²⁺ transporter involved in Strategy I Fe uptake at the root plasma membrane. *IRT1* is upregulated under both Fe deficiency and Zn excess, and *irt1* mutants are unable to take up adequate Fe²⁺ for survival [167]. *IRT1* is co-regulated with the root ferric reductase *Ferric Reduction Oxidase 2 (FRO2)*, which reduces Fe³⁺ to Fe²⁺ at the root surface to make Fe available for IRT1 uptake [164, 168]. *Arabidopsis H⁺-ATPase (AHA)* genes, *AHA1*, *AHA2* and *AHA7* are upregulated in the root epidermis and are involved in proton extrusion at

the root plasma membrane for rhizosphere acidification [169]. However, AHA2 is thought to be the major H⁺-ATPase involved in Strategy I Fe uptake (**Figure 1.4**)[169].

IRT1 has a broad substrate specificity and is also capable of transporting Zn²⁺, Mn²⁺, Co²⁺ and Cd²⁺ into the cytoplasm, and as a result when IRT1 is upregulated under Fe deficiency, root accumulation of these other metals also occurs [170]. This is especially problematic in the case of Zn, which can outcompete Fe for transport and protein-binding sites, further exacerbating the Fe deficiency response and IRT1-mediated Zn uptake. Consequently, IRT1 is subject to non-Fe metal-dependent ubiquitination and internalisation to prevent excessive uptake of these other substrates when locally present in the soil [171, 172]. AHA2 and FRO2 are also subject to post-transcriptional inhibition under Fe replete conditions to prevent root Fe accumulation [173, 174]. However, post-transcriptional mechanisms acting on AHA2 and FRO2 are yet to be characterised and are distinct from IRT1 internalisation despite physical interaction of IRT1, FRO2 and AHA2 as a tripartite complex at the plasma membrane [175].

Secretion of Fe-solubilising phenolic compounds at the root surface is also an important component of Strategy I Fe uptake (**Figure 1.4**)[176]. These Fe deficiency-responsive root exudates are key in mobilising apoplastically-bound Fe that comprises as much as 75% of root Fe content, as well as insoluble Fe under high pH conditions [177]. Catechol coumarins derived from the phenylpropanoid pathway are especially important and the best-studied of these Fe-solubilising compounds [178]. The major coumarins involved in the Fe deficiency response include scopoletin and its oxidised derivatives, such as fraxetin, sideretin and esculetin [179-182]. Key enzymes involved in coumarin biosynthesis, such as *Feruloyl-CoA 6'-Hydroxylase 1 (F6'H1)*, *Scopoletin-8-hydroxylase (S8H)*, and *Cytochrome P450 82C4 (CYP82C4)* as well as *Pleiotropic Drug Resistance 9 (PDR9/ABCG37)*, which encodes the ATP-binding cassette (ABC) transporter involved in coumarin secretion, are upregulated under Fe-limiting conditions (**Figure 1.4**)[183, 184]. Prior to secretion, coumarins require deglycosylation by enzymes such as Beta-glucosidase 42 (BGLU42), which catalyses the conversion of scopolin to scopoletin (**Figure 1.4**)[185]. Disruption of phenolic efflux or biosynthesis greatly impairs the ability of plants to take up Fe³⁺ sources in high pH environments, as evidenced by the poor growth of *f6'h1* and *pdr9* mutant phenotypes [186]. The exact mechanism by which coumarins enhance Fe solubility in the rhizosphere is not fully understood, although

there is evidence for chelation as well as potential reduction of Fe^{3+} species [178]. The types of coumarin accumulated and secreted also show spatial and environment-specific responses. For example, scopoletin secretion occurs mainly at root hairs, whereas fraxetin secretion occurs mainly in epidermal cells, with PDR9 additionally functioning in cortical to epidermal transport of coumarins [187]. Moreover, fraxetin secretion occurs mainly in response to high pH, while sideretin predominates under low pH, showing that complex metabolic changes involving coumarins and associated secondary metabolic pathways are a key part of the adaption to low Fe conditions [187].

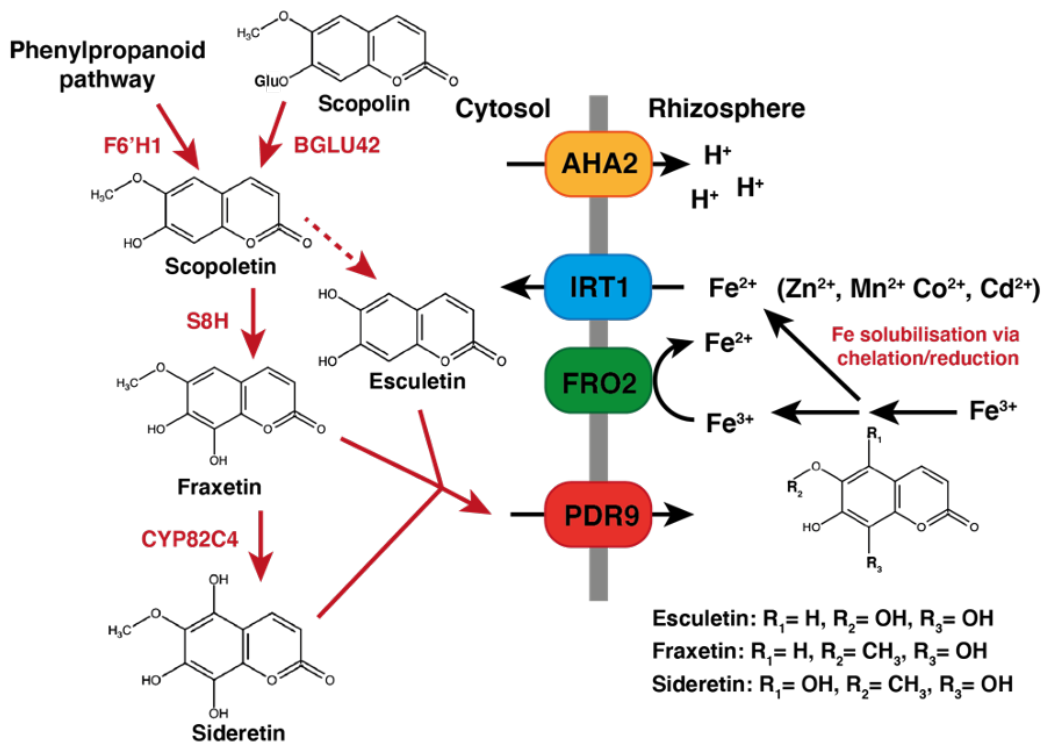


Figure 1.4: Strategy I Fe uptake in *A. thaliana*.

Under Fe deficiency conditions, upregulation of the phenylpropanoid pathway and enzymes such as *Feruloyl-CoA 6'-Hydroxylase 1 (F6'H1)*, *Scopoletin-8-hydroxylase (S8H)* and *Cytochrome P450 82C4 (CYP82C4)* increases the biosynthesis of the coumarins scopoletin, fraxetin and sideretin. Coumarins are deglycosylated by beta-glucosidase (BGLU) enzymes, such as BGLU42 which catalyses the deglycosylation of scopoline. Aglycone coumarins are secreted into the rhizosphere by Pleiotropic Drug Resistance 9 (PDR9/ABCG37) where they solubilise Fe³⁺ through chelation and reduction. Acidification of the rhizosphere through proton extrusion by Arabidopsis H⁺-ATPase 2 (AHA2) further aids Fe solubilisation. When mobilised Fe³⁺ reaches the root surface it is reduced to Fe²⁺ by Ferric Reduction Oxidase 2 (FRO2), making it available for root uptake by the major Fe²⁺ uptake transporter Iron-regulated Transporter 1 (IRT1). IRT1 has broad substrate specificity and is able to uptake Zn²⁺, Mn²⁺, Co²⁺ and Cd²⁺. Adapted from [188].

Natural Resistance-Associated Macrophage Protein (NRAMP) family transporters are metal/H⁺ antiporters with a broad substrate specificity for divalent cations [189]. *A. thaliana* has six *NRAMP* genes [190], with *NRAMP1*, *NRAMP3*, *NRAMP4* and *NRAMP6* involved in Zn and Fe homeostasis. *NRAMP1* encodes a plasma-membrane root transporter, primarily functioning in Mn²⁺ root uptake under deficiency conditions [191]. However, recent studies have also shown a cooperative role with *NRAMP1* and *IRT1* in Fe²⁺ uptake under Fe sufficiency conditions, as well as Zn²⁺ uptake in *A. halleri*, with overexpression of *AhNRMP1* in rice found to enhance Fe and Zn content [192, 193]. *NRAMP3*, *NRAMP4* and *NRAMP6* are discussed in **1.2.5** in relation to their roles in subcellular transport.

1.2.2 Zn and Fe chelators

In the neutral pH conditions of the plant cytosol and nucleus, Zn and Fe have a propensity to bind to a range of organic molecules, which greatly restricts movement and has the potential to interfere with the homeostasis of other metals. Thus, in the symplast Zn²⁺ and Fe²⁺ ions are generally bound to chelators to prevent cellular damage and aid translocation. In the cytoplasm, non-chelated free Zn²⁺, the 'labile pool', is kept in the pM range [194]. In the xylem, conditions are slightly more acidic at ~pH 5.5, while in the phloem they are more alkaline, having implications for the ligands that Fe and Zn are found associated with, which is discussed in more detail below [195].

Nicotianamine (NA)

Nicotianamine (NA) is a non-proteinogenic amino acid synthesised from three molecules of S-adenosyl methionine (SAM) in a one-step reaction catalysed by NA Synthase (NAS) enzymes [196]. NA is a high affinity chelator able to form stable complexes with a broad range of metals, including Fe²⁺, Fe³⁺, Zn²⁺, Mn²⁺, Co²⁺ and Cu²⁺ and has been demonstrated to play an important role in long distance metal transport and vacuolar storage [197, 198]. NA-metal complexes show the greatest stability around pH 6.5, so it is likely that NA functions primarily in the phloem and symplastic cell-to-cell movement of metals (**Figure 1.5 and 1.6**)[199]. The *A. thaliana* genome encodes four *NAS* genes, *NAS1*, *NAS2*, *NAS3* and *NAS4*, which all show metal-dependent regulation,

including upregulation in response to Zn and Fe deficiency, and Zn excess [200]. The *NAS* genes are partially functionally redundant, showing differential spatial expression and mutant phenotypes. For example, *NAS1*, *NAS2* and *NAS4* are expressed in roots and upregulated under Fe deficiency, with *NAS1* and *NAS4* also expressed in leaves, while *NAS3* is expressed in leaves and flowers but is repressed under low Fe conditions [198]. Of the single mutants, *nas4* shows the greatest sensitivity to Fe deficiency conditions, likely linked to its central role in long distance transport demonstrated by its expression in the root stele [198].

As NA binds both Zn^{2+} and Fe^{2+} , whilst having a slightly higher binding affinity for Zn^{2+} over Fe^{2+} , this has implications for the role of NA and *NAS* genes in Fe and Zn-cross homeostasis [199]. For example, *NAS* overexpression lines with increased NA content show enhanced Fe translocation to shoots, and consequently enhanced tolerance to Fe deficiency and Zn excess [201, 202]. Moreover, overexpression of the *ZIF1* vacuolar NA transporter leads to immobilisation of Zn in roots, but causes interveinal chlorosis in shoots through Fe sequestration, highlighting the importance of NA in metal storage and regulating Zn and Fe distribution [203].

The role of elevated NA in Zn tolerance is further demonstrated by its function in Zn hyperaccumulator species. In *A. halleri*, constitutive overexpression of *AhNAS2* leads to enhanced root Zn content, which contributes to metal hyperaccumulation through conferring efficient root-to-shoot Zn transport [204, 205]. NA is also associated with hypertolerance in *A. halleri* through secretion into the rhizosphere which restricts uptake into the symplast [206].

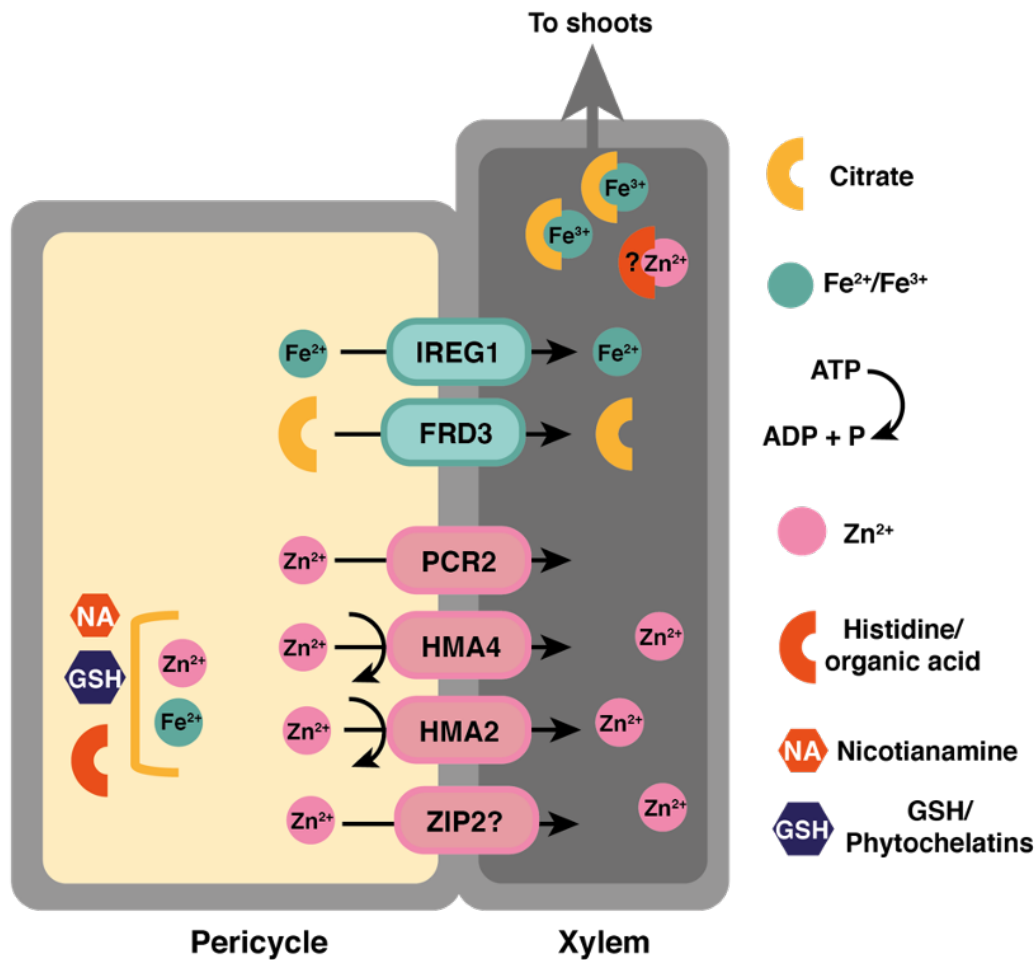


Figure 1.5: Chelation and xylem loading of Zn and Fe.

Zn and Fe are loaded into the xylem by transporters at the plasma membrane of root pericycle cells. In the symplast of the root pericycle, Zn and Fe are mainly associated with chelators such as nicotianamine (NA), glutathione (GSH) and derived phytochelatin, histidine or organic acids. Zn²⁺ is transported into the apoplastic space of the xylem by Plant Cadmium Resistance 2 (PCR2), and ATP-dependent Heavy Metal ATPase 2 (HMA2) and 4 (HMA4), as well as possibly by Zrt-/Irt-like Protein 2 (ZIP2), where it is then transported to the shoots predominantly as free Zn²⁺ ions, with a small amount associated with histidine and organic acids. Fe²⁺ and citrate are transported into the xylem by Iron-Regulated Transporter 1/Ferroportin 1 (IREG1/FPN1) and Ferric Reductase Defective 3 (FRD3). Fe is translocated to shoots predominantly as Fe³⁺-citrate complexes.

Glutathione (GSH)

Glutathione (GSH) is a non-protein thiol that functions in a wide range of biological processes in plants, notably in abiotic and biotic stress responses, and in reactive oxygen species (ROS) scavenging in the ascorbate-glutathione cycle [207]. GSH is synthesised in a two-step reaction. The first is the production of γ -glutamylcysteine from glutamate and cysteine (Cys) by plastid-localised γ -glutamylcysteine synthetase (GSH1)[208]. In the second step, a glycine is added by glutathione synthetase (GSH2), which is found in the cytosol and plastids, to produce GSH [209]. There is a growing body of evidence for the role of GSH in metal homeostasis, particularly in Zn detoxification and Fe deficiency tolerance through metal chelation in the symplast (**Figure 1.5**)[210]. Elevated GSH levels occur under high Zn and low Fe growth conditions, with GSH acting as both antioxidant and metal homeostasis component [211, 212]. Increases in shoot GSH content through foliar application or overexpression of *GSH1* enhances root-to-shoot translocation of Zn [208]. It has also been found that *gsh1* mutants, which show reduced GSH content, are defective in Fe-mediated Zn tolerance due to an inability to accumulate shoot Fe [212]. Later studies showed that reduced Fe transport in *gsh1* mutants is associated with impaired nitric oxide (NO) signalling upstream of the Fe deficiency response, indicating a regulatory role for GSH as well [213].

Phytochelatins (PCs)

GSH is the precursor of phytochelatins (PCs), which are also important for tolerance to Zn excess growth conditions. PCs are non-ribosomally produced proteins, synthesised by PC synthases (PCSs), and structurally are $(\gamma\text{-Glu-Cys})_n\text{-Gly}$ polymers, where $n = 2\text{-}7$ [214]. There are two known *PCS* genes in *A. thaliana*, *PCS1* and *PCS2*, both of which are induced in response to Zn excess and have been linked to Zn tolerance, as well as to survival under excess of non-essential metals such as Cd, mercury (Hg), Pb and arsenic (As)[215]. *PCS1* expression is important for Zn transport to shoots, as well as for Zn detoxification through cytosolic buffering (**Figure 1.5**). Consequently, *pcs1* mutants show reduced leaf Zn content under standard growth conditions and sensitivity to Zn excess [216, 217]. The physiological function of *PCS2* still remains obscure, although its

constitutive expression suggests a role in maintaining homeostasis under Zn sufficiency conditions [218].

Metallothioneins (MTs)

Metallothioneins (MTs) are small Cys-rich proteins found in both prokaryotic and eukaryotic systems that bind a range of heavy metals [219]. Plant MTs are divided into four types based upon the arrangement of their Cys residues [220]. Seven functional MTs have been identified to date in *A. thaliana*, and they play central roles in micronutrient homeostasis and heavy metal tolerance in a number of different tissues [221]. *MT1a*, *MT2a*, *MT2b* and *MT3* have been linked to Cu chelation primarily in leaves [222], while Type 4 MTs function in Zn chelation and homeostasis in developing seeds [223]. *MT4a* and *MT4b* act together to load Zn into developing seed and are important in supplying Zn to the metalloproteome during seed development and germination [223]. *MT4a* is expressed in vascular tissues of the embryo during later stages of development and is thought to function in Zn transport, whereas *MT4b* is expressed highly throughout the embryo and functions mainly in Zn storage [224]. Silencing of *MT4a* and *MT4b* expression reduces seed Zn accumulation and impairs seed development, with overexpression having the opposite effect and increasing seed Zn content and viability [223].

1.2.3 Long distance transport

Once at the root pericycle, nutrients are actively transported out of the symplast and into the xylem, which is a key regulatory step in controlling ion transport to the shoot (**Figure 1.5**)[195]. At the shoots, Zn and Fe are unloaded into the xylem parenchyma cells and subsequently into mesophyll cells for metalloproteome utilisation, or into the apoplast for further transport or loading into the phloem. Lateral transport of nutrients between xylem and phloem cells also occurs to aid nutrient tissue distribution, as the transpiration stream in the xylem is not sufficient to reach distant developing organs. Transport in the phloem functions to remobilise micronutrients to sink tissues, such as developing leaves or seeds, as well as in shoot-to-root systemic nutrient signalling [195].

Zn loading into the xylem: HMA2, HMA4 and PCR2

The Heavy Metal-Associated (HMA) transporters are 1B P-type ATPases involved in Zn detoxification and long-distance transport [225]. The *A. thaliana* genome encodes eight HMA transporters, which are divided into two subgroups based upon their metal specificity – the Cu/silver (Ag) subgroup and the Zn/Co/Cd/Pb subgroup [226]. *HMA1*, *HMA2*, *HMA3* and *HMA4* are in the Zn/Co/Cd/Pb subgroup and have all been shown to play a role in Zn homeostasis [225]. *HMA2* and *HMA4* are expressed in the pericycle and xylem parenchyma and play central roles in Zn root-to-shoot transport through loading of Zn into xylem vessels, especially under Zn-limiting growth conditions (**Figure 1.5**)[225]. The *hma2 hma4* double mutant is severely defective in root-to-shoot transport and shows shoot Zn deficiency symptoms while over accumulating Zn in roots [225]. While only *HMA2* expression is upregulated in response to low Zn, the HMA4 protein has an exposed Zn-binding domain which is thought to potentially confer post-translation Zn-mediated regulation [227, 228]. HMA1 and HMA3 function in detoxification, and as such are described in **1.2.4**.

Alongside HMA2 and HMA4, the small plasma membrane transporter Plant Cadmium Resistance 2 (PCR2) has also been implicated in the loading of Zn into the xylem (**Figure 1.5**)[229]. *PCR2* is expressed in the pericycle and the epidermis and shows upregulation under both Zn deficiency and Zn excess growth conditions [229]. Additionally, the *pcr2* mutant is sensitive to both low and high Zn growth conditions and shows Zn and Fe root accumulation [229]. As such, PCR2 has been proposed to have a dual function in both xylem loading of Zn under deficiency conditions and in Zn detoxification through extrusion at the root surface during excess. As previously mentioned, ZIP2 has also been proposed to function in Zn long distance transport (**Figure 1.5**)[156].

The acidic environment of the xylem (~pH 5.5) enables Zn to be predominantly transported as unchelated Zn²⁺ ions, although a small amount is found associated with organic acids, such as citrate and malate, amino acids such as histidine (**Figure 1.5**)[77]. The relative contributions of these chelators to Zn homeostasis in *A. thaliana* is not fully understood, but their role in metal hyperaccumulator species has been more extensively studied and can be used to infer potential functions. For example, work in *A. halleri* suggested that Zn in xylem sap may be associated mainly with citrate and malate [230],

while it has been shown that exogenous application of histidine to *Noccaea caerulescens* can enhance Zn loading into the xylem and high levels of histidine are found in the xylem sap of numerous hyperaccumulator species [231].

Fe loading into the xylem: IREG1/FPN1, FRD3 and citrate

A. thaliana has three *IRON-REGULATED/Ferroportin (IREG/FPN)* genes, which show high protein similarity to the mammalian Fe transporter IRON-REGULATED 1 (IREG1)[232]. *IREG2/FPN2* and *IREG3/FPN3* encode Fe transporters which localise to the vacuolar and plastid membranes respectively, and are discussed in **1.2.4** [233, 234]. The third *IREG* gene, *IREG1/FPN1*, localises to the plasma membrane of stelar cells and is thought to be involved in Fe²⁺ efflux into the xylem, with *fpn1* loss of function mutants showing chlorosis and shoot Fe deficiency (**Figure 1.5**)[233].

In addition to NA, Fe is chelated by a range of organic acids such as citrate, malate and succinate [235]. However, in the xylem Fe is found predominantly associated with citrate, generally as a tri-Fe³⁺, tri-citrate complex [236]. It has therefore been hypothesised that citrate and the citrate efflux transporter, Ferric Reductase 3 (FRD3) which loads citrate into the apoplast, are central to long distance transport of Fe in the xylem (**Figure 1.5**)[237]. *FRD3* is expressed in the root pericycle and encodes a plasma membrane-localised member of the multidrug and toxic compound extrusion (MATE) family of transporters [238]. The *frd3* knockout mutant is severely impaired in root-to-shoot Fe translocation, and consequently shows constitutive activation of the Fe deficiency response while accumulating high levels of Fe in roots due to the sustained Fe deficiency signal from shoots [237, 238]. Higher *FRD3* expression has additionally been linked to enhanced Zn tolerance, likely through improved shoot Fe nutrition, with *FRD3* also undergoing differential splicing under Zn excess [239].

Zn and Fe xylem and phloem transport: Oligopeptide Transporters (OPTs)

The lateral distribution, loading and unloading of Fe and Zn in the xylem and phloem is largely associated with two clades of the Oligopeptide Transporter (OPT) family, the YELLOW STRIPE-LIKE (YSL) transporters and OPTs. YSLs are involved in the transport of metal-NA chelates, predominantly Fe²⁺-NA, Zn²⁺-NA and Cu²⁺-NA [140]. A.

thaliana has eight *YSL* genes, of which three are implicated in Zn and Fe homeostasis [240]. *YSL1* and *YSL3* are highly expressed in senescing leaves and are involved in remobilisation of Fe²⁺-NA, Zn²⁺-NA, Cu²⁺-NA and Mn²⁺-NA complexes for phloem transport to sink tissues, particularly seeds (**Figure 1.6**)[241]. *YSL1* and *YSL3* localise to the plasma membrane and function in apoplastic loading of metal-NA complexes at companion cells during long distance phloem transport [241]. Impaired phloem transport in the *ysl1 ysl3* double knockout mutant results in reduced shoot Fe content and toxic Zn accumulation, leading to the onset of Fe deficiency symptoms [241]. *YSL2* also plays a central role in Fe²⁺-NA long distance transport and distribution, by regulating lateral movement and unloading of Fe-NA complexes from the xylem at source tissues (**Figure 1.6**)[240]. *YSL2* is the only Zn-responsive *YSL* gene, showing repression under Zn-deficiency. However, this is thought to be a secondary effect of the increased Fe content seen under Zn deficiency conditions, rather than a direct role in Zn homeostasis [240].

A close phylogenetic relative of the *YSLs*, *OPT3*, is also involved in long distance Fe transport in the phloem but is believed to transport Fe²⁺ rather than a metal-chelate complex [242]. *OPT3* is expressed in the vasculature and upregulated under Fe deficiency conditions and has an especially important role in loading of Fe into seeds, with the *opt3-1* knockout mutation being embryo lethal (**Figure 1.6**)[242]. *OPT3* is additionally proposed to function in remobilisation of Fe²⁺ from the xylem or source tissues to the phloem for recirculation and systemic Fe signalling (**Figure 1.6**)[243, 244]. This role in Fe shoot-to-root signalling was proposed after characterisation of the *opt3-2* partial knockout mutant demonstrated a constitutive Fe deficiency phenotype despite Fe accumulation in roots and shoots [242-244].

Prior to xylem unloading, Fe³⁺-chelate complexes require the reduction of Fe³⁺ to Fe²⁺. It has been suggested that *FRO6*, or another shoot-expressed plasma membrane-localised *FRO* gene may be responsible, although further evidence is required to confirm this [245]. The transporters involved in xylem unloading of Fe²⁺ or Zn²⁺ into shoots are also yet to be identified, but the ZIP transporter family members are likely candidates.

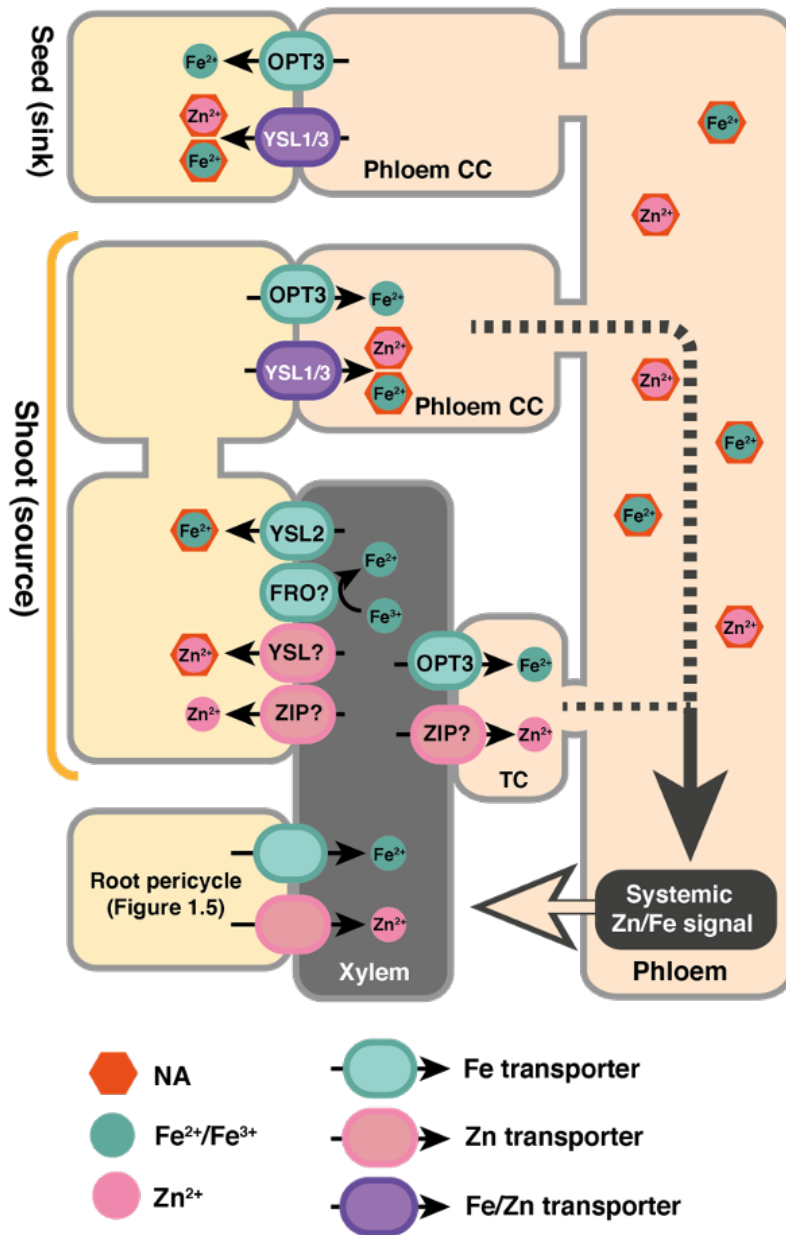


Figure 1.6: Long distance Zn and Fe transport in the xylem and phloem.

Zn and Fe undergo long distance transport in the xylem (see **Figure 1.5** for overview of transporters involved in xylem loading) towards shoot source tissues, where YELLOW STRIPLE-LIKE 2 (YSL2) unloads Fe-nicotianamine (NA) from the xylem. It is also thought that a Ferric Reduction Oxidase (FRO) enzyme is involved in reduction of Fe^{3+} to Fe^{2+} in the xylem for transport into the symplast by an unknown transporter. The transporters involved in Zn unloading from the xylem are not yet known, but YSL and Zrt-/Irt-like Proteins (ZIP) transporters are likely involved. Zn and Fe are loaded into the phloem from shoot source

tissues, with Oligopeptide Transporter 3 (OPT3) transporting Fe^{2+} and YSL1 and YSL3 Fe-NA and Zn-NA complexes. OPT3 is also involved in the lateral transport of Fe^{2+} from the xylem to the phloem, and it also likely a ZIP transporter performs a similar function for Zn^{2+} . In the phloem, Zn and Fe are transported mainly complexed with NA. Phloem-mobile Zn and Fe or an associated unknown signalling molecule are recirculated to the roots and act as a systemic nutrient signal. Zn and Fe transported in the phloem is also recirculated to sink tissues, such as seeds and developing leaves, where OPT3, YSL1 and YSL3 act in phloem unloading. CC = companion cell. TC = transfer cells. Adapted from [246].

1.2.4 Subcellular sequestration and mobilisation

In the symplast, ion movement is restricted by transport into vacuoles for storage, particularly under metal excess conditions when enhanced root vacuolar sequestration restricts root-to-shoot transport. Vacuoles are the major storage organelle of Zn and Fe, with as much as 80% of cellular Zn and 50% of Fe contained within the vacuole as either free ions or associated with low molecular weight ligands, such as NA [247]. There is also evidence for excess Zn, Fe and heavy metal storage in trichomes and other subcellular organelles as well [242, 247, 248]. The balance of sequestration and remobilisation is not only critically important for regulating cytoplasmic metal concentrations, but also maintains metalloproteome function in subcellular compartments [140]. This is especially important for chloroplasts and mitochondria, which demand a high amount of Fe and Zn to support photosynthetic and respiratory processes. A summary of the transporters involved in subcellular compartmentalisation of Zn and Fe are shown in **Figure 1.7**.

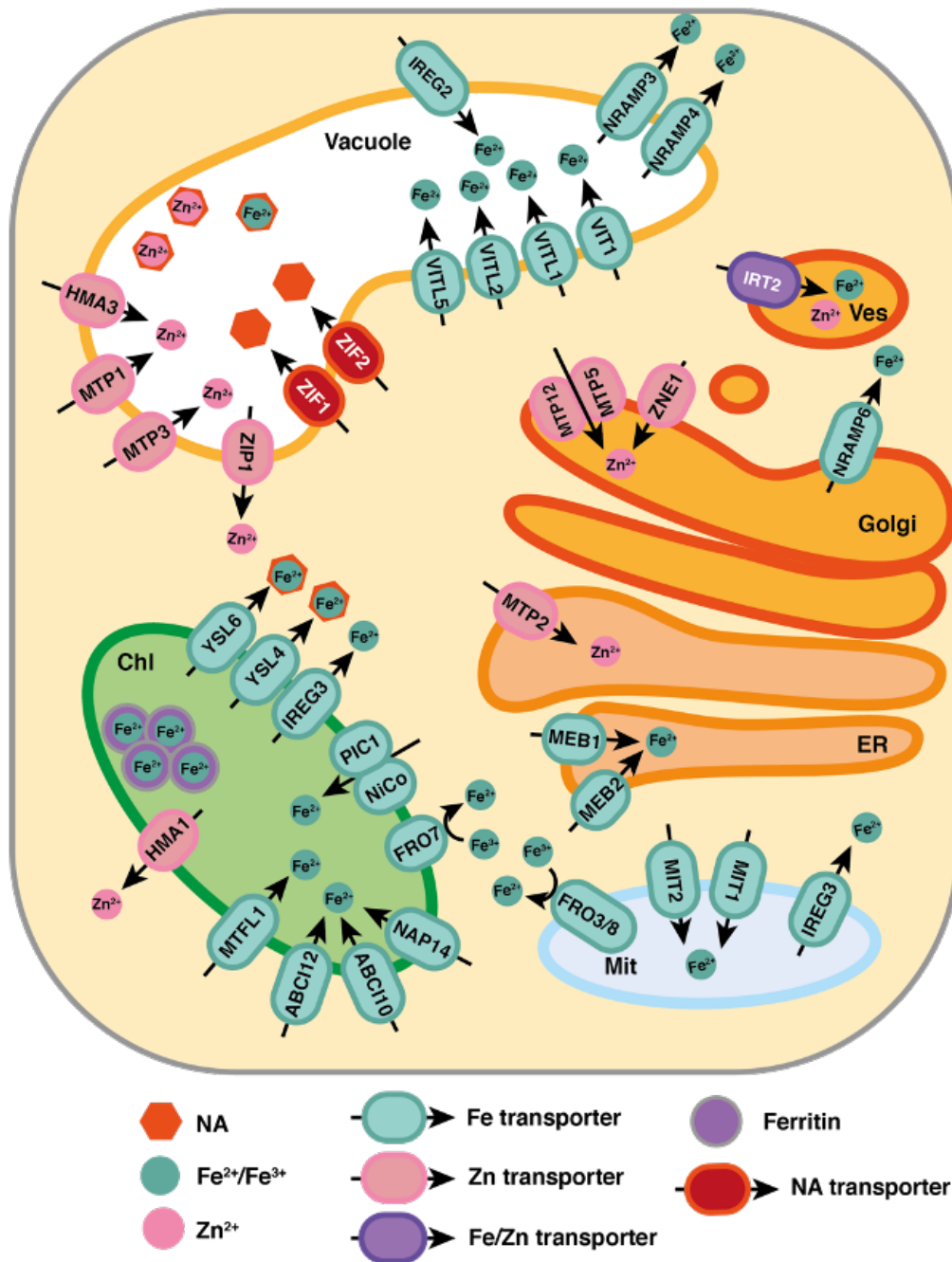


Figure 1.7: Subcellular transport of Zn and Fe.

Transporters involved in sequestration and mobilisation of Zn and Fe in organelles. At the vacuolar membrane Zinc-Induced Facilitator 1 (ZIF1) and ZIF2 import NA, where it associates with Zn and Fe for storage. Zn^{2+} is imported into the vacuole by Heavy Metal APTase 3 (HMA3), Metal Tolerance Protein 1 (MTP1) and MTP3, and Zn^{2+} is thought to be exported by Zrt-/Irt-like Protein 1 (ZIP1). Fe^{2+} is imported into the vacuole by Iron-Regulated 2/Ferroportin 2 (IREG2/FPN2), Vacuolar Iron Transporter 1 (VIT1). VIT-Like 1 (VITL1), VITL2

and VITL5, and Fe^{2+} is exported from the vacuole by Natural Resistance-Associated Macrophage Protein 3 (NRAMP3) and NRAMP4. IRT2 imports Zn^{2+} and Fe^{2+} into subcellular vesicles. At the Golgi, Zn^{2+} is imported by Zinc Nutrient Essential 1 (ZNE1), MTP5 and MTP12, and Fe^{2+} is exported by NRAMP6. At the ER, Zn^{2+} is imported by MTP2, and Fe^{2+} is imported by Membrane Protein of Endoplasmic Reticulum 1 (MEB1) and MEB2. At the chloroplast membrane, Fe^{3+} is reduced to Fe^{2+} by Ferric Reduction Oxidase (FRO7) and imported into the chloroplast stroma by the Permease In Chloroplast 1 (PIC1) and the Nickel-Cobalt (NiCo) translocon, as well as Mitoferritin-like 1 (MTFL1), and ABC transporters ABCI10, ABC12 and ABCI11/NAP14. Inside the chloroplast, Fe^{2+} is associated with ferritin proteins for storage. Fe^{2+} and Fe^{2+} -NA stores are mobilised from chloroplasts by IREG3, Yellow Stripe-Like 4 (YSL4) and YSL6. Zn^{2+} is exported from chloroplasts by HMA1. At the mitochondrial membrane, Fe^{3+} is reduced to Fe^{2+} by FRO3 and FRO8, and imported into the mitochondrial stroma by Mitochondrial Iron Transporter 1 (MIT1) and MIT2. Fe^{2+} is mobilised from mitochondria by IREG3. Ves = vesicles. Golgi = Golgi apparatus. ER = endoplasmic reticulum. Mit = mitochondria. Chl = chloroplasts. Tissue-specific expression, transporter-antiporter and ATPase properties not shown for simplification.

Zn subcellular compartmentalisation: MTPs, ZNE1 and HMAs

The MTP family were introduced in **1.2.1** in relation to the role of MTP2 in radial transport of Zn. However, many other MTP transporters function in the subcellular compartmentalisation of Zn. For example, MTP1 and MTP3 are both vacuolar Zn transporters, with non-redundant roles in Zn tolerance (**Figure 1.7**)[249, 250]. *MTP1* expression is not Zn-regulated, but plays an important role under Zn excess in vacuolar storage and detoxification in roots and shoots [250]. RNAi-mediated silencing of *MTP1* results in reduced leaf Zn accumulation, as well as hypersensitivity to high Zn conditions likely due to failure to sequester excess Zn^{2+} ions [250]. Thus, MTP1 functions in Zn detoxification in dividing tissues and the shoot. *MTP3* is upregulated in response to high Zn, Mn and Co, and low Fe conditions in the root epidermis and cortex [249]. Silencing of *MTP3* by RNAi results in reduced root storage of Zn and subsequent hypersensitivity to increased Zn as a result of elevated shoot Zn content [249]. As such, MTP3 promotes root Zn storage under low Fe and Zn excess conditions, which in turn limits Zn root-to-shoot translocation.

MTP12 and MTP5 are additionally involved in Zn²⁺ transport into subcellular organelles, but they form a heteromeric complex to transport Zn²⁺ into the Golgi for Zn-dependent protein function within the *cis*-Golgi apparatus (**Figure 1.7**)[251]. *MTP12* and *MTP5* do not show Zn-dependent regulation and it has also been shown that their activity is insufficient to reduce cytosolic Zn²⁺ concentrations under Zn excess [251]. Consequently, it is thought that their transport activity helps maintain Zn-dependent protein function within the Golgi, rather than having a role in detoxification.

Zinc Nutrient Essential 1 (ZNE1) was recently identified as a Golgi-localised Zn²⁺ transporter involved in sequestration in leaves under Zn excess and Fe deficiency conditions [252]. ZNE1 was originally annotated as ZIP13, however phylogenetic analysis and predicted protein domain composition suggest that ZNE1 does not belong to any known transporter families [252]. The *zne1* mutant shows growth impairment under Zn excess and Fe deficiency, but does not have altered metal content. This suggests that similar to MTP12, ZNE1 may function primarily in supplying Zn to the Golgi metalloproteome and subcellular distribution [252].

HMA1 and HMA3 are members of the Heavy Metal ATPase family involved in subcellular Zn²⁺ transport. HMA1 localises to the chloroplast envelope and functions as both a Cu²⁺ and Zn²⁺ transporter, with proposed roles in Zn detoxification through Zn extrusion from chloroplasts, which are highly sensitive to the balance of Zn and Fe (**Figure 1.7**)[253]. Accordingly, the *hma1* knockout mutant shows sensitivity to Zn excess growth conditions and accumulates Zn in shoots [253]. HMA3 is also thought to function in Zn detoxification through transport of Zn²⁺ and Cd²⁺ into the vacuole, with *hma3* mutants showing a Zn and Cd hypersensitive phenotype and a hypertolerance phenotype when *HMA3* is overexpressed (**Figure 1.7**)[254]. The Columbia-0 (Col-0) accession of *A. thaliana* contains a loss-of-function *HMA3* allele due to a base-pair deletion causing a frame-shift and subsequent premature stop codon [225]. Loss of HMA3 transporter function in Col-0 increases the sensitivity of this accession to Zn and Cd, highlighting the key role of HMA3 in metal tolerance [255].

NA vacuolar partitioning: ZIF transporters

Zinc-Induced Facilitator 1 (ZIF1) and ZIF2 are Major Facilitator Superfamily (MFS) transporters localised to the tonoplast with roles in Zn and Fe sequestration through

regulating subcellular NA distribution (**Figure 1.7**)[256, 257]. MFS transporters are found in all organisms and are a superfamily of membrane proteins involved in the transport of a wide range of small organic molecules [258]. The *A. thaliana* genome encodes over 90 putative MFS genes, although relatively few have been characterised [259]. *ZIF1* and *ZIF2* both encode vacuolar transporters upregulated in response to Zn excess and Fe deficiency, with *zif1* and *zif2* mutants displaying Zn hypersensitive phenotypes [256, 257]. *ZIF1* has been shown to regulate NA partitioning, promoting vacuolar Zn storage in roots, while maintaining Fe translocation to shoots under Zn excess conditions [203]. *ZIF1* overexpressing lines show enhanced immobilisation of NA and Zn in roots, but this causes NA deficiency in shoots and subsequent impaired symplastic movement of Fe in shoots and chlorosis [203]. Thus, *ZIF1* and NA are key components in maintaining Zn and Fe balance and distribution. Although, *ZIF2* transport is not yet fully characterised, it appears to perform a similar function either through the transport of Zn²⁺, NA or another Zn-associated small molecule (**Figure 1.7**)[203, 256]. *ZIF2* mRNA undergoes Zn-responsive alternative splicing favouring the expression of a longer mRNA variant (*ZIF2.2*) in response to high Zn growth conditions. The *ZIF2.2* 5' untranslated region greatly enhances translation efficiency of the downstream protein-coding region, leading to increased tolerance to Zn [257].

Fe vacuolar partitioning: VIT and NRAMP transporters

Vacuolar Iron Transporters (VITs) are a small family of nodulin-like proteins with functions in the subcellular compartmentalisation of Fe [260, 261]. Transporters in this family show homology to the CCC1 vacuolar Fe²⁺ transporter from *Saccharomyces cerevisiae* and can complement growth of the *ccc1* mutant [262]. In *A. thaliana* five members of this family, *VIT1*, *VIT1-Like 1* (*VITL/VTL*), *VITL2*, *VITL5*, and *Nodulin-Like3*, are upregulated in response to Fe excess and have been implicated in Fe²⁺ transport into vacuoles to prevent toxicity (**Figure 1.7**)[263, 264]. *VIT1* is expressed in the vasculature, mainly in the xylem parenchyma of developing embryos, where it functions to ensure adequate Fe storage and correct distribution within seeds [263]. Loss-of-function *vit1* mutants do not have altered Fe content but show reduced Fe accumulation in seed endodermal layers and increased Fe accumulation in subepidermal layers, and as a result show poor germination and growth under low Fe [263]. *VITL1*, *VITL2* and *VITL5* are

additionally thought to participate in Fe sequestration in vacuoles, with overexpression of *VITL1*, *VITL2* and *VITL5* able to complement growth of the *vit1-1* mutant and partially restore Fe partitioning to seeds (**Figure 1.7**)[264]. *VITL1* is expressed in the root vasculature and is thought to function in root Fe storage and regulation of Fe translocation to shoots, as *MTP3* does for Zn [265]. The tissue-specific expression of *VITL2*, *VITL5* and *Nodulin-like3* genes *in planta* and their relative contributions to Fe homeostasis are not fully understood. Although, knockout mutants of *vit15* and *nodulin-like3* show decreased Fe partitioning to roots, suggesting they may play a similar role in vacuolar root storage as *VITL1* [265]. *IREG2/FPN2* also plays a role in vacuolar Fe²⁺ influx, predominantly in the epidermis and cortex (**Figure 1.7**)[233].

Two closely related homologs of *VIT1*, *Membrane Protein of Endoplasmic Reticulum 1 (MEB1)* and *MEB2* can also complement the Fe²⁺ and Mn²⁺ excess hypersensitive growth phenotype of the yeast *cc1* mutant [266]. *MEB1* and *MEB2* localise to the ER and are thought to sequester excess Fe in the ER lumen of roots (**Figure 1.7**)[266].

NRAMP3 and *NRAMP4* are both vacuolar-localised Fe²⁺-transporters involved in mobilisation of Fe stores under Fe-limiting growth conditions (**Figure 1.7**)[267, 268]. Similarly to *VIT1*, *NRAMP3* and *NRAMP4* are expressed mainly in the vasculature, suggesting that vacuoles in the stele are important sites of Fe storage in *A. thaliana* [269]. The *nramp3 nramp4* double knockout mutant shows impaired growth and germination under Fe deficiency, highlighting a role for these transporters in Fe mobilisation during early seedling development [270]. Reduced Fe remobilisation in the *nramp3 nramp4* mutant also causes Zn hypersensitivity, while increased expression is associated with Zn hypertolerant and accumulator species [271]. *NRAMP6* has recently been identified as localising to the Golgi/trans-Golgi in lateral roots and plays an essential role in lateral root development under low Fe conditions through releasing Fe from the Golgi into the cytosol (**Figure 1.7**)[272].

There is also evidence for metal compartmentalisation into subcellular vesicles. For example, *IRT2* is co-regulated in epidermal cells with *IRT1* and *FRO2* and is primarily involved in maintaining Fe homeostasis in root outer cell layers [273]. *IRT2* localises to the endomembrane of intracellular vesicles and under Fe deficiency conditions is

thought to compartmentalise Fe taken up through IRT1 [273]. There is also evidence for Zn^{2+} transport capabilities in yeast and *in planta* [273, 274].

Fe chloroplast partitioning: Ferritins and the PIC1-NiCo translocon

In leaves, as much as 90% of Fe is found stored in chloroplasts [72]. Excess free Fe^{2+} ions can lead to ROS production and cellular damage, and thus, in chloroplasts Fe is stored associated with ferritin proteins in the stroma [275]. Ferritins are highly conserved in eukaryotes and form a 24 subunit oligomer cage, capable of storing up to 4,500 Fe^{3+} ions in its core [275]. *A. thaliana* has four *Ferritin (FER)* genes, *FER1-4*, of which *FER1*, *FER3* and *FER4* encode chloroplast targeted proteins upregulated under Fe excess, while *FER2* ferritin proteins are localised to the plastids of seeds [276]. There is also evidence for *FER4* ferritin proteins having a role in Fe storage in mitochondria [277]. Similar to Fe uptake at the root surface, Fe import into chloroplasts is thought to use a reduction-based import strategy involving FRO7, Permease In Chloroplast 1 (PIC1) and the Nickel-Cobalt (NiCo) transporter (**Figure 1.7**)[278]. PIC1 and NiCo are thought to form a translocon, whereby NiCo is able to sense and bind Fe^{2+} , made available at the chloroplast outer envelope by FRO7-mediated reduction, and then transfer Fe to Fe^{2+} -permeable PIC1 at the inner envelope [279-281]. *PIC1* overexpression results in increased Fe accumulation in chloroplasts, causing ROS production and leaf chlorosis, reminiscent of *fer* mutant phenotypes [280].

A number of other transporters has also been connected to Fe import into chloroplasts. For example, *Mitoferritin-like 1 (MTFL1)* is upregulated in leaves under Fe excess alongside *PIC1*, with *mtfl1* knockout mutants showing reduced leaf Fe accumulation and *FER1* expression (**Figure 1.7**)[282]. ABC transporters *ABC10*, *NAP14/ABC111* and *ABC112* have also been implicated in energy-coupled transport of Fe^{2+} across in the inner envelope of the chloroplast, with loss-of-function mutants showing impaired chloroplast development and reduced chloroplast Fe content (**Figure 1.7**)[283, 284].

Mitochondrial Iron Transporters 1 (MIT1) and MIT2, which are members of the mitochondrial carrier family, have recently been shown to play a role in mitochondrial Fe^{2+} import. MIT1 and MIT2 function is especially important during embryogenesis and under low Fe growth conditions (**Figure 1.7**)[285]. FRO3 and FRO8 are proposed to

function at the mitochondrial membrane to aid Fe²⁺ availability for import (**Figure 1.7**)[245].

Fe export from chloroplasts is critically important for detoxification and buffering stromal Fe concentrations. IREG3/FPN3, also known as Multiantibiotic Resistance 1 (MAR1), is targeted to chloroplasts and mitochondria and plays an important role in Fe²⁺ or Fe-NA efflux from plastids (**Figure 1.7**)[234]. *MAR1/IREG3* is constitutively expressed in leaves, while in roots *MAR1/IREG3* is upregulated in response to local Fe deficiency signals, likely in order to mobilise mitochondrial Fe stores to meet adjusted metabolic demands [234]. The *mar1* knockout mutant shows Fe accumulation in plastids and abnormal mitochondrial development as a result [234].

Two YELLOW STRIPE-LIKE transporters, YSL4 and YSL6, have been linked to Fe²⁺-NA efflux from chloroplasts under Fe excess conditions, with the *ysl4 ysl6* double mutant showing sensitivity to Fe excess due to overaccumulation of Fe in chloroplasts (**Figure 1.7**)[286]. The role of YSL4 and YSL6 in detoxification is thought to be especially important during plastid differentiation during embryogenesis and in senescing leaves [286]. Although YSL6 localisation to the chloroplast envelope has been demonstrated, there have also been contradictory reports of YSL4 and YSL6 localisation to the tonoplast and to the ER with roles in Mn and Ni detoxification [287]. As such, YSL4 and YSL6 function may not be restricted to chloroplast Fe detoxification.

1.2.5 Regulation of Zn and Fe homeostasis

Fluctuations in Zn and Fe availability require appropriate regulation of transporters and chelators to maintain adequate micronutrient supply to all tissues and organelles. A number of transcription factors, post-transcriptional mechanisms and signalling pathways have been identified as regulating Zn and Fe homeostasis. Further details on the main transcription factors involved in regulating the Zn and Fe deficiency transcriptional response are discussed in **3.1**, **4.1** and **5.1**.

Zn deficiency: bZIP19 and bZIP23

Basic leucine zipper (bZIP) transcription factors bZIP19 and bZIP23 are the main regulators of the Zn deficiency response in *A. thaliana* (**Figure 1.8**)[159]. bZIP19 and

bZIP23 are closely related paralogues that are thought to have evolved through a gene duplication event and, along with the salt stress-responsive bZIP24, they form the F-bZIP subgroup [159]. Loss-of-function *bzip19 bzip23* double mutants are hypersensitive to Zn deficiency and fail to upregulate a suite of ZIP (*ZIP1/3/4/5/9/10/12* and *IRT3*) and NAS (*NAS2* and *NAS4*) genes, as well as other genes involved in Zn uptake and distribution, such as *Defensin-like (DEFL)* genes (**Figure 1.8**)[159, 288, 289]. Initial analysis of *bzip19* and *bzip23* single mutants found no obvious phenotypes, suggesting that bZIP19 and bZIP23 were fully functionally redundant [159]. However, subsequent investigation of the *bzip19* mutant found a Zn-hypersensitive phenotype and evidence that bZIP19 and bZIP23 targets are only partially overlapping, showing that the transcription factors are only partially functionally redundant [288]. *ZIP4*, *ZIP5* and *ZIP9* are mainly regulated by bZIP19 which is expressed more highly in roots, while *ZIP12* is predominantly regulated by bZIP23 which is expressed more highly in shoots [159, 288]. Direct Zn²⁺ binding by bZIP19/23 has recently been demonstrated to regulate activation of downstream gene expression, and consequently show that these transcription factors also act as cellular Zn sensors [290]. Under Zn deficiency, lack of Zn²⁺ binding to the Zinc Sensing Motif (ZSM) of the Cys/His-rich N-terminal domain of bZIP19/23 allows transcription factor dimerisation and subsequent DNA binding (**Figure 1.8**)[290]. bZIP19/23 recognise a 10 bp *Zinc Deficiency Response Element (ZDRE, RTGTCGACAY)* binding motif in the promoter of target genes (**Figure 1.8**)[159].

While bZIP19/23 are responsive to local Zn deficiency signals, there is also evidence for regulation of the root Zn deficiency response by a systemic shoot-borne signal [162]. Overexpression of *Thlaspi goesingense MTP1 (TgMTP1)* in *A. thaliana* shoots drives Zn compartmentalisation into shoot vacuoles and subsequent enhanced shoot Zn accumulation as a result of activation of the systemic Zn deficiency response [291]. Grafting experiments with the *TgMTP1* overexpression lines demonstrated that activation of the root Zn deficiency response was a result of a shoot-borne Zn deficiency signal [291]. Utilisation of the *hma2 mtp2* mutant, which is impaired in root-to-shoot transport and consequently shows constitutive shoot Zn deficiency signalling, demonstrated that *HMA2* and *MTP2* are regulated by shoot Zn status in a bZIP19/23-independent manner [162]. However, the exact nature of the shoot-borne signal and the sensor of this systemic signal in roots is still not understood.

Hormonal signalling pathways have been linked to Zn homeostasis in plants. For example, studies have shown a link between Zn and auxin signalling, with Zn affecting Indole Acetic Acid (IAA) metabolism, as well as auxin being involved in regulation of Zn-dependent changes in ROS metabolism and growth [292, 293]. Moreover, altered Zn accumulation and distribution in *hma2 hma4* double mutants results in impaired jasmonic acid (JA) and ethylene signalling, indicating crosstalk and regulation of abiotic and biotic stress signalling pathways [294]. However, there is currently no evidence showing direct interaction between Zn regulatory proteins and hormone signalling pathway components, and further work needs to be carried out to understand the relationship between Zn homeostasis and other signalling pathways

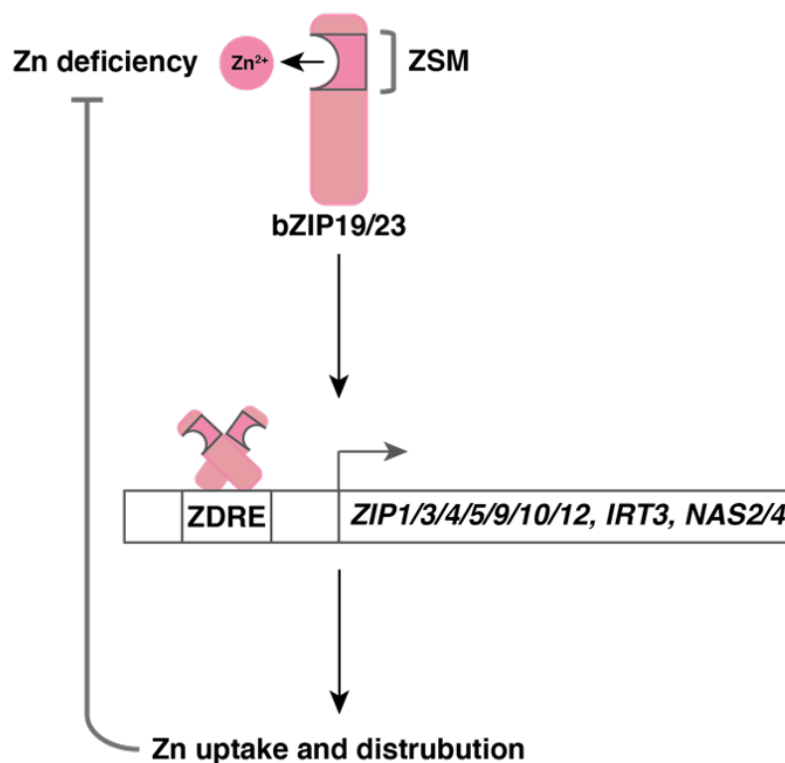


Figure 1.8: Transcriptional regulation of Zn deficiency responses by bZIP19 and bZIP23.

Zn deficiency-responsive transcription factors bZIP19 and bZIP23 directly bind Zn²⁺ through a Zinc Sensing Motif (ZSM). Under Zn deficiency, unbinding of Zn²⁺ from the ZSM promotes bZIP19/23 dimerisation and upregulation of genes involved in Zn uptake and distribution, such as *Zrt-/Irt-Like Proteins (ZIP)* transporters and *Nicotianamine Synthase (NAS)* genes.

Fe deficiency: bHLH signalling cascade and FIT

In comparison to Zn homeostasis, far more is understood about the transcriptional response to Fe deficiency and the signalling pathways that regulate it. To date, no central regulators of the Zn excess response have been identified, but the Fe deficiency transcriptional cascade is upregulated in response to high Zn, and as such Fe-responsive genes are often used as markers of Zn toxicity.

The *A. thaliana* Fe deficiency transcriptional response is regulated by a hierarchical signalling cascade of basic helix-loop-helix (bHLH) transcription factors, which controls the expression and protein abundance of the central transcription factor *FER-like Fe deficiency-induced transcription factor (FIT)* (**Figure 1.9**) [295]. At the top of this signalling cascade are Clade IVc transcription factors, bHLH34, bHLH104, bHLH105/ILR3 (IAA-LEUCINE RESISTANT3) and bHLH115, and bHLH121/URI (Upstream Regulator of IRT1, Clade IVb), which upregulate the expression of *bHLH38*, *bHLH39*, *bHLH100* and *bHLH101* (Clade Ib) [296-300]. In turn, Ib bHLH transcription factors upregulate *FIT* expression [301, 302]. Under Fe deficiency, FIT and Ib bHLH transcription factors (bHLH38, bHLH39, bHLH100 and bHLH101) activate the expression of *IRT1*, *FRO2* and other genes involved in Fe uptake and mobilisation in the roots [303]. Under Fe sufficiency, FIT protein accumulation is negatively regulated by BRUTUS-LIKE 1 (BTSL1) and BTSL2 E3 ubiquitin ligases, which are proposed to act as cellular Fe sensors (**Figure 1.9**) [304, 305]. *BTSL1* and *BTSL2* expression is upregulated by bHLH transcription factors upstream of FIT, as well as by FIT itself, thus creating a negative feedback loop to regulate FIT protein abundance and prevent excessive Fe uptake [304, 305]. A closely related BTSL homologue, BRUTUS (BTS), also negatively regulates the Fe deficiency response by targeting IVc bHLH proteins and bHLH121/URI for proteasomal degradation (**Figure 1.9**) [304, 306, 307]. The bHLH signalling cascade and BTS, BTSL proteins are described in further detail in **4.1** and **5.1**.

A number of hormonal and small molecule signalling pathways converge on FIT to regulate Fe uptake in response to developmental and environmental cues [308]. For example, ethylene, auxin, NO and calcium (Ca²⁺) signalling positively regulate Fe uptake (**Figure 1.9**) [309, 310]. The interaction of FIT with two transcription factors involved in ethylene signalling, Ethylene Insensitive 3 (EIN3) and EIN3-Like 1 (EIL1), promotes FIT

stabilisation and allows accumulation under Fe deficiency (**Figure 1.9**)[311]. This EIN3/EIL1-FIT stabilising complex is also recruited by Mediator subunit 25 (MED25) and MED16, which form part of the Mediator transcriptional regulatory complex, to the promoter of Fe-responsive genes, further enhancing FIT-dependent gene expression (**Figure 1.9**)[312, 313]. This positive effect of ethylene on Fe uptake is simultaneously balanced with ethylene-dependent repression of *IRT1* and *AHA2* by Ethylene Response Factor 4 (ERF4) and ERF72 (**Figure 1.9**)[314, 315]. Auxin and NO accumulation occurs in Fe deficient plants and plays a key role in stimulating lateral root development to enhance Fe uptake, with auxin thought to act upstream of NO [316, 317]. NO has also been demonstrated to promote FIT stabilisation through interaction with the ethylene signalling pathway, with NO upregulating the expression of genes involved in ethylene synthesis, such as *S-adenosylmethionine synthetase 1 (SAM1)*, and ethylene also reciprocally increasing NO accumulation in roots [318, 319]. The 14-3-3 protein, GENERAL REGULATORY FACTOR11 (GRF11), additionally acts downstream of NO signalling and activates *FIT* expression under Fe deficiency, with FIT in turn also inducing *GRF11* expression in a feedback loop (**Figure 1.9**)[320]. Fe deficiency causes a rise in cytosolic Ca²⁺ in the primary root, and this activates the CBL-CIPK11 pathway ultimately leading to CIPK11-dependent phosphorylation of FIT (**Figure 1.9**)[321]. Phosphorylated FIT shows enhanced nuclear accumulation, interaction with bHLH39 and downstream gene activation [321].

In contrast, JA, cytokinins (CKs) and gibberellin (GA) negatively regulate Fe uptake (**Figure 1.9**). JA inhibits FIT-dependent gene expression via the JA master regulator bHLH6/MYC2 protein [322]. MYC2 inhibits the expression of *FIT* and *Ib bHLH* genes, while also regulating the expression of Clade IVa *bHLH18*, *bHLH19*, *bHLH20* and *bHLH25* which promote FIT protein degradation via the 26S proteasome pathway (**Figure 1.9**)[322]. Inhibition of *IRT1* expression by CK is unaffected in the *fit-1* knockout mutant, and as such it is proposed that repression of primary root growth by CK alters nutrient uptake in a FIT-independent manner (**Figure 1.9**)[323]. GA signalling repressive DELLA proteins can bind to FIT, bHLH38 and bHLH39 and prevent binding to target gene promoters (**Figure 1.9**)[324]. Under Fe deficiency, DELLA proteins accumulate in the root meristem and restrict root elongation, while simultaneously being excluded from the epidermis of the differentiation zone, allowing de-repression of FIT and *Ib bHLH* proteins

to promote Fe uptake [324]. Other proteins which interact with FIT to repress its activity include the abiotic stress-responsive Zinc Finger of Arabidopsis thaliana 12 (ZAT12) and in the root stele Fe deficiency and Zn excess-responsive FIT-Binding Protein (FBP) acts to suppress *NAS* gene expression (**Figure 1.9**)[201, 324, 325].

In addition to the bHLH signalling cascade, WRKY46 has also been implicated in regulating Fe homeostasis [326]. Under Fe deficiency, WRKY46 represses the expression of *VITL1*, which functions in vacuolar storage of Fe in the root stele, and subsequently promotes enhanced translocation to shoots [326]. There is also evidence for phosphate-dependent regulation of Fe homeostasis, with phosphate deficiency-responsive transcription factors, Phosphate Starvation Response 1 (PHR1) and PHR1-Like 1 (PHL1), regulating the expression of *FER1* [327]. PHR1 has also been shown to regulate the expression of *ZIP2* and *ZIP4*, providing evidence for complicated crosstalk between Zn, Fe and phosphorous homeostasis [328].

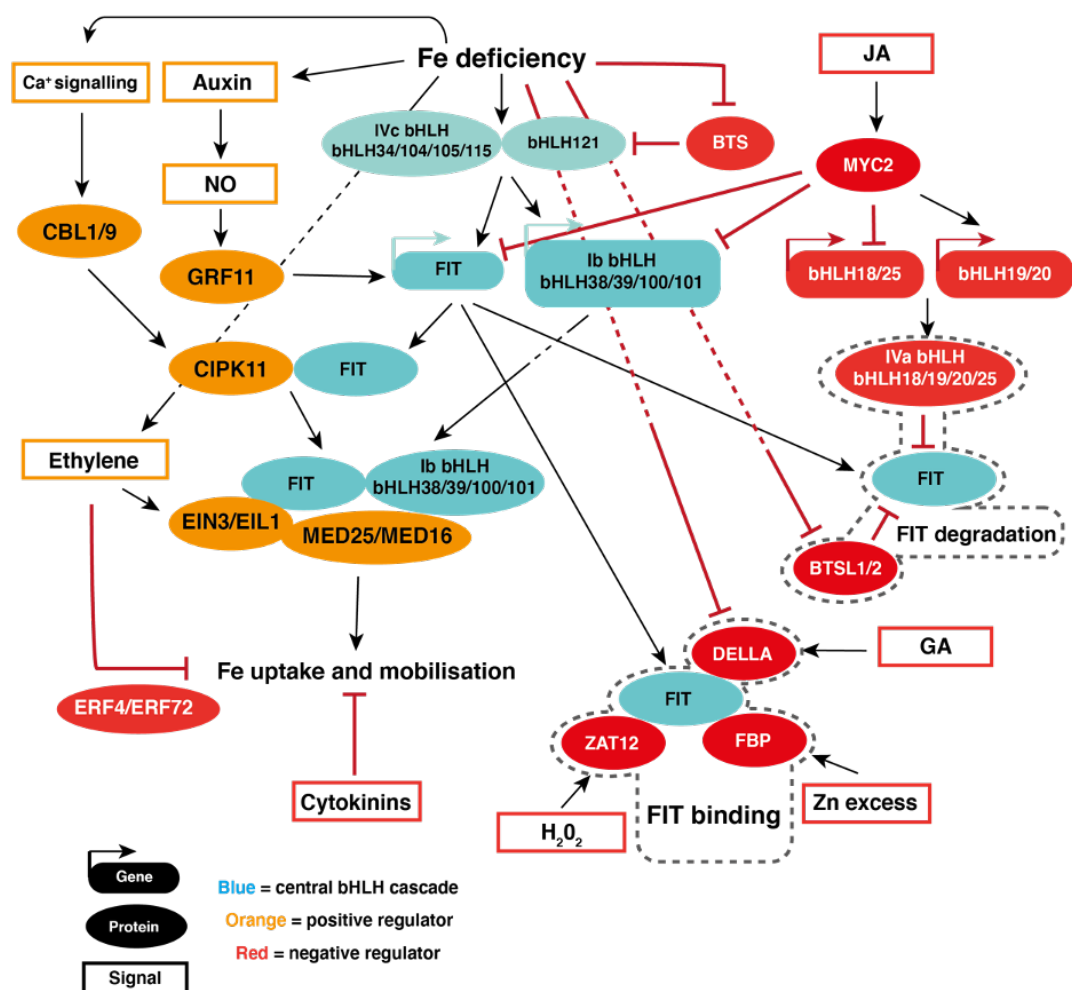


Figure 1.9: Regulation of the Fe deficiency response.

In roots, Fe deficiency activates a basic helix-loop-helix (bHLH) transcription factor cascade (shown in blue), with the IVc bHLH (bHLH34, bHLH104, bHLH105/ILR3 and bHLH115) and bHLH121/URI activating the expression of *Ib* bHLH (bHLH38, bHLH39, bHLH100 and bHLH101) and *FER*-like Fe deficiency Induced Transcription factor (*FIT*). *FIT* and *Ib* bHLH transcription factors activate the expression of genes involved in Fe uptake and mobilisation. A number of signalling pathways are activated by Fe deficiency and positively regulate (shown in orange) Fe uptake through interaction with *FIT*. Ca²⁺ signalling activates CBL1/9 and downstream CIPK11-dependent phosphorylation of *FIT*. Auxin accumulates and activates nitric oxide (NO) signalling pathways, including General Regulatory Factor 11 (GRF11) that activates *FIT* expression. Ethylene accumulates and promotes *FIT* stabilisation through Ethylene Insensitive 3 (EIN3) and EIN3-Like 1 (EIL). Mediator subunit 25 (MED25) and MED16 also participate in EIN3/EIL1-*FIT* stabilisation and enhance recruitment to target gene promoters. Fe uptake is simultaneously subject to negative regulation (shown in red) by ethylene through Ethylene Response Factor 4 (ERF) and ERFF72-dependent inhibition of Fe uptake genes. IVc transcription factors and bHLH121/URI are subject to proteasomal degradation by BRUTUS (BTS), and *FIT* is targeted by BRUTUS-LIKE 1 (BTSL1) and BTSL2 in response to Fe sufficiency. Jasmonic acid (JA) activates bHLH6/MYC2 which inhibits the expression of *FIT* and *Ib* bHLH genes. MYC2 also regulates the expression of *IVa* bHLH (bHLH18, bHLH25, bHLH19, bHLH20), which interact with *FIT* to promote proteasomal degradation. DELLA proteins downstream of gibberellin (GA), FIT-Binding Protein (FBP) downstream of Fe deficiency and Zn excess signals and Zinc finger of Arabidopsis Thaliana 12 (ZAT12) downstream of hydrogen peroxide (H₂O₂) all bind to *FIT* to prevent interactions with *Ib* bHLH proteins. Adapted from [310].

1.3 Objectives

1.3.1 Aims of this project

Zn and Fe are essential micronutrients for plant and human health, and the manipulation of Zn and Fe homeostasis to optimise micronutrient uptake and distribution for biofortification strategies is of great interest. Zn and Fe homeostasis is closely interlinked, with excess of one often causing deficiency of the other, and a

number of transporters, chelators and regulatory proteins have been recognised as important points of Zn and Fe interactions. However, there still remain a number of major gaps in our understanding of how plants sense, signal and regulate both Zn and Fe individually, as well as in relation to one another. Proteins involved in inhibition of the Fe deficiency response have notably been shown to be important in regulating tolerance to Zn excess as well, such as FIT-repressive proteins BTSL2 and FBP [201, 329].

Furthering understanding of the genes and proteins involved in regulating Zn and Fe uptake, balance and distribution not only helps inform future biofortification efforts but can also provide new perspectives on the functions of previously characterised genes. This project focusses on identifying novel genes involved in Zn and Fe cross-homeostasis in *A. thaliana* through utilising both forward and reverse genetic approaches. There is specific emphasis on investigating mechanisms of tolerance to Zn excess, which still remains poorly understood at a regulatory level.

1.3.2 Overview of thesis contents

Chapter 3: Establishing luciferase-based mutant screens to identify novel genes in the Zn homeostasis network

To establish luciferase-based mutant screens looking for novel genes involved in Zn homeostasis, publicly available microarray and gene expression data were used to identify genes that were robustly upregulated in *A. thaliana* in response to Zn deficiency or Zn excess. The expression of these genes was then verified under proposed mutant screening conditions using quantitative real-time PCR (qRT-PCR), leading to the selection of the *ZIP5* promoter for use in the deficiency screen, and the *FRO3* promoter in the excess screen. *ZIP5* and *FRO3* promoters were cloned into a construct containing the firefly luciferase (*LUC*) gene, subsequently transformed into *A. thaliana* and screening conditions were optimised by testing bioluminescence imaging of p*ZIP5:LUC* and p*FRO3:LUC* transgenic plants. Zn deficiency was most successfully induced by growing plants in low Zn liquid media in 96-well plates, while Zn excess was induced by growing plants continuously on agar plates supplemented with 200 μ M ZnSO₄.

Homozygous T₃ lines were identified and then mutagenised using EMS. The M₂ population was screened for candidate mutants which had lost *LUC* expression, with 2,000 individuals from the p*ZIP5:LUC* population imaged and 18,000 from the p*FRO3:LUC* population. Initial screening failed to identify a candidate mutant of interest, with silencing observed in some p*ZIP5:LUC* lines and a number of false positives identified in the p*FRO3:LUC* population due to wild type seed contamination. However, the work in this chapter successfully established a resource of two mutant screens with optimised high throughput screening protocols for future research.

Chapter 4: The Fe-mediated Zn tolerance phenotype of the bts1x2 mutant reveals a role for BTSL proteins in Fe and Zn cross-homeostasis

To identify the molecular mechanisms underlying Zn tolerance, and Zn and Fe cross-homeostasis, characterisation of the *bts1 bts2* (*bts1x2*) double mutant, which shows constitutive activation of the Fe deficiency response, was undertaken. Compared to wild type and *bts1* single mutants, the *bts1x2* double mutant showed enhanced tolerance to Fe and Mn deficiency, and Zn excess. The *bts1* single mutants showed partial tolerance phenotypes, supporting previous evidence for partial functional redundancy between the BTSL proteins [305, 329]. The *bts1x2* mutant showed enhanced Fe uptake capacity under low Fe and Zn excess growth conditions, demonstrated by overexpression of *IRT1* and *FRO2*, and higher *FRO2* activity compared to wild type. This resulted in enhanced shoot Fe content in *bts1x2* under standard growth conditions, as well as reduced Zn shoot content under Zn excess, ultimately conferring Fe-mediated Zn tolerance.

Interestingly, despite enhanced Fe uptake capacity in the *bts1x2* mutant, wild type accumulated more root Fe under Zn excess growth conditions than the mutant. This wild type root Fe appeared to be apoplastic Fe³⁺ accumulation likely caused by post-transcriptional inhibition of *FRO2* and reduced symplastic Fe uptake capacity.

To determine if altered nutrient homeostasis also impacted growth and development of the *bts1x2* mutant, stage-based phenotyping of the whole life cycle was carried out on Zn supplemented soil. The *bts1x2* mutant also showed a Zn tolerance phenotype on soil, with wild type showing a greater Zn-dependent delay in flowering

time and reduced growth rate than the mutant. The *bts1x2* mutant also showed a genotype-specific delay in floral transition, with the elongated vegetative growth phase also conferring enhanced rosette growth rate and size.

Chapter 5: Transcriptomic analysis reveals a novel role for BTSL proteins in FIT-independent gene regulation

To further characterise the *bts1x2* Fe-mediated Zn tolerance phenotype, and answer some of the outstanding questions from the model proposed in **Chapter 4**, RNA-sequencing (RNA-seq) analysis of wild type and mutant response to Zn excess was carried out. Consistent with the Zn tolerance phenotype, the *bts1x2* mutant did not show differential expression of Fe deficiency and Zn excess-responsive genes in shoots. In roots, the *bts1x2* mutant showed constitutive expression of both FIT-dependent and FIT-independent Fe deficiency-responsive genes, which was further enhanced on high Zn. This misregulation of FIT-independent genes was confirmed by qRT-PCR and suggests that BTSL proteins likely target additional Fe deficiency-responsive transcription factors, with IVc bHLH and bHLH121/URI being the most probable candidates.

The *bts1x2* mutant showed opposite transcriptional responses in shoots and roots, indicating antagonistic Fe sensing and signalling. To determine whether BTSL proteins have a role in responding to systemic shoot Fe signals, a split root assay was conducted. It was found that the *bts1x2* mutants fail to downregulate the root Fe deficiency transcriptional network in response to shoot Fe sufficiency signals. Furthermore, a small subset of Fe deficiency-responsive genes expressed in the stele independently of BTSL regulation maintain responsiveness to systemic signalling. As such, the BTSL proteins regulate the root Fe-deficiency response in a cell-specific manner through responding to both local and systemic signals.

1.3.3 Contributions to thesis

All experiments in this thesis were carried out by me (C.S.) unless otherwise stated. Plant material was provided by Dr Kalyani Kallam and Dr Jorge Rodriguez-Celma (both John Innes Centre, UK). ICP analysis was performed by technical staff at University of East Anglia (Norwich, UK). All contribution by collaborators including experimental

work, plant material and primers, are acknowledged in **Chapter 2** and fully and appropriately acknowledged in the legends pertaining to display items (figures and tables).

Chapter 2: Materials and Methods

All chemicals were sourced from Sigma-Aldrich® (subsidiary of Merck KGaA©, Germany) unless stated otherwise. If chemicals are available from Sigma-Aldrich only the catalogue number is given.

For plant materials, all *Arabidopsis thaliana* wild-type (Col-0) and mutant lines were sourced from lab stocks unless stated otherwise.

2.1 Plant maintenance

2.1.1 Plant materials

Arabidopsis thaliana Columbia-0 accession (Col-0) plants were used throughout as the wild-type reference and as the genetic background for mutants or transformants. *pFRO3:LUC*, *bts1-1* (*bts1*, SALK_015054), *bts2-2* (*bts2*, SALK_048470) and *bts1-1x2-2* (*bts1x2*) seeds were provided by Dr Jorge Rodriguez-Celma (John Innes Centre, Norwich). All photographs of plants were taken by JIC Scientific Photography Department (John Innes Centre).

2.1.2 *A. thaliana* agar plate growth conditions

Seeds were surface sterilised with 50 mL 70% (v/v) EtOH, followed by shaking (150 rpm) for 15 min with 35 mL dH₂O, 4 mL 10% (v/v) bleach and 1 mL 10% (w/v) sodium dodecyl sulphate (SDS). Seeds were then washed six times with dH₂O, inverting the tube with each wash and left to vernalise at 4 - 6 °C for 48 h in the dark. For the luciferase assay, seeds were plated on 100 mm² square plates (R & L Slaughter Ltd., Upminster, UK) containing ¼ strength Murashige and Skoog (MS) medium (M5524), 1% (w/v) agar (AGA03, Formedium Ltd., Norfolk, UK), 0.75% (w/v) sucrose buffered to pH 5.7, containing 7.5 µM ZnSO₄ for standard growth conditions and 200 µM ZnSO₄ for Zn excess. Zn deficiency conditions were induced through either transfer to ¼ MS plates supplemented with 50 µM TPEN (N,N,N',N'-tetrakis(2-pyridylmethyl)ethane-1,2-diamine, P4413) or spraying with 50 µM TPEN for 3 days. In all other experiments, modified Hoagland medium (2.1.4) with chelator-washed agar (2.1.3) was used. Seedlings were grown vertically in a controlled environment room (CER) maintained at 23 °C with a photoperiod of 16 h light (90 µmol m⁻² s⁻¹) and 8 h dark. Plants were used at 14-d-old after vernalisation for experiments, unless otherwise stated.

2.1.3 Preparation of chelator-washed agar

For experiments characterising the *btsI* mutants in **Chapters 4 and 5**, agar was washed in order to remove contaminating cations using an adapted method [162]. In a 2 L Erlenmeyer flask, 30 g agar (Type M, A4800) was washed three times with 1 L 50 mM EDTA (E9884) pH 8. The first two washes were for 5 h and the final wash overnight. Agar was then washed six times with dH₂O, with all washes carried out for 1 h, except the final wash which was overnight. Washing was achieved through continuous stirring using a magnetic stirrer at room temperature followed by straining through Miracloth (475855, Merck Millipore Ltd., Watford, UK). Agar was then air-dried on filter paper (185 mm diameter, FT3205185, Sartorius Ltd., UK) at room temperature for 1 h and used to immediately make modified Hoagland medium (2.1.4).

2.1.4 Modified Hoagland medium

Phenotyping of *btsI* mutants in **Chapters 4 and 5** was carried out on 0.25x modified Hoagland medium [330] supplemented with 1.5% (w/v) chelator washed agar (section 2.1.3), 1% (w/v) sucrose buffered to pH 5.7, using a modified recipe [331]. Nutrient composition of the medium is described in **Table 2.1**, unless specified otherwise.

2.1.5 *A. thaliana* 96-well plate growth conditions

For *A. thaliana* growth in liquid medium, seeds were surface sterilised as described in 2.1.2. Single seeds were dispensed into each well of white 96-well plates (655074, Greiner Bio-One, Austria) containing 200 µL of ¼ MS medium supplemented with ZnSO₄ as specified using a wooden toothpick. Plates were covered with a transparent lid (656171, Greiner Bio-One) and transferred to a CER maintained at 23 °C with a photoperiod of 16 h light (90 µmol m⁻² s⁻¹) and 8 h dark. Seedlings were used at 12-d-old.

Nutrient	Stock concentration	Final concentration
Ca(NO ₃) ₂	1 M	1.5 mM
KH ₂ PO ₄	1 M	0.28 mM
MgSO ₄	1 M	0.75 mM
KNO ₃	1M	1.25 mM
CuSO ₄	0.5 mM	0.5 μM
ZnSO ₄	1 mM	1 μM
MnSO ₄	5 mM	5 μM
H ₃ BO ₃	25 mM	25 μM
Na ₂ MoO ₄	0.1 mM	0.1 μM
KCl	50 mM	50 μM
MES, pH 5.7	1 mM	3 mM
Fe(NO ₃) ₃ [HBED]	10 mM	5 μM

Table 2.1: Nutrient composition of 0.25x modified Hoagland medium.

From [329]

2.1.6 *A. thaliana* soil growth conditions

For seed collection and soil experiments, plants were grown on a peat mix; 600 L Levington F2 peat (Scotts, Ipswich, UK), 100 L 4 mm grit, 196 g Exemptor® (chloronicotinyl insecticide, GB84080896A, Bayer CropScience Ltd., UK). Seed trays were grown in a long day CER maintained at 22 °C with a photoperiod of 16 h light (90 μmol m⁻² s⁻¹) and 8 h dark.

For soil Zn excess experiments in **Chapter 4**, soil was first dried overnight at 45 °C and then mixed for 2-3 h with either a ZnSO₄ water solution to reach a final concentration of 1000 mg/kg DW⁻¹ ZnSO₄ or with the same volume of dH₂O as a control. Soil was then dried overnight again and used immediately.

2.1.7 *A. thaliana* split root plates

Col-0 and *bts1x2* seeds were sterilised and germinated on ¼ MS as described in **2.1.2**. To generate split roots, at 5-d-old the primary root was excised and seedlings grown for an additional 5 d. Seedlings with two main roots of similar length were transferred to 100 mm² round split plates (Gosselin™, 15438784, Fisher Scientific Ltd., UK) containing modified Hoagland as described in **2.1.4**. supplemented with either 1 µM ZnSO₄, 100 µM ZnSO₄ or 0 µM FeHBED (N,N'-bis(2-hydroxybenzyl)ethylenediamine-N,N'-diacetic acid, 35369-53-0, Santa Cruz Biotechnology Inc, Texas, US). For control plates, the media was the same on both halves of the plates, otherwise plates contained one half 1 µM ZnSO₄, and the other either 100 µM ZnSO₄; 1 µM ZnSO₄; 0 µM FeHBED; or 100 µM ZnSO₄ and 0 µM FeHBED.

2.2 *A. thaliana* growth phenotyping

2.2.1 Root length measurements

Plants were grown vertically on agar plates and scanned at 14 d with a ruler for scale using Epson Perfection V550 Photo scanner (Epson, Suwa, Japan), scan definition set at 300 dpi. Root length was then measured using ImageJ (National Institutes of Health, USA) v 1.51s software. Root lengths were averaged from *ca.* 80 seedlings spread across three independent replicates. Statistically significant differences between mean values were determined using two-way ANOVA with Tukey honestly significant difference (HSD) test, with significant p-values within conditions denoted by * < 0.05, ** < 0.01, *** < 0.001 and within genotypes by letters (p < 0.05). Statistical analysis was run in RStudio (v 3.4.2) and graphs were made in GraphPad Prism 8 (GraphPad Software Inc.).

2.2.2 Leaf surface area measurements and growth stage phenotyping

For the soil growth assay in **Chapter 4**, seedlings were grown vertically on ¼ MS agar plates for 10 d and then transferred to soil. Plants were then photographed every other day between 16- and 30-d-old using a FinePix S5700 digital camera (Fujifilm, Tokyo, Japan). Leaf surface area was measured using Image J. Growth stage phenotyping was carried out as described [332] from germination until completion of flowering. Statistical analysis was performed as described in **2.2.1**.

2.3 Quantitative reverse transcription-PCR (qRT-PCR)

2.3.1 RNA extraction

Total RNA was extracted from 100 mg leaf or root tissue sample taken from pooled 14-d-old seedlings using RNeasy Plant Mini Kit (74904, QIAGEN, Hilden, Germany). Samples were flash frozen in a 2 mL Eppendorf tube using liquid nitrogen and ground to a fine powder with stainless steel ball bearings (3mm, M31G100, Simply Bearings Ltd., UK) using a TissueLyser LT homogeniser (85600, QIAGEN). RNA was then extracted per the manufacturer's instruction, with a final elution volume of 30 µL. RNA quality and concentration were measured using a NanoDrop™ 2000 spectrophotometer (ND-2000, Thermo Fisher Scientific, USA).

2.3.2 cDNA synthesis

cDNA synthesis was carried out in 20 µL final volume reactions using 200 – 500 ng mRNA using Invitrogen™ M-MLV reverse transcriptase (28025013, Thermo Fisher Scientific) according to the manufacturer's instructions. mRNA was heat treated for 5 min at 70 °C. Each 20 µL reaction was prepared on ice as follows: 10 µL RNA (200 ng/µL), 1 µL oligo dT primers (500 µg/mL), 1 µL dNTPs (10 mM), 2 µL DTT (0.1 M), 4 µL 5X first strand buffer (250 mM Tris-HCl, 375 mM KCl, 15mM MgCl, pH 8.3) and 1 µL M-MLV reverse transcriptase. Reactions were run in a Mastercycler® pro (Eppendorf UK Ltd.,

Stevenage, UK) with the programme as follows: 50 min at 37 °C and then 15 min at 70 °C. A no template control and a no reverse transcriptase reaction were run as negative controls. cDNA was diluted 1:10 to give a final volume of 200 µL and stored at –20 °C.

2.3.3 Quantitative real-time PCR (qRT-PCR)

qRT-PCR was carried out in 20 µL reactions on 96-well plates (AB0700W, Thermo Fisher Scientific) using diluted cDNA and SYBR® Green JumpStart™ ReadyMix™ (S4438). Each 20 µL was prepared on ice as follows: 10 µL SYBR ReadyMix, 5 µL cDNA, 3 µL dH₂O, 1 µL forward primer (10 µM) and 1 µL reverse primer (10 µM). Primers used in qRT-PCR analysis are shown in **Table 2.2**.

Each plate contained three technical triplicates for each reaction, including two reference genes (*ACTIN2* and *TIP41*) and controls, with each plate run as technical triplicates, and each experiment repeated for three independent biological replicates.

Reactions were run in a C1000™ CFX96 Touch™ Real-Time PCR Detection System (Biorad, Hercules, California, USA). The PCR programme was as follows: 3 min at 95 °C, followed by 40 cycles of 30 s at 94 °C, 30 s at 63 °C, 30 s at 72 °C and one cycle 30 s 50 °C, finishing with melt curve analysis (65 °C to 95 °C, increments of 0.5 °C). Data were exported to Excel (Microsoft® Office 2016) using CFX Manager (v. 3.1.1517.0823, Biorad) software.

The expression of target genes was calculated using the difference in mean C_t value of target genes and reference genes, where C_t corresponds to the cycle number at which fluorescence intensity reaches a threshold of 0.6. Expression values were then converted to relative expression ratio using the $2^{-\Delta C_t}$ method [333] with fold changes represented as relative to Col-0 under control conditions. Mean relative expression ratio and standard error of the mean (SEM) were calculated in Excel. Where applicable, statistical analysis was performed as described in **2.2.1**.

Gene name	Primer name	Sequence (5' – 3')	Source
ZIP4	ZIP4 F	TCTCTCAGGCACAGTTCAGG	C Stanton
	ZIP4 R	CCAGTATCCCCTCAGTGACC	
ZIP5	ZIP5 F	CGGGATTGTTGGCGTGAAT	Assuncao <i>et al.</i> [159]
	ZIP5 R	CCAAGACCCTCGAAGCATTG	
IRT3	IRT3 F	CAGTCTCCTTGCACAATCCG	C Stanton
	IRT3 R	ATTGAAAGACGACGCCACTG	
DEFL203	DEFL203 F	GACTCCCAAAGGCGGTAG	C Stanton
	DEFL203 R	CAGTGCGTCTCGTTGTCTTC	
DEFL206	DEFL206 F	CACCGAAATCCTGAAGAGCG	C Stanton
	DEFL206 R	GACTCCCTCAACACGTCCAG	
NAC096	NAC096 F	GTTCCGGTTTCATCCTACGG	C Stanton
	NAC096 R	AGTACCATTCCATGTCCCGG	
ZIF1	ZIF1 F	TCTGGGGAATTGTGGCTGAT	C Stanton
	ZIF1 R	GGCCTTCATTGTTCCAAGCA	
IRT2	IRT2 F	TCACCTTCACCGTATCTCCG	C Stanton
	IRT2 R	CGGCTGAAAAGAGGAGAGGT	
FRO3	FRO3 F	CCCGGCGATTAGAAGGAGAT	C Stanton
	FRO3 R	GTTCCGCGACTGGAGAAATC	
MTP3	MTP3 F	GCTTATCTTCACGTGCTGGG	C Stanton
	MTP3 R	TCTCTCGTGGTGTGACTCC	
PCR2	PCR2 F	ACGCGTTGATAGCCGTAGTA	C Stanton
	PCR2 R	ACTCATATCGTAACCGCGGT	
AT3G61930	AT3G61930 F	AGGAAGAGGAAGACACGTGG	C Stanton
	AT3G61930 R	ATGTAACTTCCACGCCGTTG	
ACTIN2	ACTIN2 F	GATGAGGCAGGTCCAGGAATC	Czechowski <i>et al.</i> [334]
	ACTIN2 R	GTTTGTACACACAAGTGCAT	

Gene name	Primer name	Sequence (5' – 3')	Source
<i>UBQ10</i>	<i>UBQ10</i> F	ATTGATCTTCGCCGAAAGC	C Stanton
	<i>UBQ10</i> R	CTTGGCCTTCACGTTGTCAA	
<i>IRT1</i>	<i>IRT1</i> F	CACCATTCGGAATAGCGTTAGG	Rodriguez-Celma <i>et al.</i> [305]
	<i>IRT1</i> R	CCAGCGGAGCATGCATTTA	
<i>FRO2</i>	<i>FRO2</i> F	TTACCCGATCGACCACAACAC	Rodriguez-Celma <i>et al.</i> [305]
	<i>FRO2</i> R	CCGCACTACAAGTCGCCATTAT	
<i>bHLH38</i>	<i>bHLH38</i> F	TTTCACAACTTCGGTTGGCC	Rodriguez-Celma <i>et al.</i> [305]
	<i>bHLH38</i> R	CTGACGAAACAGATACTCCCAAGCT	
<i>bHLH39</i>	<i>bHLH39</i> F	GGCCATCAACGGGAGAGTAC	Rodriguez-Celma <i>et al.</i> [305]
	<i>bHLH39</i> R	GCTCCATAAGTCTCTCCGG	
<i>IMA1</i>	<i>IMA1</i> F	TGATTGTAATTTAGGAGGAAACAAAA	Grillet <i>et al.</i> [335]
	<i>IMA1</i> R	TCAATCCACAAGTAAACATCTATGG	
<i>FER1</i>	<i>FER1</i> F	TCCCCAGTTAGCTGATTTTCG	Grillet <i>et al.</i> [335]
	<i>FER1</i> R	CTTTGCCGATCATCCTTAGC	
<i>TIP41</i>	<i>TIP41</i> F	GTGAAAACACTGTTGGAGAGAAGCAA	Grillet <i>et al.</i> [335]
	<i>TIP41</i> R	TCAACTGGATACCTTTTCGCA	

Table 2.2: Primers used for qRT-PCR analysis.

2.4 Generation of transgenic *A. thaliana* lines

2.4.1 Genomic DNA extraction

Genomic DNA (gDNA) was extracted from Col-0 plants grown on ¼ MS plates using the cetyltrimethylammonium bromide (CTAB) method. Thus, 100 mg of leaf tissue was flash frozen in a 2 mL Eppendorf tube using liquid nitrogen. Samples were ground into a fine powder with a TissueLyser LT homogeniser (85600, QIAGEN) using sterile

stainless steel ball bearings (3 mm, M31G100, Simply Bearings Ltd., UK) at 50 s⁻¹ for 1 min. Samples were vortexed with 500 µL CTAB buffer (2 % (w/v) CTAB (H9151), 2.5 M NaCl (S7653), 0.1 M Tris (10708976001), 20 mM EDTA), incubated at 55 °C for 15 min and then centrifuged for 5 min at 10 000 rpm. The supernatant was treated with 2 µL RNase A (10 mg/mL, EN0531, Thermo Fisher Scientific) for 15 min at 37 °C before inversion with 250 µL chloroform:isoamyl alcohol (24:1, C0549). The solution was then centrifuged for 1 min at 13 000 rpm. DNA was then precipitated from the aqueous phase by adding 50 µL 7.5 M ammonium acetate (A1542) followed by 500 µL ice cold EtOH (51976). The solution was centrifuged at 13,000 rpm for 1 min and the pellet then washed twice with 70 % (v/v) ice cold EtOH before air drying for 15 min. The pellet was resuspended in 30 µL TE buffer (10 mM Tris, 0.1 mM EDTA, pH 8.0). DNA quality and concentration were measured on a NanoDrop™ 2000 spectrophotometer (ND-2000, Thermo Fisher Scientific).

2.4.2 Promoter cloning

To generate the Zn-responsive luciferase constructs used in **Chapter 3**, promoter regions of selected Zn-responsive genes were taken as 3 kbp upstream from the transcription start site. Promoter sequences were amplified in 50 µL PCR reactions using gDNA and KOD Hot Start DNA Polymerase (71086, Merck Millipore Ltd.). Each 50 µL reaction was prepared in 0.2 mL PCR tubes (PCR1126, 4titude Ltd, Wotton, UK) on ice as follows: 5 µL 10x KOD Hot Start DNA Polymerase Buffer, 3 µL MgSO₄ (25 mM), 5 µL dNTPs (2 mM), 1.5 µL forward primer (10 µM), 1 µL reverse primer (10 µM), 1 µL KOD Hot Start DNA Polymerase, 100 ng gDNA, dH₂O to make 50 µL final volume. Primers with 5' *attB* adaptor sequences are shown in **Table 2.3**.

PCR reactions were run in a Mastercycler® pro (Eppendorf) thermocycler. The PCR programme was as follows: 2 min at 95°C, followed by 40 cycles of 20 s at 95°C, 10 s at 50–55°C, 1 min at 70°C, finishing with a final extension for 10 min at 68°C. Fragment size was verified by running 5 µL of the PCR reaction on 1.5% agarose gel (A20080, Melford Laboratories Ltd., UK) with 1% ethidium bromide. The remaining 45 µL of PCR reaction was purified using Wizard® SV Gel and PCR Clean-Up System (A9281, Promega,

Madison, USA) according to manufacturer's instructions and sequenced as described in

2.4.3.

Gene name	Primer name	Sequence (5' – 3')	Product size	Source
<i>ZIP5</i>	<i>ZIP5</i> attB1 F	attB1- AGAAAGTGCAATTTTTACCAATGATT	2638 bp	K Kallam (JIC)
	<i>ZIP5</i> attB2 R	attB2- CTTATCGATTAGGGTTTGAATTTGAA		
<i>DEFL206</i>	<i>DEFL206</i> attB1 F	attB1- GATAACGCATTTCCATGAT	3031 bp	C Stanton
	<i>DEFL206</i> attB2 R	attB2- TTAGTTCATTAATAAAGTTG		
<i>FRO3</i>	<i>FRO3</i> attB1 F	attB1- GTGGAATTGTAGTAAGTAACTGT	2861 bp	J Rodriguez- Celma (JIC)
	<i>FRO3</i> attB2 R	attB2- GAAAGCTGGGTCGGCGGCCACCTT		
<i>AT3G61930</i>	<i>AT3G61930</i> attB1 F	attB1- CCAAGTCTCAATGAATAC	3086 bp	C Stanton
	<i>AT3G61930</i> attB2 R	attB2- TTCTTGATCTTTCTTG		

Table 2.3: Primers used in the Gateway cloning of Zn-responsive promoters.

attB1 = GGGGACAAGTTTGTACAAAAAAGCAGGCT

attB2 = GGGGACCACTTTGTACAAGAAAGCTGGGT

2.4.3 DNA sequencing

DNA sequencing was performed by LightRun GATC Biotech service (Eurofins Genomics, UK). DNA-primer preparations were sent in 20 µL reactions as follows: 5 µL DNA, 2.5 µL primer (10 µM) and 12.5 µL dH₂O. Primers used for sequencing are shown in

Table 2.4.

Gene name	Primer name	Sequence (5' – 3')	Source
<i>ZIP5</i>	<i>ZIP5</i> F1	GAAAGTGCAATTTTTACCAATGA	K Kallam
	<i>ZIP5</i> F2	AATCATCCGACGGCTTTCAC	
	<i>ZIP5</i> F3	ATATGTATGACCATGCCGCA	
	<i>ZIP5</i> F4	ACGCATTTCCCTTTTCTTATCAA	
<i>DEFL206</i>	<i>DEFL206</i> F1	CAGTCTCCTTGACAATCCG	C Stanton
	<i>DEFL206</i> F2	ATTGAAAGACGACGCCACTG	
	<i>DEFL206</i> F3	GACTCCCAAAGGCGGTAG	
<i>FRO3</i>	<i>FRO3</i> F1	GTGGAATTGTAGTAAGTAACTGT	C Stanton
	<i>FRO3</i> F2	GGCCTGCAAATAACCGTCAT	
<i>AT3G61930</i>	<i>AT3G61930</i> F1	CCAAGTCTTCAATGAATAC	C Stanton
	<i>AT3G61930</i> F2	CCCCAAGACGGAGAAGG	
	<i>AT3G61930</i> F3	CGGTGCACTCAATTACGT	
	<i>AT3G61930</i> F4	CTCCGTTTCCGTTTCGATCT	
	<i>AT3G61930</i> F5	CAAGAAAGATCAAGAA	
<i>LUC</i>	<i>LUC</i> F1	ATGGAAGACGCCAAAAACAT	C Stanton
	<i>LUC</i> F2	TGGCAATCAAATCATTCCGGA	

Table 2.4: Primers used in sequencing.

2.4.4 Gateway® cloning

Promoter fragments were integrated into pDONR207 entry vectors in 10 μ L BP reactions prepared on ice as follows: 5 μ L *attB*-PCR product (20 ng/ μ L), 1 μ L pDONR207 (150 ng/ μ L), 2 μ L BP Clonase II enzyme mix (11789100, Thermo Fisher Scientific) and 2 μ L pH 8.0 TE buffer. Entry vectors were then cloned into pGWLuc destination vectors in 10 μ L LR reactions prepared on ice as follows: 5 μ L entry clone (20 ng/ μ L), 1 μ L pGWLuc (150 ng/ μ L), 2 μ L LR Clonase II enzyme mix (11791020, Thermo Fisher Scientific) and 2

μ L pH 8.0 TE buffer. Both BP and LR reactions were run overnight at 25 °C and terminated by incubating with 1 μ L Proteinase K for 10 min at 37 °C. After each BP and LR reaction, 1 μ L of reaction mixture was cloned into *E. coli* as described in **2.4.5** and plasmid sequences verified as described in **2.4.6**. Dr Kalyani Kallam had previously generated the pZIP5:LUC expression clones.

2.4.5 Heat shock transformation of *Escherichia coli* (*E. coli*)

Heat shock transformation of *E. coli* was carried out using 1 μ L of BP or LR reaction from **2.4.4** and 20 μ L of component *E. coli* strain DH5 α (maintained in the Sanders/Miller lab). The procedure was as follows: 20 min on ice, 30 s at 42 °C and 2 min on ice. 1 mL of liquid Super Optimal Broth with Catabolite repression (SOC) medium was added [336] and then incubated with shaking for 1 h (250 rpm) at 37 °C. The reaction was then plated on Lysogeny broth (LB) [337] agar plates containing 10 μ g/mL gentamycin and incubated overnight at 37 °C. Plasmids from transformed colonies were extracted using QIAprep[®] Spin Miniprep Kit (27104, Qiagen).

2.4.6 Colony PCR

Colony PCR was carried out on positive *E. coli* transformants in order to validate the transformed gene of interest. PCR reactions used Taq DNA Polymerase (4114, NEB, Ipswich, MA, USA) and each 25 μ L reaction was prepared on ice as follows: 2.5 μ L 10X Standard Taq Reaction Buffer, 0.5 μ L dNTPs (10 mM), 0.5 μ L forward primer (10 μ M), 0.5 μ L reverse primer (10 μ M), 0.1 μ L Taq DNA polymerase and 20.9 μ L dH₂O, with bacterial colony samples added using a sterile pipette tip. The primers used are shown in **Table 2.4**. Reactions were run in a Mastercycler[®] pro (Eppendorf) thermocycler with the following PCR programme: 30 s at 95°C, followed by 30 cycles of 30 s at 95°C, 10 s at 50 - 5 °C, 1 min at 68°C, finishing with a final extension for 5 min at 68 °C. Fragment size was verified by running the PCR product on 1.5% agarose gel (Melford) with 1% ethidium bromide, and then purified using Wizard[®] SV Gel and PCR Clean-Up System (Promega) and sent for sequencing (**2.4.3**).

2.4.7 Electroporation of *Agrobacterium tumefaciens* (*A. tumefaciens*)

Transformation of expression clones into *Agrobacterium* was carried out using 20 μL of electro-competent *A. tumefaciens* strain AGL1 (maintained in Sanders/Miller lab) and 5 ng of plasmid DNA in 0.1 cM electroporation cuvettes (1652083, BioRad) chilled on ice. Electroporation was carried out using a Gene Pulser™ (Biorad) with the following conditions: 25 μF , 2.4 kV, 200 Ω , 5 s and 1 mL of SOC media added immediately afterwards. The mixture was then incubated with shaking for 2 h (250 rpm) at 28 °C and plated on LB agar plates containing 10 $\mu\text{g}/\text{mL}$ tetracycline, 50 $\mu\text{g}/\text{mL}$ rifampicin, 100 $\mu\text{g}/\text{mL}$ carbenicillin and 50 $\mu\text{g}/\text{mL}$ kanamycin and incubated for 2 d at 28 °C.

2.4.8 Floral dipping transformation of *A. thaliana*

A. thaliana (Col-0) plants were grown in a long day CER (2.1.6) and at flowering the first bolt was cut and the plant grown for an additional 6 d to encourage secondary bolt proliferation. *Agrobacterium* transformed with the expression clone (2.4.7) was grown in a large liquid LB culture containing 10 $\mu\text{g}/\text{mL}$ tetracycline, 50 $\mu\text{g}/\text{mL}$ rifampicin, 100 $\mu\text{g}/\text{mL}$ carbenicillin and 50 $\mu\text{g}/\text{mL}$ kanamycin at 28 °C and then pelleted by centrifugation at 5000 g for 20 min. The pellet was resuspended in 200 mL 5 % (v/v) sucrose to an $\text{OD}_{600} = \sim 0.8$, and 40 $\mu\text{L}/\text{mL}$ Silwet L-77 (306302161, Fisher Scientific) added. The aerial parts of *A. thaliana* were then submerged in the *Agrobacterium* solution for 1 min with gentle agitation, and plants laid horizontally in autoclave bags and covered in the dark for 24 h. Plants were then uncovered and returned to standard growth conditions until seeds were harvested.

2.5 Generation of mutant screening populations

2.5.1 Selection of homozygous T_3 lines

T_1 seeds were sown directly on soil and subjected to BASTA® (Glufosinate ammonium, Bayer Cropscience) selection by spraying with 2.5 mL/L three times between 14- and 25-d-old to identify positive transformants. T_2 seeds were then grown

on ¼ MS agar plates supplemented with 20 µg/mL BASTA® and luminescence imaged (2.6) to check for luciferase expression. T₃ lines were further subjected to BASTA® and luminescence selection. Homozygous T₃ lines with 100 % luminescence were sent for a copy number check of the luciferase gene to identify single transgene insertion lines and the transgene sequence verified by sequencing (2.5.2 and 2.4.3). Selected lines were taken to T₄ to bulk seeds for mutagenesis.

2.5.2 Copy number analysis

Copy number analysis of the luciferase transgene was performed by iDNA Genetics (Norwich, UK). For each sample, 100 – 500 mg of fresh young leaf tissue was sent for copy number analysis.

2.5.3 Ethyl methanesulfonate (EMS) mutagenesis

In 50 mL falcon tubes, ~ 5000 seeds were submerged in 0.1 % (v/v) KCl (P9333) and left for 12 h on a rocker at room temperature. The KCl solution was removed and 20 mL pH 5.0 phosphate buffer (0.1 M) added. EMS (M0880) was then added to a final concentration of 75 mM and the sealed falcon tube placed on a rocker for 6 h. The EMS solution was discarded and the seeds washed twice with sodium thiosulfate solution (0.1 M, 72049) and then twice with dH₂O. Seeds were dried on filter paper and immediately transferred to soil for M₁ seed collection. All steps were carried out in an autoclave bag under a fumehood and all EMS waste was disposed of in 0.1 M sodium thiosulfate solution.

2.6 Bioluminescence imaging

2.6.1 Bioluminescence on agar plates

Seedlings were grown for 14 d as described in 2.1.2. Prior to imaging, seedlings were sprayed with 1 mM luciferin solution (L-8220, Carbosynth Ltd., UK) and incubated in the dark for 10 min. Luciferin-treated plates were imaged using a NightOwl II LB 983

(Berthold Technologies GmbH & Co KG, Germany) *in vivo* imaging system (560 λ, 60 s exposure). Images were processed using the indiGO™ software (Berthold Technologies).

2.6.2 Bioluminescence imaging in 96-well plates

Seedlings were grown for 12 d as described in 2.1.4. Prior to imaging, all liquid media was removed from wells and replaced with 100 μL fresh ¼ MS Zn-free media supplemented with 10 μM luciferin (Carbosynth). Plates were incubated in the dark for 4 h and then imaged using a NightOwl II LB 983 (Berthold Technologies) imaging system (560 λ, 5 s exposure). Images were processed with indiGo™ software (Berthold Technologies).

2.7 Biochemical and histochemical methods

2.7.1 Chlorophyll quantification

Shoots were excised from 14-d-old seedlings (*ca.* 50 mg) and flash frozen in a 2 mL Eppendorf tube using liquid nitrogen. Samples were homogenised with a TissueLyser LT (QIAGEN) using sterile stainless steel ball bearings at 50 s⁻¹ for 1 min. Samples were incubated in 2 mL 100 % (v/v) MeOH at room temperature with shaking (350 rpm) for 10 min and then centrifuged for 5 min at 10000 g. 1 mL of solution was transferred to a transparent cuvette (10151710, Fisher Scientific) on ice and absorbance measured at 650 and 665 nm using a spectrophotometer to calculate the total chlorophyll concentration:

$$\text{Chl } (\mu\text{g/ml}) = (22.5 \times A_{650}) + (4 \times A_{665})$$

Statistical analysis was performed as described in 2.2.1.

2.7.2 Inductively Coupled Plasma-Optical Emission Spectrometry (ICP-OES)

For the elemental analysis of *A. thaliana* tissues, root and shoot samples were harvested separately (*ca.* 200 mg). Apoplastic cations were desorbed from roots by washing samples in ice cold 2 mM CaSO₄ and 10 mM EDTA for 10 min followed by 0.3

mM bathophenanthroline disulphonate and 5.7 mM sodium dithionite [191]. Samples were washed twice with dH₂O then dried for 48 h at 65 °C and the dry weight recorded. Dried samples were then digested in 2 mL 65 % (v/v) HNO₃ (1004410250) and 0.5 mL H₂O₂ (216763) for 4 h at 95 °C. The digested solution was then diluted to 15 mL with ultrapure water. Fe, Zn and Mn concentrations of samples were determined using ICP-OES performed by Biological Services, UEA, Norwich. Statistical analysis was performed as described in **2.2.1**.

2.7.3 Ferric chelate reductase (FCR) assay

Roots (*ca.* 200 mg) from 14-d-old seedlings were excised, transferred to a 2 mL Eppendorf tube and submerged in 700 µL of assay solution (0.1 mM Fe(III)-EDTA (E6760) and 0.3 mM ferrozine (160601)). Samples were incubated in the dark for 30 min at room temperature. The solution was then transferred to a transparent cuvette (Fisher Scientific) and absorbance at 562 nm measured using a spectrophotometer [338]. Root surface FCR activity was calculated assuming a molar extinction coefficient of 28.6 mM⁻¹ cm⁻¹:

$$\text{FCR activity } (\mu\text{mol Fe(II)}/\text{g root FW}/\text{h}) = \frac{\left(\frac{A_{562}}{28.6}\right) \times 700}{\text{root FW} \times 2}$$

Statistical analysis was performed as described in **2.2.1**.

2.7.4 Perls' stain and DAB intensification

Whole 7-d-old *A. thaliana* seedlings were washed with ice cold 2 mM CaSO₄ and 10 mM EDTA for 10 min, followed by two dH₂O washes. Samples were then incubated in 2 mL of Perls' staining solution (4 % (v/v) HCl (H1758) and 4 % (w/v) K-ferrocyanide (P3289)) for 45 min, with the first 15 min carried out under vacuum. Samples were washed with dH₂O and incubated in peroxide inhibition solution (0.07 % (w/v) NaN₃ (S2002) and 0.3 % (v/v) H₂O₂ prepared in 100 % MeOH) for 1 h. Seedlings were then washed with pH 7.4 phosphate buffer (0.1 M) and incubated with 2 mL DAB (diaminobenzidine, D5637) solution (pH 7.4 phosphate buffer (0.1M), 0.025 % DAB,

0.005 % H₂O₂, 0.005 % CoCl₂ (60818)) for 30 min [339]. Samples were then washed again with dH₂O and roots imaged using a stereomicroscope (Leica M205).

2.8 RNA sequencing

2.8.1 Preparation of samples

Col-0 and *bts1x2* seedlings were grown vertically for 14 d on modified Hoagland medium supplemented with standard (1 μM) or excess (100 μM) ZnSO₄ (**2.1.4**). Shoots and roots were then harvested separately (*ca.* 100 mg), flash frozen in liquid nitrogen and RNA extraction carried out as described in **2.3.1**. Quality check was then carried out on a 2100 Bioanalyzer Instrument (G2939BA, Agilent Technologies, CA, USA) using the Agilent RNA 6000 Nano Kit (5067-1511, Agilent Technologies) as per the manufacturer's instructions. Samples were diluted to 100 ng/μL and a total volume of 30 μL sent for sequencing.

2.8.2 RNA-sequencing (RNA-seq)

Construction of cDNA sequencing libraries and next generation sequencing (NGS) was carried out by Novogene (HK) Company Ltd. (Hong Kong). Libraries were generated using NEBNext® Ultra™ RNA Library Prep Kit for Illumina (NEB) and then sequenced on an Illumina Novaseq 6000 (Illumina, Ca, USA) using 150 bp paired end reads. Quality control was carried out on raw reads using FastQC [340].

2.8.3 Read alignment and differential gene expression (DGE)

Reads were pseudoaligned to the TAIR10 transcriptome (TAIR10_cdna_20101214_updated.fa) and transcript abundance calculated using Kallisto (v 0.46.1) [341] on the NBI high-performance computing (HPC) platform (NBI, Norwich, UK). DGE analysis was then performed using Sleuth [342] in R Studio with a 2-fold ($\log_2FC > 1$) cut off and a 5 % false discovery rate (adjusted p-val, $qval < 0.05$) using pairwise comparisons between samples. Sleuth was also used to run principal

component analysis. Kallisto and Sleuth were both run in R Studio. Results were verified by also performing differential gene expression (DGE) analysis with EdgeR on the Degust platform [343] and the top results compared.

2.8.4 Bioinformatic analysis of RNA-seq data

Shoot and root data were analysed separately. Gene list comparisons and Venn diagrams were generated using Gene List Comparator [344]. Hierarchical clustering of significantly differentially expression genes based on fold change (FC) difference from the mean was performed using Morpheus (available at <https://software.broadinstitute.org/morpheus/>.) [345] based on Pearson correlation and average linkage method, as well as generation of Heatmaps. Gene Ontology (GO) [346] for biological processes and Kyoto Encyclopedia of Genomes and Genes (KEGG) pathway [347-349] enrichment analysis was performed using David (Database for Annotation, Visualization and Integrated Discover) [350, 351] filtered with an adjusted p-value (Benjamini < 0.05).

Chapter 3: Establishing luciferase-based mutant screens to identify novel genes in the Zn homeostasis network

3.1 Introduction

3.1.1 Forward genetic screens investigating nutrient homeostasis in *A.*

thaliana

Forward genetics provides a powerful approach to identifying novel genes or mutant alleles associated with a specific signalling pathway or biological process. The fundamental basis of forward genetics also makes it an unbiased approach, as genes are mapped by linkage with a phenotype of interest and therefore is not reliant upon prior knowledge of potential candidate genes. One of the first examples of this approach can be seen in Thomas Hunt Morgan's work on *Drosophila* from the early 1900s, where he utilised mutants with eye and wing phenotypes to establish the chromosome theory of inheritance and early genetic mapping practices [352, 353]. Since then, advances in our understanding of genetics, molecular biology techniques and technology have led to the development of high-throughput mutant screens, which are now used extensively in the study of model organisms and species of interest across most biological fields including bacteria [354], yeast [355, 356], mammals [357, 358] and plants [359-361].

In plants, *A. thaliana* is often used as the model organism of choice, and as such there are a wealth of examples where mutant screens have been used to explore signalling pathways in *A. thaliana*. Mutant screens have been particularly successful in identifying genes and novel mutant alleles associated with nutrient homeostasis networks including potassium (K) [362], sulphur (S) [363-365], magnesium (Mg) [366], phosphate [367, 368], Mn [369] - and of particular interest - Zn [256] and Fe [304, 370, 371]. Mutant screens have also identified new regulatory interactions between nutrient networks, such as for phosphate and As [372], phosphate and Fe [373] as well as for Zn and Fe [212]. It is noted that other screening approaches looking at protein-protein interactions, such as yeast two-hybrid screens [300, 302, 374], as well as protein interactions with cis-regulatory regions, such as yeast one-hybrid screens [159, 314, 375, 376], have also proved to be useful approaches in identifying important transcription factors and regulatory proteins involved in Fe and Zn homeostasis. However, these protein screens are far more targeted and limited in their outputs, and as such a genetic

screen has far more potential in identifying new genes and novel mutant alleles associated with Zn homeostasis, as well as Zn and Fe cross-homeostasis.

3.1.2 Mutagenesis techniques in *A. thaliana*

In a forward genetic screen, a parental population functional in the biological process of interest is treated with a mutagen. The offspring of these treated lines generates a mutant screening population containing individuals with random mutations throughout the genome, some of which show abnormal phenotypes relating to the process of interest. In *A. thaliana*, commonly used techniques include chemical mutagenesis utilising reagents such as EMS to generate point mutations [377], ionising radiation utilising gamma rays or fast neutron irradiation to generate deletions and substitutions [378] or insertional mutagenesis using T-DNA or transposons [379, 380]. Each of these techniques has their own respective merits and disadvantages. For instance, EMS and irradiation are fairly straightforward procedures carried out on seeds, although EMS has been shown to be a more efficient mutagen than radiation, and also does not require specialised facilities and equipment [381]. The subsequent point mutations or small deletions produced by these techniques can generate both loss-of-function or gain-of-function mutant alleles, as well as weaker alleles of mutants which are normally embryo lethal. However, it is difficult to reach saturation in these mutant populations due to the compromise between using a mutagen dose strong enough to increase the chances of generating mutations in all genes, but not so strong that seeds are non-viable [381]. Moreover, map-based cloning of single point mutations or deletions can be a long and labour-intensive process, requiring extensive back-crossing to remove additional background mutations to identify a causative mutation of interest [382]. However, the increasing affordability and accessibility of whole genome sequencing, with the added development of software designed to support sequenced-based mapping, is making the mutation mapping stage of EMS and irradiation mutagenesis much less of a barrier than it once was [383].

With insertional mutagenesis, loss-of-function mutations are far more likely, although gain-of-function mutations can be induced using activation tagging [379]. Insertions have a higher chance of disrupting normal gene function and thus compared

to EMS or radiation mutagenesis it is easier to reach saturation in a mutant screening population. Moreover, the inserted fragment acts as a tag, such that flanking sequencing of the genome can be easily sequenced and the locus of the mutation identified [380]. However, screening populations are more work to set up, requiring *Agrobacterium* mediated transformation of *A. thaliana*, and can result in multiple insertions as well as chromosomal rearrangements which can severely complicate mutant analysis [384].

Based on the relative ease of EMS, its successful deployment in other nutrient homeostasis screens and its ability to generate viable mutant alleles of otherwise embryo lethal mutants, EMS appears to be the most appropriate choice for a Zn homeostasis mutant screen.

3.1.3 Luciferase as a reporter gene in mutant screens

Forward genetic mutant screens require a robust phenotype that can easily be screened for in the mutant population using non-destructive methods. Previously, screens have utilised growth phenotypes to help identify candidate genes involved in nutrient homeostasis. For example, *GSH1* was identified in a mutant screen that looked for individuals impaired in Fe-mediated Zn tolerance [212] and the novel mutant allele of *NRAMP1*, *nramp1-3*, was identified in a screen looking for mutants hypersensitive to Mn deficiency [369]. However, this screening method can be laborious if specific phenotypes have to be measured, such as root length, and some mutations may not necessarily produce a strong growth phenotype which could easily be missed in a high throughput screen. An alternative method utilises reporter gene expression driven by a cis-regulatory element associated with the signalling network of interest as a phenotypic readout. This approach is much more rapid and suited to identifying subtle mutant phenotypes.

One of the most commonly used reporter genes in mutant screens is firefly luciferase (*LUC*). *LUC* is an oxidative enzyme which catalyses the ATP-dependent conversion of its substrate luciferin to oxyluciferin [385, 386]. During the reaction a photon is released at 560 nm, and this light emission can be captured using a photon counting CCD camera (**Figure 3.1**). The protein shows poor regeneration after this reaction, and *LUC* mRNA and protein both have very short half-lives [387]. Together, this

means that the expression localisation and intensity of a LUC transgene can be followed *in planta* in real time. In a LUC-based mutant screen, *LUC* expression is driven by a promoter known to contain cis-elements that interact with the signalling network of interest. For instance, in Fe deficiency screens, *LUC* is often fused to the promoter of *IRT1*, the main Fe uptake transporter which is strongly upregulated under low Fe conditions [304, 370, 388]. As such, putative mutants can be easily selected based on their deviation of *LUC* expression from the parental line. To continue the *pIRT:LUC* example, mutants could be selected based on lack or overexpression of *LUC* expression under Fe deficiency, or alternatively if *LUC* is expressed under Fe sufficiency conditions, or even if it is induced in the wrong tissue type. Thus, LUC-based mutant screens offer rapid, high throughput and flexible screening of mutant populations but are dependent upon robust growth and imaging conditions, as well as a parental line for reference during screening.

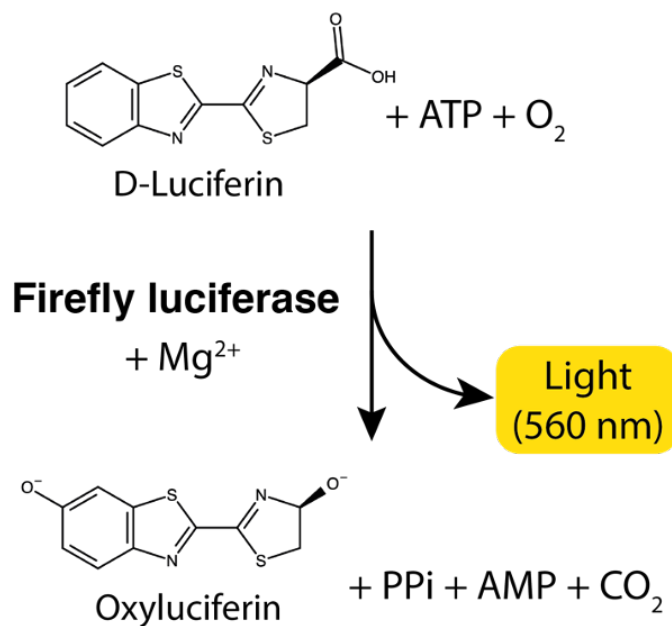


Figure 3.1: The bioluminescent firefly luciferase reaction.

Schematic showing the conversion of D-luciferin, adenosine triphosphate (ATP) and O₂ to oxyluciferin, pyrophosphate (PPi), adenosine monophosphate (AMP) and carbon dioxide (CO₂). The reaction is catalysed by firefly luciferase and a Mg²⁺ cofactor. A photon of light is emitted at 560 nm as part of the reaction giving the reaction its bioluminescent properties.

3.1.4 Filling in the gaps of the Zn homeostasis network

The current model of Zn homeostasis in *A. thaliana* is gradually becoming more comprehensive, however there still remain a number of exciting possibilities that have yet to be explored that could be answered through a forward genetics approach. For example, the response to Zn deficiency is thought to be regulated by both local and systemic signals [162]. Local Zn deficiency signalling is mediated by the activity of bZIP19 and bZIP23 transcription factors, which are able to bind Zn²⁺ directly through N-terminal Cys/His-rich motifs [159, 290]. Zn²⁺ binding prohibits bZIP19/23 dimerisation, and consequently prevents expression of downstream deficiency-responsive genes such as Zn uptake transporters, *ZIP4* and *ZIP9*, and Zn mobilisation genes, such as *NAS2*, under Zn sufficiency conditions [290]. However, it is not known whether bZIP19 and bZIP23 are also regulated by interaction with other transcription factors or regulatory proteins responsive to Zn and Zn-related signalling pathways, as is seen with Fe deficiency-responsive transcription factors (**Figure 3.2**) [308, 310]. Moreover, the exact role of Zn transporters and chelators involved in regulating the labile pool of Zn²⁺ available to bind bZIP19/23 is not fully understood (**Figure 3.2**) [389]. It is also possible that there are other Zn sensors or regulators as not all Zn-responsive genes have the bZIP19/23 binding Zinc Deficiency Responsive Element (ZDRE) in their promoters. There is relatively little known about the systemic Zn signal, apart from that it regulates the expression of *HMA2* and *MTP2* in roots in a bZIP19/23-independent manner and is likely phloem-mobile [162]. As such, there is a wealth of opportunity to explore Zn deficiency sensing and signalling in shoots, as well as genes involved in Zn shoot-to-root communication and transport (**Figure 3.2**).

Compared to Zn deficiency, no Zn-specific regulators of Zn excess have been identified to date, but rather Zn toxicity is defined by the secondary Fe deficiency response and subsequent transcriptional cascade it induces [27]. However, it is possible that there are Zn-specific transcription factors involved in this response, or regulatory proteins that can interact with the Fe homeostasis network under these conditions (**Figure 3.2**). Currently, there are a few proteins posited to act as Fe-sensors in *A. thaliana*, but whether these sensors are also responsive to Zn, or whether there are Zn excess-sensors is also not known (**Figure 3.2**). Furthermore, the contribution of various

transporters and chelators to Fe and Zn distribution and their role in Zn homeostasis under excess conditions is still not completely understood. Systemic Fe deficiency signalling is also an important part of the Zn excess response, being one of the earliest responses identified [27]. However, much the same as Zn deficiency, the nature of this signal, the transporters involved and possible root-responsive proteins are yet to be identified (**Figure 3.2**). As such, the Zn excess screen could provide evidence of Zn-specific toxicity response regulators, and also give a fuller picture of Fe and Zn cross-homeostasis in *A. thaliana*.

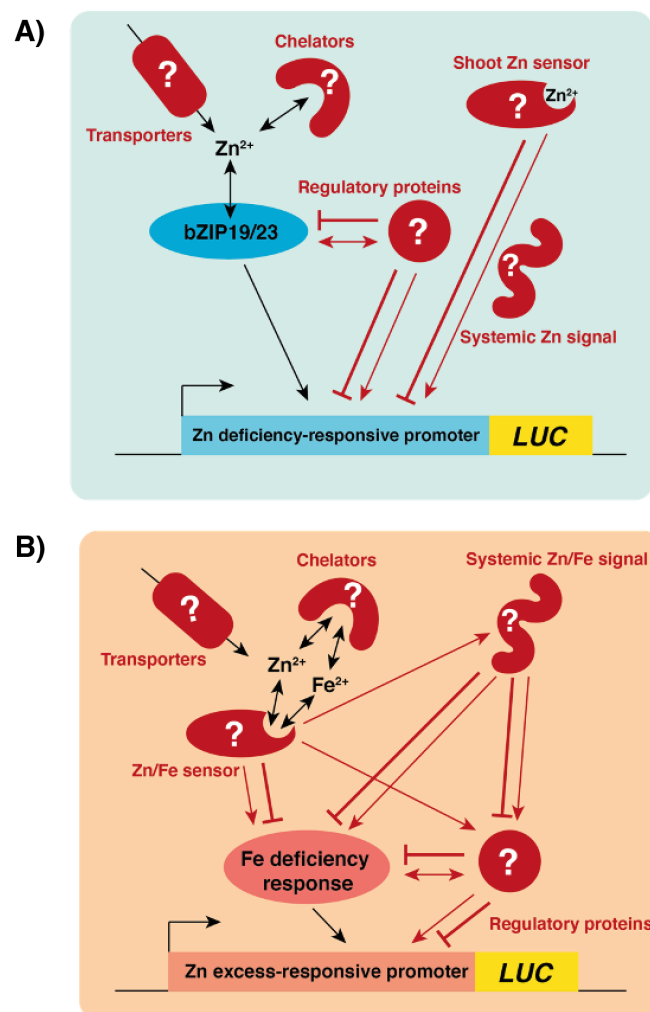


Figure 3.2: Schematic showing possible gaps in the Zn homeostasis network that a forward genetic screen could fill.

Schematics highlighting possible genes that could be identified in a luciferase-based mutant screen utilising A) a Zn deficiency-responsive promoter or B) a Zn excess-responsive promoter. Unknowns are highlighted in red with a question mark. *LUC* = luciferase gene.

3.1.5 Aims of this chapter

This chapter describes the establishment of two LUC-based mutant screens for identification of novel genes involved in Zn deficiency and Zn excess signalling. The first section of this chapter describes the selection of candidate Zn-responsive promoters to drive *LUC* expression, and the subsequent generation of mutant populations. The optimisation of screening conditions through testing varying growth conditions and LUC imaging protocols is then described, as well as the results of initial screening of mutant populations. The aim was to generate mutant populations which can be utilised for high throughput screening to discover previously unidentified mutant lines impaired in Zn homeostasis, as well as Zn and Fe cross-homeostasis.

3.2 Results

3.2.1 Selection of candidate Zn deficiency and Zn excess-responsive promoters

The development of Zn-responsive LUC-based reporter lines for a forward genetic screen firstly required the identification of Zn-responsive promoters. As such, candidate Zn-regulated genes which are robustly upregulated in response to Zn deficiency or Zn excess were selected from publicly available expression studies. A published microarray dataset of *A. thaliana* (Col-0) grown hydroponically under low (0.05 μM ZnSO₄), standard (2 μM ZnSO₄) and excess (25 μM ZnSO₄) Zn growth conditions was analysed for genes that were differentially regulated in both shoots and roots in response to either low or high Zn [390]. These genes were then filtered for those that were only upregulated and then cross-referenced with other expression studies (see **Table 3.1** for references). This identified six Zn deficiency-responsive candidate genes – three Zn transporters (*ZIP4*, *ZIP5* and *IRT3*), two defensin-like proteins (*DEFL203* and *DEFL206*) and an NAC domain-containing protein (*NAC096*). Six Zn excess-responsive candidate genes were also identified – three Zn transporters (*ZIF1*, *IRT2*, *MTP3* and *PCR2*), a ferric chelate reductase (*FRO3*) and a hypothetical protein (*AT3G61930*) (**Table 3.1**). A number of these Zn excess-responsive genes are also induced under Fe

deficiency, so the Zn excess screen could also help identify genes involved in Fe and Zn cross-homeostasis.

	Gene ID	Gene name	Log2FC		References
			Shoot	Root	
Zn deficiency	AT1G10970	<i>Zinc Transporter 4 (ZIP4)</i>	2.27	1.62	[153, 159, 228, 390, 391]
	AT1G05300	<i>Zinc Transporter 5 (ZIP5)</i>	0.60	1.49	[159, 390]
	AT1G60960	<i>Iron-Regulated Transporter 3 (IRT3)</i>	0.53	0.51	[159, 390, 391]
	AT2G36255	<i>Defensin-Like Protein 203 (DEFL203)</i>	1.05	2.37	[288, 390]
	AT3G59930	<i>Defensin-Like Protein 206 (DEFL206)</i>	1.12	2.48	[288, 390]
	AT5G46590	<i>NAC Domain-Containing Protein 96 (NAC096)</i>	0.77	0.51	[390]
Zn excess	AT5G13740	<i>Zinc-Induced Facilitator 1 (ZIF1)</i>	0.95	0.96	[256, 390]
	AT4G19680	<i>Iron-Regulated Transporter 2 (IRT2)</i>	0.11	3.40	[390, 392]
	AT1G23020	<i>Ferric Reductase Oxidase 3 (FRO3)</i>	1.73	1.95	[228, 390]
	AT3G58810	<i>Metal Tolerance Protein A2/3 (MTPA2/MTP3)</i>	0.10	1.96	[249, 390]
	AT1G14870	<i>Plant Cadmium Resistance 2 (PCR2)</i>	0.77	0.25	[229, 390]
	AT3G61930	<i>Hypothetical protein</i>	0.40	3.13	[303, 390]

Table 3.1: Zn deficiency and Zn excess-responsive genes selected as promoter candidates for the luciferase-based mutant screen

Genes were selected based on fold change (Log2FC) taken from [390] and additional expression studies indicated in references column.

3.2.2 qRT-PCR analysis of candidate Zn deficiency-responsive promoters

Expression of the selected candidate Zn deficiency-responsive genes was then tested under the growth conditions to be potentially used in the screen (**Figure 3.3**). A Zn chelator, TPEN, was used to induce Zn deficiency. This is because low-level Zn contaminants found in agar are sufficient to support healthy growth in *A. thaliana* and chelator-washing the agar before media preparation was not feasible for high throughput screening. At 11 days old, seedlings were either sprayed with 50 μ M TPEN solution (spray) or transferred to 50 μ M TPEN supplemented plates (transfer) for 3 days. All candidate genes were upregulated in shoots and roots in response to TPEN spray and transfer, apart from *NAC096* which only showed low expression in roots in response to TPEN spraying (**Figure 3.3**). Transfer to TPEN supplemented plates appeared to induce less variation in expression compared to spraying, and as such, was focussed on as the Zn deficiency screening condition. Of the remaining five genes, *ZIP5* was taken forward for use in the screen as it showed upregulation in both roots and shoots under the screening growth conditions and a construct containing the *ZIP5* promoter fused to *LUC* was readily available (p*ZIP5:LUC* generated by Dr Kalyani Kallam, John Innes Centre)(**Figure 3.3B**). *ZIP4*, *IRT3*, *DEFL203* and *DEFL206* all showed more than 10-fold upregulation in root and shoots (**Figures 3.3A, C, D and E**). However, the use of *ZIP4* as bait in a previous screen [159] and difficulties in cloning *IRT3* and *DEFL203*, meant that only *DEFL206* was taken forward alongside *ZIP5* for use in the Zn deficiency screen.

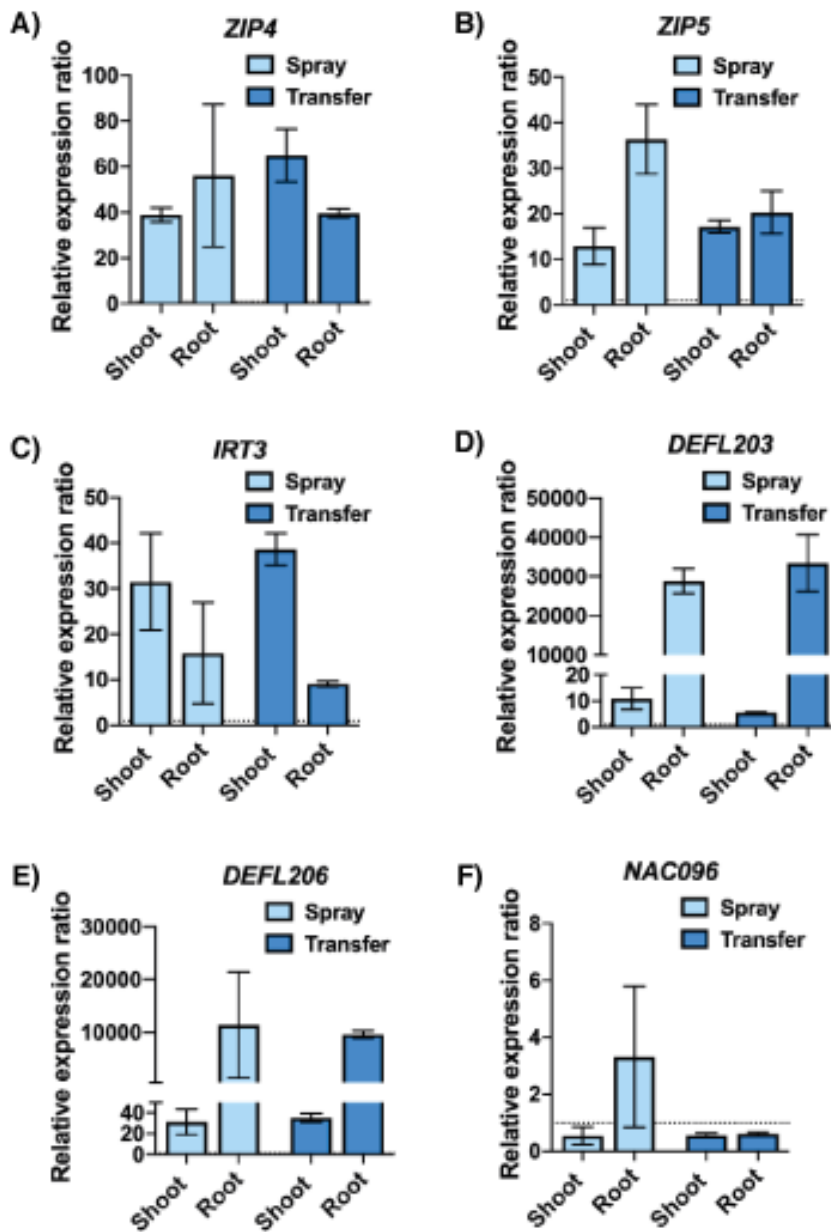


Figure 3.3: Quantitative reverse transcription-PCR (qRT-PCR) analysis of candidate Zn deficiency-responsive genes for promoter selection.

The expression of A) *ZIP4*, B) *ZIP5*, C) *IRT3*, D) *DEFL203*, E) *DEFL206* and F) *NAC096* in 14-d-old Col-0 seedlings grown on ¼ MS agar plates either sprayed with 50 µM TPEN solution (spray) or transferred to plates supplemented with 50 µM TPEN (transfer) for 3 d before the end of growth. Fold change is relative to expression under standard growth conditions (expression level set as “1” indicated by dotted line) and normalised to reference genes *ACTIN2* and *UBQ10*. Data represent mean values (\pm SEM) from three independent experiments, each comprising six plants per genotype and condition, and each repeated as three technical replicates.

3.2.3 qRT-PCR analysis of candidate Zn excess-responsive promoters

Expression analysis of the six candidate Zn excess-responsive genes was next carried out (**Figure 3.4**). Gene induction was tested in seedlings that were transferred to 200 μ M ZnSO₄ supplemented agar plates for either 3 or 5 days. All genes showed higher fold induction after 5 days, and so this was focussed on as the growth condition for use in the Zn excess screen (**Figure 3.4**). All genes were upregulated in response to Zn excess, although, consistent with the microarray data, *MTP3* and *AT3G61930* were not induced in shoots and *PCR2* was not induced in roots (**Figures 3.4D, E and F**). As a transgenic *A. thaliana* line expressing *LUC* under the control of the *FRO3* promoter (p*FRO3:LUC*) had already previously been generated by Dr Jorge Rodriguez-Celma (John Innes Centre), and the gene showed over 10-fold upregulation under Zn excess, *FRO3* was taken forward as one of the promoters for the LUC screen (**Figure 3.4C**). Of the remaining candidate genes, *ZIF1*, *MTP3* and *PCR2* expression was relatively low compared to *IRT2* and *AT3G61930*, and of these *AT3G61930* showed the highest upregulation and so was taken forward alongside *FRO3* for the Zn excess mutant screen.

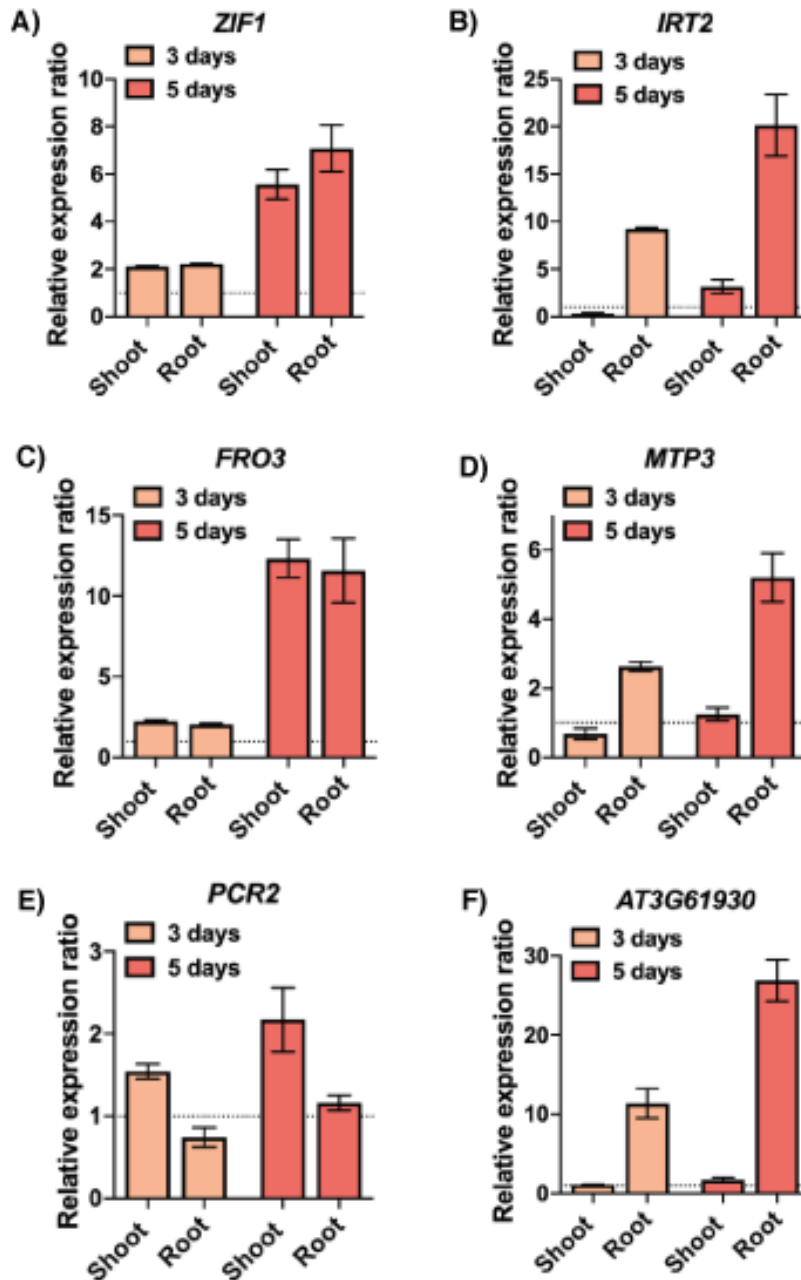


Figure 3.4: Quantitative reverse transcription-PCR (qRT-PCR) analysis of candidate Zn excess-responsive genes for promoter selection.

The expression of A) *ZIF1*, B) *IRT2*, C) *FRO3*, D) *MTP3*, E) *PCR2* and F) *AT3G61930* in 14-d-old Col-0 seedlings grown on ¼ MS agar plates and then transferred to 200 μM ZnSO₄ supplemented plates either 3 d or 5 d before the end of growth. Fold change is relative to expression under standard growth conditions (expression level set as “1” indicated by dotted line) and normalised to reference genes *ACTIN2* and *UBQ10*. Data represent mean values (± SEM) from three independent experiments, each comprising six plants per genotype and condition, and each repeated as three technical replicates.

3.2.4 Generation of pZIP5/DEFL206/FRO3:LUC primary transformants

Following the selection of ZIP5, DEFL206, FRO3 and AT3G61930 for use in the mutant screens, promoter cloning, transformation and selection of homozygous T₃ lines for mutagenesis was carried out. **Figure 3.5** gives an overview of transformation to T₃ selection. It is to be noted that Dr Kalyani Kallam (John Innes Centre) carried out generation of the pZIP5:LUC vectors, and Dr Jorge Rodriguez-Celma (John Innes Centre) produced the T₂ pFRO3:LUC populations (lines 1.1 – 1.12 and 2.1 – 2.12). Briefly, 3 kb upstream of each gene was taken as the promoter region and cloned into luciferase vectors (**Supplementary Figure A1, Appendix A**). The luciferase construct which also included a herbicide resistance gene, *bar*, against BASTA, was then transformed into *A. thaliana* (Col-0) through *Agrobacterium tumefaciens* floral dipping and successful T₁ transformants identified through herbicide selection on soil (**Figure 3.5**). At this stage, six pZIP5:LUC lines (named 1 – 6) and eight pFRO3:LUC lines (named 1 – 8) were successfully identified (**Figure 3.5**), but no successful pAT3G61930:LUC transformants, so only pFRO3:LUC was utilised in the Zn excess screen.

T₂ populations were then screened for luciferase expression, with 100 seedlings per line screened and then 50 individuals which showed consistent strong luciferase expression were selected for seed collection (**Figure 3.5**). This was in order to select at least one homozygous line with a single transgene insertion. Although only 12 individuals for each of the two pFRO3:LUC lines gifted were available, this was still sufficient. T₃ populations were then again screened for luciferase expression and BASTA resistance. The germination and luminescence percentages were recorded to identify lines which showed Mendelian segregation indicative of a single transgene insertion event. T₃ lines should show no luminescence, 75% expression or 100% expression corresponding to T₂ individuals with no insertion, hemizygous or homozygous insertions respectively (**Figure 3.5**). Lines which showed 100% luminescence representing homozygous lines were selected for seed bulking and EMS mutagenesis. At this stage no single insertion lines for pDEFL206:LUC lines could be identified so this gene was not utilised in a Zn deficiency screen (**Supplementary Figure A2, Appendix A**). Homozygous lines which showed strong consistent luciferase expression were identified for pZIP5:LUC (line 5.23) and pFRO3:LUC

(line 1.10) and their transgene copy number verified prior to EMS mutagenesis and generation of the mutant screening population. (Figure 3.5).

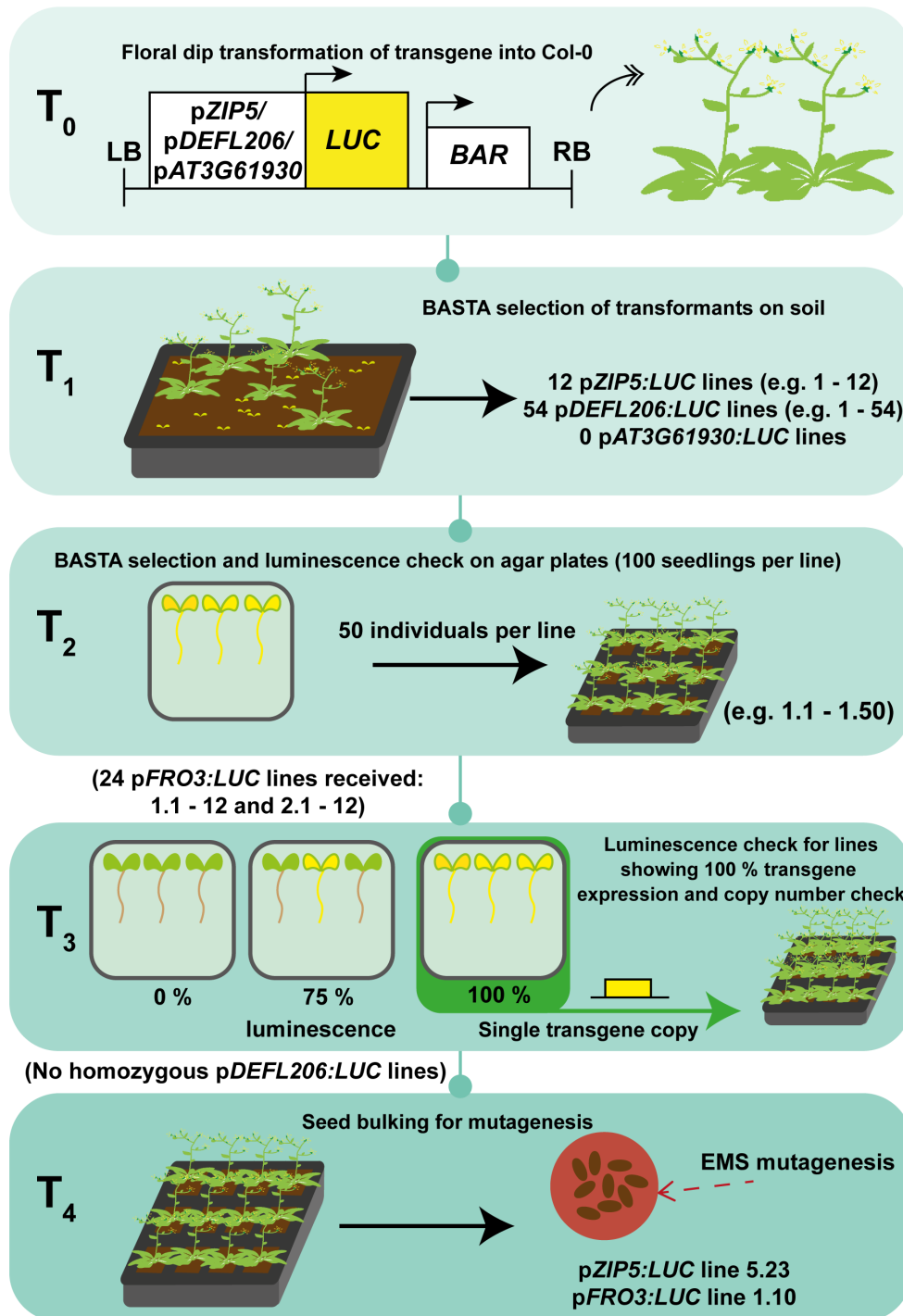


Figure 3.5: Overview of selection of pZIP5/FRO3:LUC primary transformant lines.

T₁ transgenic lines of pZIP5:LUC (construct produced by Dr Kalyani Kallam), pDEFL206:LUC and pAT3G61930 were produced by *Agrobacterium* floral dip transformation of Col-0 followed by BASTA selection of seeds on soil, with 12 pZIP5:LUC T₁ lines (named 1 – 12), 54

pDEFL205:LUC lines (1 – 54), but no *pAT3G61930:LUC* transformant lines identified. T₂ seeds were screened for luciferase expression and BASTA resistance, with 50 individuals per line selected (named 1.1 – 1.50), with 24 *pFRO3:LUC* T₂ lines (1.1 – 1.2 and 2.1 – 2.12) gifted at this stage by Dr Jorge Rodriguez-Celma. T₃ lines were screened for luciferase expression and BASTA resistance, checking for Mendelian segregation of the transgene. Homozygous lines showing 100% luminescence for *pZIP5:LUC* (line 5.23) and *pFRO3:LUC* (line 1.10) were copy number checked and seed bulked for EMS mutagenesis. No homozygous lines were identified for *pDEFL206:LUC*. LB = Left Border; RB = Right Border; BAR = BASTA resistance gene. Adapted from [393].

3.2.5 Optimisation of Zn deficiency screening conditions

Luciferase-based mutant screens are reliant upon robust transgene expression under the screening conditions used, as well as the methods for growth and seedling preparation being feasibly scaled-up for high throughput screening. As such, various growth and imaging conditions were tested for screen optimisation. First, luminescence imaging was carried out on homozygous T₃ *pZIP5:LUC* seedlings grown under the conditions used for qRT-PCR, namely no treatment as a control, or Zn deficiency induced through spraying with 50 µM TPEN solution or transfer to 50 µM TPEN plates (**Figures 3.6A, B and C**). There appeared to be low-level luciferase expression in aerial tissue around the shoot apical meristem on control plates, which is further enhanced by spraying with TPEN (**Figures 3.6A and B**). As indicated by the qRT-PCR data (**Figure 3.3**), this shows that TPEN spraying produces variable gene induction and is not suitable for screening conditions. Meanwhile, transfer to TPEN plates leads to strong luciferase expression in both shoots and roots consistently in all seedlings, and plants show more visible Zn deficiency symptoms, such as growth stunting (**Figure 3.6C**). However, the background expression of *pZIP5:LUC* on untreated agar plates could be problematic at the screening stage, so growth in 96-well plates with liquid MS media was also tested (**Figure 3.6D**). Liquid media removes the issue of Zn contaminants from agar as well as the potential pleiotropic effects of chelator use.

Omitting ZnSO₄ from liquid media (0 μM) is successful in inducing Zn deficiency and high levels of luciferase expression in all seedlings, with no residual luminescence seen at increasing Zn concentrations (1 μM, 2 μM, 5 μM, 10 μM and 25 μM)(**Figure 3.6D**). Moreover, 96-well plates are more suited for high throughput imaging, with exposure time only 5 s compared to 60 s for agar plates, more seedlings grown per plate, and more plates capable of being imaged at once (**Supplementary Table A1, Appendix A**). Although germination is compromised in 96-well plates, with ~10% of seedlings failing to grow, this is not an issue for mutant screening as mutations should be present in multiple individuals within the same line. Taken together, this led to the selection of the 96-well plate imaging system with liquid media for the Zn deficiency screen.

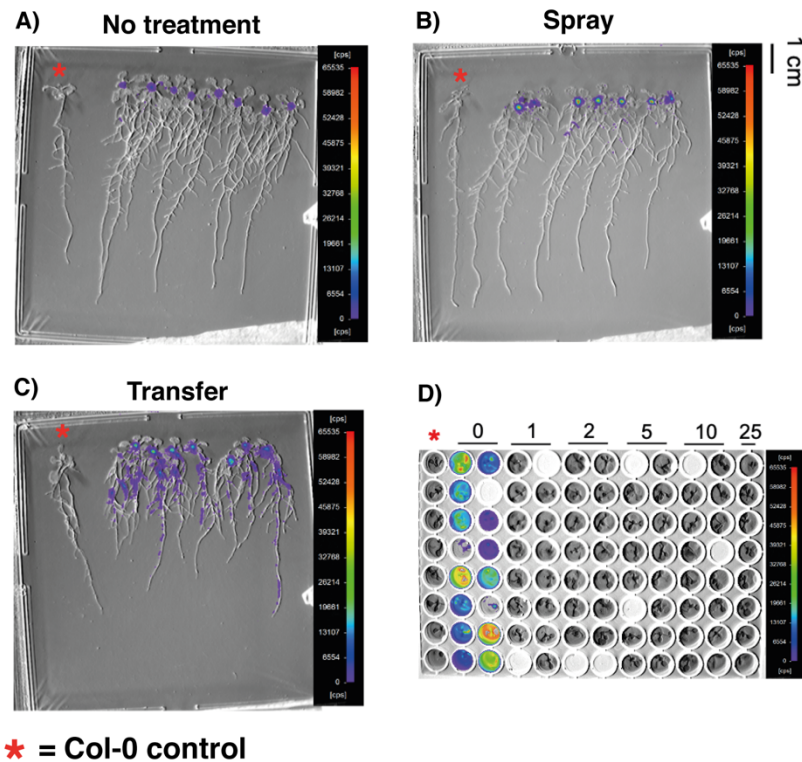


Figure 3.6: Optimisation of luminescence imaging of pZIP5:LUC lines for the Zn deficiency screen.

pZIP5:LUC seedlings were imaged at 14-d-old after growth on ¼ MS agar plates A) with no treatment, B) spraying with 50 μM TPEN solution (spray) for 3 d or C) transfer to 50 μM TPEN plates (transfer) for 3 d. D) 12-d-old seedlings grown in liquid ¼ MS supplemented with various ZnSO₄ concentrations (0 μM, 1 μM, 2 μM, 5 μM, 10 μM and 25 μM). Seedlings were incubated with luciferin prior to imaging. Red asterisk indicates Col-0 control; cps = counts per second.

3.2.6 Optimisation of Zn excess screening conditions

Optimisation of the Zn excess screen using homozygous T₃ *pFRO3:LUC* lines was next carried out. At 14 days old, no luciferase expression is seen when seedlings are grown on control untreated plates (**Figure 3.7A**). Zn excess was induced through transferring seedlings to 200 μ M ZnSO₄ supplemented agar plates for 5 days or through continual growth on Zn supplemented plates (**Figures 3.7B and C**). While transfer successfully induces transgene expression, consistent with qRT-PCR data, growing seedlings continuously on Zn excess produces higher luciferase expression, inducing Zn toxicity more consistently and reduces the time it takes to prepare seedlings for imaging (**Figures 3.7B and C**). Growth in liquid media in 96-well plates was also tested, however, luciferase expression is not detectable under these growth conditions (**Figures 3.7D and E**). This is most likely because transgene expression is seen most strongly in the root. As such, continuous growth on 200 μ M ZnSO₄ supplemented plates was selected as the screening conditions for Zn excess mutants.

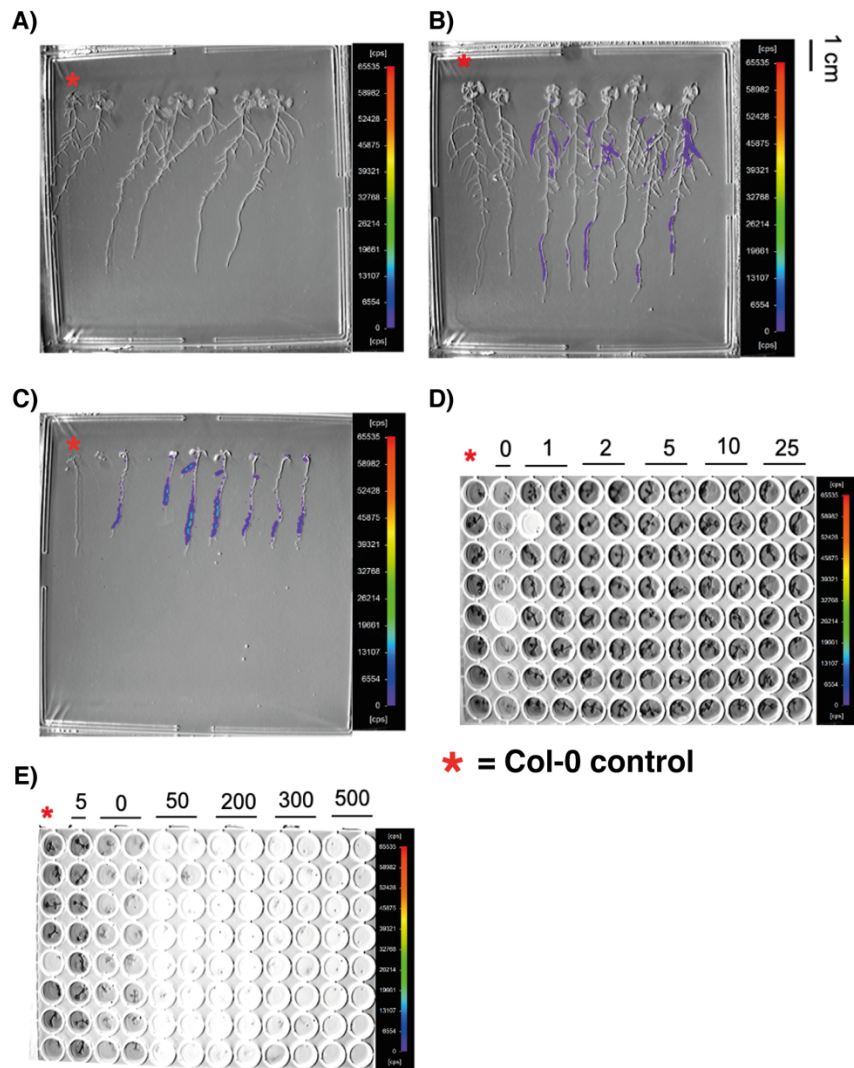


Figure 3.7: Optimising luminescence imaging of pFRO3:LUC lines for the Zn excess screen.

pFRO3:LUC seedlings were imaged at 14-d-old after growth on ¼ MS agar plates with A) no treatment, B) transfer to 200 μM ZnSO₄ plates for 5 d or C) continuous growth on 200 μM ZnSO₄ plates. D-E) 12-d-old seedlings grown in liquid ¼ MS supplemented with various ZnSO₄ concentrations D) 0 μM, 1 μM, 2 μM, 5 μM, 10 μM and 25 μM; E) 5 μM, 0 μM, 50 μM, 200 μM, 300 μM and 500 μM. Seedlings were incubated with luciferin prior to imaging. Red asterisk indicates Col-0 control; cps = counts per second.

3.2.7 Initial screening of M₂ populations

Following EMS mutagenesis, M₀ seeds (~5,000) were sown directly on soil and seed from the resultant M₁ lines collected in pools, with 40 pools in total. LUC screening

of the M₂ population was then carried out to identify p*ZIP5:LUC* and p*FRO3:LUC* individuals which did not show luminescence under Zn deficiency or Zn excess respectively. Initial screening of the p*ZIP5:LUC* population was carried out, with roughly 2,000 individuals from 20 different pools imaged. Most lines showed strong luciferase expression, although the germination problem previously noted from growth in liquid media was still seen (**Figure 3.8A**). However, seedlings from one particular pool showed that all individuals lacked luciferase expression under all conditions (**Figure 3.8B**). Amplification and sequencing of the transgene from individuals in this pool showed that there were no mutations in the *ZIP5* promoter sequence or *LUC*, which could suggest that the *LUC* transgene is being silenced in this line.

For screening of the p*FRO3:LUC* M₂ population, 18,000 individuals were screened, with 252 individuals identified as candidate mutants lacking luciferase expression (**Figures 3.9A and B**). Of these, 230 were found to be false positives due to luciferase expression in the M₃ generation. The remaining 22 lines were found to still show no expression in the M₃ line which could suggest that they are true candidate mutants (**Figure 3.9C**). However, the transgene could not be amplified from these lines, indicating that the lack of luciferase expression was due to absence of the transgene itself. This could be for a number of reasons, but the most likely is that these individuals are wild type contamination seed which entered the screening population during seed collection. Screening on BASTA confirmed this. Further screening of these populations is still required to identify a successful mutant candidate, but the results here show that *ZIP5* and *FRO3* promoters can be successfully utilised to drive reporter gene expression in forward genetic screens.

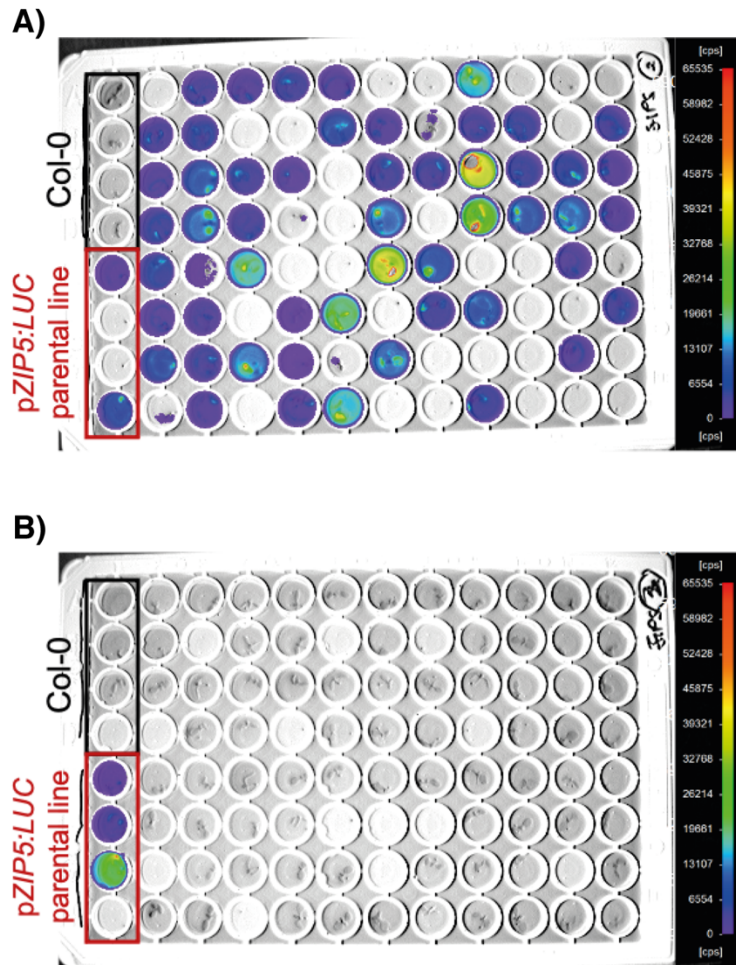


Figure 3.8: Screening of pZIP5:LUC M₂ population.

A) Representative plate of pZIP5:LUC M₂ screening population. B) Plate of pZIP5:LUC M₂ line showing silencing of the luciferase transgene. 12-d-old seedlings grown in liquid ¼ MS with ZnSO₄ omitted from the recipe (0 µM Zn). Seedlings were incubated with luciferin prior to imaging. Parental (outlined in red box) and Col-0 (outlined in black box) controls shown in left hand lane.

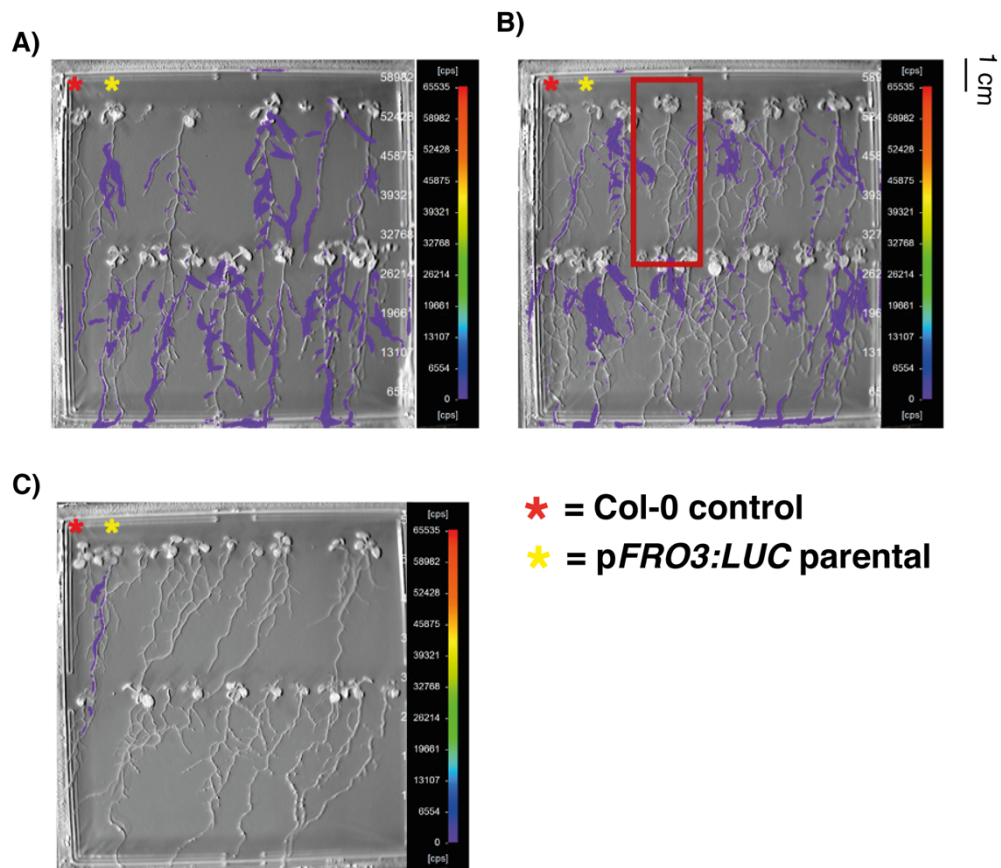


Figure 3.9: Screening of *pFRO3:LUC* M₂ population.

A) Representative plate of *pFRO3:LUC* M₂ screening population with no candidate mutant. B) Representative plate of *pFRO3:LUC* M₂ screening population with candidate mutant highlighted in red box. C) Representative plate of *pFRO3:LUC* M₃ false positive line. Seedlings were imaged at 14-d-old after continuous growth on 200 μM ZnSO₄ plates. Seedlings were incubated with luciferin prior to imaging.

3.3 Discussion

3.3.1 Expansion of screening conditions to identify candidate mutants

Through generating the *pZIP5:LUC* and *pFRO3:LUC* mutant populations (Figure 3.5), as well as optimising high throughput screening protocols (Figures 3.6 and 3.7), a resource that can be exploited in future screens has been established. Although initial screening yielded no mutants of interest, there is still great potential in identifying both

loss-of-function and gain-of-function mutants within these populations by expanding the screening conditions. For instance, in the screening protocol used here, the focus was on identifying mutants with loss of transgene expression under Zn deficiency or Zn excess, but it is also possible to look for individuals showing *LUC* overexpression. Furthermore, the specific induction of *pZIP5:LUC* (**Figure 3.6**) and *pFRO3:LUC* (**Figure 3.7**) under Zn stress conditions also means that mutants showing constitutive *LUC* expression under control conditions could also be identified. With *pFRO3:LUC*, specific Zn and Fe cross-homeostasis mutants could also be explored by looking for mutants that maintain high *LUC* expression under Fe supplemented Zn excess conditions. This could identify mutants which lack the Fe-mediated Zn tolerance phenotype.

3.3.2 The *pFRO3:LUC* screen

Early screening of the *pFRO3:LUC* mutant population appeared promising, with 253 candidate mutants identified as failing to induce transgene expression (**Figure 3.9**). However, rescreening in the M_3 generation demonstrated that these were false positives, with a small subset of these found to be wild type contaminant seed, but the majority appeared to be related to experimental error during screening. This error most likely occurred during the luciferin incubation stage, which on agar plates involves spraying seedlings with a concentrated luciferin solution. As such, compared to the 96-well approach, where seedlings are incubated in media supplemented with a specific amount of luciferin, spraying has a greater chance of applying uneven dosages or missing seedlings to give false positives. Another contributing factor to the high number of false positives in the Zn excess screen could be linked to the choice of promoter. Compared to some of the other genes tested, *FRO3* was not as highly upregulated as *IRT2* and *AT3G61930* (**Figure 3.4**). Perhaps use of a stronger promoter could also further help reduce the issue of false positives.

Although the use of liquid media in the *pZIP5:LUC* screen proved the most effective way to induce Zn deficiency-responsive gene expression and a more consistent luciferin application, it did impact the rate of germination (**Figure 3.6 and 3.8**). This should not be too problematic, as multiple mutants of the same gene should be present within the screening population. However, it is far from ideal, increasing the number of

seedlings that have to be screened and raising the possibility of missing a mutant of interest. Overall, these issues with the *pZIP5:LUC* and *pFRO3:LUC* screens represent the compromise that often happens between scalability and quality in developing suitable screening conditions.

3.3.3 Further screening of the M₂ population to identify candidate mutants

Forward genetic screens are somewhat of a high risk, high reward strategy. In theory, mutagenesis should achieve saturation within a screening population such that there are multiple mutants for each gene within the genome. However, this can be hard to achieve with EMS as not all point mutations result in disruptions to transcription and translation that produce a phenotype, with premature stop codons accounting for ~5% of EMS mutations and missense mutations ~65% [394]. EMS also induces G/C to A/T substitutions more frequently than other possible base changes, which can further limit mutation possibilities [395]. This reduced saturation in the mutagenised population means that a large number of individuals often have to be screened, with one estimate suggesting that as many as 135,000 M₁ lines could be required to give five-fold coverage of the *A. thaliana* genome, although less than 50,000 lines should be sufficient to obtain a high probability of finding a given G:C base pair mutagenised [396]. Random sampling probability also plays a contributing factor to how many M₂ seedlings have to be screened before a mutant of interest is found. For instance, there are examples in the literature where eight mutant lines were obtained from a screen of 15,000 [369], four mutant lines from a screen of 60,000 [397], at least one mutant line of interest from a screen of 30,500 [370] and 132 candidates from a screen of 75,000 [398]. To date, only 2,000 M₂ seedlings from *pZIP5:LUC* and 18,000 from the *pFRO3:LUC* populations have been screened (3.2.7). Thus, it is likely that further screening of these mutant populations across varied screening conditions could lead to the identification of novel mutant alleles associated with the Zn homeostasis network.

3.3.4 Transgene silencing and wild-type seed contamination issues in screens

During screening, a pool of pZIP5:LUC lines was identified that appeared to show transgene silencing (**Figure 3.8B**). This loss of expression was not related to an interesting mutation as it was found across all seedlings from a collected pool of multiple lines, rather than specific individuals as would be expected. Transgene silencing can occur through two different mechanisms, either at the transcriptional level, when promoter and cis-regulatory elements are methylated or histones deacetylated, or post-transcriptionally, when mRNA is targeted for degradation [399, 400]. Transgene silencing in *A. thaliana* is most often seen for genes that have not been codon optimised or are highly expressed due to a constitutive or strong promoter [401, 402]. Silencing can also occur due to exposure to stress conditions [403]. However, the firefly luciferase gene has not been widely reported to suffer from transgene silencing in *A. thaliana*, as appears to be a major problem in other species, such as sugarcane [404]. Moreover, the ZIP5 promoter is not particularly strong, and it is uncommon to see differences in transgene expression between lines descended from a common homozygous transformant line (i.e. the same T₃ line). One possible explanation could be stress exposure, possibly occurring during M₁ seed collection of this particular pool of lines, but again, it would be surprising for such consistent silencing across multiple lines. Another possibility could be simple experimental error, for instance with DNA contamination from control lines occurring during PCR and subsequent sequencing obscuring wild type seedling contamination, as appeared to happen in a pool of pFRO3:LUC M₁ lines. However, the BASTA resistance of the non-expressing pZIP5:LUC lines suggest that this is also not likely to be the case. Although an obvious answer for these anomalous lines is yet to be found, it perhaps highlights the importance of setting up robust screening lines and conditions, and potential problems that can arise during screening that are not often discussed in the literature.

3.3.5 Outlook for future Zn homeostasis mutant screens

Since the inception of the screen, there have been a number of developments in the literature which could provide useful direction for future Zn homeostasis mutant screens. For the Zn deficiency screen, it could be interesting to specifically explore the Zn systemic signal through utilising the promoters from *MTP2*, *HMA2*, or other non-bZIP19/23 regulated genes [162]. Moreover, had a homozygous line for p*DEL206:LUC* been found (**Supplementary Figure A2, Appendix A**), this could have yielded some really interesting results regarding the regulation of *DEFL* proteins not only under Zn deficiency, but also in Zn and Fe cross-homeostasis, with growing evidence for their role in Fe deficiency and Zn excess as well [228, 308, 405, 406]. Similarly, *NAS* genes are upregulated in response to both Zn deficiency [289] and Zn excess [228], thus *NAS2:LUC* reporter lines could be an extremely useful resource for future screens, with both low and high Zn being able to be investigated in the same mutant population.

**Chapter 4: The Fe-mediated Zn tolerance
phenotype of the *bts/1x2* mutant reveals
a role for BTSL proteins in
Fe and Zn cross-homeostasis**

4.1 Introduction

4.1.1 BTSL1 and BTSL2 are closely related homologs of BTS

Under Fe deficiency and Zn excess, genes involved in Fe acquisition, distribution and assimilation are upregulated in order to increase root Fe uptake capacity and translocation to shoots [166]. The key regulators of this transcriptional response form a hierarchical signalling cascade of bHLH transcription factors. The Clade IVc bHLH proteins (bHLH34, bHLH104, bHLH105/ILR3 and bHLH115)[296, 297, 375], and the recently identified bHLH121/URI [298-300], are the most upstream regulators identified to date, with their activity directly activating *FIT* expression, as well as indirectly via upregulation of Ib bHLH genes (*bHLH38*, *bHLH39*, *bHLH100*, *bHLH101*)[295]. However, the IVc and *bHLH121/URI* genes themselves are not transcriptionally responsive to Fe [298, 300] and none of the bHLH proteins has a discernible Fe-binding motif, which leaves the regulatory mechanism of cellular Fe and Zn concentrations on this signalling cascade as an open question. One likely process is the activity of Fe-dependent E3 ubiquitin ligases that target these transcription factors for 26S-proteasome-dependent degradation.

The first of these E3 ubiquitin ligases identified was BTS, a protein with three hemerythrin (HHE) cation-binding domains at its N-terminus and a C-terminal Really Interesting New Gene (RING) E3 ligase and CHY Zn-finger domain (**Figure 4.1**)[307, 407]. Similar to its rice homologs, HRZ1 and HRZ2 [407], the E3 ligase activity of BTS negatively regulates Fe deficiency through targeting key bHLH transcriptional regulators for proteasomal degradation in response to cellular Fe sufficiency [306, 307]. Two closely related homologs of BTS only found in dicotyledonous species, the partially functionally redundant BTSL1 and BTSL2, were also recently identified as E3 ubiquitin ligases with an Fe deficiency repressive function [304, 305]. BTSL1 and BTSL2 have a highly similar protein domain structure to BTS, although BTSL proteins only have two functional HHE domains and one HHE-like domain, which could potentially impact the cellular Fe concentrations that they are responsive to (**Figure 4.1**)[305]. The structure bears striking resemblance to mammalian F-box/LLR protein 5 (FBXL5), a hemerythrin motif protein from a multi-subunit E3 ligase whose activity targets iron regulatory proteins 1 and 2 (IRP1 and IRP2) for proteasomal degradation [408-410], and mammalian E3 ligase

Pirh2/RCHY1 [411] (**Figure 4.1**), which share distant homology to BTS [305]. BTS and BTSL stabilisation, and thus regulation of E3 ligase activity by cellular Fe concentration, is thought to be dictated by Fe binding to HHE domains [305] again with similarity to FBLX5 which is stabilised by Fe and oxygen binding [408, 409]. However mutagenesis of the HHE domains in BTS shows that Fe binding has a destabilising effect [306] and that Zn is also found bound to the HHE domains [407]. Therefore, it is likely that the Fe, and maybe Zn-mediated, regulation of BTS and BTSL proteins is more complicated than a switch in protein stabilisation alone.

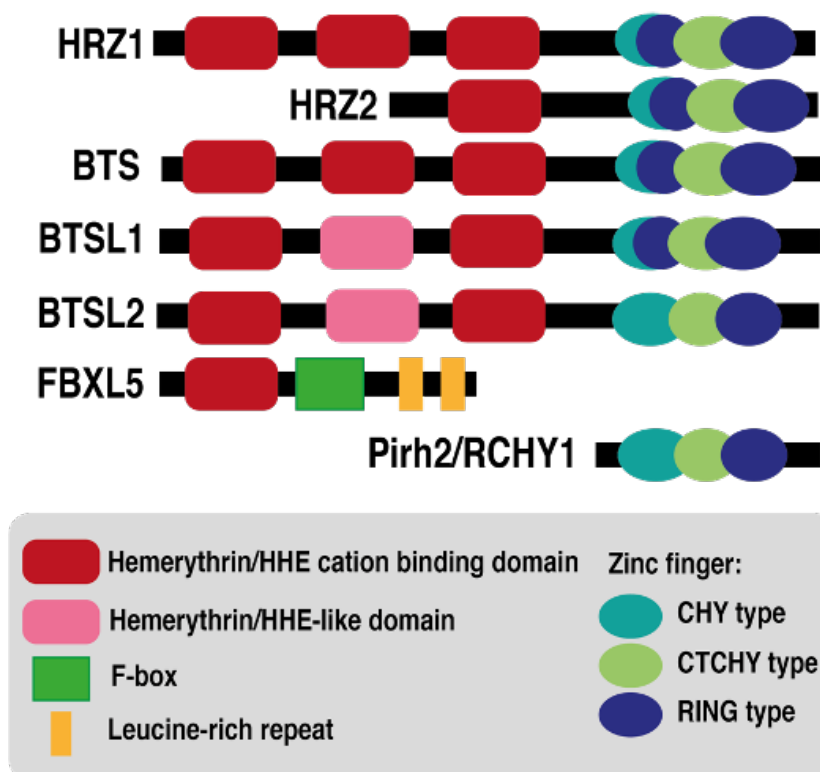


Figure 4.1: Domain organisation of BTS, BTSL and closely related hemerythrin domain-containing E3 ligases involved in Fe homeostasis.

Schematic of the domain organisation of *A. thaliana* BTS and BTSL proteins, closely related rice homologs HRZ1 and HRZ2 and mammalian hemerythrin-domain protein FBXL5 and E3 ligase Pirh2/RCHY1. Adapted from [305, 407].

4.1.2 BTSL1 and BTSL2 regulate FIT protein turnover

There are a number of key differences between BTS and BTSL proteins that highlight their distinct functions. BTS represses the Fe deficiency response by regulating protein turnover of three of the IVc bHLH transcription factors (bHLH104, ILR3 and bHLH115)[306] and bHLH121/URI [300] at the top of the transcriptional cascade, as well as VOZ1 and VOZ2 transcription factors, which negatively regulate cold and drought stress signalling [412]. Meanwhile, the only currently identified target of BTSL1/2 is FIT (**Figure 4.2A**)[305]. This difference in targets is reflected in their expression patterns. *BTS* is expressed in leaves and the root stele [306], while *BTSL1* and *BTSL2* are expressed in root epidermal and cortical cells where FIT is predominantly active, with *BTSL2* also expressed in the endodermis and in the stele around the differentiation zone [305]. Continual turnover of FIT under both Fe sufficient and deficient conditions helps maintain a small but responsive pool of protein, which can rapidly alter expression Fe uptake genes in response to fluctuations in Fe availability and other environmental signals [308]. Enhanced promotion of FIT degradation by BTSL proteins under Fe sufficiency leads to reduced expression of FIT-regulated *IRT1* and *FRO2* and as such prevents excessive Fe uptake [305]. In turn, as FIT accumulates under Fe deficiency, it activates the expression of Fe uptake genes, as well as *BTSL2*, creating a negative feedback loop to regulate itself and maintain the aforementioned protein turnover (**Figure 4.2B**)[305].

4.1.3 *bts* and *btsl* mutants are tolerant to Fe deficiency

Loss-of-function *bts* and *btsl* mutants show that de-repression of the Fe deficiency response leads to Fe accumulation and enhanced tolerance to Fe deficient growth conditions [304]. Analysis of the non-embryo lethal mutant allele, *bts-3*, demonstrated that accumulation of IVc bHLH proteins leads to constitutive upregulation of downstream Fe deficiency-responsive genes, including major regulators *PYE*, *lb bHLH* genes and *FIT* [304]. Constitutive activation of the Fe deficiency response results in excessive Fe uptake and accumulation, notably in shoots and seeds, as well as enhanced Zn and Mn uptake due to the broad substrate specificity of *IRT1*. Although enhanced Fe

uptake confers tolerance to Fe deficiency, it also makes the mutants more sensitive to high Fe growth conditions [304]. Fe overaccumulation in the seed also explains why a number of *bts* mutants are non-viable, highlighting the important role of BTS in preventing Fe toxicity. The *bts/1 bts/2 (bts/1x2)* double mutant also shows enhanced Fe uptake and tolerance to Fe deficiency, although is not as sensitive to excess Fe as *bts-3* [304]. Fe accumulation in *bts/1x2* occurs through failure to maintain FIT protein turnover and reduce FIT protein accumulation under Fe sufficiency conditions, and consequently FIT-downstream genes involved in Fe uptake are constitutively upregulated [305]. Compared to the double mutant, *bts/1* and *bts/2* single mutants have been reported as having no obvious Fe phenotype [304, 329], although one study has shown that the *bts/2* mutant does appear to retain chlorophyll under Fe deficiency, showing a phenotype stronger than *bts/1*, but not as strong as the *bts/1x2* double mutant [304, 305].

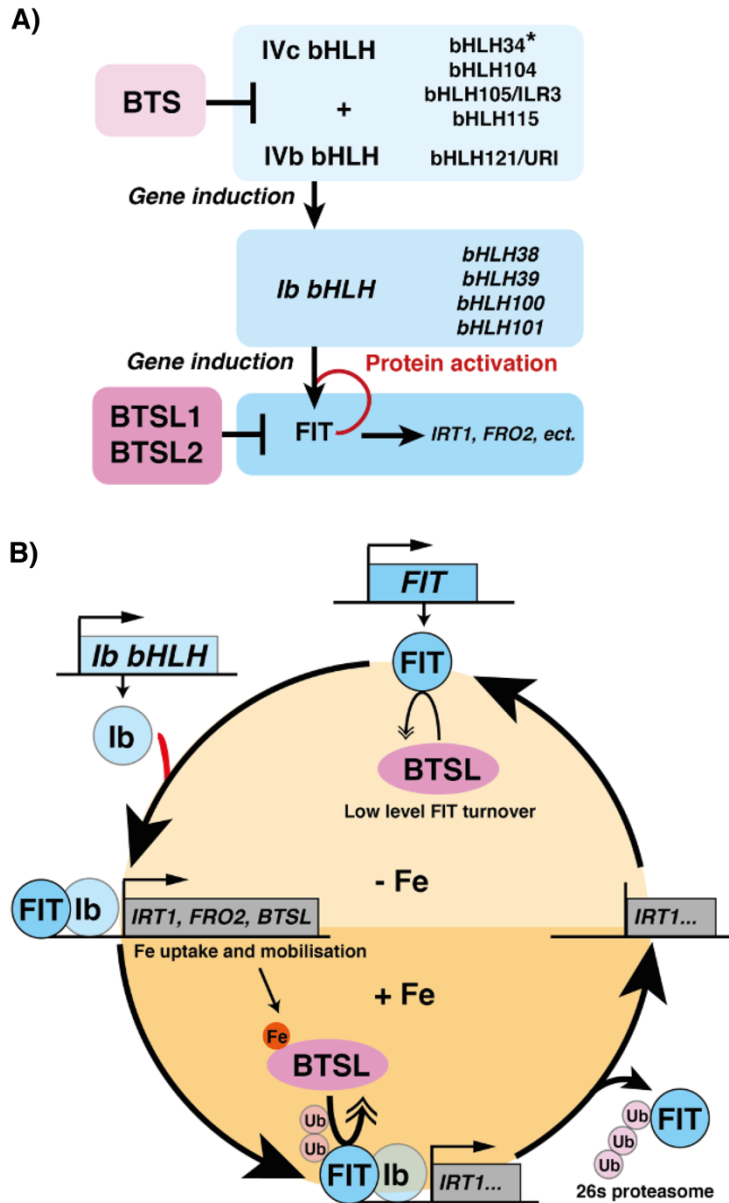


Figure 4.2: Role of BTS and BTSL proteins in the Fe deficiency transcriptional cascade.

A) BTS and BTSL targets within the bHLH transcription factor signalling cascade. Clade IVc (bHLH34, bHLH104, bHLH105/ILR3 and bHLH115) and Clade IVb (bHLH121/URI) bHLH transcription factors activate the expression of Clade Ib bHLH (*bHLH38*, *bHLH39*, *bHLH100* and *bHLH101*) genes [296, 301, 375, 413]. Ib bHLH proteins form stabilising interactions with FIT to induce expression of downstream genes, such as *IRT1* and *FRO2*, as well as *FIT* [301, 302, 308]. BTS targets IVc and IVb bHLH proteins, apart from bHLH34 (indicated by asterisk) [300, 306] and BTSL1 and BTSL2 proteins target FIT for proteasomal degradation in response to Fe sufficiency [304, 305]. Adapted from [308]. B) Model of BTSL1 and BTSL2 Fe-dependent targeting of FIT. Under Fe deficiency (-Fe), FIT is transcriptionally upregulated and FIT protein

accumulates, although is subject to low level turnover by BTSL proteins. FIT forms heterodimers with Ib bHLH transcription factors and activates the expression of Fe uptake genes as well as *BTSL1* and *BTSL2*. Increased Fe uptake (+Fe) stabilises BTSL proteins, promoting ubiquitination (Ub) and degradation of FIT protein, which in turn prevents excessive Fe uptake. Adapted from [305].

4.1.4 The *bts/2* mutant is tolerant to Zn excess

Another study investigating the role of BTSL proteins in *A. thaliana* characterised the Zn excess tolerance phenotype of the *bts/2* mutant, as demonstrated through increased biomass and chlorophyll content compared to wild type [329]. In wild type, Zn excess results in accumulation of Zn in all tissue types and Fe overaccumulation in roots, however in *bts/2* this metal overaccumulation is significantly reduced. Fe deficiency- and Zn excess-responsive genes, *ZIF1* and *FRO3*, also fail to be upregulated in *bts/2* shoots under Zn excess, an indication that the mutant is not showing transcriptional Zn stress responses [329]. Based on this phenotype, as well as evidence from microarray datasets that show *BTSL2* upregulation in response to both Fe deficiency and Zn excess [228, 303], a potential role for BTSL2 in Fe and Zn cross-homeostasis has been suggested.

The *bts/2* mutant is not the only example in which de-repression of the Fe deficiency response confers Zn excess tolerance. FIT-binding protein (FBP) was recently identified in a yeast two-hybrid screen for FIT-interacting proteins [201]. FBP is expressed in the root stele and in these cell types it inhibits FIT's ability to interact with its target promoters through binding to the bHLH domain. Consequently, *NAS1*, *NAS2* and *NAS4* genes are constitutively overexpressed in the *fbp* mutant, leading to an increase in root NA content [201]. Increased NA content promotes Zn sequestration in root vacuoles via the ZIF1 transporter, while enhancing Fe root-to-shoot translocation. The authors suggest that this phenotype shows that FBP acts as a point of Fe and Zn homeostatic interaction, modulating FIT activity to balance Fe and Zn distribution. With the strong Fe phenotype of the *bts/1 bts/2* mutant in mind, analysis of its growth phenotype on Zn excess could reveal an even more pronounced tolerance than is seen in *bts/2* or *fbp*, and

this offers further insight into the potential role BTSL proteins may play in Fe and Zn interactions.

4.1.5 Fe and Zn nutrition affect flowering time

While the current studies on *btsl* mutants describe the metal-associated seedling phenotypes, later stage developmental characteristics and soil phenotyping have not yet been investigated. With a lot of interest surrounding the manipulation of Fe and Zn homeostasis [414] centred on possible applications in biofortification, it is also important to see how changes in metal uptake and distribution might affect important yield-defining parameters such as development and flowering time.

Flowering time in plants is regulated by a number of environmental factors and abiotic signalling pathways, including deficiency or excess of macro- and micronutrients [415, 416]. Generally, nutrient stress is reported as inducing early flowering [417, 418], however conflicting reports in the literature suggest that correlation of nutrition with flowering time is not as straightforward as this. For example, while the majority of studies suggest that nitrate deficiency accelerates flowering time, extremely low nitrate availability actually causes a delay in flowering time, as is similarly seen under high nitrate, resulting in a U-shaped flowering response curve to nitrate availability in *A. thaliana* [419-421]. Compared to other heavy metals and macronutrients, there is not as much research surrounding the influence of Zn on flowering time, and most of this focusses on the more agriculturally relevant condition of Zn deficiency. Work in *Salvia* suggests that heavy metal stress from Pb, Cu or Zn delay flowering [422], as well as evidence that Zn concentration correlated positively with flowering time in *Arabidopsis arenosa* [423]. Zn deficiency has additionally been shown to delay flowering time in *A. thaliana* [424], so it is possible that flowering time may show a 'U-shaped' response curve to Zn as it does with nitrate. The mechanistic effect of Zn on flowering time is not fully understood, although a genome-wide association study (GWAS) has identified the *FLOWERING TIME (FT)* gene as a likely target [424], and excess Zn has also been linked to extended circadian period length [425].

There is also evidence of the impact of Fe on flowering time. Plastid Fe homeostasis and ferritins have been linked to floral development and fertility [426] as

well as shown to interact with components of the circadian period and regulate cycle length [371, 427]. Consistent with the delay in flowering on high Zn soil, Fe deficiency also results in a late flowering phenotype [427, 428]. Loss of function *bhlh100 bhlh101* mutants, which are hypersensitive to Fe deficiency, also show a further delay in flowering phenotype [428], so it is possible that *bts1x2* with the opposite Fe phenotype might be early flowering.

4.1.6 Aims of this chapter

Understanding the molecular mechanisms underlying the Zn tolerance phenotypes of *A. thaliana* mutants provides an opportunity to gain further insight into Zn and Fe cross-homeostasis, as well as to identify novel components involved in micronutrient interactions. Based upon the enhanced Fe uptake in *bts1* mutants and the Fe-mediated Zn tolerance phenotype observed in Fe homeostasis mutants, such as *fbp* and *bts12* [201, 329], it was hypothesised that the *bts1x2* double mutant would show Zn hypertolerance. The Zn tolerance phenotype could then be used to explore the potential role of BTSL proteins in Zn and Fe cross-homeostasis.

The first part of this chapter describes experiments characterising the *bts1* and *bts12* single mutants and *bts1x2* double mutant grown on varying Zn, Fe and Mn concentrations. The latter half focusses on analysing the Zn tolerance phenotype of the *bts1x2* mutant through elemental and gene expression analysis, as well as growth-stage based phenotyping of the entire life cycle. The overall aim was to further define the *bts1* mutant phenotypes and to create a model for the function of BTSL1 and BTSL2 proteins under Zn excess growth conditions, which could then be further explored using transcriptomics in **Chapter 5**.

4.2 Results

4.2.1 The *bts1x2* double mutant Zn tolerance phenotype

A double knockout mutant for *BTSL1* and *BTSL2* (*bts1x2*) was previously generated by Dr Jorge Rodriguez-Celma (John Innes Centre) through crossing of T-DNA

mutant lines obtained from the Nottingham Arabidopsis Stock Centre [305]. The mutant line for *BTSL1* (*bts1-1*, SALK_015054) contains an insertion in the second exon, which results in loss of *BTSL1* full length transcript [304]. The *BTSL2* mutant line (*bts2-2*, SALK_048470) contains an insertion in the sixth exon, which also results in complete loss of full length transcript (**Supplementary Figure B1, Appendix B**)[305].

In order to investigate whether the *bts1x2* double mutant showed tolerance to Zn excess, as had been previously described for the *bts2* single mutant [329], the phenotype of Col-0 (wild type), *bts1*, *bts2* and *bts1x2* on different Zn concentrations was characterised (**Figure 4.3**). Increasing Zn concentrations (50 μ M and 100 μ M ZnSO₄) resulted in a significant reduction in shoot biomass in all genotypes, with Col-0 biomass reduced by 41% between control (1 μ M) and 100 μ M Zn growth conditions, *bts1* by 24%, *bts2* by 25% and *bts1x2* by 39% (**Figure 4.3B**). Despite a similar reduction in shoot biomass for Col-0 and *bts1x2*, the double mutant was larger than Col-0 and the single mutants under control conditions, and as such under Zn excess *bts1x2* maintained a greater shoot biomass compared to Col-0, as do the single mutants (**Figure 4.3B**). Chlorophyll content was also impacted, with Col-0 and *bts1* already showing a 31% and 28% decrease at 50 μ M Zn respectively (**Figure 4.3C**). Col-0, *bts1* and *bts2* showed even more severe chlorosis when the media concentration was further increased to 100 μ M Zn, with a significant reduction in chlorophyll content of 63%, 51% and 41% respectively. In contrast, *bts1x2* chlorophyll levels were not significantly affected by Zn concentrations (**Figure 4.3C**). Primary root length was significantly reduced in all genotypes at higher Zn concentrations, and although *bts2* and *bts1x2* root length was significantly shorter under control growth conditions, Col-0 and *bts1* primary root length was far more impacted by increasing Zn, with 44% and 38% reductions in length at 100 μ M Zn respectively, compared to only 32% and 27% in *bts2* and *bts1x2* (**Figure 4.3D**). These results show that *bts1x2* was more tolerant to Zn excess than Col-0 and *bts1* single mutants, with the single mutants showing partial tolerance phenotypes.

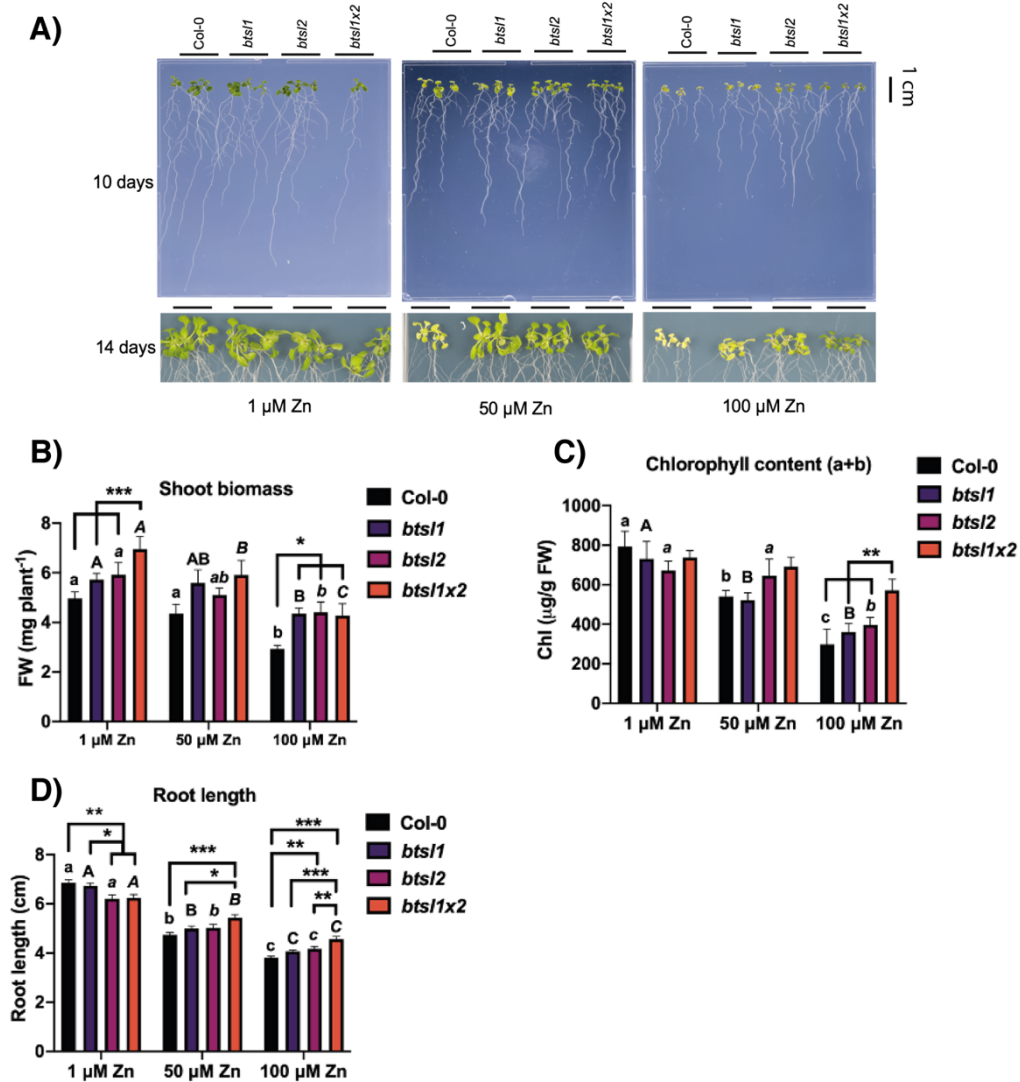


Figure 4.3: The growth phenotype of Col-0, *bts1*, *bts2* and *bts1x2* on varying Zn concentrations.

A) Representative photographs of Col-0, *bts1*, *bts2* and *bts1x2* 10-d-old and 14-d-old seedlings, B) shoot fresh weight (FW) and C) total chlorophyll content (chl) of 14-d-old seedlings and D) primary root length of 10-d-old seedlings grown continuously on modified Hoagland medium supplemented with increasing Zn concentrations (1 μM, 50 μM and 100 μM ZnSO₄). Data represent mean values (± SEM) from three independent experiments, each comprising six plants per genotype and condition. Statistically significant differences are indicated by asterisks (within conditions, *p < 0.05, **p < 0.01, ***p < 0.001) or letters (within genotype, p < 0.05) as determined by two-way ANOVA followed by Tukey HSD post-hoc test. Non-significant differences are not indicated.

4.2.2 The *bts1x2* mutant Fe deficiency tolerance phenotype

The *bts1x2* mutant has previously been shown to be more tolerant to Fe deficiency, with only *bts2* out of the single mutants showing any Fe phenotype [305]. In order to verify *bts1* mutant tolerance to low Fe under the growth conditions used here, the effect of different Fe concentrations on the growth of Col-0, *bts1*, *bts2* and *bts1x2* was investigated (**Figure 4.4**).

Fe deficiency (0 μ M Fe) significantly reduced shoot biomass in all genotypes, with a 48% reduction in Col-0 weight compared to control conditions (5 μ M Fe), 49% reduction in *bts1*, 53% reduction in *bts2*, and *bts1x2* the least affected with only a 40% reduction in shoot weight (**Figure 4.4B**). All of the *bts1* mutants retained a greater shoot biomass under low Fe growth conditions (**Figure 4.4B**). Reduced Fe concentrations cause severe chlorosis in Col-0 and *bts1*, with a 46% and 26% reduction in chlorophyll content respectively (**Figure 4.4C**). In contrast, *bts2* and *bts1x2* chlorophyll was not significantly affected by Fe deficiency and both maintained a significantly higher chlorophyll content than Col-0, with *bts1x2* chlorophyll concentration significantly higher than *bts1* as well (**Figure 4.4C**). Increasing Fe concentrations to 50 μ M had no significant effect on shoot biomass or chlorophyll content in any of the genotypes. Primary root length was reduced by Fe deficiency in all genotypes, with Col-0 length reduced by 53%, *bts1* by 43%, *bts2* by 31% and *bts1x2* by 34% (**Figure 4.4D**). Increasing media Fe content to 50 μ M lead to a significant 10% reduction in *bts1x2* primary root length compared to control conditions, and *bts2* and *bts1x2* root length also significantly shorter compared to Col-0 and *bts1* at this higher Fe concentration (**Figure 4.4D**). Reduced primary root length in *bts2* was already observed under control conditions (**Figure 4.4D**). Taken together, these data corroborate previous findings that *bts1x2* was more tolerant to Fe deficiency than Col-0 and the *bts1* single mutants [304], and both *bts1* and *bts2* also showed some Fe deficiency tolerance phenotypes. The reduction in primary root length seen in *bts2* and *bts1x2* at higher Fe concentrations, and in *bts2* under control conditions, could also suggest sensitivity to high Fe in these mutants. As *BTSL1* and *BTSL2* are partially functionally redundant, with *bts1x2* showing the strongest mutant phenotype, in agreement with [304], characterisation of *BTSL* gene function in Zn and Fe cross-homeostasis throughout the rest of this chapter is carried out in the double mutant.

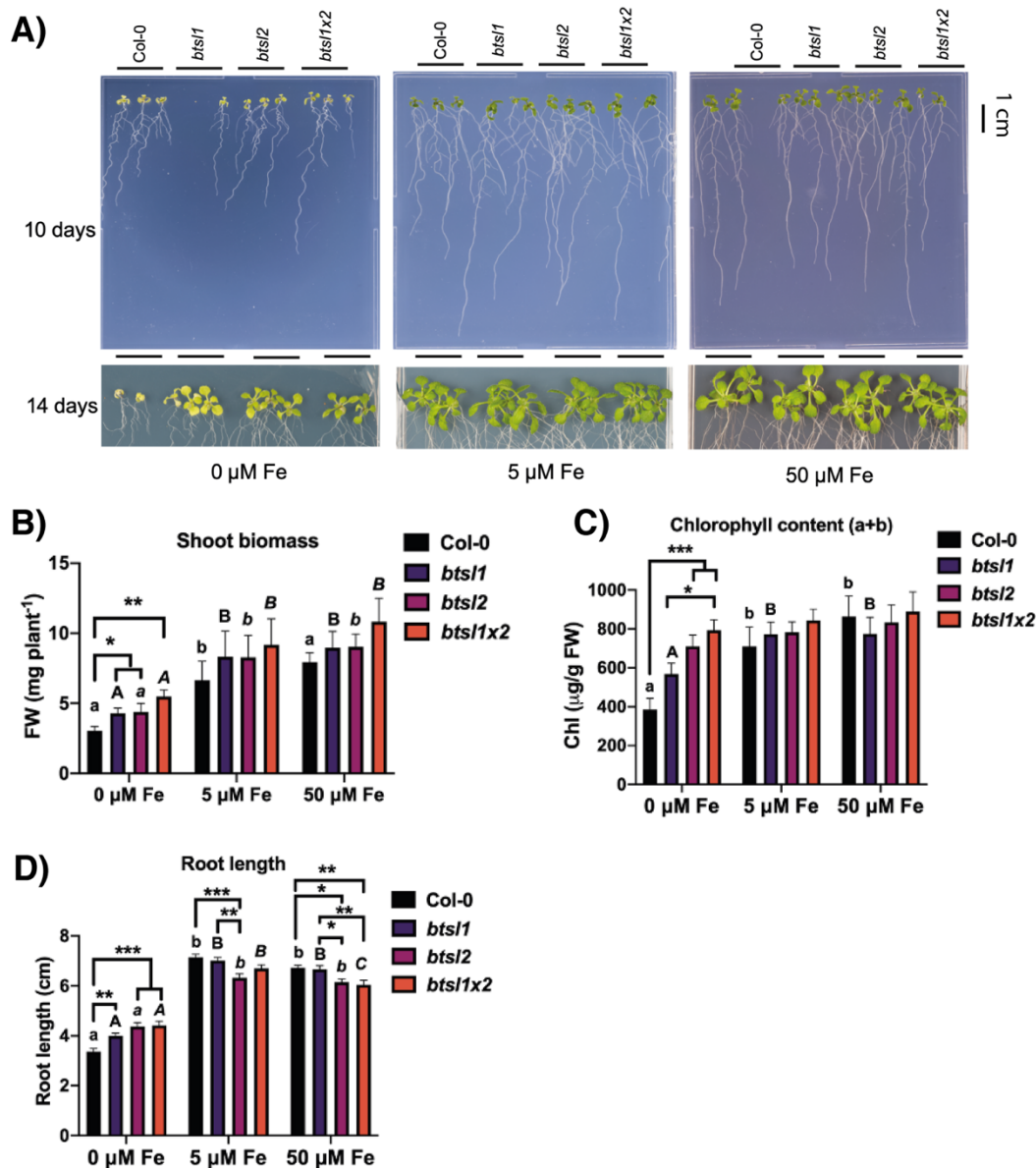


Figure 4.4: The growth phenotype of Col-0, *bts1*, *bts2* and *bts1x2* on varying Fe concentrations.

A) Representative photographs of Col-0, *bts1*, *bts2* and *bts1x2* 10-d-old and 14-d-old seedlings, B) shoot fresh weight (FW) and C) total chlorophyll content (chl) of 14-d-old seedlings and D) primary root length of 10-d-old seedlings grown continuously on modified Hoagland medium supplemented with increasing Fe concentrations (0 μM, 5 μM and 50 μM ZnSO₄). Data represent mean values (± SEM) from three independent experiments, each comprising six plants per genotype and condition. Statistically significant differences are indicated by asterisks (within conditions, *p < 0.05, **p < 0.01, ***p < 0.001) or letters (within genotype, p < 0.05) as determined by two-way ANOVA followed by Tukey HSD post-hoc test. Non-significant differences are not indicated.

4.2.3 The *bts1x2* mutant phenotype on varying Mn growth conditions

The broad substrate specificity of many divalent cation transporters, including the major Fe uptake transporter IRT1, means that altered Fe and Zn homeostasis has implications for the nutrition of other divalent micronutrients, such as Mn [170]. In order to investigate whether Mn homeostasis is also affected by loss of BTSL proteins, the growth phenotype for Col-0 and the *bts1x2* mutant on different Mn concentrations was investigated (**Figure 4.5**). Both Col-0 and *bts1x2* shoot biomass was significantly reduced by Mn deficiency (0 μ M Mn), however *bts1x2* was less impacted with a 67% biomass reduction compared to 79% in Col-0 (**Figure 4.5B**). Mn excess also resulted in significant biomass reductions, however *bts1x2* appeared more sensitive to high Mn growth conditions, with a 17% reduction in biomass already seen at 50 μ M Mn and 47% at 250 μ M Mn, compared to Col-0 which showed no change in biomass at 50 μ M and was reduced by only 37% at 250 μ M Mn (**Figure 4.5B**). Only Col-0 chlorophyll content was affected by changing Mn, with significant increases of 44% under Mn deficiency and 25% under Mn excess (**Figure 4.5C**). Altered chlorophyll content could be linked to altered Fe uptake under varying Mn growth conditions, however it was unusual that chlorophyll content was not reduced under deficiency conditions as would be expected. Primary root length was reduced in both genotypes in high Mn growth conditions, but there were no genotypic differences aside from the reduced *bts1x2* root length under control (5 μ M Mn) conditions, which was already noted in **4.2.1** and **4.2.2**, and at 50 μ M Mn (**Figure 4.5D**). Taken together, these data suggest that *bts1x2* was slightly more tolerant to Mn deficiency and sensitive to Mn excess than wild type, although it was a subtle phenotype.

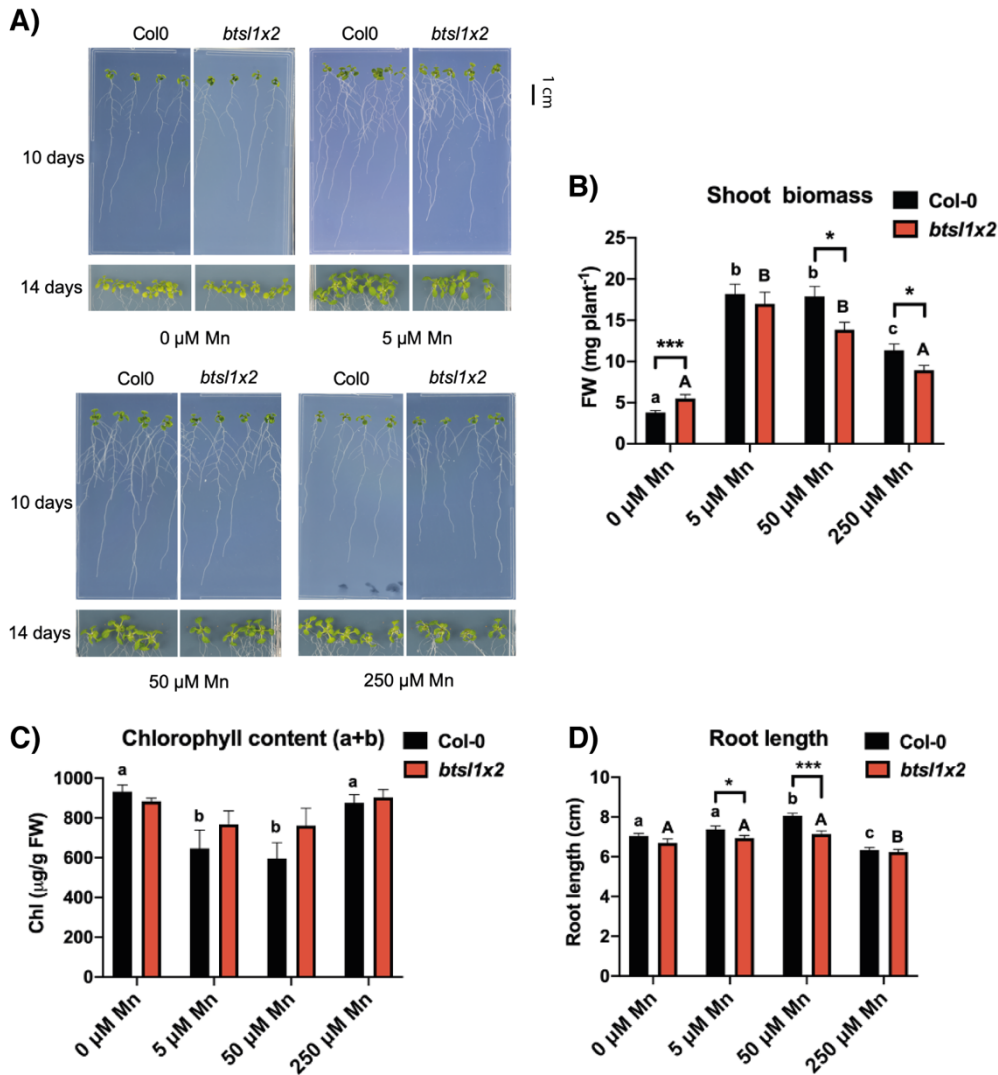


Figure 4.5: The growth phenotype of Col-0, *bts1*, *bts2* and *bts1x2* on different Mn concentrations.

A) Representative photographs of Col-0, *bts1*, *bts2* and *bts1x2* 10-d-old and 14-d-old seedlings, B) shoot fresh weight (FW) and C) total chlorophyll content (chl) of 14-d-old seedlings and D) primary root length of 10-d-old seedlings grown continuously on modified Hoagland medium supplemented with increasing Mn concentrations (0 μM, 5 μM and 50 μM and 250 MnSO₄). Data represent mean values (± SEM) from three independent experiments, each comprising six plants per genotype and condition. Statistically significant differences are indicated by asterisks (within conditions, *p < 0.05, **p < 0.01, ***p < 0.001) or letters (within genotype, p < 0.05) as determined by two-way ANOVA followed by Tukey HSD post-hoc test. Non-significant differences are not indicated.

4.2.4 Zn, Fe and Mn content of *bts/1x2* mutant under Zn excess

The Fe and Mn deficiency tolerance phenotype of the *bts/1x2* mutant could be linked to increased Fe and Mn uptake capacity. Fe and Mn can compete with Zn for uptake and translocation, which could reduce shoot Zn content and confer tolerance to excess Zn. In order to test the contribution of altered metal content and distribution to *bts/1x2* Zn hypertolerance, the Fe, Zn and Mn content of shoots and roots under Zn excess was investigated by ICP-OES. Under control conditions (1 μM Zn), there was no significant difference in the Zn content in shoots or roots between Col-0 and *bts/1x2*, with both roughly having a root-to shoot (root/shoot) ratio of 1 (**Figures 4.6A and B**). Under Zn excess (100 μM Zn), both genotypes showed a significant increase in shoot and root Zn concentrations, with Col-0 shoot and root Zn content increasing 23-fold and 89-fold respectively, and *bts/1x2* shoot and root Zn content by 17-fold and 69-fold (**Figure 4.6A**). Although *bts/1x2* accumulated 15% less Zn in shoot tissues compared to Col-0 under Zn excess, both genotypes still showed a similar increase in Zn root/shoot ratio to ~ 3.8 (**Figures 6A and B**). The similar ratio was likely due to a lower, but non-significant, Zn root content in *bts/1x2* under Zn excess as well.

Under control conditions, *bts/1x2* accumulated significantly more Fe in shoots than Col-0, but there was no genotypic difference in root Fe or root/shoot ratio (**Figures 4.6C and D**). At increasing Zn concentrations, shoot Fe content was not significantly impacted, although it was slightly reduced in both genotypes. However, root Fe concentrations increased 5-fold and 2-fold in Col-0 and *bts/1x2* respectively (**Figure 4.6C**). The increased root Fe content resulted in a notable increase in the Fe root/shoot ratio to 8.2 for Col-0 and to 3 for *bts/1x2* (**Figure 4.6D**). As such, Zn excess reduced Fe translocation to shoots in both genotypes, although *bts/1x2* was less affected than Col-0.

Zn exposure and loss of BTSL proteins also affected Mn content. Under control conditions, *bts/1x2* shoot Mn was 20% greater than Col-0, but under Zn excess it was 11% lower than Col-0 (**Figure 4.6E**). Root Mn content was dramatically reduced in both genotypes under Zn excess, leading to a reduction in Mn root/shoot ratio, although there was no genotypic difference (**Figure 4.6E and F**). Thus, Zn was able to outcompete Mn

for uptake under Zn excess, and additionally in *bts/1x2* Mn translocation to the shoot was reduced.

Taken together with the Fe data, the *bts/1x2* mutant showed enhanced Fe and Mn uptake under control conditions, which supports association of the Zn tolerance phenotype with enhanced Fe and Mn nutrition in *bts/1x2*. However, the overall Fe and Mn concentration under Zn excess was lower in *bts/1x2*, which suggests that metal distribution and ratios, rather than total concentration, underlie the Zn tolerance phenotype. It has previously been shown that increasing shoot Fe concentration can ameliorate the detrimental effects of Zn excess, even when shoot Zn levels are at toxic concentrations [212]. Indeed, Fe-mediated Zn tolerance was observed when Col-0 and *bts/1x2* are grown under Zn excess conditions supplemented with increasing Fe (**Supplementary Figure B2, Appendix B**). Thus, the Zn-to-Fe (Zn/Fe) ratio was also investigated to see if the Zn tolerance phenotype of *bts/1x2* could be linked to a reduced Zn/Fe content in shoots. Under control conditions, the Zn/Fe ratio was close to 1 for both genotypes in shoots and roots, although the *bts/1x2* shoot Zn/Fe ratio was 22% lower than Col-0 due to the increased Fe content (**Figure 4.6G**). The accumulation of Zn in all tissues under Zn excess caused a significant increase in the Zn/Fe ratio in shoots and roots of both genotypes, with the ratio in Col-0 shoots increasing by 36-fold and roots by 16-fold, and in *bts/1x2* shoots by 24-fold and roots by 31-fold (**Figure 4.6G**). In comparison to Col-0 under Zn excess, the *bts/1x2* shoot ratio was 33% lower and the root ratio 94% higher (**Figure 4.6G**).

Taken together, these data show that the *bts/1x2* mutant has enhanced Fe and Mn uptake under standard growth conditions, which is consistent with previous work by Hindt *et al.* [304]. Under Zn excess the mutant maintained a higher degree of Fe translocation to the shoot and shoot Zn accumulation is reduced. Subsequently, *bts/1x2* shoot Zn/Fe ratio was reduced, decreasing competition for Fe binding sites and Zn toxicity symptoms. Moreover, *bts/1x2* showed reduced Fe overaccumulation in roots under Zn excess, which could suggest changes in Fe uptake capacity under these conditions.

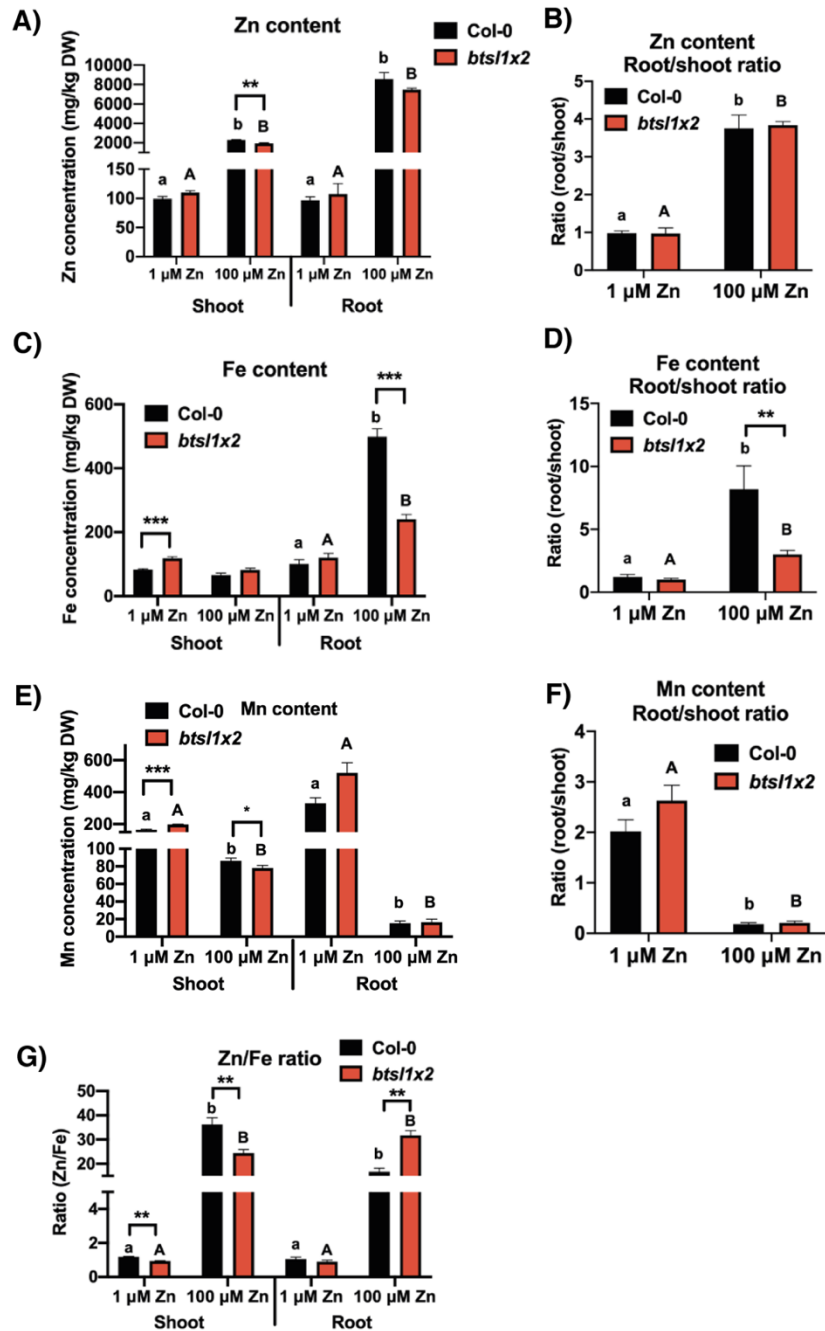


Figure 4.6: Zn, Fe and Mn accumulation in Col-0 and *bts1x2* roots and shoots under Zn excess.

The accumulation and root-to-shoot (root/shoot) ratio of A-B) Zn, C-D) Fe, E-F) Mn and G) the Zn-to-Fe (Zn/Fe) ratio in Col-0 and *bts1x2* 14-d-old seedlings grown continuously on standard (1 μM) or Zn excess (100 μM) agar plates. Data represent mean values (\pm SEM) from three independent experiments, each comprising ten plants per genotype and condition. Statistically significant differences are indicated by asterisks (within conditions, * $p < 0.05$, ** $p < 0.01$, *** $p < 0.001$) or letters (within genotype, shoots and roots analysed separately $p < 0.05$) as determined by two-way ANOVA followed by Tukey HSD post-hoc test. Non-significant differences are not indicated.

4.2.5 The *bts1x2* mutant constitutive Fe deficiency root response

The reduced root Fe accumulation in *bts1x2* under Zn excess compared to Col-0 cannot easily be explained through enhanced Fe translocation to the shoot, as the shoot Fe content is not increased accordingly. The root Fe overaccumulation phenotype was verified through Perls' staining followed by DAB intensification, which is used to indicate the presence of Fe³⁺, Fe²⁺ and H₂O₂. Col-0 showed strong apoplastic staining along the entirety of the mature root ('1' and '2') under Zn excess, while *bts1x2* notably only showed Fe accumulation in root hairs at the top of the root ('1', **Figure 4.7A**).

In order to investigate whether this reduced root Fe accumulation in *bts1x2* was associated with lower expression of Fe uptake genes under Zn excess, qRT-PCR analysis of *IRT1* and *FRO2* expression under Fe deficiency and Zn excess was carried out (**Figure 4.7B**). *IRT1* and *FRO2* were chosen as they encode the main transporter and ferric chelate reductase involved in Strategy I Fe uptake at the root surface [164, 165], and previous research has also shown that these genes are constitutively overexpressed in *bts1* mutants under control and low Fe conditions [304, 305]. Within genotypes, *IRT1* and *FRO2* were significantly upregulated in response to Fe deficiency and Zn excess in Col-0 and *bts1x2*, with similar upregulation seen under both conditions (**Figure 4.7B**). However, both genes were highly overexpressed in *bts1x2* under Fe deficiency, with *IRT1* showing 154-fold upregulation compared to 40-fold in Col-0, and *FRO2* upregulated 129-fold compared to only 39-fold in Col-0 (**Figure 4.7B**).

The same overexpression pattern was also seen in *bts1x2* under Zn excess, with *IRT1* upregulated 156-fold in *bts1x2* compared to 46-fold in Col-0, and *FRO2* 120-fold upregulated in *bts1x2* compared to 23-fold in Col-0 (**Figure 4.7B**). *IRT1* and *FRO2* also showed significant upregulation in *bts1x2* under control conditions, with 34-fold and 23-fold upregulation respectively compared to Col-0 control expression, which was normalised to 1 (**Figure 4.7B**).

As the reduced *bts1x2* root Fe accumulation cannot be explained by reduced transcription of Fe uptake genes, it was possible that post-transcriptional regulation was responsible. Ferric-chelate reductase (FCR) assays are used as a readout of *FRO2* activity, which has been shown to undergo post-transcriptional inhibition under non-Fe deficiency conditions [173]. FCR activity was significantly elevated in both Col-0 and

bts1x2 in response to Fe deficiency and Zn excess as expected from upregulation of *FRO2* transcript under these conditions (**Figure 4.7C**). While FCR activity levels were similar under both low Fe and high Zn for *bts1x2* and thus correlated closely with expression data, in Col-0 FCR activity under Zn excess was half that seen under Fe deficiency (**Figure 4.7C**). Taken together, the constitutive upregulation of Fe uptake genes in *bts1x2* roots and enhanced Fe uptake capacity previously observed under low Fe conditions, was also extended into Zn excess growth conditions. Furthermore, Fe overaccumulation in roots under Zn excess does not affect the transcription of Fe uptake genes but does lead to post-transcriptional inhibition of FRO2 activity in Col-0. Reduced FCR activity and deep Perls' staining in Col-0 under Zn excess could suggest that the high root Fe content in Col-0 could be due to apoplastic Fe³⁺ accumulation.

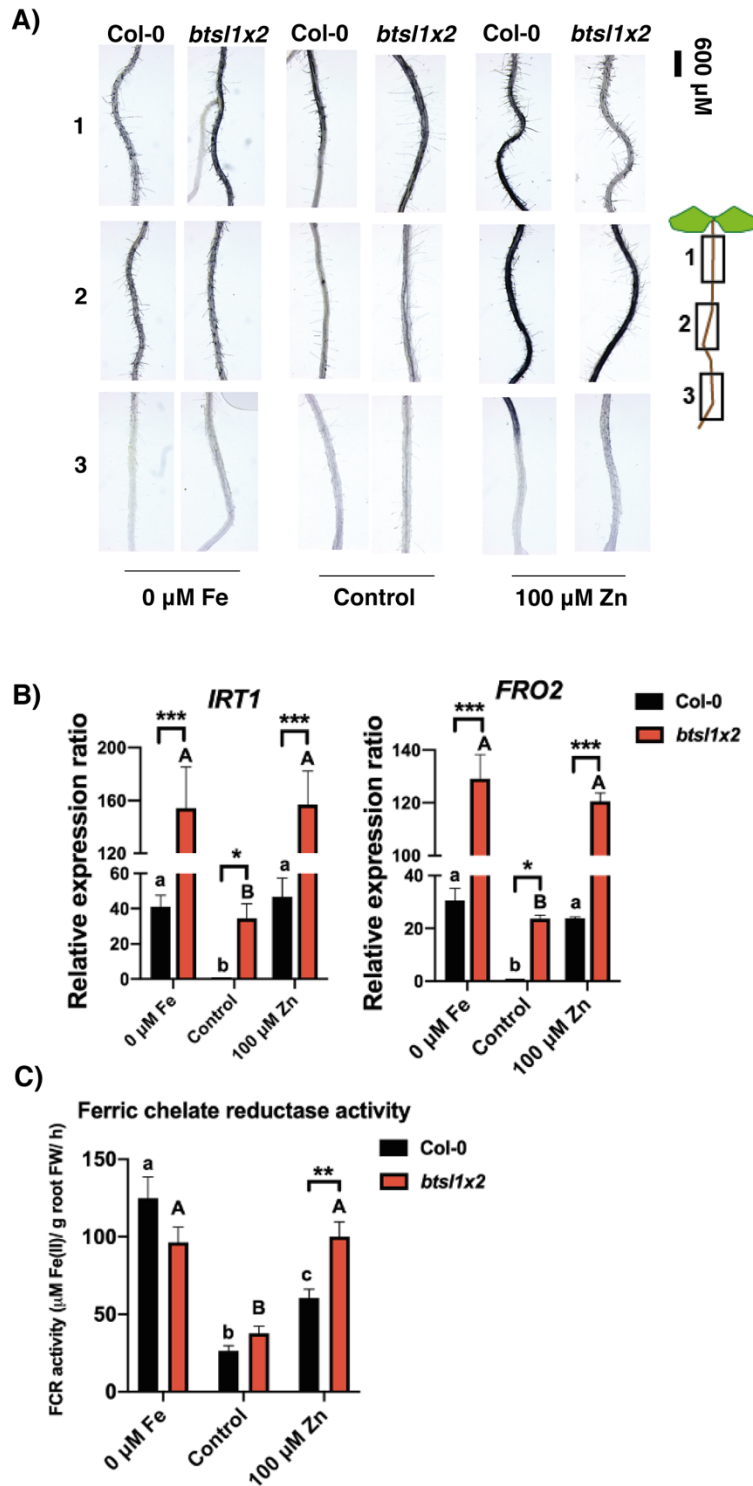


Figure 4.7: Perls' staining, *IRT1* and *FRO2* expression and ferric chelate reductase activity of Col-0 and *bts1x2* roots under Fe deficiency and Zn excess.

A) Representative photos of Fe accumulation along the root apoplast (1 = mature zone (top of the root); 2 = mature zone (mid-root); 3 = elongation/differentiation zone) of 7-d-old Col-0 and *bts1x2* seedlings as shown through Perls' staining followed by DAB intensification. B) qRT-PCR analysis of Fe uptake genes, *IRT1* and *FRO2*, in roots of 14-d-old seedlings. Fold change is relative

to Col-0 control (expression level set as “1”) and normalised to reference genes *ACTIN2* and *TIP41*. Data represent mean values (\pm SEM) from three independent experiments, each comprising five plants per genotype and condition, and each repeated as three technical replicates. C) Ferric chelate reductase (FCR) activity in roots of 10-d-old Col-0 and *bts1x2* seedlings. Data represent mean values (\pm SEM) from three independent experiments, each comprising four plants per genotype and condition. Seedlings were grown continuously on Fe deficiency (0 μ M FeHBED), control (5 μ M FeHBED, 1 μ M ZnSO₄) or Zn excess (100 μ M ZnSO₄) agar plates. Statistically significant differences are indicated by asterisks (within conditions, * p < 0.05, ** p < 0.01, *** p < 0.001) or letters (within genotype, p < 0.05) as determined by two-way ANOVA followed by Tukey HSD post-hoc test.

4.2.6 The *bts1x2* mutant is late flowering and has increased growth rate

Plant nutrition strongly influences developmental timing, with both Zn and Fe deficiency shown to delay flowering time, as well as mutations in Fe homeostasis regulators [424, 427, 428]. As *bts1x2* shows altered metal content, it was hypothesised that the mutant would also show changes in developmental timing, as is seen in *bhlh100* *bhlh101* mutants [428]. Growth stage-based phenotyping as described by Boyes *et al.* [332] was carried out on Col-0 and *bts1x2* grown on Zn excess supplemented agar plates and soil. Plate-based phenotyping of early developmental stages showed no significant difference in timing of developmental progression between genotypes or Zn treatment (**Figure 4.8A**). Later stage development was monitored on soil that was supplemented through watering with either 1000 mg ZnSO₄ kg⁻¹ DW soil or no Zn. In Col-0, Zn supplementation delayed flowering by 3 days, starting from the emergence of the first flower bud (5.10) to the end of flowering (6.9, **Figure 4.8B**). This delay in flowering was even more pronounced in *bts1x2*, irrespective of Zn treatment, with the end of flowering occurring 10 days later compared to Col-0 control (**Figures 4.8B and C**). Zn supplementation of *bts1x2* caused delays in rosette growth early on (1.10) and also in emergence of the first flower bud (5.10), but developmental progression was comparable to *bts1x2* control conditions by the end of flowering (**Figure 4.8B**).

Next, growth rate was calculated through measuring rosette surface area between 16 and 30 days old (**Figure 4.9**). Zn treatment significantly impacted rosette size

and growth rate in both genotypes (**Figures 4.9A-D; Supplementary Figure B3, Appendix B**). Genotypic differences in rosette size were not apparent until 28 days old, where *bts1x2* started showing significantly greater rate of rosette expansion and rosette size (**Figures 4.9B-D; Supplementary Figure B3, Appendix B**). The *bts1x2* mutant also showed increased rosette diameter and leaf number at bolting, which could suggest that the increased rosette size was associated with the delay to floral transition as has been shown in *A. thaliana* grown on Zn deficient soils (**Figures 4.9E and F**)[424]. Taken together, the *bts1x2* Zn tolerance phenotype was also extended to soil growth conditions, and any Zn-dependent impact on developmental timing in the mutant was not apparent at the end of growth. The *bts1x2* mutant showed a delay in floral transition and increased growth rate under both Zn sufficiency and excess, which could be linked to the altered metal content and distribution of *bts1x2*.

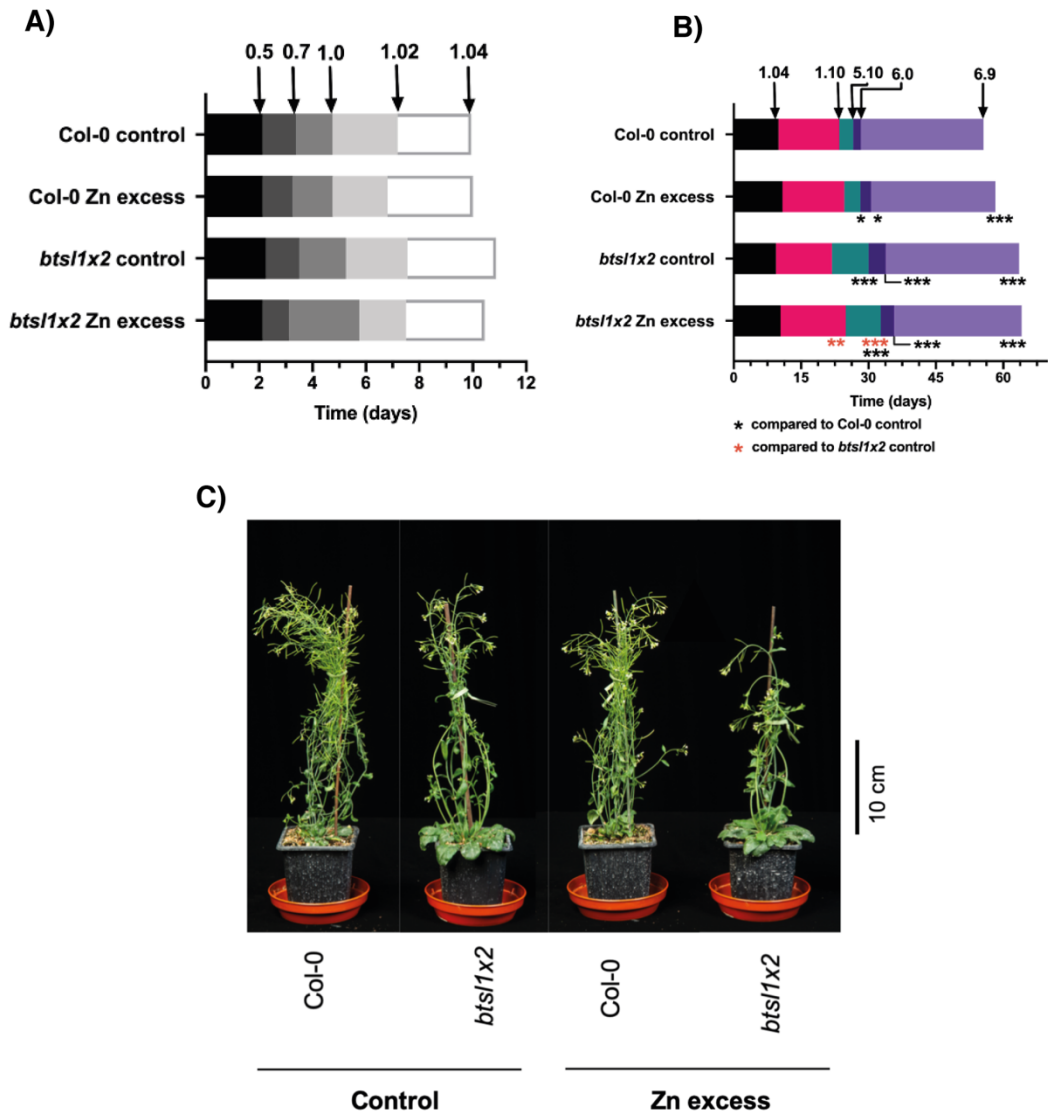


Figure 4.8: Stage-based growth phenotyping of Col-0 and *bts1x2* under Zn excess.

Progression of Col-0 and *bts1x2* development when grown on A) agar plates supplemented with control (1 μM) or excess (100 μM) ZnSO_4 and B) soil supplemented with Zn (1000 mg kg^{-1} DW soil) or without (control). Arrows indicate the day that the growth stage defined by the associated number was reached and size of the blocks the number of days between growth stages. Data represent mean values from three independent experiments, each comprising ten plants per genotype and condition. Statistically significant differences are indicated by asterisks (* $p < 0.05$, ** $p < 0.01$, *** $p < 0.001$) as determined by two-way ANOVA followed by Tukey HSD post-hoc test. Non-significant differences are not indicated. 0.5 = radicle emergence; 0.7 = hypocotyl and cotyledon emergence; 1.0 = cotyledons fully open; 1.02 = 2 rosette leaves > 1 mm; 1.04 = 4 rosette leaves > 1 mm; 1.10 = 10 rosette leaves > 1 mm length; 5.10 = first flower buds visible; 6.0 = first flower open; 6.9 = flowering complete. C) Representative photos of 50-d-old Col-0 and *bts1x2* plants used for the soil-based phenotyping.

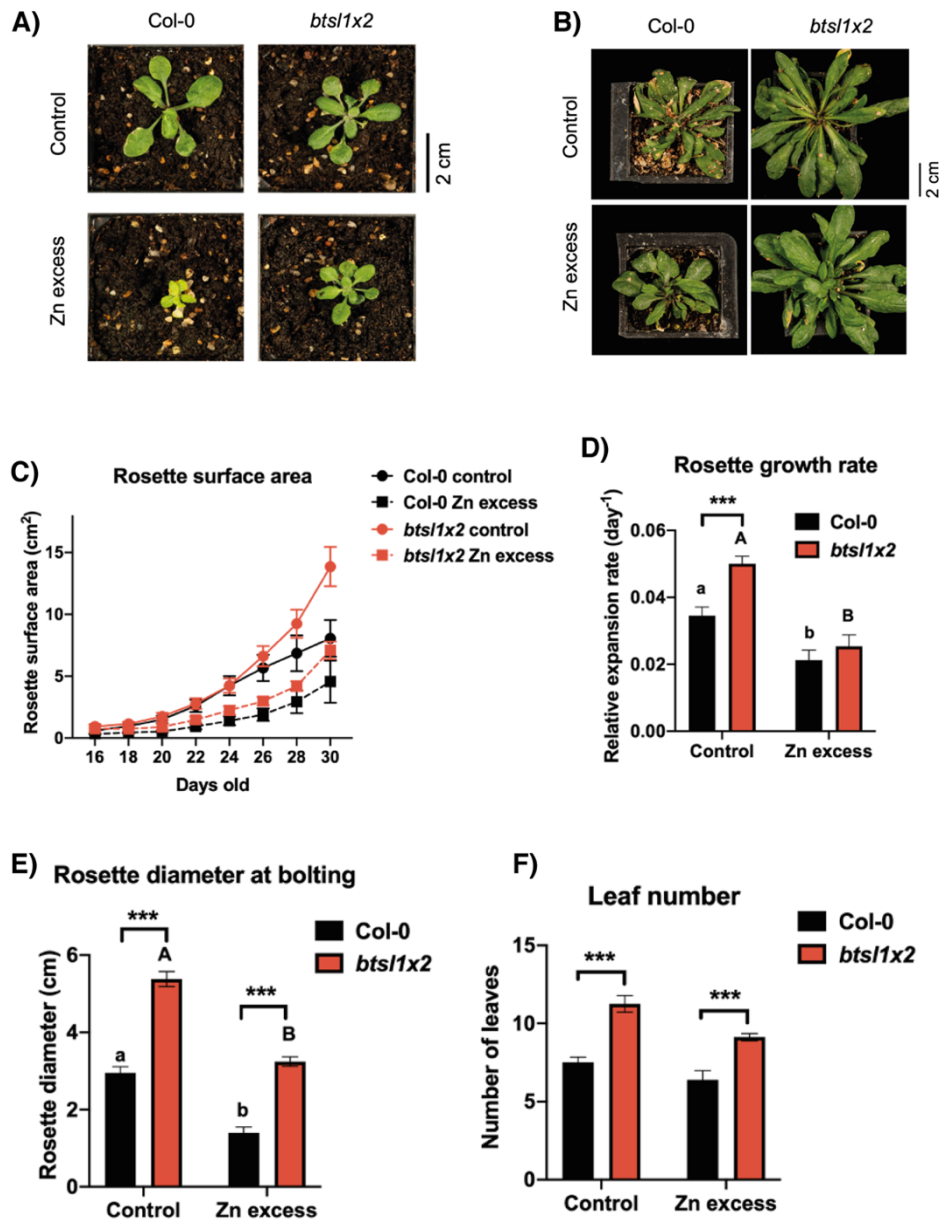


Figure 4.9: Rosette phenotyping of Col-0 and *bts1x2* grown on Zn excess soil.

Representative photos of Col-0 and *bts1x2* plants grown on control and Zn excess soil at A) 22-d-old and B) 50-d-old with the bolts removed. C) Rosette surface area measurement of Col-0 and *bts1x2* plants grown on control and Zn excess soil from 16-d-old to 30-d-old. D) Rosette growth rate (day⁻¹) calculated by the gradient of a linear fit model applied to data from **Figure 4.9C** represented as log(rosette surface area mm²) against age (days old). E) Rosette diameter and F) leaf number at the start of bolting. Data represent mean values (\pm SEM) from three independent experiments, each comprising ten plants per genotype and condition. Statistically significant differences are indicated by asterisks (within conditions, * $p < 0.05$, ** $p < 0.01$, *** $p < 0.001$) or letters (within genotype, $p < 0.05$) as determined by two-way ANOVA followed by Tukey HSD post-hoc test.

4.3 Discussion

4.3.1 BTSL1 and BTSL2 have partial functional redundancy

In this chapter, characterisation of the *bts1* and *bts2* single mutants alongside the *bts1x2* double mutant demonstrates the intermediate phenotype of the single mutants, confirming the partial redundancy of these two genes (**Figures 4.3 and 4.4**). Some previous reports have suggested that the *bts/* single mutants have no obvious Fe phenotype [304, 329], but the data shown here are consistent with other findings that *bts2* shows an Fe deficiency tolerance phenotype, although it is less pronounced than the *bts1x2* Fe tolerance phenotype (**Figure 4.3**)[305]. The *bts2* Zn tolerance phenotype was also replicated, although the phenotype does not appear as obvious as previously found, with no significant chlorophyll retention (**Figure 4.5**)[329]. In comparison to *bts2*, *bts1* appears phenotypically closer to wild type, with the only obvious metal phenotype being increased shoot biomass compared to wild type under Zn excess and Fe deficiency (**Figures 4.3 and 4.4**). The slightly stronger *bts2* phenotype suggests that BTSL2 may play a more predominant role than BTSL1. This could be related to the differences in expression pattern between the *BTSL* genes, with *BTSL2* expressed across more cell types than *BTSL1* [305]. *BTSL2* is also mainly expressed in the differentiation zone with root hairs, an important area of nutrient uptake, as well as in the stele which is an important centre for regulation of Fe transport, and correlates more closely with *FIT* expression patterns [303, 429]. In comparison *BTSL1* is mainly expressed in the upper half of the root [305]. Additional experiments exploring parameters which might affect protein activity, such as differences in bHLH targets, metal-binding kinetics and spatio-temporal expression at the cellular level, are needed to fully elucidate the functional differences between BTSL1 and BTSL2. In **Chapter 5**, gene expression analysis of selected Fe-deficiency responsive genes in the *bts/* single and double mutants under Fe deficiency and Zn excess further explores phenotypic differences between BTSL1 and BTSL2.

4.3.2 BTSL1 and BTSL2 proteins regulate Fe, Zn and Mn uptake

The broad substrate specificity of many Fe transporters, notably the major Fe uptake transporter IRT1 [170, 430] and a number of other ZIP transporters [156], results in Fe homeostasis perturbations impacting the nutrition of other divalent cations, such as Zn, Mn and Cu [431-433]. Upregulation of these transporters under Fe deficient conditions results in Zn and Mn overaccumulation, and vice versa [203, 212, 304, 328, 434]. The constitutive upregulation of FIT-dependent Fe uptake genes under control conditions in *bts1x2* results in Fe and Mn accumulation in shoots (**Figure 4.6**). Then under Zn excess, Mn and Zn shoot accumulation is reduced, as is root Fe accumulation compared to wild type (**Figure 4.6**). Thus, BTSL activity not only regulates Fe uptake, as the current model for its role in Fe homeostasis would suggest, but also Zn and Mn uptake, and Fe translocation. The influence that BTSL proteins exert on Zn and Mn could be a secondary consequence of the altered expression of Fe transporters with a broad substrate specificity that BTSL regulates, with BTSL only interacting with Fe ions or signalling proteins. Alternatively, Zn and Mn may also be able to interact with BTSL proteins through direct binding or homeostasis signalling components, and thus BTSL proteins could be regulators of these metal homeostasis networks as well. At present, it is clear that the cross-talk between these networks is affected by genes indirectly downstream of BTSL activity, and as such suggests a role for BTSL proteins in Fe, Zn and Mn cross-homeostasis. By regulating Fe, Zn and Mn in a co-ordinated manner this could help balance the homeostasis of these nutrients and prevent secondary nutrients deficiency and excesses. A proteomics or transcriptomics approach could be utilised to identify which genes and proteins in addition to *IRT1* are responsible for the altered Zn and Mn homeostasis, as well as to look for candidates that could signpost other cationic micronutrient networks that may be misregulated in the mutant, such as Cu and Ni.

There are also well-documented links between Fe and phosphate homeostasis, with phosphate able to complex Fe into insoluble precipitates in soils and consequently phosphate excess results in activation of the Fe deficiency response [435]. Zn is further involved in this interaction, resulting in complicated tripartite interaction between Fe, Zn and phosphate signalling pathways [436]. As such, it would be interesting to see if phosphate homeostasis is also affected by loss of *BTSL1* and *BTSL2* or if the *bts1x2*

mutant also shows a phosphate excess tolerance phenotype. The transcriptomics carried out in **Chapter 5** looks to explore the misregulation of genes involved in the homeostasis of non-Fe nutrients.

4.3.3. *bts1x2* enhanced Fe uptake capacity confers Fe-mediated Zn tolerance

Despite accumulating high levels of Zn in shoots, the *bts1x2* mutant does not show severe Zn toxicity symptoms (**Figures 4.3 and 4.6A**). The reduced shoot Zn/Fe ratio observed in the mutant under Zn excess compared to wild type suggests that there is less competition between Zn and Fe protein binding sites and ultimately maintaining shoot Fe proteome function (**Figure 4.6G**). A similar Fe-mediated Zn tolerance can be achieved through supplying additional Fe in the growth medium under Zn excess (**Supplementary Figure B2, Appendix B**) [212]. The *bts1x2* tolerance phenotype is also reminiscent of the *A. halleri* Zn hyperaccumulator, which shows a similar shoot Fe-Zn balance but through the opposite mechanism of low-level *FIT* and *IRT1* expression to limit leaky uptake of Zn [212]. Fe-mediated Zn tolerance is achieved through these two divergent mechanisms because of the nature of Fe and Zn competition, whereby Zn is prioritised for translocation and Fe is prioritised for uptake, with increasing Fe root content slowing Zn uptake into the plant [212]. Thus, by increasing the root Fe concentration before high levels of Zn accumulate, plants are able to maintain Fe translocation and reduce Zn shoot accumulation. In *A. halleri* this is accomplished by strictly regulating Zn influx through Fe transporters, and in *bts1x2* by greatly enhancing Fe availability in the environment through high FRO2 activity, and consequently Fe uptake and translocation over Zn. In contrast, wild type *A. thaliana* does not activate the root Fe deficiency response until Zn interferes with shoot Fe sensing, likely mediated by BTS, by which point the Fe-Zn balance is already in the favour of Zn [27].

A contributing factor to the suppression of *A. halleri* *IRT1* expression is that conservation of Fe shoot content prevents deficiency signalling from shoots [432]. Reduced chlorosis and Zn toxicity symptoms in *bts1x2* shoots suggests that shoot Fe deficiency signalling in the mutant is also likely suppressed. However, this would mean antagonistic Fe signalling between shoots and roots, or a root insensitivity to shoot-borne Fe signals, with shoots showing Fe sufficiency but roots showing a heightened Fe

deficiency response. Current models suggest that BTSL proteins act as primary Fe-sensors for local Fe fluctuations, while BTS is the internal Fe sensor responding to shoot signalling [305]. However, the phenotype presented here hints at a role for BTSL proteins in responding to systemic Fe signalling. Further investigation of the BTSL proteins function in responding to local and systemic signals is carried out in **Chapter 5**.

A drawback of the experimental approach taken here is that it is a static snapshot of the response to continuous growth on Zn excess conditions. A number of approaches allowing non-invasive real-time imaging and tracking of nutrient uptake and distribution have been developed, such as gamma-ray imaging [437], other real-time radioisotope imaging systems [438, 439] and Förster resonance energy transfer (FRET) imaging [440]. It would be interesting to test the spatio-temporal mechanism of Fe-mediated Zn tolerance proposed here for *bts/1x2* using some of these techniques. Spatio-temporal nutrient distribution could be combined with modelling analyses which could incorporate how changes in transporter and chelator abundance with differing substrate affinities affects nutrient homeostasis balance.

4.3.4 BTSL1 and BTSL2 attenuate FIT-dependent gene expression under Fe deficiency and Zn excess

The currently proposed function of BTSL proteins in Fe homeostasis centres around their role in preventing Fe uptake under Fe sufficiency growth conditions through promoting FIT degradation [305]. The importance of regulating FIT protein abundance is demonstrated in the Fe and Mn excess sensitivity phenotype of *bts/1x2* (**Figures 4.5; Supplementary Figure B2, Appendix B**) [304, 305]. BTSL proteins also maintain continual FIT protein turnover under all growth conditions, such that a small responsive pool of FIT protein is available to rapidly respond to changes in Fe availability an abiotic signalling [304, 305]. The value of regulating FIT abundance even when it is active under Fe deficiency was appreciated as an important regulatory mechanism prior to BTSL identification [441, 442]. Low-level FIT turnover under Fe deficiency and Zn excess conditions could be demonstrated through the attenuated *IRT1* and *FRO2* expression observed in wild type compared to *bts/1x2* (**Figure 4.7**). Interestingly, FIT-dependent

gene expression is attenuated to a similar degree under both conditions, which could suggest a similar mechanism or signal is regulating BTSL activity under these conditions. Fe-dependent BTSL stabilisation through HHE binding is the popular model for regulation of BTSL activity [305], however root Fe content varies greatly between Fe deficiency and Zn excess, so Fe concentration alone is unlikely to be the signal. Zn has also been found bound to the HHE domains of closely related BTS and HRZ proteins [407] and Zn accumulation occurs under both growth conditions. As such, it is possible that Zn may be capable of binding BTSL HHE domains and controlling their activity, and thus BTSL proteins could be regulated by a Zn/Fe ratio rather than absolute Fe concentration itself. It would be interesting to carry out metal binding assays with the BTSL proteins and additionally see how this affects ubiquitination activity.

In contrast, failure to turnover Fe-deficiency activated FIT protein leads to accumulation and strong overexpression of FIT-dependent genes in the *bts1x2* mutant [305]. However, overexpression of *FIT* and protein accumulation alone is not sufficient to activate downstream Fe deficiency responses [303] and requires heterodimer formation with *lb* bHLH transcription factors [301, 302]. There is evidence that *bHLH38* and *bHLH39* are also overexpressed in *bts1x2* [305], which could suggest that further upstream regulators, such as *IVc* bHLH or *bHLH121/URI*, are also misregulated in *bts1x2*. The transcriptomics carried out in **Chapter 5** looks to identify additional FIT-independent differentially expressed genes in *bts1x2* that could explain *lb* bHLH overexpression and subsequent FIT activation.

4.3.5 Root Fe overaccumulation in wild-type under Zn excess

One of the striking phenotypes of Zn excess is the overaccumulation of Fe in roots, which compared to wild type is reduced in *bts1x2* (**Figures 4.6C and 4.7**). Reduced root Fe accumulation in *bts1x2* could be explained again by enhanced Fe translocation to shoots before high root Zn accumulation occurs (**4.3.3**). However, shoot Fe in *bts1x2* does not show a resulting increase to make this a sufficient explanation. An alternative explanation is that the wild type root Fe accumulation is not FIT-mediated cytoplasmic build-up, but rather occurring as apoplastic Fe³⁺. This collecting of Fe in the apoplast also occurs in response to phosphate deficiency-induced root Fe overload, mainly in the form

of malate-Fe³⁺, triggering ROS production, callose deposition and ultimately root growth inhibition [443]. As a method, Perls' stain stains labile nonhaem-Fe in the form of both Fe²⁺ and Fe³⁺ [444], while DAB allows detection of H₂O₂ [445]. As such, the deep staining seen along the root surface of wild type seedlings grown under Zn excess in response to these stains (**Figure 4.7**), as well as the reduced root length (**Figure 4.3**) is in agreement with high apoplastic Fe³⁺. The presence of high apoplastic Fe³⁺ in the ICP samples could suggest a more thorough root washing technique is required for the elemental analysis (**2.7.2**). However, any solubilised Fe can freely enter the root apoplast, including inside the root up to the Casparian strip [163] which could pose difficulty in removing all bound cations if the overload is as great as thought. Confirmation of this Fe³⁺ accumulation requires techniques that look at cellular and subcellular Fe distribution, such as synchrotron x-ray fluorescence [304, 446], or cross-sectional Perls' staining of the root, combined with more sensitive elemental analysis techniques which can give isotope information, such as ICP-MS [447].

Apoplastic Fe³⁺ accumulation could also explain, or be a result of, attenuated *IRT1* and *FRO2* expression, and reduced *FRO2* activity in wild type compared to *bts1x2* (**Figure 4.7**). *FRO2* activity, which reduces Fe²⁺ to Fe³⁺, is the rate-limiting step of Fe uptake and is subject to post-transcriptional inhibition under Fe sufficiency conditions [173]. The *IRT1* transporter also undergoes post-translational regulation, with a proposed metal-sensing ability that promotes its own internalisation and vacuolar degradation in response to elevation of non-Fe substrates in the soil, such as Zn and Mn [172]. Thus, post-transcriptional inhibition of *FRO2* activity and *IRT1* internalisation caused by cytoplasmic Fe and Zn overload slows the rate of Fe reduction at the root surface for uptake, but in turn leads to Fe³⁺ accumulation in the apoplast. In contrast, *IRT1* and *FRO2* are highly overexpressed in *bts1x2*, which is likely accompanied by a greater amount of protein at the plasma membrane [305]. Hence, even though post-transcriptional feedback is also occurring in *bts1x2*, as exemplified by FCR activity not being correlated exactly with the high *FRO2* expression, there is still sufficient amount of *FRO2* protein to maintain Fe³⁺ reduction at the root surface into the more soluble Fe²⁺. Interestingly, *FRO2* activity is similar under both Fe deficiency and Zn excess in *bts1x2*, which could suggest that this post-transcriptional control may be regulated by a signal which is constant under both these conditions, such as shoot-borne signal or the root Fe

content, although further elemental analysis of *bts1x2* under Fe deficiency is required to confirm this. Furthermore, analysis of IRT1 protein localisation through use of GFP fusion proteins is required to investigate whether regulation of Fe uptake into the symplast is also a contributing factor to reduced Fe accumulation.

4.3.6 Soil phenotyping of *bts1x2*

The soil phenotyping experiments in this chapter demonstrate that Zn excess reduces rosette growth rate and delays flowering time in wild type (**Figures 4.8 and 4.9**). The late flowering phenotype is consistent with previous reports of a positive correlation between flowering time and Zn concentration [422, 423]. In contrast to the Zn deficiency-induced delay in flowering [424], elongation of the vegetative growth phase under Zn excess does not lead to a biomass increase, as shown by the reduced growth rate and rosette size compared to control conditions (**Figure 4.9**). A lack of biomass increase is likely because of stress-induced growth inhibition mediated by ROS production, or a fitness disadvantage conferred through Zn excess-mediated lengthening of the circadian period [425]. Furthermore, differences in developmental timing and rosette size are not obvious until later stages of development, which could suggest that Zn-induced Fe limitation is not an influencing factor on development until then (**Figures 4.8 and 4.9**).

Unlike the Zn-stress induced delay in flowering seen in wild type, *bts1x2* flowering is delayed irrespective of Zn growth conditions and accompanied by an increase in rosette size and growth rate under control conditions (**Figures 4.8 and 4.9**). The *bts1x2*-specific developmental phenotype could be due to a number of factors, including altered metal content or misregulation of Fe homeostasis genes that also interact with circadian clock components. For instance, plastid-localised ferritin proteins, which are involved in Fe storage and regulation of oxidative stress, mediate Fe homeostatic influences on floral development [426]. The triple ferritin mutant, *atfer1-3-4*, or mutations in genes that affect ferritin chloroplast content, show excessive Fe uptake, ROS production and subsequent impaired floral development [426, 448]. The influence of Fe on floral development is also linked to reciprocal interaction between Fe homeostasis and the circadian clock, with *FER1*, *IRT1* and *bHLH39* showing circadian

regulation, and Fe deficiency associated with lengthening of the circadian period [371, 425]. As such, the enhanced Fe content of *bts/1x2* may help maintain an optimal circadian period length under both Zn sufficiency and excess conditions, explaining the lack of further flowering time delay on Zn treatment (**Figure 4.8**). Expression analysis of key circadian clock flowering time genes is needed to investigate this theory. Improved Fe nutrition, and therefore photosynthetic capacity, could also contribute to the increased growth rate observed. However, it is also possible that these phenotypes could be a pleiotropic effect of the T-DNA insertion mutation, and only through investigation of alternative mutant alleles and complementation studies will this become apparent.

4.3.7 Proposed model for the *bts/1x2* Fe-mediated Zn tolerance phenotype

Based on the observations discussed here, and the characterisation of the wild type and *bts/1x2* response to various metal conditions presented in this chapter, a model for the role of BTSL proteins under Zn excess (**Figure 4.10A**), as well as a model for the Fe-mediated Zn tolerance in *bts/1x2* (**Figure 4.10B**), is proposed. In wild type under Zn excess, Zn accumulates in roots and outcompetes Fe for uptake and translocation to shoots, leading to a high Zn/Fe shoot ratio [27](**Figure 4.10A**). The resultant Fe deficiency signal from shoots inhibits BTSL and allows FIT protein accumulation and upregulation of *IRT1* and *FRO2*, enhancing Fe, as well as further Zn uptake, at the root surface (**Figure 4.10A**). The increased root Fe content post-transcriptionally inhibits *FRO2* [173], and enhanced Zn concentrations may lead to post-transcriptional internalisation of *IRT1* [172], ultimately leading to apoplastic accumulation of Fe^{3+} in roots (**Figure 4.10A**). In comparison, in *bts/1x2* under Zn excess enhanced FIT protein accumulation results in enhanced *IRT1* and *FRO2* expression compared to wild type [304, 305], and enhanced Fe translocation to shoots (**Figure 4.10B**). As such, there is a reduced Zn/Fe shoot ratio and a lower Fe deficiency signal from shoots compared to wild type, although some Fe deficiency signalling further activates the Fe uptake response in *bts/1x2* roots (**Figure 4.10B**). Accumulating root Fe post-transcriptionally inhibits *FRO2*, but increased *FRO2* and *IRT1* protein content at the plasma membrane compared to wild type maintains high Fe uptake and prevents the apoplastic Fe^{3+} accumulation (**Figure 4.10B**). Some Zn-dependent internalisation of *IRT1* as a result of the high root Zn/Fe ratio likely prevents

toxic accumulation of Zn and Fe in roots [172]. However, there remain a number of gaps in this explanation, which are indicated by a question mark ('?') in the schematic. Two of these questions are addressed in the following chapter, namely the mechanism upregulating *Ib bHLH* gene expression and subsequent FIT activation [305] and the responsiveness of BTSL proteins to systemic Fe signals. The other major unknown, which would be an important avenue for future research, is the mechanism of metal-dependent regulation of BTSL proteins, and the potential differences in metal binding and sensing between these BTSL1/2 and BTS. The answers to these questions will provide valuable insight into the role of BTSL proteins in Fe sensing, signalling and cross-homeostasis networks.

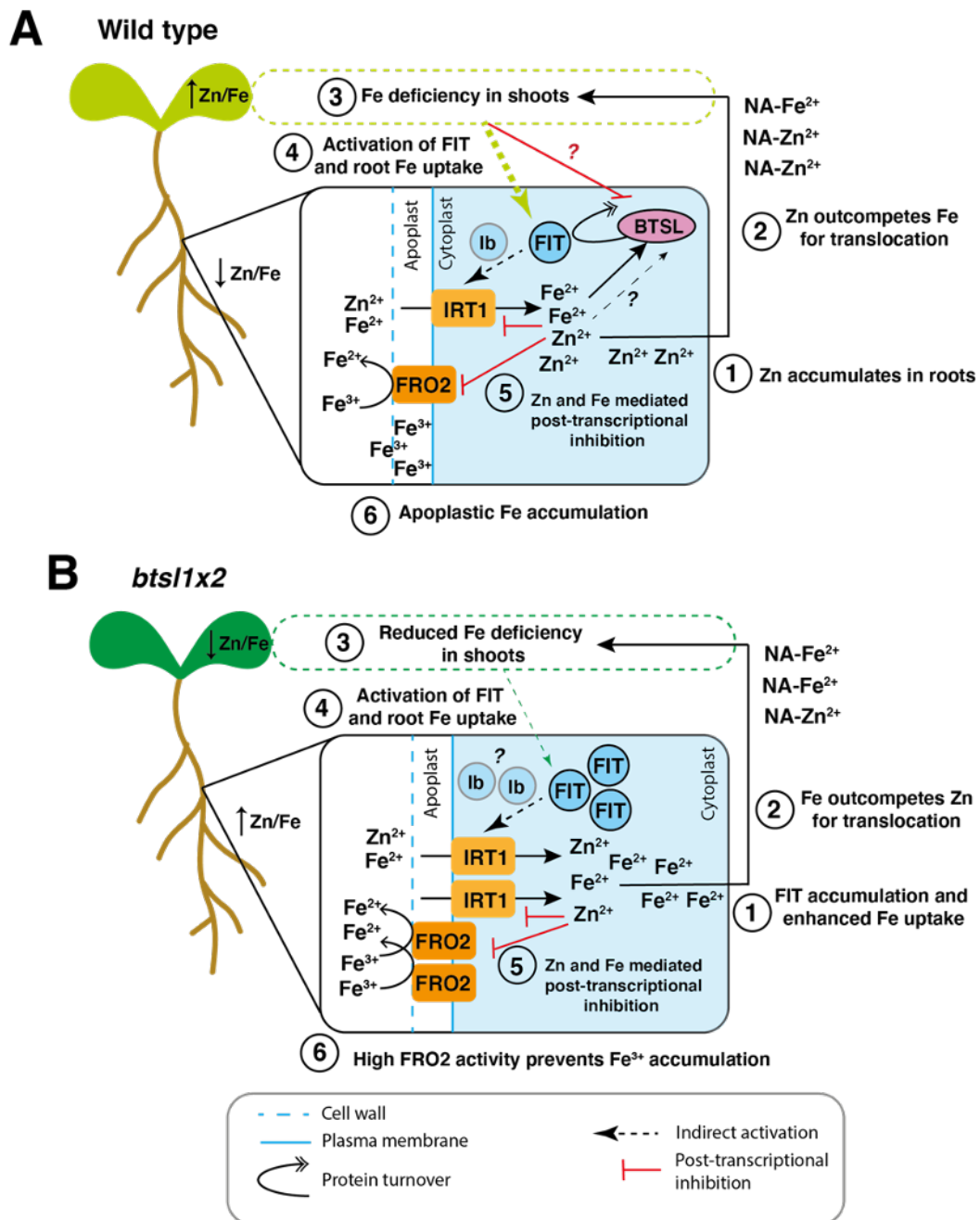


Figure 4.10: Proposed model for the Fe-mediated Zn tolerance phenotype of *bts1x2*.

A) A simplified model of the wild-type response to Zn excess. Under Zn excess, Zn accumulates in roots (1), leading to Zn outcompeting Fe for translocation to shoots (2) [27] and a high shoot Zn/Fe ratio. This triggers a strong shoot Fe deficiency signal (3) which potentially inhibits BTSL proteins. The root Fe deficiency response is activated via FIT accumulation and upregulation of FIT-dependent genes, such as *IRT1* and *FRO2*, via FIT-Ib bHLH heterodimer formation (4) [301, 303]. Enhanced Zn and Fe uptake into the cytoplasm leads to post-transcriptional feedback inhibition of *FRO2* [173] and likely *IRT1* (5) [172] and subsequent accumulation of Fe^{3+} in the apoplast. BTSL maintains FIT protein turnover and

may be regulated by the increasing root Fe and Zn concentrations [304, 305]. B) Simplified model of the *bts1x2* response to Zn excess. Loss of BTSL proteins allows FIT protein accumulation and activation of *IRT1* and *FRO2* expression potentially via enhanced Ib bHLH transcription factor expression and accumulation (1) [304, 305]. Fe outcompetes Zn for translocation to the shoots (2) leading to a reduced shoot Zn/Fe ratio and shoot Fe deficiency signal than is seen in wild type (3). Subsequent further activation of the root Fe deficiency response via FIT and increased Fe and Zn uptake (4). Accumulating root Fe and Zn post-transcriptionally inhibits *FRO2* [173] (5), but high levels of protein maintain Fe reduction to prevent apoplastic Fe³⁺ accumulation (6). Enhanced internalisation of *IRT1* as a consequence of the higher root Zn/Fe ratio likely prevents excessive cation uptake and toxicity [172]. NA = nicotianamine. ? = outstanding question.

4.3.8 New advances in the understanding of BTSL1 and BTSL2 function

This chapter initially set out to characterise the physiological and molecular mechanisms conferring the Zn tolerance phenotype of the *bts1x2* double mutant, and to explore whether this could show a role for BTSL proteins in Zn and Fe cross-homeostasis. Other proteins involved in repression of the Fe deficiency response, such as FBP, have previously been shown to function in Zn and Fe distribution, and consequently micronutrient interactions [201]. Characterisation of the *bts1* mutants on various metal growth conditions confirmed the Zn tolerance phenotype of *bts1x2*, and also demonstrated the partial functional redundancy of the *bts1* single mutants (**Figure 4.3**). Elemental analysis of *bts1x2* under Zn excess showed that BTSL proteins, similar to FBP, also play a role in balancing the uptake and translocation of Zn and Fe, as well as regulating Fe and Mn uptake under Fe sufficiency conditions (**Figure 4.6**). It also showed that the Fe-mediated Zn tolerance phenotype of *bts1x2* is underpinned by reduced competition between Fe and Zn for uptake and root-to-shoot transport conferred through constitutive expression of Fe uptake genes and *FRO2* activity (**Figure 4.7**), although further work is required to understand how constitutive FIT-dependent gene expression is possible in the mutant. Altered metal distribution in the mutant also impacts development, flowering time and rosette growth rate and size, which could be

an interesting phenotype for increasing crop yield in dicotyledonous crop species (**Figures 4.8 and 4.9**). Taken together, the findings presented in this chapter lead to the proposition of a model for the novel role of BTSL proteins in Fe and Zn cross-homeostasis (**Figure 4.10**), which can be further clarified through transcriptomic analysis in **Chapter 5**.

**Chapter 5: Transcriptomic analysis
reveals a novel role for BTSL proteins in
FIT-independent gene regulation**

5.1 Introduction

5.1.1 Investigating the Fe-mediated Zn tolerance phenotype of *bts/1x2* through transcriptomics

In **Chapter 4**, characterisation of the *bts/1x2* mutant revealed an Fe-mediated Zn tolerance phenotype associated with constitutive overexpression of FIT-dependent Fe uptake genes, *IRT1* and *FRO2*. A previous publication has shown that *bts/1x2* roots accumulate high levels of FIT protein, a central regulator of Fe deficiency, and consequently fail to downregulate the expression of FIT-dependent *IRT1* and *FRO2* [305]. However, the *bts/1x2* mutant also showed altered metal distribution, with reduced Zn accumulation in shoots and Fe in roots compared to wild type (**Chapter 4**). A number of key genes involved in Fe and Zn translocation and distribution, such as *ZIF1*, *FRO3* and *NAS4*, are largely regulated in a FIT-independent manner by the PYE regulon [307]. The mis-regulation of *bHLH38* and *bHLH39* in *bts/1x2* mutants has also previously been reported [305] although no other FIT-independent genes have been investigated to date in the mutant. Therefore, a transcriptomics approach could give an unbiased overview of which genes are additionally affected by loss of BTSL protein function and contribute towards the altered metal distribution and tolerance phenotype in the double mutant.

Transcriptomic analysis can reveal global and tissue-specific RNA expression patterns indicating changes in signalling and metabolic pathways in response to a chosen experimental condition. Microarray analysis and RNA-sequencing (RNA-seq) have successfully been used in a number of *A. thaliana* mutant studies to identify genes and transcriptional regulatory networks that are responsive to Fe [300, 335, 449-451], Zn [162, 390], and other nutrients [452, 453]. While transcriptomics can be a powerful tool in helping shape and inform hypotheses, alone it only captures one aspect of molecular regulation. Additional regulatory mechanisms that transcription and translation are subject to can be missed, as well as protein-protein and metabolite interactions that can affect downstream activity of expressed genes. As such, when interpreting transcriptomic results, it is important to keep the spatial, temporal and resolution limits of this approach in mind.

5.1.2 RNA-seq analysis as a tool for transcriptomic analysis in *A. thaliana*

RNA-seq was developed in 2008 following advances in next generation sequencing (NGS) technologies which facilitated the use of high-throughput sequencing to map and quantify transcriptomes [454-459]. Compared to hybridisation-based techniques, such as microarrays, RNA-seq is highly sensitive and is not limited to genomes that have already been sequenced. This makes RNA-seq an extremely useful technique for investigating non-model species, alternative splicing and non-coding RNA. Moreover, RNA-seq captures expression changes in genes that are omitted from microarrays, such as Fe homeostasis genes *bHLH38*, *bHLH100* and *IMA2*, which are not found on the Arabidopsis ATH1 microarray [300]. Advances in RNA sample preparation protocols, NGS technologies and computational power over the past decade have helped significantly reduce the cost of RNA-seq, making it now a widely used standard technique [460]. Subsequently, a diverse range of bioinformatics analytical techniques have been developed for interpreting the wealth of data RNA-seq experiments provide. These include programmes for read mapping, differential gene expression (DGE) and splicing analysis, as well as annotation and visualisation tools for the output of these analyses [461]. The initial steps of RNA-seq analysis, read mapping to a reference genome and transcript quantification, can be very time consuming and require lots of computational power. However, for model organisms, such as *A. thaliana*, with a well-annotated reference transcriptome the time and power taken for these initial steps can be significantly reduced through using pseudoalignment tools such as Kallisto [341]. Kallisto also comes with a partner programme, Sleuth [342], for downstream DGE analysis, making RNA-seq an ideal approach for quick and straightforward analysis of the *A. thaliana* transcriptome.

5.1.3 The FIT-dependent transcriptional response network

Our understanding of the transcriptional response of *A. thaliana* to low Fe has grown dramatically over the past decade. A combination of RNA-seq [335, 462-464] and microarray experiments [465-467] with co-expression analyses [305, 308, 465, 468] have found that ~1300 genes are upregulated and ~1250 downregulated in roots on exposure

to Fe deficiency, with the major Fe deficiency-responsive gene networks also induced in response to Zn excess [390]. These genes show cell-type specific expression depending upon their upstream regulator and include not only metal homeostasis genes, but genes involved in developmental, hormonal and stress signalling pathways [469]. These Fe deficiency-responsive gene networks can be classified as FIT-dependent or FIT-independent.

FIT-dependent genes are only expressed in roots and mainly in the epidermal cell layer, although there is some *FIT* expression seen in the stele (**Figure 5.1**)[308, 469]. To date, 448 FIT-regulated genes have been identified in *A. thaliana* roots, with the regulation of these genes reliant upon FIT and Ib bHLH transcription factor (bHLH38, bHLH39, bHLH100 and bHLH101) heterodimer formation [302, 465]. An important group of FIT-dependent genes is involved in Fe uptake and include *IRT1* and *FRO2* [173, 303] and genes involved in the biosynthesis and secretion of Fe mobilising small molecules, such as *S8H*, *CYP82C4*, *F6'H1* and *ABCG37*, which produce coumarins [181, 182, 470]. The β -glucosidase *BGLU42* involved in the synthesis of Fe-mobilising phenolics compounds is indirectly FIT regulated via MYB10 and MYB72 [185]. Closely related *IRT1* homolog, *IRT2*, which has an unspecified role in maintaining Fe homeostasis in epidermal cells, is also subject to FIT-dependent upregulation [273]. *NAS1* and *NAS2* involved in NA synthesis for Fe and Zn distribution [471] are also expressed in a FIT-dependent manner, as is *NAS4* indirectly through MYB10 and MYB72 activation [201, 472]. *NAS4*, *MYB10* and *MYB72* are also subject to FIT-independent regulation and expressed in cells closer to the central root cylinder so are not found to cluster with FIT in co-expression networks [308]. Vacuolar transporters involved in the detoxification of heavy metals, such as *IREG2/FPN* for Fe, Ni and Co [233, 473] and *MTPA2/MTP3* for Zn [249], as well as transporters involved in the compensatory uptake of other metals, such as *COPT2* for Cu [474] and *ZIP2*, one of the few FIT-repressed genes, for Mn and Zn uptake [156]. Some FIT-regulated genes also function to feedback and regulate FIT itself, such as negative-regulator *BTSL2*, although not *BTSL1* [305], and the NO-responsive positive-regulator *GRF11* [320].

FIT is also receptive to, and an important regulator of, developmental signals, largely in adjusting root morphology to optimise Fe uptake via stimulation of root hair growth and branching, and primary root elongation [475]. As such, genes such as *RHS13* [476], *EXPA7* [477] and *EXPA18* [478] which are involved in root hair elongation, and cell wall peroxidase *PER7* [479] and xylogucan endotransglucosylases *XTH12* and *XTH13* [480] which function in cell wall modifications and lengthening are also FIT-regulated.

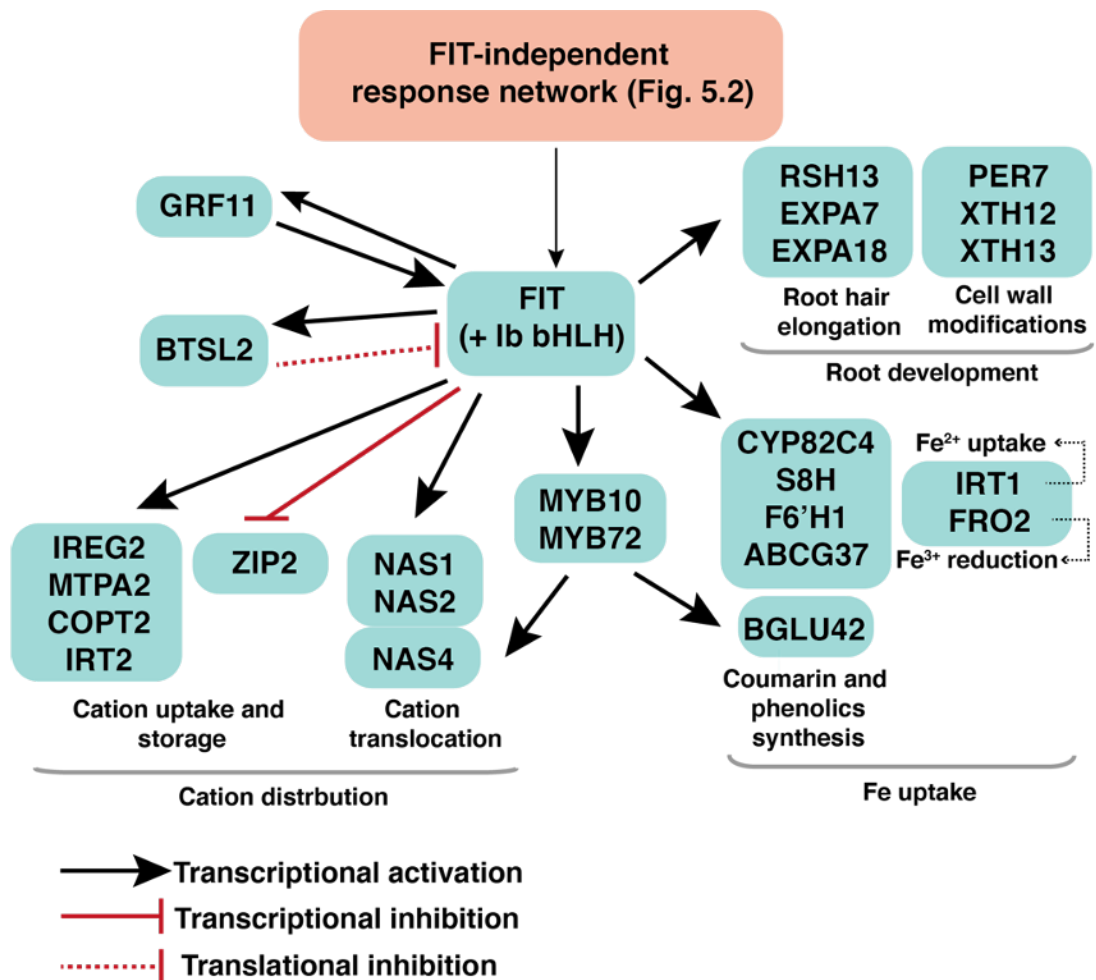


Figure 5.1: The FIT-dependent Fe deficiency response network.

Schematic of the FIT-dependent regulon showing selected genes and their functions. GRF11 = 14-3-3 protein. BTSL2 = ubiquitin E3 ligase. IREG2 = Ni and Co vacuolar importer. MTPA2 = Zn vacuolar importer. COPT2 = Cu transporter. IRT2. = Fe²⁺ transporter. ZIP2 = Zn and Mn transport. NAS1, NAS2 and NAS4 = nicotianamine synthase. MYB10 and MYB72 = MYB transcription factors. CYP82C4 = fraxetin hydroxylase. S8H = scopoletin hyxroxylase. F6'H1 = feruloyl CoA ortho-hydroxylase. ABCG37 = coumarin exporter. BGLU42 = β-glucosidase. IRT1

= Fe²⁺ uptake transporter. FRO2 = ferric chelate reductase. RSH13 = root hair-specific apoplastic protein. EXPA7 and EXPA18 = root hair expansins. PER7 = peroxidase. XTH12 and XTH13 = xyloglucan endotransglucosylases. *lb* bHLH = bHLH38, bHLH39, bHLH100 and bHLH101. FIT = Clade IIIa+c. Adapted from [308].

5.1.4 The FIT-independent transcriptional response network

FIT-independent gene expression occurs in both roots and shoots, and genes in this regulon are mainly involved in metal translocation and distribution (**Figure 5.2**)[308]. Four members of the IVc bHLH Clade (bHLH34, bHLH104, bHLH105/ILR3 and bHLH115) are the most upstream regulators of this response network, activating the expression of a IVb bHLH (*bHLH121/URI*) [299], which then form heterodimers to regulate downstream target genes. These include *lb* bHLH genes, *bHLH38*, *bHLH39*, *bHLH100* and *bHLH101*, which form stabilising activating heterodimers with FIT to activate the response network [302, 375, 428], as well as with *FIT* directly [299]. IVc transcription factors also form heterodimers with *bHLH11*, which exert a negative effect on FIT-dependent gene expression by preventing upregulation of *lb* bHLH genes [481]. *BTS*, *BTSL1* and *BTSL2* are upregulated by IVc and bHLH121/URI activity [300], with *BTS* forming a negative feedback loop to promote bHLH104, ILR3, bHLH115 and bHLH121/URI protein turnover [296, 300, 306, 307], while *BTSL1* and *BTSL2* negatively regulate FIT protein abundance [304, 305]. A number of genes involved in Fe signalling and transport are also directly activated by IVc and bHLH121/URI. These include Fe deficiency-induced signalling peptides *IMA1*, *IMA2* and *IMA3* [335, 482] and phloem transporter *OPT3*, which is thought to function in shoot-borne signalling processes [244].

IVc and bHLH121/URI transcription factors also activate the expression of *PYE* [307], which itself forms a repressive complex with ILR3 to downregulate genes involved in metal distribution, such as *NAS4* [202], vacuolar Zn-NA importer *ZIF1* [256], the mitochondrial ferric chelate reductase *FRO3* [245] and vacuolar Fe exporter *NRAMP4* [267]. *ZIF1* and *NAS* genes especially play an important role in Fe-Zn balance, with higher expression of these genes associated with Zn tolerance phenotypes [200, 201, 256]. Fe sequestration genes, such as Fe storage proteins *FER1*, *FER3* and *FER4* [448, 483],

vacuolar Fe importers *VTL1* and *VTL2* [264] and Fe assimilation protein *NEET* [484], as well as *PYE* itself [413] are also subject to repression by *PYE-ILR3*. These *PYE*-repressed genes are also antagonistically activated by *bHLH121/URI* and IVc *bHLH* activity, either directly as is seen for *FER1*, *FER3*, *FER4*, *VTL2*, *NEET*, *NRAMP4* and *FRO3* [300, 485], or indirectly via *MYB10* and *MYB72* as is seen for *NAS4* [375]. *ZIF1* is activated by IVc transcription factors, but not by *bHLH121/URI* [300]. *ZIF1* and *NAS* genes also play important roles in Zn storage and distribution.

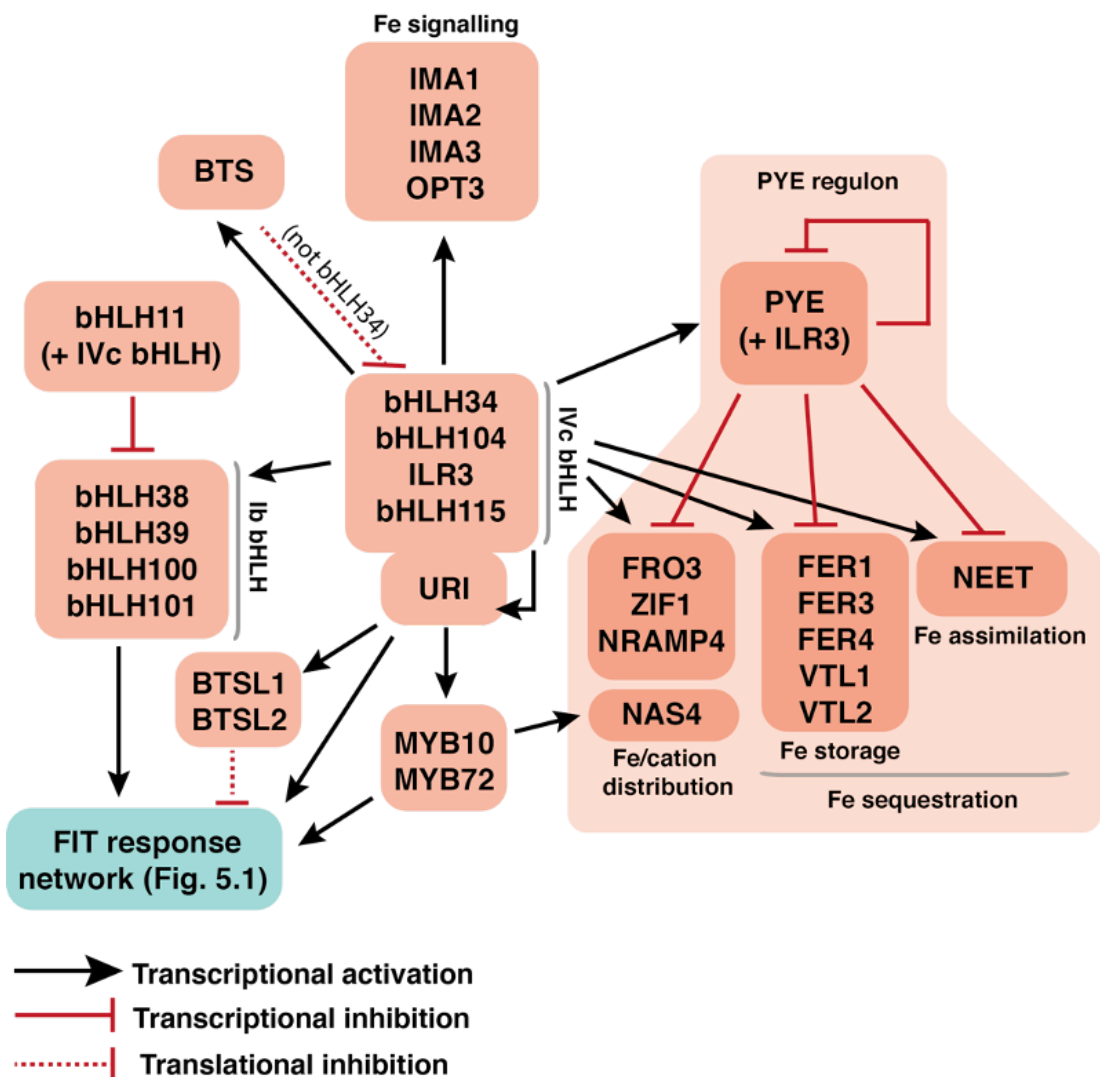


Figure 5.2: The FIT-independent Fe deficiency transcriptional response network.

Schematic of the FIT-dependent regulon showing selected genes and their functions. IMA1, IMA2, IMA3 = Fe signalling peptides. OPT3 = phloem Fe and Fe signalling transporter. BTS, BTSL1 and BTSL2 = ubiquitin E3 ligase. bHLH11 = Clade IVb bHLH. bHLH38, bHLH39, bHLH100 and bHLH101 = Clade Ib bHLH. MYB10 and MYB72 = MYB transcription factors. ZIF1 =

vacuolar Zn-NA importer. FRO3 = mitochondrial ferric chelate reductase. NRAMP4 = vacuolar Fe exporter. NAS4 = nicotianamine synthase. FER1, FER3, FER4 = ferritin Fe storage proteins. VTL1 and VTL2 = vacuolar Fe importer. NEET = Fe-S protein. PYE and bHLH121/URI = Clade IVb bHLH. bHLH34, bHLH104, bHLH105/ILR3 and bHLH115 = Clade IVc bHLH. Adapted from [308].

5.1.5 Antagonistic gene regulation by bHLH121/URI and PYE

Both bHLH121/URI and PYE are members of the IVb bHLH Clade and share a common subset of downstream genes, where they bind to the same G-box motif (*CACGTG*) in target gene promoters [485]. These target genes include Fe storage proteins (*FER1*, *FER3* and *FER4*) [485], vacuolar Fe importers (*VTL1* and *VTL2*) [264] and Fe assimilation protein *NEET* [300]. However, bHLH121/URI and PYE have antagonistic roles in the regulation of these genes [298-300, 307]. While bHLH121/URI forms heterodimers with all four IVc bHLH transcription factors and activates the expression of downstream target genes, PYE represses gene expression through forming complexes with ILR3 [307, 413].

Fe-dependent changes in the cellular distribution of bHLH121/URI, PYE and ILR3 within the root helps balance their activity to optimise Fe homeostasis gene expression. Under Fe sufficiency, bHLH121/URI is found mostly in the stele, where ILR3 is also found to accumulate, with lower amounts of ILR3 also seen in epidermal and cortical cells [298, 486]. In contrast, only low levels of PYE are found in the stele under these conditions [307]. Thus, the expression of genes associated with Fe storage is activated by the preferential heterodimerisation of bHLH121/URI and IVc bHLH transcription factors [298, 300]. Under Fe deficient conditions, bHLH121/URI is then found to accumulate in epidermal and cortical cells, where it activates the expression of *FIT* and other genes associated with FIT-dependent gene expression and Fe uptake [299, 300]. On the other hand, PYE and ILR3 are found across all cell types, but the reduction of bHLH121/URI in the stele allows formation of the ILR3-PYE repressive complex to occur more often, subsequently leading to downregulation of genes involved in Fe sequestration and transport [298, 307, 486].

bHLH121/URI activity and protein abundance is further regulated through Fe-dependent phosphorylation [298, 300]. The mechanism for this phosphorylation is currently unknown, although it has been suggested that CIPK11, which also regulates FIT activity through phosphorylation, could be involved [321]. Under Fe deficiency, phosphorylated bHLH121/URI protein accumulates, with this phosphorylation also promoting interactions with its IVc bHLH partners and subsequent nuclear localisation and downstream gene expression [299]. In turn, active phosphorylated bHLH121/URI is targeted for proteasomal degradation through BTS-dependent ubiquitination, helping maintain continual protein turnover and sensitivity to Fe signalling [300]. Whether phosphorylation state is a contributing factor to bHLH121/URI cellular localisation is yet to be explored.

5.1.6 Implications of Fe sensing and signalling in Fe and Zn cross-homeostasis

Root Fe uptake and the Fe deficiency transcriptional network is regulated by both local environmental and shoot-borne systemic Fe signals. The exact mechanisms regulating this sensing and signalling however, still remain a fairly open question [246, 487]. It has been suggested that both apoplastic and cytoplasmic Fe concentrations mediate local activation of FIT-dependent gene expression in roots, as demonstrated through modulating apoplastic Fe pools through Fe resupply after deficiency [168], and characterisation of mutants impaired in subcellular Fe distribution [267, 268]. Hormonal regulation of FIT, notably early on in the Fe deficiency response, has also implicated auxin, ethylene, NO, abscisic acid (ABA) and GA as positive regulators of Fe deficiency signalling [316, 487-490], and JA and CKs as negative regulators [323, 491].

Systemic signalling has been shown to have an overriding effect on local Fe signalling. Split root and grafting experiments, and foliar Fe application demonstrate that roots exposed to low Fe conditions will not mount an Fe deficiency response if the shoot has adequate Fe levels [168, 246]. The importance of this cross-talk between local and systemic signalling suggests that root Fe sensors are able to integrate both signalling pathways, with shoot-borne signals travelling radially through the root, or that multiple sensors and signals exist in an intercellular signalling cascade. Both BTS and BTSL proteins

have been suggested to play a role in Fe-sensing in roots [304, 305, 307, 407, 487]. Based on the expression of BTS in the shoots and the stele – which is the first cell layer to respond to Fe deficiency in roots [469] - and BTSL proteins predominantly in the epidermis, the current model posits that BTS regulates root Fe deficiency in response to systemic signalling and internal Fe concentrations, while BTSL proteins are responsive to local Fe [305]. However, based on the importance of the aforementioned cross-talk, and evidence that FIT-dependent gene expression is responsive to shoot-derived signals from co-expression analysis [308], it is also likely that BTSL proteins may be important for both signalling pathways.

Based on the number of phloem-associated transporters and proteins which have been found vital for shoot-to-root communication, the current model for systemic signalling centres around shoot-borne phloem-transported signals. For instance, Fe deficiency-responsive IMA signalling peptides [335], OPT3-mediated loading of Fe into the phloem [243], as well as phloem Fe bound to ligands, such as citrate, which requires the FRD3 transporter [237], NA [471], and the tripeptide GSH [212] are all thought to play a part. It is notable that NA and GSH are also important for Fe and Zn cross-homeostasis [203, 212, 492], implying that Fe sensing and signalling also incorporates cross-talk with other divalent cations. Indeed, Zn interference with Fe binding to sensors, ligands and proteins has been suggested to be the mechanism of activation of Fe deficiency under Zn excess conditions [27].

5.1.7 Aims of this chapter

Characterisation of the *bts1x2* mutant in **Chapter 4** identified an Fe-mediated Zn tolerance phenotype, suggestive of a novel role for BTSL proteins in Zn and Fe cross-homeostasis. However, the known function of BTSL proteins as negative regulators of FIT protein accumulation is insufficient to explain overexpression of FIT-dependent genes and *bHLH* genes in the *bts1x2* mutant [305]. As such, an unbiased transcriptomics approach could reveal new functions of BTSL proteins in the regulation of Zn and Fe homeostasis genes, as well further understanding of the molecular mechanisms underpinning the Fe-mediated Zn tolerance phenotype.

This chapter describes the data from an RNA-seq experiment carried out on Col-0 and *bts1x2* to investigate the transcriptomic responses to Zn excess. After two weeks of continual growth on either control or Zn excess media, separated shoots and roots were analysed using RNA-seq. The first section of this chapter gives an overview of experimental design, quality control and differential gene expression (DGE) analysis. The transcriptomic changes in the shoots are then described through hierarchical clustering of significantly differentially expressed genes (DEGs) and Gene Ontology (GO) analysis of clusters, with metal homeostasis genes highlighted. This is then repeated for the root data. The aim was to identify genes that are misregulated in *bts1x2* that could further develop and test the proposed Zn tolerance model from **Chapter 4 (Figure 4.10)**, as well as explore which FIT-independent genes in addition to *bHLH38* and *bHLH39* are affected by loss of BTSL protein function.

The final part of the chapter investigates the transcriptional response of *bts1x2* in responding to systemic Fe signalling under Fe deficiency and Zn excess through split root experiments. The purpose of this was to test the current model of BTSL proteins as local Fe sensors, as well as to investigate the role of BTSL Fe-sensing in the Zn tolerance phenotype.

5.2 Results

5.2.1 RNA-sequencing experimental design and quality control

RNA was extracted from shoot and root tissues of two week-old Col-0 and *bts1x2* seedlings grown on either control (1 μM ZnSO_4) or Zn excess (100 μM ZnSO_4) media. Samples were collected from three biological replicates for each genotype and treatment, except for *bts1x2* Zn excess shoot tissue, which only had two replicates due to contamination of third replicate. RNA samples showed high quality and no degradation, so were suitable for sequencing (**Supplementary Table C1 and Figure C1, Appendix C**). Paired-end RNA sequencing was carried out using the Illumina Novoseq platform. Quality analysis of the sequenced reads using FastQC showed ~ 30 million reads per samples and high sequence quality, ranging between 33–40 (Phred score), with 40 being the highest score possible (**Supplementary Table C2, Appendix C**).

RNA-seq reads were then mapped to the *A. thaliana* transcriptome using Kallisto, a pseudoalignment tool that has been shown to give similar results to other commonly used genome alignment programs, but much more rapidly [341]. On average, Kallisto successfully mapped 94.28 % of reads in total, with 92.91 % of these being unique (**Table 5.1**).

Genotype	Tissue	Treatment	Rep	Reads	Reads pseudoaligned	Unique reads pseudoaligned	% Pseudoaligned	% Pseudoaligned Unique
Col-0	Shoot	1 μ M Zn	1	28753615	27672343	27154693	96.2%	94.4%
Col-0	Shoot	1 μ M Zn	2	32996397	31776305	31199779	96.3%	94.6%
Col-0	Shoot	1 μ M Zn	3	30663868	29521478	29011520	96.3%	94.6%
Col-0	Root	1 μ M Zn	1	30617168	29062819	28722825	94.9%	93.8%
Col-0	Root	1 μ M Zn	2	28515861	27083875	26746473	95.0%	93.8%
Col-0	Root	1 μ M Zn	3	27118347	25777491	25458739	95.1%	93.9%
Col-0	Shoot	100 μ M Zn	1	37145299	35450601	34859903	95.4%	93.8%
Col-0	Shoot	100 μ M Zn	2	30325010	29048413	28584584	95.8%	94.3%
Col-0	Shoot	100 μ M Zn	3	28698744	27476783	27063971	95.7%	94.3%
Col-0	Root	100 μ M Zn	1	30285796	30285796	28484460	95.1%	94.1%
Col-0	Root	100 μ M Zn	2	29986048	28522067	28206335	95.1%	94.1%
Col-0	Root	100 μ M Zn	3	31801542	30195887	29857910	95.0%	93.9%
<i>bts1x2</i>	Shoot	1 μ M Zn	1	31202788	30030129	29460569	96.2%	94.4%

Genotype	Tissue	Treatment	Rep	Reads	Reads pseudoaligned	Unique reads pseudoaligned	% Pseudoaligned	% Pseudoaligned Unique
<i>bts1x2</i>	Shoot	1 μ M Zn	2	33591017	32281917	31686381	96.1%	94.3%
<i>bts1x2</i>	Shoot	1 μ M Zn	3	25994973	24832229	24371040	95.5%	93.8%
<i>bts1x2</i>	Root	1 μ M Zn	1	28603626	27155068	26831345	94.9%	93.8%
<i>bts1x2</i>	Root	1 μ M Zn	2	32971800	31176638	30766418	94.6%	93.3%
<i>bts1x2</i>	Root	1 μ M Zn	3	31168763	29297325	28906940	94.0%	92.7%
<i>bts1x2</i>	Shoot	100 μ M Zn	1	33500432	32096345	31501161	95.8%	94.0%
<i>bts1x2</i>	Shoot	100 μ M Zn	2	30008688	28775448	28285848	95.9%	94.3%
<i>bts1x2</i>	Root	100 μ M Zn	1	31093476	28041027	27741651	90.2%	89.2%
<i>bts1x2</i>	Root	100 μ M Zn	2	26910577	23691008	23434737	88.0%	87.1%
<i>bts1x2</i>	Root	100 μ M Zn	3	28345177	23060085	22809754	81.4%	80.5%

Table 5.1: Summary of RNA-seq samples pseudoalignment.

Pseudoalignment was carried out using Kallisto against the *A. thaliana* transcriptome.

5.2.2 Principal component analysis (PCA) demonstrates divergent transcriptomic responses of Col-0 and *bts/1x2* to Zn excess

After mapping, differentially expressed (DE) transcripts were identified using Sleuth [342]. Principal component analysis (PCA) was then carried out on shoot and root whole transcript data to investigate variance between samples. Preferably intergroup variability, representing treatment and genotypic difference, should be greater than intragroup variability, which represents experimental replicates, and this can be visualised by plotting principal component (PC) 1 against PC2. Shoot samples clustered mainly by genotype and treatment, although Col-0 and *bts/1x2* control samples showed almost no intergroup variation, suggesting little transcriptomic difference between the two genotypes under control conditions (**Figure 5.3A**). Col-0 Zn excess samples also clustered further away from controls than *bts/1x2* Zn excess samples, showing that Col-0 shoots showed a more divergent transcriptomic response to Zn excess than *bts/1x2* (**Figure 5.3A**). The majority of the variance was captured by PC1 and PC2, with PC1 accounting for 73.18% of variance and PC2 24.30%, so no further PCs were investigated (**Figure 5.3B**). Transcript loading shows the relative contribution of individual transcripts to each PC and can reveal particular transcripts or subsets of transcripts which may be strongly influencing variation. The primary transcripts contributing to PC1 and PC2 loading were associated mainly with photosynthesis, such as *CAB1* (AT1G29930), *LHCA1* (AT3G54890) and *LHCB3* (AT5G54270), and translation, such as *RCA* (AT2G39730) and *RBCS1A* (AT1G67090)(**Figures 5.3C and D**). This initial result suggested that Zn excess might differentially affect photosynthesis and protein translation in Col-0 and *bts/1x2*. A summary of the top ten transcripts and their gene description can be found in **Supplementary Table C3, Appendix C**.

PCA of root samples showed greater intergroup variability compared to intragroup variability, with sample replicates clustering together, although it was notable that Col-0 and *bts/1x2* control samples again clustered closely together (**Figure 5.4A**). PC1 and PC2 accounted for the majority of variation, explaining 70.7% and 14.0% respectively (**Figure 5.4B**). Transcript loading for PC1 showed that *BGLU23* (AT3G09260), a beta-glucosidase associated with the defense response, largely contributed to PC1 variation, and to a lesser extent cell wall organising genes *EXT3* (AT1G21310) and *EXT21*

(AT2G43150) and metal responsive genes *ATMT1* (AT1G07600) and *ATMS1* (AT5G17920)(Figure 5.4C). PC2 loading transcripts were largely associated with Fe uptake and the Fe deficiency response, and included *IRT1* (AT4G19690), *FRO2* (AT1G01580), *AHA2* (AT4G30190) and *ABCG37* (AT3G53480)(Figure 5.4D). A summary of loading transcripts and their gene descriptions can be found in **Supplementary Table C4, Appendix C**. Based on the clustering of root samples and transcript loading of PC1 and PC2, Col-0 and *bts1x2* appeared to show genotype-specific root transcriptomic responses to Zn excess, largely characterised by differential expression of Fe homeostasis genes.

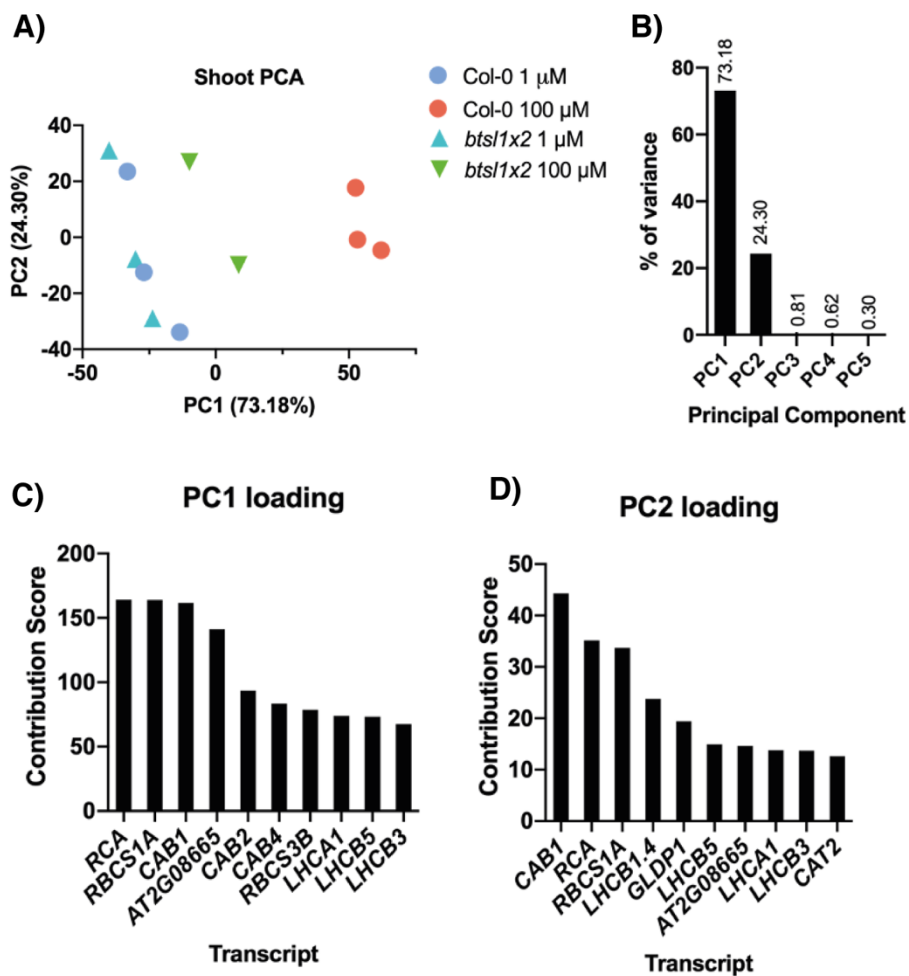


Figure 5.3: Principal component analysis (PCA) of shoot sample transcripts.

A) PCA plot of all experimental replicates of shoot samples, PC1 = principle component 1, PC2 = principle component 2, (%) is the percentage of variance explained by each PC. B) Percentage of variance between shoot samples explained by PC 1–5. C-D) Loading plot for the top ten transcripts in C) PC1 and D) PC2 contributing to variation.

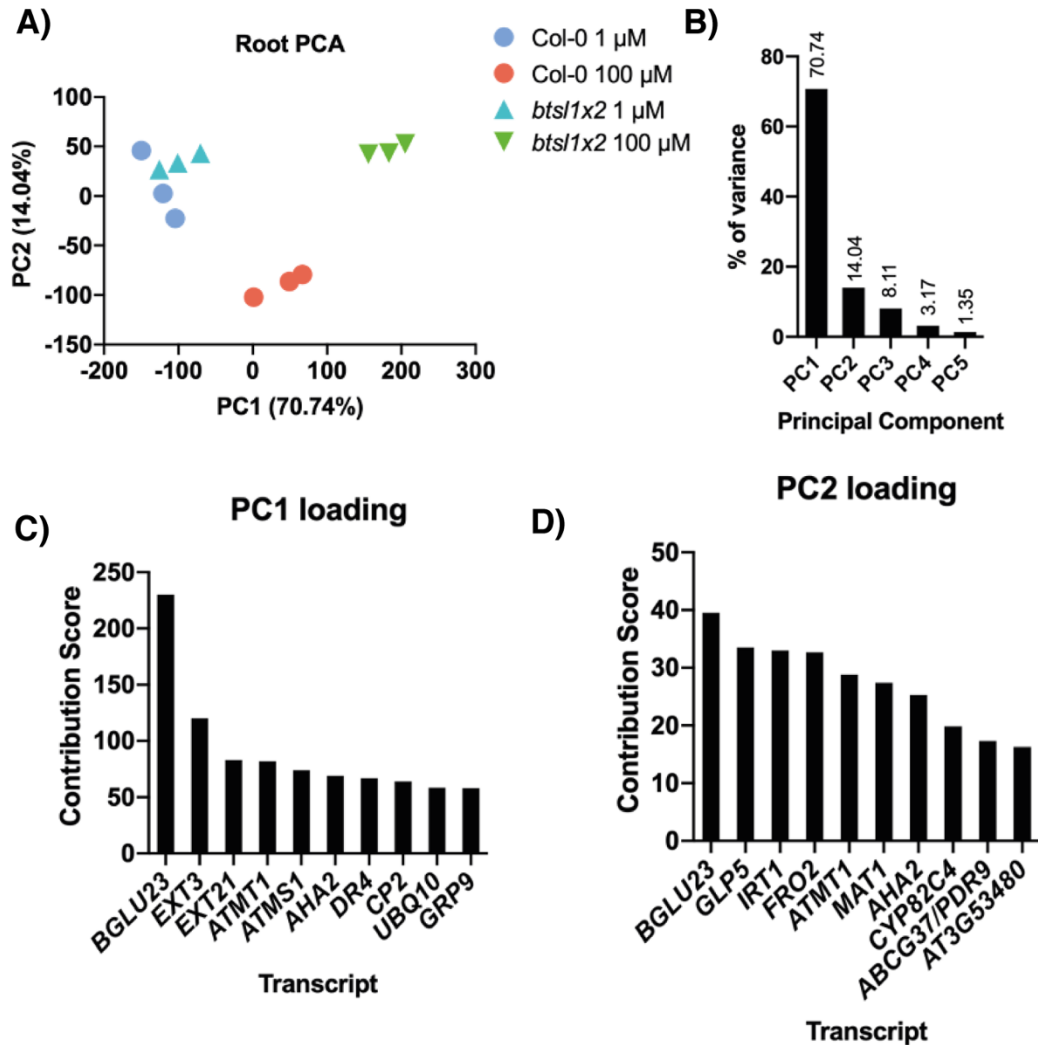


Figure 5.4: Principal component analysis (PCA) of root sample transcripts.

A) PCA plot of all experimental replicates of shoot samples, PC1 = principle component 1, PC2 = principle component 2, (%) is the percentage of variance explained by each PC. B) Percentage of variance between shoot samples explained by PC 1–5. C-D) Loading plot for the top ten transcripts in C) PC1 and D) PC2 contributing to variation.

5.2.3 Genotype-specific Differential Gene Expression (DGE) in wild-type and *bts/1x2* under Zn excess

Pairwise comparisons were next run to identify the number of DEGs between Col-0 and *bts/1x2* under basal and Zn excess growth conditions. Significantly DEGs were filtered based on absolute \log_2 fold change (FC) of ≥ 1 (2 x FC) and false discovery rate

(FDR) adjusted p-value < 0.05. The number of DEGs up- (+) or downregulated (-) between each pairwise comparison and their overlap is summarised in **Figures 5.5 and 5.6**. The overlap of all pairwise comparisons is summarised in **Supplementary Tables C5 and C6, Appendix C**.

In *bts1x2* shoots under control (1 μ M Zn) conditions, there were only 15 DEGs relative to Col-0, with 2 upregulated and 13 downregulated (**Figure 5.5A**). Of these, both the upregulated genes, and 5 of the downregulated genes were also DE in *bts1x2* in response to Zn excess relative to Col-0 (**Figures 5.5B and C**). This suggested that these genes are unlikely to be Zn responsive in *bts1x2*. Under Zn excess relative to Col-0, 1277 genes were DE in Col-0 (981 upregulated, 296 downregulated), compared to only 75 in *bts1x2* (54 upregulated, 21 downregulated)(**Figure 5.5A**). A further 4 genes are upregulated and 2 downregulated in *bts1x2* relative to *bts1x2* control, but not relative to Col-0 control, likely due to low mRNA levels in *bts1x2* under control conditions relative to Col-0 (**Figures 5.5B and C**). Of these Zn- responsive genes, 50 were DE in both Col-0 and *bts1x2* shoots (40 upregulated in both, 9 downregulated in both, 1 upregulated in Col-0 and downregulated in *bts1x2*)(**Figures 5.5B and C; Supplementary Table C5, Appendix C**).

In *bts1x2* roots under control conditions, 44 genes were DE relative to Col-0 control (32 upregulated, 12 downregulated)(**Figure 5.6A**). Of this gene set, 5 of those upregulated and 8 of those downregulated were also DE in *bts1x2* under Zn excess relative to Col-0, suggesting that these were potentially not Zn responsive but rather DE in *bts1x2* under all conditions (**Figures 5.6B and C**). However, 23 of the upregulated genes and 1 of those downregulated were also DE in Col-0 or *bts1x2* in response to Zn relative to their genotype control (**Figures 5.6B and C**). This suggests that a number of Zn-responsive genes were DE in *bts1x2* roots under control conditions and were further up- or downregulated under Zn treatment. Under Zn excess relative to Col-0 control, 489 genes were DE in Col-0 (168 upregulated, 321 downregulated) and 460 were DE in *bts1x2* (298 upregulated, 162 downregulated), with an additional 22 genes upregulated and 66 downregulated in *bts1x2* relative to *bts1x2* control (**Figure 5.6**). Of these, 172 genes were DE in both Col-0 and *bts1x2* roots in response to Zn (85 upregulated, 87 downregulated)(**Figures 5.6B and C**).

Overall, this suggested that *bts/1x2* shoots showed a less pronounced transcriptomic response to Zn excess than Col-0, which can be explained by the reduced toxicity symptoms observed in the mutant (see **Chapter 4**). Meanwhile, Col-0 and *bts/1x2* roots showed partially overlapping, but largely unique root transcriptomic responses to Zn, with *bts/1x2* also showing constitutive expression of a number of Zn-responsive genes.

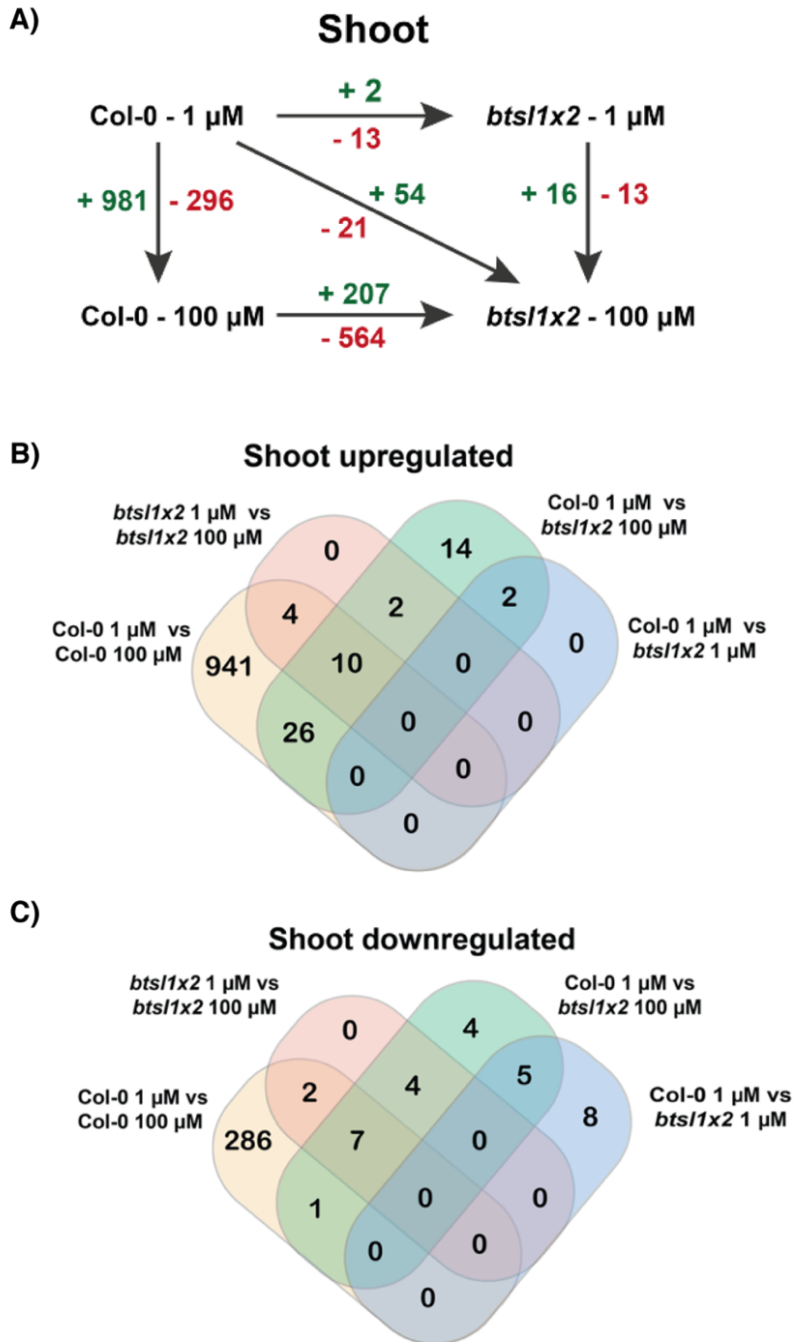


Figure 5.5: Significantly differentially expressed genes (DEGs) in Col-0 and *bts1x2* shoots grown under control (1 μM Zn) or Zn excess (100 μM Zn) conditions.

A) Number of significantly upregulated (+) or downregulated (-) genes between all pairwise comparisons. B-C) Venn diagrams showing the number of significantly B) upregulated and C) downregulated DEGs in four pairwise comparisons of interest (Col-0 1 μM Zn vs *bts1x2* 1 μM Zn; Col-0 1 μM Zn vs Col-0 100 μM Zn; Col-0 1 μM Zn vs *bts1x2* 100 μM Zn; *bts1x2* 1 μM Zn vs *bts1x2* 100 μM Zn) and the overlap between these gene sets.

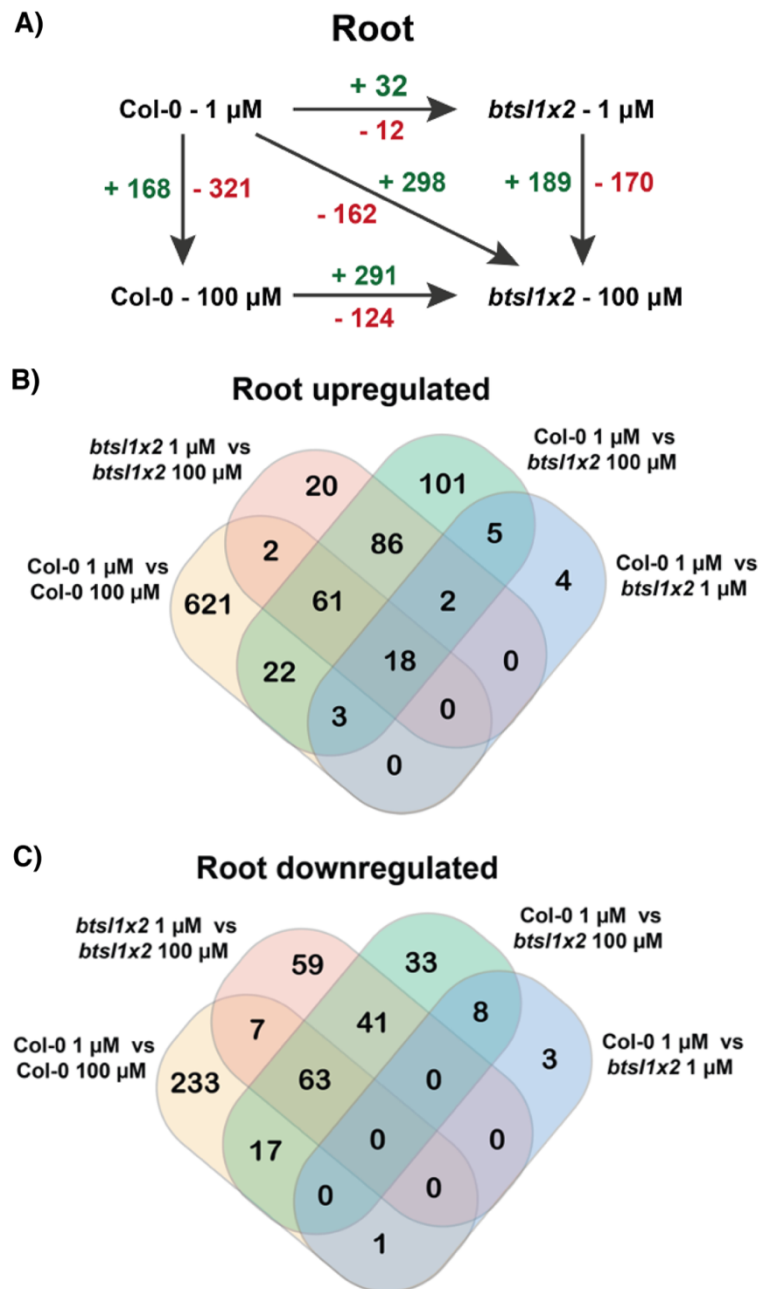


Figure 5.6: Significantly differentially expressed genes (DEGs) in Col-0 and *bts1x2* roots grown under control (1 μM Zn) or Zn excess (100 μM Zn) conditions.

A) Number of significantly upregulated (+) or downregulated (-) genes between all pairwise comparisons. B-C) Venn diagrams showing the number of significantly B) upregulated and C) downregulated DEGs in four pairwise comparisons of interest (Col-0 1 μM Zn vs *bts1x2* 1 μM Zn; Col-0 1 μM Zn vs Col-0 100 μM Zn; Col-0 1 μM Zn vs *bts1x2* 100 μM Zn; *bts1x2* 1 μM Zn vs *bts1x2* 100 μM Zn) and the overlap between these gene sets.

5.2.4 Hierarchical clustering of shoot Differentially Expressed Genes (DEGs)

In order to identify different patterns between the Col-0 and *bts1x2* shoot transcriptomic response to Zn, hierarchical clustering of the 1311 significantly DE shoot genes was performed and Gene Ontology (GO) enrichment analysis for biological processes was carried out on the 8 major clusters (**Figure 5.7; Supplementary Dataset**). GO enrichment analysis was also run on larger subsets of genes consisting of the genes that were significantly up- or downregulated uniquely in Col-0, *bts1x2* or both in order to capture terms that might be missed when only looking at smaller selected clusters and verify the clustering analysis (**Supplementary Figure C2, Appendix C**). These larger subsets were also annotated for Kyoto Encyclopedia of Genes and Genomes (KEGG) metabolic pathways (**Supplementary Figure C3, Appendix C**). Selected Fe and Zn homeostasis genes that were DE in Col-0 or *bts1x2* shoots are shown in **Table 5.2**.

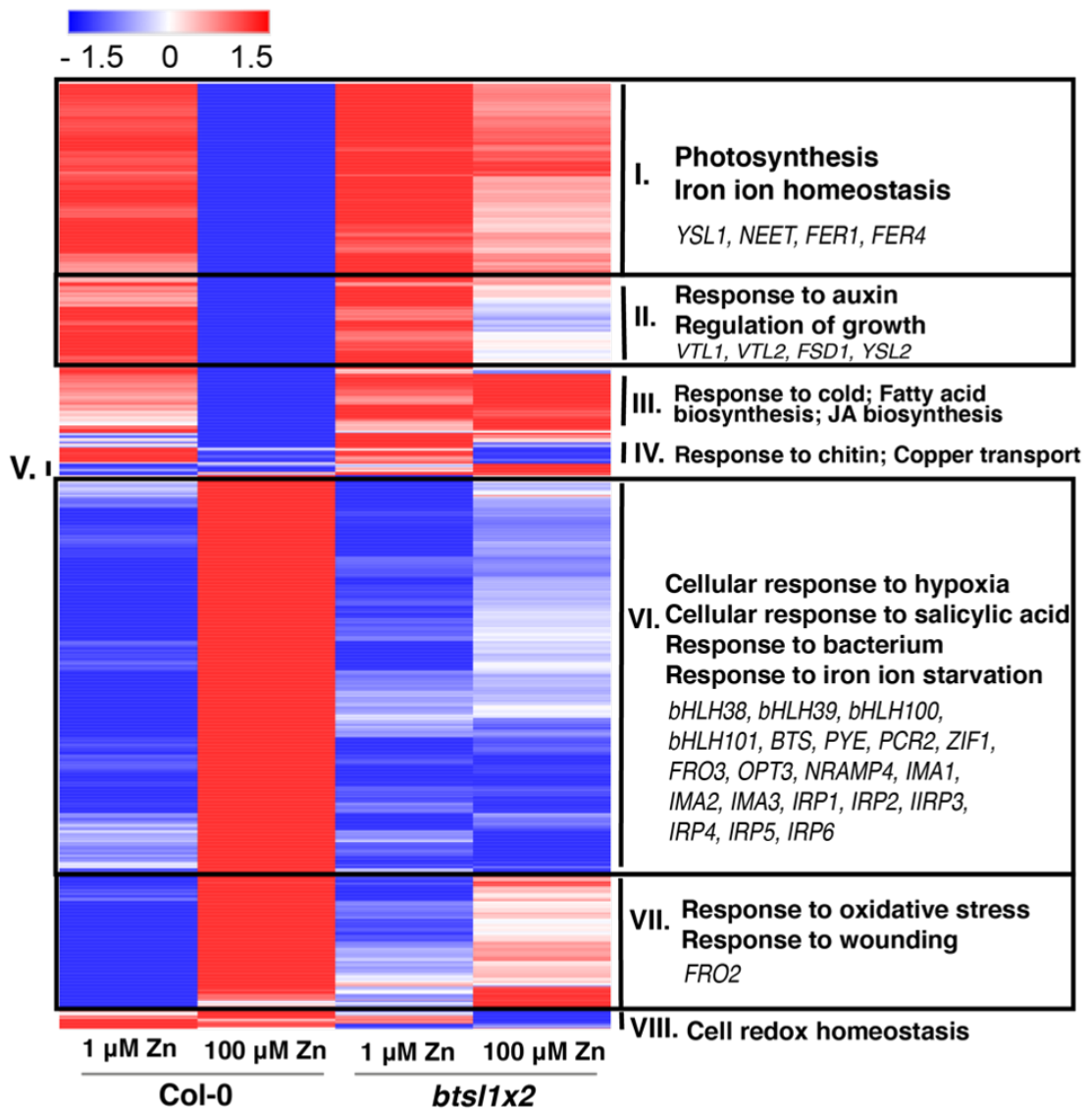


Figure 5.7: Hierarchical clustering analysis of Zn-responsive genes in Col-0 and *bts1x2* shoots.

Major clusters are numbered I-VIII and annotated for significantly ($p_{adj} < 0.05$) enriched GO terms and Fe/Zn homeostasis genes. Expression is represented as standard deviation from the mean.

	Gene ID	Gene name	Col-0 1 Zn vs Col-0 100 Zn		Col-0 1 Zn vs <i>bts/1x2</i> 100 Zn		<i>bts/1x2</i> 1 Zn vs <i>bts/1x2</i> 100 Zn	
			qval	log2FC	qval	log2FC	qval	log2FC
Cluster I	AT4G24120	<i>Yellow Stripe Like 1 (YSL1)</i>	3.35E⁻¹⁰	-1.86	0.98	0.13	0.99	-0.23
	AT5G51720	<i>NEET</i>	4.23E⁻²⁶	-6.08	0.96	-0.42	0.99	-0.84
	AT5G01600	<i>Ferritin 1 (FER1)</i>	4.10E⁻¹⁴	-2.56	0.99	-0.47	0.99	-0.29
	AT2G40300	<i>Ferritin 4 (FER4)</i>	3.56E⁻³⁸	-3.00	0.99	0.02	0.99	-0.32
Cluster II	AT1G21140	<i>Vacuolar Iron Transporter-Like 1 (VTL1)</i>	2.72E⁻⁰⁶	-2.54	0.04	-1.38	0.01	-1.12
	AT1G76800	<i>Vacuolar Iron Transporter-Like 2 (VTL2)</i>	1.24E⁻¹³	-2.49	0.03	-1.07	1.03E⁻¹⁰	-1.40
	AT4G25100	<i>Fe-superoxide Dismutase 1 (FSD1)</i>	5.95E⁻²⁰	-6.14	5.33E⁻¹³¹	-3.30	3.07E⁻⁴⁶	-3.35
	AT5G24380	<i>Yellow Stripe Like 2 (YSL2)</i>	9.12E⁻⁰⁷	-1.80	6.19E⁻⁰³	-1.80	0.01	-1.12
Cluster VI	AT3G56970	<i>bHLH38</i>	1.28E⁻²³	6.49	0.43	1.68	-	-
	AT3G56980	<i>bHLH39</i>	1.29E⁻²⁴	5.83	0.70	1.26	-	-
	AT2G41240	<i>bHLH100</i>	1.06E⁻¹⁵	6.19	0.97	0.49	-	-
	AT5G04150	<i>bHLH101</i>	1.41E⁻⁰⁸	3.28	0.97	0.27	8.41E⁻⁰⁵	3.22
	AT3G18290	<i>Brutus (BTS)</i>	3.88E⁻²⁷	2.00	0.67	0.26	0.03	0.52
	AT3G47640	<i>Popeye (PYE)</i>	1.02E⁻⁰³	1.41	0.98	0.06	0.99	0.11
	AT1G14870	<i>Plant Cadmium Resistance 2 (PCR2)</i>	3.50E⁻⁰⁷	3.04	0.55	1.35	0.49	1.29
	AT5G13740	<i>Zinc-Induced Facilitator 1 (ZIF1)</i>	5.04E⁻⁰⁶	1.86	0.98	0.126	0.99	0.18
	AT1G23020	<i>Ferric Reductase Oxidase 3 (FRO3)</i>	3.47E⁻⁰⁹	2.02	0.94	0.44	0.9	0.55
	AT4G16370	<i>Oligopeptide transporter 3 (OPT3)</i>	1.48E⁻⁰⁷	1.76	0.89	0.23	0.99	0.40

Gene ID	Gene name	Col-0 1 Zn vs Col-0 100 Zn		Col-0 1 Zn vs <i>bts/1x2</i> 100 Zn		<i>bts/1x2</i> 1 Zn vs <i>bts/1x2</i> 100 Zn	
		qval	log2FC	qval	log2FC	qval	log2FC
AT5G67330	Natural Resistance Associated Macrophage Protein 4 (NRAMP4)	0.02	1.17	0.98	-0.11	0.99	-0.04
AT1G47400	Fe-uptake Inducing Peptide 3/Ironman 1 (FEP3/IMA1)	1.24E ⁻¹¹	5.02	0.96	0.80	-	-
AT1G47395	Fe-uptake Inducing Peptide 2/Ironman 2 (FEP2/IMA2)	3.63E ⁻²⁷	5.20	0.96	0.65	-	-
AT2G30766	Fe-uptake Inducing Peptide 1/Ironman 3 (FEP1/IMA3)	9.60E ⁻¹⁸	3.14	0.98	-0.15	-	-
AT1G47400	Iron-Responsive Protein 1 (IRP1)	1.24E ⁻¹¹	5.02	0.96	0.80	-	-
AT1G47395	Iron-Responsive Protein 2 (IRP2)	3.63E ⁻²⁷	5.20	0.96	0.65	-	-
AT2G14247	Iron-Responsive Protein 3 (IRP3)	1.99E ⁻⁰⁴	5.54	0.9	0.85	0.40	3.07
AT1G13609	Iron-Responsive Protein 4 (IRP4)	1.75E ⁻¹⁹	5.76	0.92	0.77	-	-
AT3G56360	Iron-Responsive Protein 5 (IRP5)	0.03	1.09	0.99	-0.10	0.94	0.35
AT5G05250	Iron-Responsive Protein 6 (IRP6)	2.84E ⁻⁰⁶	2.67	0.97	0.40	0.08	2.39
Cluster VII AT1G01580	Ferric Reductase Oxidase 2 (FRO2)	0.01	1.25	0.16	1.03	3.90E ⁻⁰³	1.26

Table 5.2: Selected Fe- and Zn-homeostasis genes that were significantly (qval < 0.05, log2FC > 1) DE in Col-0 or *bts/1x2* shoots in response to Zn excess.

Expression values too low to give a readout are indicated by a '-'.

Cluster I

Cluster I contained genes that showed similar steady state mRNA levels in both genotypes under control conditions, and were then significantly downregulated in Col-0 under Zn excess (**Figure 5.7**). Multiple photosynthetic genes involved in the electron transport were found in this cluster, such as chlorophyll A/B binding proteins *LHCA1*, *LHCA3* (AT1G61520), *CAB1*, *CAB2* (AT1G29920) and *CAB3* (AT1G29910), light harvesting complexes *LHCB3* and *LHCB5* (AT4G10340) and photosystem subunits associated with both photosystems such as *PSBY* (AT1G67740) and *PSAL* (AT4G12800). Fe plays a major role in many photosynthetic proteins and the electron transport chain. Under Zn excess, Zn is able to disrupt Fe proteomic function leading to a reduction in photosynthetic capacity and chlorophyll biosynthesis. A number of Fe homeostatic genes that are known to be downregulated on Fe starvation were also in this cluster. These included the Fe-S cluster binding protein *NEET*, metal-NA transporter *YSL1* and the ferritin Fe storage proteins *FER1* and *FER4* (**Table 5.2**). These results were consistent with enrichment of photosynthetic and Fe homeostasis-associated genes in the Col-0 uniquely downregulated gene set (**Supplementary Figures C2 and C3, Appendix C**). This downregulation of photosynthetic genes and genes associated with Fe storage and transport was consistent with the higher shoot Zn/Fe ratio and chlorosis of Col-0 under Zn excess.

Cluster II

Cluster II consisted of genes that showed a similar level of expression in both genotypes under control conditions. Genes were then strongly downregulated in Col-0 in response to Zn, and partially downregulated in *bts1x2* (**Figure 5.7**). A number of these genes were associated with auxin responses and signalling, including 16 members of the auxin early response SAUR gene family, *IAA29* (AT4G32280) and homeobox gene *HAT2* (AT5G47370). Fe deficiency is thought to reduce polar auxin transport from roots to shoots [493], and that this reduction in shoot auxin is linked to Fe deficiency induced growth stunting and repression of photosynthesis [494]. Auxin-associated GO terms were also overrepresented in the Col-0 uniquely downregulated gene set, as well as plant hormone signal transduction pathways (**Supplementary Figures C2 and C3,**

Appendix C). Although this cluster was not enriched in metal homeostasis genes, three Fe homeostasis-related genes were identified. These were vacuolar Fe import proteins *VTL1* and *VTL2*, Fe-superoxide dismutase *FSD1* which was involved in oxidative stress detoxification, and metal-NA transporter *YSL2* (**Table 5.2**). The differential expression of auxin-related genes and some genes involved in Fe homeostasis in *bts/1x2* shoots were indicative that *bts/1x2* shoots were responding to excess Zn, although to a lesser extent than Col-0, which was again consistent with the higher Zn/Fe ratio in Col-0 shoots (**Chapter 4**).

Cluster III

Cluster III contained genes that were expressed more highly in *bts/1x2* under control conditions compared to Col-0. Under Zn excess, genes were downregulated in Col-0 and either partially upregulated or showed no change in expression in *bts/1x2* in comparison to control conditions (**Figure 5.7**). There was an overrepresentation of genes involved in the response to cold, fatty acid and JA biosynthesis. These include *KCS5* (AT1G25450), *KCS6* (AT1G68530) and *AOS* (AT5G42650) which function in both long chain fatty acid and JA biosynthetic pathways. These processes could be related to either altering fatty acid composition in response to oxidative stress [495], or perhaps linked to JA signalling, which has been shown to have a role in abiotic stress and alter Fe deficiency signalling [496, 497]. Differential expression of hormone signalling and stress-responsive genes between Col-0 and *bts/1x2* under Zn treatment was again consistent with different metal content and physiological stress phenotypes between the two genotypes, although this could also be linked to pleiotropic phenotypes.

Cluster IV

Cluster IV contained genes with similar levels of expression in both genotypes under control conditions, and genes were downregulated in both genotypes under Zn excess (**Figure 5.7**). Genes in this cluster were enriched for terms related to the response to chitin, such as the BTB and TAZ domain protein *BT5* (AT4G37610) and the ethylene response factor *ERF105* (AT5G51190). Fe deficiency leads to altered cellular redox states which can trigger biotic stress pathways, as well as some overlap in the regulation of Fe

and biotic-responsive genes [498]. Analysis of the Col-0 uniquely DEGs showed chitin-responsive terms also associated with the upregulated gene set, suggesting that there were large and complex transcriptomic changes related to biotic stress induction, with gene sets not simply being up- or downregulated (**Supplementary Figures C2, Appendix C**). There was an enrichment in Cu transport genes, with Cu chaperone *CCH* (AT3G56240) and plasma membrane Cu transporter *COPT2* (AT3G46900), which is also involved in Fe-Cu cross-talk. Fe deficiency leads to increased Cu shoot concentration [499], which in turn causes downregulation of these Cu transporters to help prevent Cu toxicity [500]. These data support the indication from cluster II that *bts1x2* shoots were experiencing some metal stress and suggested that Cu homeostasis could be affected in *bts1x2*.

Cluster V

Cluster V contained genes that were more highly expressed in *bts1x2* under both control and Zn excess conditions compared to Col-0 (**Figure 5.7**). This small subset of genes were not significantly enriched in any GO terms but two genes of interest, *NF-YA2* (AT3G05690) and *NF-YA10* (AT5G06510), code for CCAAT-binding complex proteins that are transcription factors involved in regulating leaf size [501]. Overexpression of these transcription factors leads to increased cell expansion and leaf growth. The *bts1x2* mutant shows increased rosette leaf area compared to Col-0 under both control and Zn excess conditions (**Chapter 4**), and higher expression of *NF-YA2* and *NF-YA10* may partially explain this phenotype.

Cluster VI

In this cluster genes showed similar low expression in both genotypes under control conditions. Under Zn excess, genes were strongly upregulated in Col-0, with partial or no upregulation in *bts1x2* compared to control conditions (**Figure 5.7**). This cluster was significantly enriched for genes involved in biotic and abiotic stress responses, including cellular response to hypoxia, salicylic acid and bacteria. A number of redox-related genes were found in this category, such as cytochrome P450 family members *CYP71A12* (AT2G30750) and *CYP71A3* (AT2G30770), 2-oxoglutarate (2-OG) and Fe(II)-dependent oxygenase family protein AT4G10500 and peroxidases, such as

PER4 (AT1G14540). As previously mentioned, ROS production and biotic stress pathways are tightly linked and both triggered by Fe deficiency. Fe starvation-responsive genes were also overrepresented in this cluster, including most of the central regulators of the Fe deficiency response, *bHLH38*, *bHLH39*, *bHLH100*, *bHLH101*, *BTS* and *PYE* (**Table 5.2**). Interestingly, *bHLH101* was significantly upregulated in *bts1x2* in response to Zn, but expression levels were still far lower than Col-0 (**Table 5.2**). Zn detoxification genes, *PCR2*, *FRO3* and *ZIF1*, and genes involved in Fe signalling and distribution, *OPT3*, *NRAMP4*, *IMA1*, *IMA2* and *IMA3* were also upregulated in Col-0 but not *bts1x2*. The IRON-RESPONSIVE PROTEIN (IRP) family, previously identified as six proteins of unknown function that are strongly induced in Fe deficient leaves, *IRP1*, *IRP2*, *IRP3*, *IRP4*, *IRP5* and *IRP6*, were also found in this cluster (**Table 5.2**). This was consistent with the GO analysis of Col-0 uniquely upregulated genes, which showed enrichment in metal homeostasis, oxidative stress and biotic stress terms (**Supplementary Figures C2 and C3, Appendix C**). The upregulation of oxidative stress and Fe deficiency related genes in Col-0, but not *bts1x2*, was consistent with *bts1x2* showing a reduced shoot Zn/Fe ratio and thus maintaining Fe sensing and systemic sufficiency signalling.

Cluster VII

In this group, genes were expressed at a similar low level under control conditions in both genotypes. Under Zn excess, genes were strongly upregulated in Col-0, and partially upregulated in *bts1x2* in comparison to control conditions (**Figure 5.7**). Genes in this cluster were enriched in terms related to oxidative stress and oxidation-reduction processes. The ferric chelate reductase *FRO2* (**Table 5.2**), as well as members of the cysteine-rich transmembrane module (CYSTM) family protein, such as *ATCYSTM1* (AT1G05340), *ATHCYSTM4* (AT2G32190) and *ATHCYSTM5* (AT2G32200), Cu/Zn superoxide dismutase *CSD1* (AT1G08830) and *CSD2* (AT2G28190) and a number of peroxidase family members belong to this group. Superoxide radicals are produced under Fe deficiency and Zn excess due to reduced photosynthetic and respiratory capacity, and upregulation of these genes helps to regulate and detoxify these species. *FRO2* activity in shoots may participate in these processes, as well as making internal Fe available to Fe deficient shoots. Higher upregulation of these genes in Col-0 than *bts1x2* was consistent again with increased Fe deficiency and Zn toxicity stress in wild type.

Cluster VIII

Cluster VIII consisted of genes that showed higher steady state mRNA levels under control conditions in Col-0 compared to *bts/1x2*. Under Zn excess, genes were downregulated in *bts/1x2*, but did not show any change in expression in Col-0 in comparison to control conditions (**Figure 5.7**). Genes in this group were enriched for cell redox homeostasis functionality, which could mainly be attributed to members of the thioredoxin superfamily – *GRXS1* (AT1G03020), *GRXS8* (AT4G15660), *GRXS7* (AT4G15670), *GRXS4* (AT4G15680) and *GRXS5* (AT4G15690). Monothiol glutaredoxins (GRXs) are redox regulatory proteins conserved across species that have been linked to Fe homeostasis regulation [502], with the *GRXS4/5/7/8* gene cluster also shown to be co-ordinately upregulated by nitrate [503], suggestive of redox and nutrient alterations in *bts/1x2* shoots. Cell redox homeostasis was also an enriched GO term for genes uniquely downregulated in *bts/1x2* shoots under Zn excess (**Supplementary Figure C2, Appendix C**). This again supported a genotype-specific transcriptomic response to Zn excess in *bts/1x2* shoots, linked to reduced shoot Zn accumulation, which in turn affected cellular redox status and homeostasis of other nutrients.

5.2.5 Hierarchical clustering of root DEGs

Hierarchical clustering of the 882 root DEGs was carried out and GO analysis performed on the seven major clusters identified (**Figure 5.8; Supplementary Dataset**). GO and KEGG pathway enrichment analysis was also performed on larger subsets of genes representing Col-0 and *bts/1x2* commonly and uniquely expressed genes (**Supplementary Figures C4 and C5, Appendix C**). Selected Fe and Zn homeostasis genes of interest are shown in **Table 5.3**.

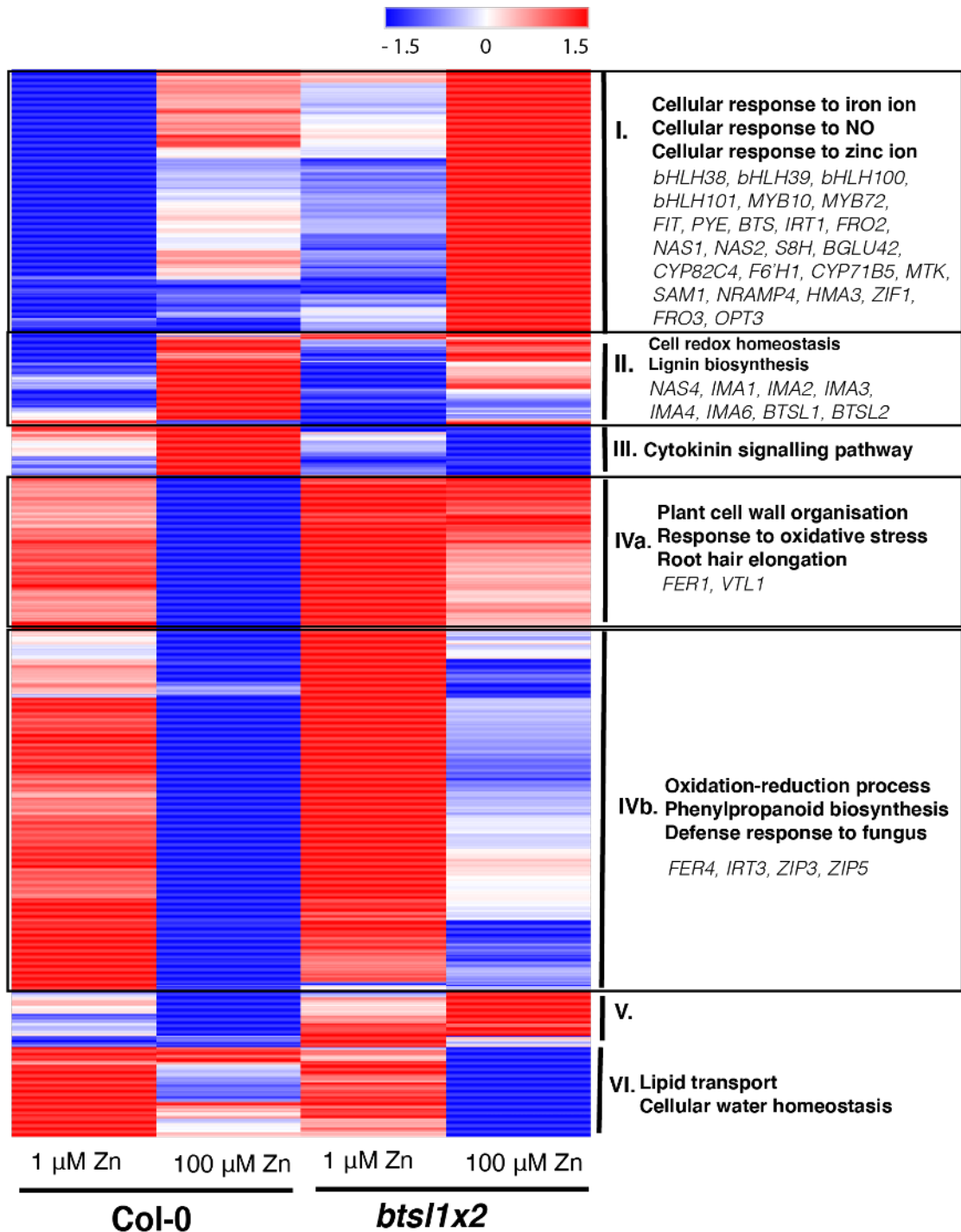


Figure 5.8: Hierarchical clustering analysis of Zn-responsive genes in Col-0 and *bts1x2* roots.

Major clusters are numbered I-VI and annotated for significantly ($p_{adj} < 0.05$) enriched GO terms and Fe/Zn homeostasis genes. Expression is represented as standard deviation from the mean.

Gene ID	Gene name	Col-0 1 Zn vs <i>bts1x2</i> 1 Zn		Col-0 1 Zn vs Col-0 100 Zn		Col-0 1 Zn vs <i>bts1x2</i> 100 Zn		<i>bts1x2</i> 1 Zn vs <i>bts1x2</i> 100 Zn	
		qval	log2FC	qval	log2FC	qval	log2FC	qval	log2FC
AT3G56970	<i>bHLH38</i>	5.71E ⁻¹¹	3.84	3.54E ⁻¹⁶	4.71	1.61E ⁻²⁴	5.52	4.48E ⁻⁵²	1.24
AT3G56980	<i>bHLH39</i>	2.04E ⁻⁷³	3.42	5.49E ⁻⁷⁰	4.07	5.46E ⁻¹⁴¹	4.67	4.48E ⁻⁵²	1.24
AT2G41240	<i>bHLH100</i>	2.57E ⁻²¹	5.50	3.44E ⁻²⁷	6.29	1.14E ⁻⁴⁴	7.55	1.52E ⁻⁵³	2.06
AT5G04150	<i>bHLH101</i>	1.83E ⁻⁰⁹	2.08	1.81E ⁻²⁹	3.05	2.81E ⁻⁶³	4.42	7.42E ⁻⁴⁸	2.33
AT3G12820	<i>Myb Domain Protein 10 (MYB10)</i>	2.82E ⁻¹⁴	1.41	2.80E ⁻¹⁶	2.49	7.02E ⁻⁵⁰	3.50	5.18E ⁻³⁷	2.08
AT1G56160	<i>Myb Domain Protein 72 (MYB72)</i>	2.10E ⁻⁰⁷	5.08	1.99E ⁻¹⁰	5.72	4.41E ⁻¹⁸	7.07	6.47E ⁻³⁹	2.03
AT2G28160	<i>Fer-Like Iron Deficiency-Induced Transcription Factor (FIT)</i>	0.99	0.29	8.07E ⁻⁰⁵	1.07	5.85E ⁻⁰⁹	1.16	3.02E ⁻³⁹	0.86
AT3G47640	<i>Popeye (PYE)</i>	5.44E ⁻⁰⁵	0.59	7.12E ⁻⁰⁸	1.03	2.20E ⁻²⁴	1.55	0.02	0.51
AT3G18290	<i>Brutus (BTS)</i>	0.36	0.17	9.63E ⁻¹⁹	0.68	1.92E ⁻³¹	1.06	8.49E ⁻²²	0.87
AT4G19690	<i>Iron-Regulated Transporter 1 (IRT1)</i>	0.96	1.87	0.03	2.94	3.94E ⁻⁰³	3.63	4.05E ⁻⁴⁶	1.75

Cluster I

Gene ID	Gene name	Col-0 1 Zn vs <i>bts1x2</i> 1 Zn		Col-0 1 Zn vs Col-0 100 Zn		Col-0 1 Zn vs <i>bts1x2</i> 100 Zn		<i>bts1x2</i> 1 Zn vs <i>bts1x2</i> 100 Zn	
		qval	log2FC	qval	log2FC	qval	log2FC	qval	log2FC
AT4G19680	<i>Iron-Regulated Transporter 2 (IRT2)</i>	3.95E ⁻⁰⁸	0.72	6.76E⁻¹⁹	1.46	1.92E⁻⁵¹	1.92	2.26E⁻⁷⁵	1.20
AT1G01580	<i>Ferric Reductase Oxidase 2 (FRO2)</i>	0.99	1.88	0.04	3.07	6.32E⁻⁰³	3.84	9.90E⁻²⁹	1.95
AT5G04950	<i>Nicotianamine Synthase 1 (NAS1)</i>	0.99	0.48	0.06	1.04	6.24E⁻⁰³	1.40	6.72E ⁻⁰⁴	0.92
AT5G056080	<i>Nicotianamine Synthase 2 (NAS2)</i>	0.99	0.41	0.05	0.68	3.21E⁻¹¹	1.87	6.25E⁻⁴¹	1.46
AT3G53480	<i>ABC Transporter G Family Member 37 (ABCG37)</i>	0.01	0.52	2.70E⁻⁰⁹	1.06	3.81E⁻³⁰	1.47	0.04	0.41
AT3G12900	<i>Scopoletin 8-Hydroxylase (S8H)</i>	0.37	2.63	0.04	2.74	2.86E⁻⁰³	3.60	5.93E⁻⁰³	1.05
AT5G36890	<i>Beta-glucosidase 42 (BGLU42)</i>	7.98E ⁻⁰⁶	0.88	8.83E⁻⁰⁹	1.39	4.01E⁻⁴²	2.42	7.81E⁻⁰⁴	1.02
AT4G31940	<i>Cytochrome P450 82, Subfamily C (CYP82C4)</i>	0.99	1.86	0.03	1.21	2.13E⁻⁰³	4.36	1.67E⁻⁰⁷	1.19
AT3G13610	<i>Feruloyl CoA Ortho-Hydroxylase 1 (F6'H1)</i>	0.03	0.74	2.00E ⁻⁰⁵	0.87	5.83E⁻³³	1.79	6.79E⁻⁰⁹	1.05
AT3G53280	<i>Cytochrome P450 71, Subfamily B (CYP71B5)</i>	5.61E ⁻⁰⁴	3.83	8.49E⁻⁰⁴	3.16	3.43E⁻¹⁰	5.17	3.13E⁻⁰⁴	1.34
AT1G49820	<i>5-Methylthioribose Kinase 1 (MTK)</i>	0.04	0.28	3.86E ⁻⁰⁹	0.94	4.67E⁻³⁰	1.39	5.65E⁻²⁹	1.11

Gene ID	Gene name	Col-0 1 Zn vs <i>bts1x2</i> 1 Zn		Col-0 1 Zn vs Col-0 100 Zn		Col-0 1 Zn vs <i>bts1x2</i> 100 Zn		<i>bts1x2</i> 1 Zn vs <i>bts1x2</i> 100 Zn	
		qval	log2FC	qval	log2FC	qval	log2FC	qval	log2FC
AT1G02500	<i>S-adenosylmethionine Synthase 1 (SAM1)</i>	1.09E ⁻⁰³	0.56	1.97E ⁻⁰⁸	0.83	7.39E⁻⁴⁶	1.36	2.24E ⁻¹²	0.80
AT5G67330	<i>Natural Resistance Associated Macrophage Protein 4 (NRAMP4)</i>	1.25E ⁻⁰⁶	0.41	7.25E ⁻¹⁸	0.69	1.27E⁻⁵¹	1.36	1.74E ⁻³⁴	0.95
AT4G30120	<i>HMA3</i>	0.62	0.70	3.51E⁻⁰⁵	1.75	1.09E⁻⁰⁷	2.04	9.57E⁻¹⁶	1.33
AT5G13740	<i>Zinc-Induced Facilitator 1 (ZIF1)</i>	0.10	0.37	1.50E ⁻³⁶	0.91	7.33E⁻⁴²	1.61	2.43E⁻²⁰	1.24
AT1G23020	<i>Ferric Reductase Oxidase 3 (FRO3)</i>	1.05E⁻¹⁰	1.15	1.56E⁻¹⁷	1.89	3.14E⁻⁴⁷	2.59	2.70E⁻⁷⁸	1.43
AT4G16370	<i>Oligopeptide transporter 3 (OPT3)</i>	3.60E⁻⁰⁸	1.27	1.40E⁻³⁶	2.41	5.07E⁻⁴⁹	3.24	1.89E⁻²⁰	1.97
AT3G58060	<i>Metal Tolerance Protein 8 (MTP8)</i>	0.72	1.72	0.04	2.14	3.06E⁻⁰³	2.95	4.00E⁻⁰³	1.22
AT3G58810	<i>Metal Tolerance Protein A2/3 (MTPA2/MTP3)</i>	0.46	1.30	5.60E⁻⁰³	1.83	1.13E⁻⁰⁴	2.38	1.58E⁻²⁹	1.07
AT5G03570	<i>Iron-Regulated Protein 2 (IREG2)</i>	0.16	0.89	6.44E⁻³⁰	1.73	2.18E⁻³⁶	1.99	2.29E⁻⁰⁴	1.09

Cluster I

Gene ID	Gene name	Col-0 1 Zn vs <i>bts1x2</i> 1 Zn		Col-0 1 Zn vs Col-0 100 Zn		Col-0 1 Zn vs <i>bts1x2</i> 100 Zn		<i>bts1x2</i> 1 Zn vs <i>bts1x2</i> 100 Zn	
		qval	log2FC	qval	log2FC	qval	log2FC	qval	log2FC
AT1G56430	<i>Nicotianamine Synthase 4 (NAS4)</i>	0.99	0.04	3.04E⁻⁴⁷	1.92	7.03E⁻²³	1.99	6.74E⁻¹⁶	1.96
AT1G47400	<i>Fe-uptake Inducing Peptide 3/Ironman 1 (FEP3/IMA1)</i>	-	-	4.69E⁻²⁶	4.71	3.93E⁻⁰⁴	2.91	1.53E⁻¹³	4.71
AT1G47395	<i>Fe-uptake Inducing Peptide 2/Ironman 2 (FEP2/IMA2)</i>	-	-	3.65E⁻³⁴	4.69	1.57E⁻⁰³	2.49	7.54E⁻⁰⁵	3.24
AT2G30766	<i>Fe-uptake Inducing Peptide 1/Ironman 3 (FEP1/IMA3)</i>	-	-	4.85E⁻⁴³	5.23	-	-	-	-
AT1G07367	<i>Ironman 4 (IMA4)</i>	-	-	1.65E⁻¹¹	4.39	1.81E⁻⁰⁴	2.83	1.27E⁻⁰⁷	3.39
AT1G07373	<i>Ironman 6 (IMA6)</i>	-	-	1.54E⁻⁶³	5.70	1.05E⁻¹³	3.82	2.17E⁻¹²	3.84
AT1G74770	<i>Brutus-Like 1 (BTSL1)</i>	0.012	-0.78	2.67E⁻¹³	1.64	0.57	0.18	3.61E⁻¹⁸	0.96
AT1G18910	<i>Brutus-Like 2 (BTSL2)</i>	5.60E⁻⁰⁴	-0.58	1.39E⁻⁰⁷	1.83	1.52E⁻⁰⁶	0.72	1.75E⁻¹⁹	1.30
AT5G01600	<i>Ferritin 1 (FER1)</i>	0.99	5.98E⁻⁰⁴	6.97E⁻¹⁴⁹	-1.63	0.02	-0.49	0.01	-0.48
AT1G21140	<i>Vacuolar Iron Transporter-Like 1 (VTL1)</i>	0.34	0.20	4.71E⁻³⁴	-1.03	0.70	-0.17	0.25	-0.38

Gene ID	Gene name	Col-0 1 Zn vs <i>bts1x2</i> 1 Zn		Col-0 1 Zn vs Col-0 100 Zn		Col-0 1 Zn vs <i>bts1x2</i> 100 Zn		<i>bts1x2</i> 1 Zn vs <i>bts1x2</i> 100 Zn	
		qval	log2FC	qval	log2FC	qval	log2FC	qval	log2FC
AT2G40300	<i>Ferritin 4 (FER4)</i>	0.99	-0.06	3.97E⁻²⁵	-1.11	7.90E ⁻⁰⁵	-0.55	1.57E ⁻⁰⁷	-0.50
AT1G60960	<i>Iron-Regulated Transporter 3 (IRT3)</i>	0.99	0.11	3.77E⁻⁶⁶	-2.68	1.46E⁻²⁵	-1.91	1.37E⁻⁷⁷	-2.02
AT2G32270	<i>Zinc Transporter 3 (ZIP3)</i>	0.99	0.34	5.81E ⁻²⁴	-2.70	4.32E ⁻¹⁷	-2.27	3.64E ⁻⁵⁷	-2.61
AT1G05300	<i>Zinc Transporter 5 (ZIP5)</i>	0.99	0.16	2.35E⁻⁵⁰	-4.27	1.18E⁻¹⁴	-3.26	1.89E⁻¹⁸	-3.42
AT5G51720	<i>NEET</i>	0.99	-0.03	9.52E⁻⁰⁵	-2.47	2.30E⁻⁰³	-1.96	2.42E⁻⁰³	-1.94

Table 5.3: Selected Fe- and Zn-homeostasis genes that were significantly (qval < 0.05, log2FC > 1) DE in Col-0 or *bts1x2* roots in response to Zn excess.

Expression values too low to give a readout are indicated by '-'.

Cluster I

Cluster I contained genes that were expressed more highly in *bts1x2* than in Col-0 under control conditions. Genes were strongly upregulated in both genotypes in response to Zn excess compared to control. Thus, this cluster contained genes that were constitutively overexpressed in *bts1x2* (**Figure 5.8**). Genes in this cluster were significantly enriched for Fe and Zn homeostasis related terms, as well as NO-responsive genes. NO acts early in the Fe-deficiency response to activate FIT-dependent gene expression [388]. Both FIT-dependent and FIT-independent genes were found in this group, including *bHLH38*, *bHLH39*, *bHLH100*, *bHLH101*, *MYB10*, *MYB72*, *FIT*, *PYE*, *BTS* and *GRF11* (**Table 5.3**). Upregulation of transcription factors higher up than FIT in the Fe deficiency signalling cascade could suggest compensatory gene regulation elsewhere in the Fe homeostasis network, or that BTSL proteins have additional FIT-independent targets, such as IVc bHLH transcription factors or bHLH121/URI.

Downstream targets of these regulators involved in Fe uptake and transport were also in this group, such as *IRT1*, *IRT2*, *FRO2*, *NAS1*, *NAS2*, *ABCG37*, *S8H*, *BGLU42*, *CYP82C4*, *F6'H1*, *CYP71B5*, *MTK*, *SAM1*, *NRAMP4*, *HMA3*, *ZIF1*, *FRO3*, *OPT3*, *MTP8* and *MTP3* (**Table 5.3**). High expression of Fe uptake and translocation genes in *bts1x2* was consistent with improved Fe nutrition in the mutant, and most notably higher expression of *NAS* genes and *ZIF1* has been linked to Zn detoxification in roots and Fe translocation to shoots. Similar GO enrichment terms were seen in Col-0 and *bts1x2* common upregulated genes, as well as *bts1x2* uniquely upregulated genes under control and Zn excess conditions (**Supplementary Figures C4 and C5**). This showed that both FIT-dependent and FIT-independent gene expression was misregulated in *bts1x2* roots under control and Zn excess conditions, with the overexpression of Fe deficiency and Zn tolerance associated genes likely contributing towards the Fe-mediated Zn tolerance phenotype of the mutant.

Cluster II

Cluster II contained genes that showed a similar level of expression in both genotypes under control conditions. Under Zn excess, genes were strongly upregulated in Col-0, and partially upregulated in *bts1x2* in comparison to control conditions (**Figure**

5.8). Genes in this cluster were enriched for cell redox homeostasis GO terms, with a number of thioredoxins present in this cluster (AT2G30540, AT3G62930, AT4G15660, AT4G15680, AT4G15690). The exact function of thioredoxins in the root Fe deficiency is still not fully understood, but their upregulation under Fe limiting conditions is well documented and it is thought they may play a role in regulating H₂O₂ production and mitochondrial redox status. Changes in cell redox homeostasis in Col-0 may also be also linked to Fe and Zn overaccumulation in roots under Zn excess, which leads to ROS production. There was also enrichment of genes associated with lignin metabolism, such as chitin synthase *MWL-2* (AT4G19370) and the cell wall-bound peroxidase *PRX25* (AT2G41480). Lignin biosynthesis and deposition is a common response to heavy metal stress and is thought to alter secondary cell wall properties to help control transport of these metals within the plant, especially through lignification of the Casparian strip [228]. The larger gene set of commonly upregulated genes was also significantly enriched in phenylpropanoid and anthocyanin biosynthesis, which are also linked to the lignin metabolic pathway (**Supplementary Figures C4 and C5, Appendix C**).

A select number of Fe homeostasis genes were also in this cluster, including the Fe deficiency signalling peptides *IMA1*, *IMA2*, *IMA3*, *IMA4* and *IMA6* (**Table 5.3**). These genes are predominantly expressed in the stele independently of BTSL regulation and their expression is induced by shoot Fe deficiency, hence reduced *IMA* expression in *bts1x2* was consistent with Fe sufficiency signalling from the shoot. *NAS4* was also in this cluster and showed similar expression levels in both genotypes (**Table 5.3**). *NAS4* is expressed in both the stele and epidermal cell layers, and subjected to both FIT-dependent and FIT-independent regulation (**Figures 5.1 and 5.2**). As such, any BTSL-dependent overexpression of *NAS4* could be balanced out by ILR3-PYE repression in the stele, although it is likely far more complicated than this. *BTSL1* and *BTSL2* were also in this cluster, showing reduced expression as expected in the mutant (**Table 5.3**). The reduced expression of redox and lignification genes in *bts1x2*, as well as lower expression of BTSL-independent Fe homeostasis genes, was consistent with reduced root Fe content and stress in roots compared to Col-0. Moreover stele-expressed Fe and Zn homeostasis gene expression was consistent with reduced Fe deficiency and Zn stress signalling from shoots in *bts1x2*.

Cluster III

Cluster III contained genes were expressed more highly in Col-0 than *bts/1x2* under control conditions. Under Zn excess, genes were strongly upregulated in Col-0 and strongly downregulated in *bts/1x2* compared to control conditions (**Figure 5.8**). Genes involved in CK signalling were enriched in this cluster, with the presence of three Type-A response regulator (ARR) genes, *ARR5* (AT3G48100), *ARR6* (AT5G62920) and *AAR7* (AT1G19050). ARRs are induced by CK and function in a negative feedback loop to downregulate CK signalling, while CK itself negatively regulates root Fe uptake [323, 504]. High expression of *AARs* in Col-0 would suggest repression of CK signalling to increase root Fe uptake, with increased CK signalling in *bts/1x2*, perhaps signalling root Fe sufficiency. This suggested differential hormonal signalling in Col-0 and *bts/1x2*, with antagonistic CK signalling and Fe deficiency-induced gene expression in *bts/1x2*, but analysis of other CK signalling components is required to confirm this.

Cluster IVa

Cluster IVa contained genes that were more highly expressed in *bts/1x2* than Col-0 under control conditions. Under Zn excess, genes were strongly downregulated in Col-0, and partially downregulated in *bts/1x2* compared to control conditions (**Figure 5.8**). Genes were enriched for GO terms associated with plant cell wall organisation, response to oxidative stress and root hair elongation, with the majority of the genes in this cluster involved in cell wall modification and root development. For instance, there were a number of peroxidases (*AT1G05240*, *AT1G05250*, *AT1G30870*, *AT3G49960* and *AT4G26010*), expansins, such as *EXPA18* (AT1G62980) and *EXPA7* (AT1G12560) and proline-rich extension-like genes, such as *EXT10* (AT5G06640), *EXT6* (AT2G24980) and *EXT13* (AT5G35190). Additional root hair-specific genes important in promoting root hair tip growth in response to redox status were also found here, including *SFH1* (AT4G34580) and *DTX31* (AT1G12950)[505]. A number of these genes, such as *EXPA7* and *EXPA18* are upregulated by FIT in response to Fe deficiency (**Figure 5.1**)[308], so overexpression in *bts/1x2* was consistent with FIT accumulation. However, downregulation on Zn exposure, especially in Col-0, suggested that Zn excess signalling was suppressing these genes, and indeed, Zn excess has been demonstrated to induce

abnormal branched root hair morphology [506], further highlighting points of cross-homeostasis between Fe and Zn.

The larger gene dataset of commonly downregulated genes was also significantly enriched for oxidation-reduction processes and anthocyanin and phenylpropanoid compound biosynthesis, which are linked to cell wall modifications and root morphology (**Supplementary Figures C4 and C5, Appendix C**).

FER1 and *VTL1*, which are both associated with Fe storage, and *FER1* additionally with oxidation-reduction processes, were both downregulated under Fe depletion conditions and were also found in this cluster (**Table 5.3**). Both genes are subject to antagonistic bHLH121/URI and PYE regulation predominantly in the stele in response to shoot-borne Fe signalling (**Figure 5.1**). Greater downregulation of *FER1* and *VTL1* in Col-0 was consistent with Fe deficiency signalling from shoots.

Cluster IVb

Similarly to IVa, cluster IVb genes were expressed more highly in *bts1x2* under both control and Zn excess conditions compared to Col-0. Under Zn excess, genes were strongly downregulated in Col-0, and partially downregulated in *bts1x2* in comparison to control conditions, but more strongly so than in cluster IVa (**Figure 5.8**). Cluster IVa and IVb also showed enrichment of similar GO terms, with oxidation-reduction processes, phenylpropanoid biosynthesis and defense response to fungus, again with the function of many of these genes linking back to redox-regulation and redox-regulated growth processes (**Figure 5.8**). The larger dataset of commonly downregulated genes also showed enrichment for oxidation-reduction processes, defense response to fungus and anthocyanin compound biosynthesis (**Supplementary Figures C4 and C5, Appendix C**). Genes in this cluster associated with redox-reaction and defense response to fungus included nine members of the peroxidase family, such as *PER4* (AT1G14540) and *PER5* (AT1G14550), ten members of the cytochrome P450 family, such as *CYP71A12* (AT2G30750) and *CYP76G1* (AT3G52970), five members of the FAD-binding Berberine family, such as AT1G26380 and AT1G26390, and five members of the DEFL family. Apoplastic Fe³⁺ accumulation in Col-0 roots under Zn excess triggered ROS production and subsequent inhibition of root growth and changes in root morphology (**Chapter 4**). ROS can also trigger changes to cell wall biosynthesis and remodelling, through genes

such as the dirigent (DIR)-like protein family, of which seven were found in this cluster [507].

A number of Fe homeostasis genes were also found in this group, including Fe-storage protein *FER4*, which was regulated in a similar manner as *FER1* (Cluster IVa). Three Zn transporters, *IRT3*, *ZIP3* and *ZIP5* were also in the cluster (**Table 5.3**). Although *ZIP5* has been linked to FIT-dependent regulation [308], the exact regulatory mechanism repressing the expression of Zn transporters under Zn excess is not yet known. However, the expression pattern here suggested that their regulation is not BTSL-dependent and may be responsive to shoot Fe and Zn signals.

Cluster V

Cluster V was a small cluster of genes which were expressed more highly in *bts1x2* than Col-0 under control conditions. Under Zn excess, genes were strongly downregulated in Col-0 and strongly upregulated in *bts1x2* compared to control (**Figure 5.8**). There was no significant enrichment for GO terms, however a few genes of interest are found in this cluster, such as the phosphate deficiency-responsive transcription factor *WRKY45* (AT3G01970) and the sulphate transporter *SULTR2;1* (AT5G10180). *SULTR2;1* is a xylem-localised transporter involved in root-to-shoot transport of sulphur and is strongly downregulated under Fe and Pi deficiency conditions [508]. This suggests that phosphate and sulphur nutrition is also affected by loss of BTSL proteins in the *bts1x2* mutant, with upregulation on *SULTR2;1* suggesting sulphur deficiency but phosphate sufficiency [328], but in contrast upregulation of *WRKY45* in the mutant suggests phosphate deficiency. There is likely complicated and antagonistic Fe, Zn, phosphate and sulphur homeostasis cross-talk and signalling in *bts1x2* due to misregulation of Fe homeostasis genes [328].

Cluster VI

The final cluster contained genes that were highly expressed in both genotypes under control conditions. Under Zn excess, genes were strongly downregulated in *bts1x2* and partially downregulated in Col-0 in comparison to control conditions (**Figure 5.8**). There was an enrichment for genes associated with lipid transport and cellular

water homeostasis, including five members of the bifunctional inhibitor/lipid-transfer protein/seed storage 2S albumin superfamily (AT1G62510, AT4G12490, AT4G12500, AT4G22460 and AT5G46900) and three tonoplast intrinsic proteins, *GAMMA-TIP* (AT2G36830), *TIP2;2* (AT4G17340) and *TIP2;3* (AT5G47450). The exact function of these genes in their response to Zn remains unclear, although the lipid-transfer proteins have been linked with Fe and Zn transcriptomic responses previously, and the *TIP* genes could indicate differential salinity of small molecule status between the two genotypes [228].

Two of the principal phosphate uptake transporters, *PHT1;4* (AT2G38940) and *PHT1;2*, (AT5G43370), known to be upregulated under phosphate deficiency were also in this group [509]. Strong downregulation in *bts1x2* was consistent with phosphate sufficiency signalling as suggested by *SULTR2;1* expression in Cluster V. *SULTR2;1* and *PHT1* genes were regulated by PHR1, a transcription factor found to be important in integrating phosphate, sulphur, Fe and Zn signals, while *WRKY45* appears to be independent of this network [328]. As such, BTSL-dependent gene expression interaction with one of these networks could explain the seemingly opposite transcriptomic phosphate responses in *bts1x2* roots.

5.2.6 qRT-PCR confirmation of overexpression of FIT-dependent and FIT-independent genes in *bts1* mutants

The RNA-seq analysis showed that both FIT-dependent and FIT-independent genes were misregulated in *bts1x2*, as is seen in the *bts-3* mutant [304]. This raised the possibility that BTSL proteins can target additional transcription factors in the Fe deficiency signalling cascade. In order to verify these findings, as well as to test possible differences in targets between BTSL1 and BTSL2, qRT-PCR analysis of selected Fe homeostasis genes in *bts1*, *bts2* and *bts1x2* roots exposed to Fe deficiency and Zn excess was carried out (**Figure 5.9**). Two members of the FIT-interacting Ib bHLH family, *bHLH38* and *bHLH39*, were selected as FIT-independent genes that influence expression of the FIT regulon, with *IRT1* and *FRO2* selected as FIT-dependent target genes. Two genes that form part of the FIT-independent PYE regulon, *ZIF1* and *FRO3*, were also selected.

All genes were induced in all genotypes on exposure to Fe deficiency or Zn excess, with similar levels of upregulation observed within genotypes (**Figures 5.9A-C**). There was no significant difference in expression of the investigated genes under control conditions, although *bts/1x2* fold change was consistently higher than the single mutants and Col-0 (**Figures 5.9A-C**). Under Fe deficiency or Zn excess, *bts/1x2* expression of all selected genes was significantly higher than Col-0 and *bts/1*, as well as *bts/2* for a number of genes (**Figures 5.9A-C**). The single mutants showed similar expression patterns across all the gene sets, with *bts/1* expression being closer to Col-0, and *bts/2* upregulation higher and closer to *bts/1x2*. This data was consistent with the partially functionally redundant phenotypes observed in **Chapter 4**.

Taken together, this data confirmed the constitutive upregulation of FIT-dependent and FIT-independent genes in *bts/1x2*, including direct targets of IVc bHLH transcription factors and bHLH121/URI higher up in the Fe deficiency signalling cascade. It also showed that BTSL1 and BTSL2 are likely to have the same targets, however BTSL2 appeared to contribute more strongly to regulation than BTSL1. With BTSL1 and BTSL2 likely targeting similar proteins as BTS, combined with constitutive strong activation of the Fe deficiency response in *bts/1x2* roots but not shoots, it draws into question the current thinking of BTSL proteins as local Fe sensors. The insensitivity of *bts/1x2* roots to shoot Fe sufficiency signalling suggests a potential role in integrating both local and systemic signalling.

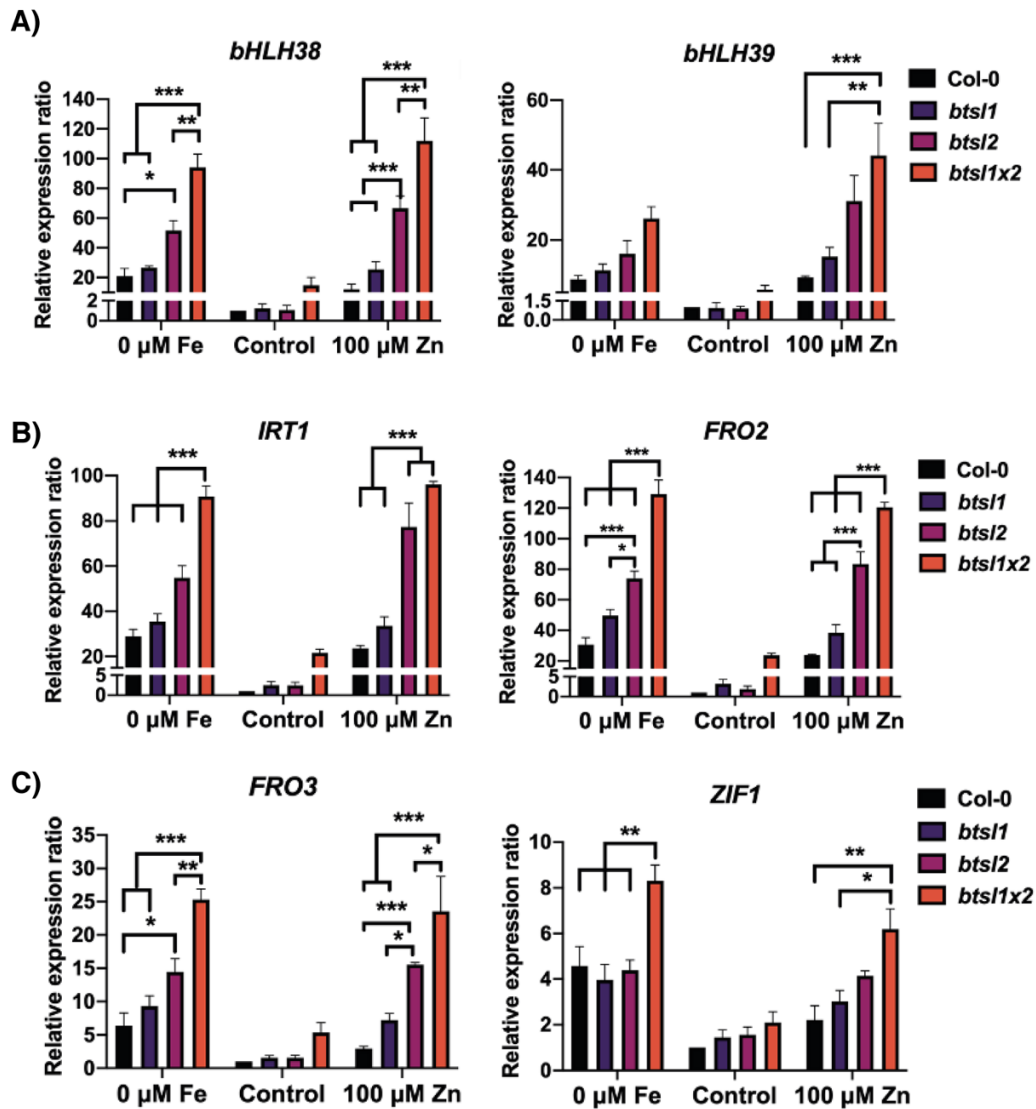


Figure 5.9: Quantitative reverse transcription PCR (qRT-PCR) analysis of selected Fe and Zn-responsive genes in Col-0 and *bts/* mutant roots in response to Fe deficiency and Zn excess.

The expression of selected Fe homeostasis genes A) FIT-interacting partners *bHLH38* and *bHLH39*, B) downstream of FIT, *IRT1* and *FRO2*, and C) FIT-independent, *FRO3* and *ZIF1*, in Col-0, *bts1*, *bts2* and *bts1x2* 14-d-old seedlings grown continuously on Fe deficiency (0 μM Fe), Zn excess (100 μM Zn) or control (5 μM Fe, 1 μM Zn) agar plates. Fold change is relative to Col-0 control (expression level set as “1”) and normalised to reference genes *ACTIN2* and *TIP41*. Data represent mean values (± SEM) from three independent experiments, each comprising five plants per genotype and condition, and each repeated as three technical replicates. Statistically significant differences are indicated by asterisks (within conditions, **p* < 0.05, ***p* < 0.01, ****p* < 0.001) as determined by two-way ANOVA followed by Tukey HSD post-hoc test. Non-significant differences are not indicated.

5.2.7 *bts1x2* mutant insensitivity to systemic Fe signalling in roots demonstrated by split-root assays

The RNA-seq analysis revealed a large difference in the shoot and root transcriptional response of *bts1x2* mutants to high Zn. BTSL-dependent Fe deficiency-responsive genes were constitutively overexpressed in *bts1x2* roots, despite phenotypic data demonstrating reduced Fe deficiency and Zn toxicity in shoots (**Chapter 4**). However, BTSL-independent genes expressed in the stele appeared to still be responsive to shoot Fe sufficiency signals in the mutant, which suggested that BTSL proteins may have a role in responding to systemic Fe signalling in certain cell types in roots.

To verify this insensitivity of BTSL-dependent gene regulation to systemic Fe signals, a split-root system was utilised, whereby a seedlings root system is simultaneously exposed to two different nutrient conditions. One half of the root system was grown on control media (5 μ M FeHBED, 1 μ M ZnSO₄) and the other on either Fe deficient (0 μ M FeHBED, 1 μ M ZnSO₄) or Zn excess (5 μ M FeHBED, 100 μ M ZnSO₄) media (**Supplementary Figure C6, Appendix C**). If *bts1x2* was insensitive to systemic Fe signalling, it was hypothesised that BTSL-dependent genes would be more highly upregulated in the half of the roots exposed to low Fe or Zn excess than those on control media (**Figure 5.10**).

In Col-0, exposure to low Fe or Zn excess media on both sides of the root system led to shoot Fe deficiency, as shown by a reduction in chlorophyll content and upregulation of *bHLH38* and *bHLH39* in shoots (**Figure 5.11A; Supplementary Figure C7B, Appendix C**). This was accompanied by activation of both the BTSL-dependent and BTSL-independent Fe deficiency response in roots, with upregulation of Fe deficiency signalling peptide *IMA1* and downregulation of Fe storage protein *FER1*, as well as upregulation of *bHLH38* and *IRT1* (**Figures 5.11B-C**). This response was attenuated if half of the roots are grown in control media, with Fe deficiency-responsive genes showing similar low-level upregulation in both halves of the root (**Figures 5.11A-C**).

In contrast, when exposed to low Fe or Zn excess on both halves of the root, *bts1x2* showed reduced shoot Fe deficiency symptoms compared to Col-0 (**Supplementary Figure C7, Appendix C**), and reduced expression of Fe deficiency-responsive genes, *bHLH38* and *bHLH39*, in shoots (**Figure 5.11A**). BTSL-independent

IMA1 and *FER1* in roots also demonstrated expression patterns consistent with systemic Fe sufficiency signalling in *bts1x2*, with *IMA1* expression lower compared to Col-0 and *FER1* higher (**Figure 5.11B**). However, BTSL-dependent *bHLH38* and *IRT1* showed high constitutive upregulation, which was only partially reduced when half of the root system is exposed to control medium (**Figure 5.11C**). Moreover, the root half exposed to Fe deficiency or Zn excess medium showed significantly higher *bHLH38* and *IRT1* expression compared to the other half exposed to control medium (**Figure 5.11C**). This suggested that *bts1x2* failed to downregulate activation of local Fe deficiency signals in response to systemic suppressive Fe sufficiency signals. This further highlighted the role of BTSL proteins in fine-tuning the local response to environmental Fe as suggested in the literature [305]. It also suggested that BTSL proteins regulate Fe uptake and distribution in specific cell types of the root in response to systemic Fe signals.

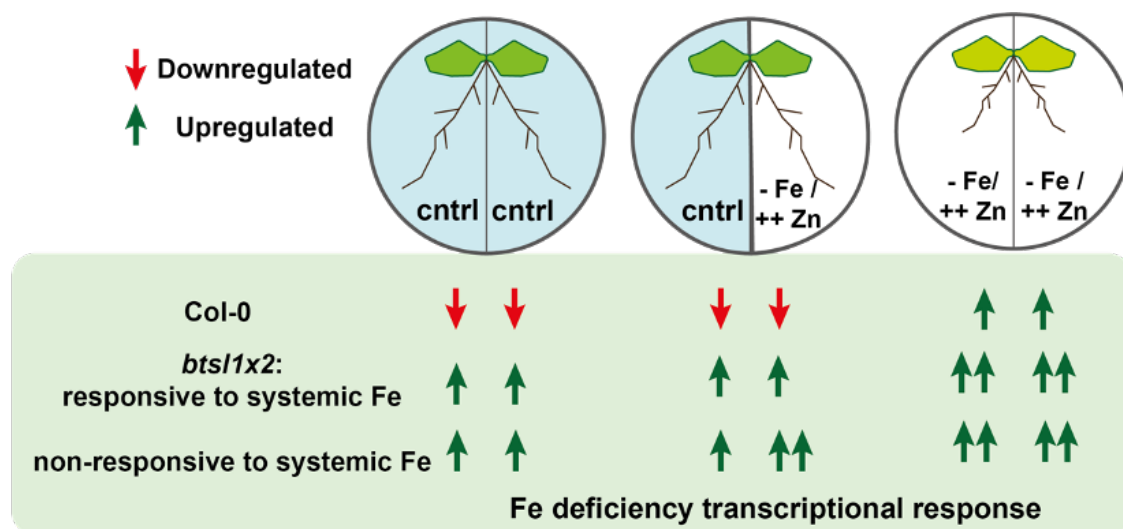


Figure 5.10: Schematic of split-root experimental set up to test systemic Fe signalling in *bts1x2*.

Seedlings were germinated on ¼ MS plates, roots excised at 5 d and then at 10-d-old transferred to split root plates containing control (cntrl, 5 µM FeHBED, 1 µM ZnSO₄), Fe deficiency (- Fe, 0 µM FeHBED, 1 µM ZnSO₄) or Zn excess (++) (5 µM FeHBED, 100 µM ZnSO₄) modified Hoagland medium in all combinations. The predicted up- (green) or downregulation (red) of the BTSL-dependent Fe deficiency-responsive genes in roots used to test systemic (long distance) Fe signalling is indicated by arrows.

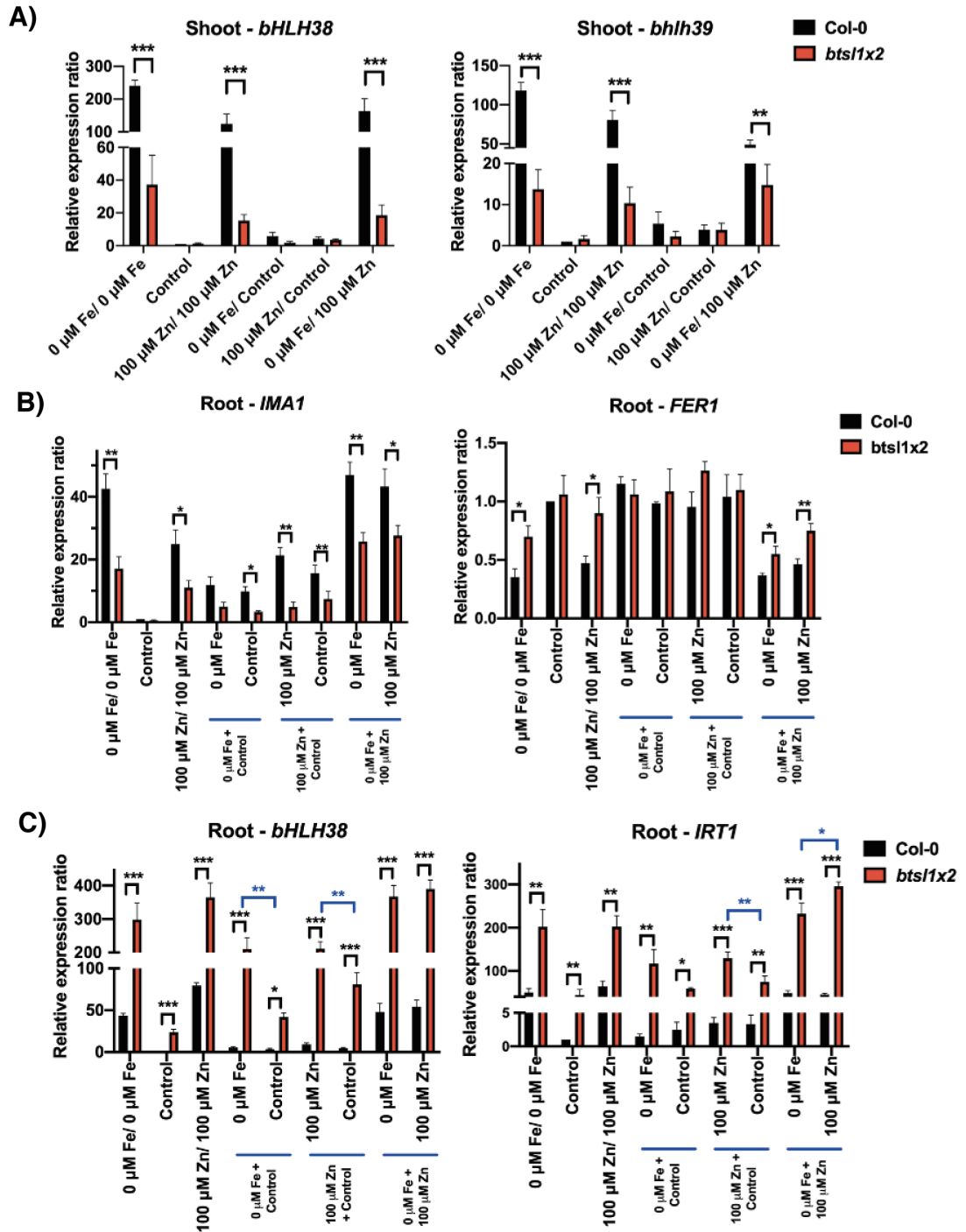


Figure 5.11: Expression of Fe deficiency-responsive genes in Col-0 and *bts1x2* seedlings grown in the split-root system.

qRT-PCR analysis of A) *bHLH38* and *bHLH39* in shoots, B) BTSL-independent *IMA1* and *FER1* and C) BTSL-dependent *bHLH38* and *IRT1* in roots of Col-0 and *bts1x2* 17-d-old seedlings grown on split root agar plates containing control (5 μM FeHBED, 1 μM ZnSO₄), Fe deficiency (0 μM FeHBED, 1 μM ZnSO₄) or Zn excess (5 μM FeHBED, 100 μM ZnSO₄) modified Hoagland medium in all combinations. Seedlings were germinated on ¼ MS plates, roots excised at 5

d and then transferred to split root plates at 10-d-old. Fold change is relative to Col-0 control (expression level set as “1”) and normalised to reference genes *ACTIN2* and *TIP41*. Data represent mean values (\pm SEM) from three independent experiments, each comprising five plants per genotype and condition, and each repeated as three technical replicates. Statistically significant differences are indicated by asterisks (black = within conditions, blue = within genotype, * $p < 0.05$, ** $p < 0.01$, *** $p < 0.001$) as determined by two-way ANOVA followed by Tukey HSD post-hoc test. Non-significant differences are not indicated.

5.3 Discussion

5.3.1 BTSL proteins negatively regulate FIT-, IVc bHLH- and bHLH121/URI-dependent gene expression

In **Chapter 4**, a model was proposed for the role of BTSL proteins in Fe homeostasis and the contribution that this has on the *bts/1x2* Zn tolerance phenotype (**Figure 4.10**). In this model, BTSL proteins regulate FIT protein turnover [304, 305] and consequently the *bts/1x2* mutant shows constitutive overexpression of FIT-dependent genes, enhanced Fe uptake and subsequent Fe-mediated Zn tolerance. However, a major question in this model was how FIT-dependent gene expression was activated when heterodimer formation with Ib bHLH transcription factors is necessary [302]. Previous reports of upregulation of *bHLH38* and *bHLH39* in *bts/1x2* provides a possible answer [305], but this in itself raises another question of how IVc bHLH and bHLH121/URI-targeted *Ib bHLH* genes are upregulated in *bts/1x2*. The transcriptomics data presented in this chapter clearly indicates that, in addition to the already identified FIT-dependent targets and *Ib bHLH* genes, the majority of the FIT-independent transcriptional network is also upregulated in *bts/1x2* roots (**Figure 5.8 and Table 5.3**).

Misregulation of FIT-independent genes could be explained by compensatory gene expression in response to upregulation of FIT-dependent genes. For instance, this is seen in *ysl* and *frd* mutants to accommodate Fe transport [471]. However, this is very unlikely as the enhanced Fe sufficiency signalling in the mutant should suppress activation of Fe deficiency-responsive transcription factors to prevent excessive Fe

uptake. Moreover, genes expressed predominantly in the stele and leaves, where BTS is expressed but not BTSL, do not show overexpression of Fe deficiency genes, and rather their expression pattern is more consistent with systemic Fe sufficiency signalling. This signifies that overexpression of Fe deficiency genes in the mutant is probably specific to BTSL-associated cells layers.

A far more plausible explanation is that BTSL proteins target both FIT and additional transcription factors involved in the FIT-independent transcriptional network. A number of the top DEGs in the mutant are direct targets of bHLH121/URI and IVc bHLH transcription factors (**Table 5.3**), such as *Ib bHLH* genes, *FIT*, and *MYB10* and *MYB72*, making these upstream regulators the most likely candidates. Three of the IVc bHLH transcription factors (bHLH104, ILR3 and bHLH115) and bHLH121/URI are regulated by BTS in an Fe-responsive manner in the stele and shoots [300, 306]. Thus, BTSL proteins could be carrying out this essential regulatory function simultaneously on upstream IVc and bHLH121/URI, and further downstream FIT, in epidermal and cortical cells, as well as in the stele of the differentiation zone. Notably these cell types are where the phosphorylated active form of bHLH121.URI accumulates under Fe deficiency [298-300]. Consequently, BTSL-dependent degradation of phosphorylated bHLH121/URI and its interacting partners under Fe sufficiency could provide an important point of control for rapidly and effectively downregulating the entire Fe deficiency response.

Further evidence supporting this proposed new role is that IVc bHLH and bHLH121/URI directly upregulate the expression of *BTS*, *BTSL1* and *BTSL2* [300]. Hence, as is seen with BTSL proteins and FIT, BTS in the stele and BTSL in epidermal cells form a negative feedback loop with IVc bHLH and bHLH121/URI to maintain protein turnover and attenuate protein accumulation under Fe deficiency. Moreover, the BTS and BTSL proteins are closely related homologs (**4.1.1**), and so it is possible that they could share similar targets. However, while based on current knowledge of bHLH121/URI target genes it is clear that bHLH121/URI-dependent gene expression is misregulated in *bts1x2*, the functional redundancy of the IVc proteins makes it difficult to say which specific ones are likely BTSL targets. Rather the case may be as is seen in *BTS*, that BTSL proteins regulate multiple IVc bHLH proteins. Protein-protein interaction studies are required to validate these upstream regulators as new BTSL targets, as well as

investigation of protein accumulation in a cell type-specific manner to see if spatial distribution of transcription factors makes this plausible.

5.3.2 Overexpression of Zn sequestration and Fe mobilisation genes contributes to the Fe-mediated Zn tolerance phenotype of *bts1x2* mutants

Enhanced Fe uptake capacity in *bts1x2* under Zn excess was demonstrated in **Chapter 4** through overexpression of *IRT1* and *FRO2* and high ferric chelate reductase activity (**Figure 4.7**). Transcriptomics of *bts1x2* reveals that additional genes involved in Fe uptake and mobilisation are also highly upregulated and further contribute to the enhanced Fe nutrition of the mutant (**Figure 5.8**). For example, coumarins and phenolic compounds, such as fraxetin, scopoletin, isofraxidin and esculetin, are secreted to help solubilise Fe³⁺ in the rhizosphere and aid availability at the root surface for reduction [179, 183]. *S8H*, *BGLU42*, *CYP82C4* and *F6'H1* are all involved in biosynthesis of these compounds [180-182, 185, 470], while *ABCG37* is required for coumarin secretion [184](**Table 5.3**). It would be useful to run metabolomics analysis on *bts1x2* root exudates to confirm increased production of Fe-solubilising compounds. *AHA2*, a plasma membrane H⁺-ATPase, plays a major role in acidification of the rhizosphere and subsequent solubilisation of Fe in response to deficiency conditions [169]. *AHA2* is upregulated in response to low Fe, with FIT being necessary but not sufficient to induce expression [510]. Upregulation of *AHA2* was not seen in wild type or *bts1x2* under Zn excess conditions. This could suggest that Zn excess does not activate the non-FIT regulatory mechanism involved in *AHA2* upregulation, or that *AHA2* is not sufficiently upregulated for detection through the RNA-seq experiment carried out here.

The transcriptomics data also shows that a number of genes involved in Fe and Zn distribution, that have been found linked to Zn tolerance, are constitutively upregulated in the mutants and overexpressed under Zn excess (**Figure 5.8**). For instance, *MTP3*, a Zn vacuolar transporter [249], and *HMA3*, a vacuolar Zn and Cd transporter [255], both regulate Zn storage in roots and are found overexpressed in *bts1x2* (**Table 5.3**). Root NA levels and the vacuolar Zn-NA importer, *ZIF1*, regulate Fe and Zn distribution within plants. High root NA concentrations combined with high *ZIF1* expression promotes Fe root-to-shoot transport, while enhancing vacuolar Zn

sequestration in roots [203, 256]. *ZIF1*, and genes involved in NA synthesis, such as *NAS1* and *NAS2*, as well as *SAM1* and *MTK*, which participate in upstream methionine cycling, are all overexpressed in *bts1x2* roots (**Table 5.3**). It has been shown that *NAS* transcripts correlate closely with NA content, although it would be useful to carry out metabolomics analysis to confirm elevated root NA levels in *bts1x2* [200].

However, increased biosynthesis of other Zn tolerance-associated metabolites and small molecules cannot be inferred from the RNA-seq data. For instance, phytochelatins and GSH are involved in Zn detoxification and Fe-Zn distribution but are not transcriptionally regulated [212, 216]. Phytochelatin synthase 1 (*PCS1*), for example, is activated by metal binding to its C-terminal domain [511]. Reduced shoot Mn accumulation is also seen in the mutant under Zn excess (**Figure 4.6E**), and this can be explained by increased expression of *MTP8* in roots, which has a role in Mn import and detoxification (**Table 5.3**)[512]. Thus, this shows that the altered metal distribution, and subsequent Fe-mediated Zn tolerance phenotype in *bts1x2* is not only due to enhanced Fe uptake, but also associated with increased expression of Zn and Mn sequestration genes in roots.

5.3.3 The expression pattern of shoot and select PYE-repressed genes is consistent with Fe sufficiency signalling in *bts1x2*

In *bts1x2*, the root Fe deficiency response is hyperactivated and Zn-responsive, demonstrating that BTSL-dependent genes are at least responsive to local Zn stress signalling (**Figure 5.8**). However, shoot genes and a subset of root genes, associated with expression in the stele, do not show large changes in expression under Zn excess (**Figures 5.7 and 5.8**). For example, in shoots *YSL1*, which is involved in unloading of Fe-NA complexes from the xylem into shoots, and *FER1* and *FER4*, are all downregulated in response to Fe deficiency and Zn excess [513, 514]. However, in *bts1x2* there is no significant change in expression under Zn excess (**Table 5.3**). Additionally, the small Fe-responsive *IMA* signalling peptides, which are phloem-mobile and positively regulate root Fe uptake in response to low shoot Fe [335] are highly upregulated in wild type on Zn exposure but fail to be induced in *bts1x2* shoots and are only partially upregulated in roots (**Tables 5.2 and 5.3**). In shoots, *IMA* gene expression is activated by IVc bHLH

activity in response to Fe deficiency, and thus reduced expression in *bts1x2* shoots indicates systemic Fe sufficiency signalling. In roots, *IMA* expression is also regulated by bHLH121/URI activity. Thus, low-level *IMA* expression in *bts1x2* roots under Zn excess could be the result of loss of BTSL function in some cell types where *IMA* is expressed. However, *IMA* is not upregulated under control conditions, and some shoot Fe deficiency marker genes such as *VTL1*, *FSD1* and *bHLH101* are also upregulated in *bts1x2* under Zn excess. This suggests that *IMA* expressing cells, likely predominantly under BTS regulation, are still responsive to low-level shoot Fe deficiency signalling in *bts1x2* under Zn excess.

Under Fe deficiency and Zn excess, PYE-ILR3 complexes accumulate in the stele and repress the expression of genes involved in Fe storage and sequestration (**Figure 5.2**). In *bts1x2* a number of these genes are not downregulated or show reduced downregulation compared to wild type, including *FER1*, *FER4*, *VTL1* and *NEET* (**Table 5.3**). This reduced induction is similar to *IMA*, again showing responsiveness of BTS-associated cells to shoot Fe status in *bts1x2*. *NAS4* is another PYE-repressed gene which is additionally repressed by FBP inhibition of FIT in the stele under Zn excess, while also being upregulated by MYB10 and MYB72 in both a FIT-dependent and FIT-independent manner [201, 472]. *NAS4* is the only *NAS* gene which is not overexpressed in *bts1x2*, but rather shows similar expression levels between mutant and wild type (**Table 5.3**). This is likely linked to the complicated differential regulation in different cell types, with *NAS4* expression being upregulated in the stele cells where BTSL2 should be active, but its expression being attenuated by PYE and BTS activity along the majority of the root.

Other PYE-repressed genes, *FRO3* and *NRAMP4*, are expressed strongly in the stele and vasculature of the differentiation zone where *BTSL2* is expressed [271, 515], while *ZIF1* is expressed in all cell types [256], which explains their overexpression in *bts1x2* (**Table 5.3**). It would be interesting to investigate this cell-type specific activity between BTSL proteins and BTS in the *bts1x2* and *bts-3* mutants, possibly by using GUS staining of selected target genes to see the cell-specific induction.

5.3.4 BTSL proteins are important for regulating root responses to local and systemic Fe signals

The currently proposed role for BTS and BTSL proteins as Fe sensors suggests that BTSL proteins are responsive to local signals, acting as an initial protection mechanism against excessive Fe uptake. Meanwhile, BTS is thought to act as the internal Fe sensor in shoots and root vasculature, regulating root Fe uptake in accordance with shoot Fe status [305]. The split root experiments carried out here suggest that BTSL proteins are also responsive to systemic Fe signalling, and they have an important function in downregulating the local response upon receiving Fe sufficiency signals (**Figure 5.11**). If the Fe-binding regulation of BTS and BTSL proteins is correct, this would suggest that the systemic signal is increased root Fe content, likely mediated by OPT3 recirculation of Fe in the phloem [243, 244]. Yet, BTSL-dependent genes show similar levels of induction under Fe deficiency and Zn excess when root Fe is low in the former and high in the latter (**Figure 4.7**)[430]. Therefore, a more likely possibility is that BTS and BTSL activity is regulated by the Zn/Fe ratio, as the Zn/Fe ratio rises in roots and shoots under both Fe deficiency and Zn excess (**Figure 4.6**). Zn binding to the HHE domains of BTS and HRZ proteins has been demonstrated [306], and thus Zn could prevent Fe-sensing by BTS and BTSL proteins and inactivate them under these conditions. The Zn/Fe sensing theory also aligns with the data presented here. For instance, *bts1x2* roots show a slightly higher Zn/Fe ratio than shoots under Zn excess, which would suggest that BTS should be less active in roots than shoots, and subsequently higher expression of Fe deficiency-responsive genes in roots should be observed (**Figure 4.6**). Indeed, shoot Fe deficiency genes are not as responsive to Zn excess as root BTS-dependent genes, such as *IMA* and *FER* (**Tables 5.2 and 5.3**). Conversely, the opposite is true in wild type (**Figure 4.6, Tables 5.2 and 5.3**).

Alongside the two Fe atoms they canonically bind, HHE domains can reversibly bind O₂ at their second Fe binding site [516]. The mammalian BTS homolog, FBXL5, has been shown to bind both Fe and O₂ at its HHE domain resulting in its activity being regulated by both Fe levels and hypoxia or ROS signalling [517]. As such, it is possible that micronutrient stress-induced ROS production also regulates BTS and BTSL function. It would be interesting to look at metal binding to HHE domains under differing oxidation

states and investigate the effect that this has on protein stability and function. Moreover, it would be interesting to see if BTS and BTSL proteins show different metal binding capabilities based on the different number of HHE motifs they possess, and if this could be related to associated with different sensing functions in their respective tissues (**Figure 4.1**).

5.3.5 BTSL2 plays a more prominent role in regulating the root Fe deficiency response than BTSL1

Characterisation of the *bts1* and *bts2* single mutants has shown that BTSL proteins are not fully functionally redundant and that the *bts2* appears to have a slightly stronger phenotype closer to *bts1x2* than *bts1* (**4.2.1 and 4.2.2**)[305]. The gene expression analysis carried out on selected Fe deficiency-responsive genes in the *bts1* single and double mutants is further evidence of partial functional redundancy between BTSL1 and BTSL2 (**Figure 5.9**). The expression pattern, which shows *bts2* gene upregulation being greater than *bts1*, is also consistent with the stronger *bts2* phenotype, and suggests that BTSL2 may play a more prominent role in regulating the root Fe deficiency response. This difference in target gene expression could be related to the differences in expression pattern of the *BTSL* genes. Although *BTSL2* is expressed across more cell types, notably in the stele of the differentiation zone, and as such could exert a greater influence on target protein abundance [305], *BTSL1* shows much higher expression levels than *BTSL2* on exposure to Fe deficiency [304]. Transcript information alone does not provide sufficient information, and as such quantification of BTSL1 and BTSL2 protein abundance is required to test this theory.

Alternatively, the BTSL proteins could have differing levels of ubiquitination activity, with BTSL2 being more active than BTSL1, and able to promote higher levels of protein turnover and degradation. Moreover, it is possible that BTSL proteins actually do have slightly differing targets. From the similar partial expression pattern of the genes analysed, it appears that both BTSL proteins regulate FIT, based on *IRT1* and *FRO2*, as well as bHLH121/URI, as evidenced by *bHLH38*, *bHLH39* and *FRO3* (**Figure 5.9**). However, *ZIF1* expression appears slightly different from the others, especially under Fe deficiency. Here, the *bts1* single mutants show wild type levels of expression (**Figure 5.9C**). *ZIF1* is

regulated by the IVc bHLH transcription factors independently of bHLH121/URI, and as such if the BTSL proteins target different IVc proteins which require interaction to induce *ZIF1* this could explain the observed phenotype. *In vitro* ubiquitination assays with the various proposed target proteins under varying metal conditions, as well as *in planta* evidence of protein-protein interaction, is necessary to investigate this possibility, but could reveal important functional differences between BTSL proteins.

5.3.6 New model for the role of BTSL proteins in the root transcriptional response to Zn excess

Based upon current knowledge of the Fe deficiency transcriptional cascade, Fe and Zn cross-homeostasis and the new proposed role for BTSL proteins under Zn excess presented here, a revised model for the response of root epidermal (**Figure 5.12A**) and stelar cell layers (**Figure 5.12B**) to Fe deficiency and Zn excess is proposed. A reduction in root Fe content, due to lower uptake or lack of phloem Fe recirculation from deficient shoots, leads to an increase in the Zn/Fe ratio. Inhibition of BTSL activity under these conditions allows the accumulation of active phosphorylated bHLH121/URI and FIT in epidermal cell layers (**Figure 5.12A**). IVc bHLH proteins and bHLH121/URI form a feedback loop with BTSL proteins by upregulating *BTSL1* and *BTSL2* expression to help maintain low level target protein turnover as a means of keeping the protein pool responsive to Fe and Zn fluctuations. FIT, IVc bHLH and bHLH121/URI accumulation activates FIT-dependent and FIT-independent gene expression which promotes Fe uptake and mobilisation (*IRT1*, *FRO2*, *S8H* and *F6'H1*), as well as enhancing Fe translocation and Zn root sequestration (*ZIF1*, *FRO2*, *NAS1* and *NAS2*). However, Zn is also able to enter roots through *IRT1*, and as such exacerbates the high Zn/Fe ratio. This feed forward loop is circumvented in *bts1x2* by enhanced Fe solubilisation in the rhizosphere facilitating Fe competition with Zn for uptake via *IRT1*, and subsequently increasing Fe uptake. Enhanced Fe content repels further Zn uptake and allows Fe to outcompete Zn for translocation to shoots, giving the mutant its Fe-mediated Zn tolerance phenotype, as well as tolerance to Fe deficiency (**Figure 4.10B**).

In the stele, IVc and bHLH121/URI upregulate a slightly different subset of genes, including *IMA* signalling peptides, *FER* genes and *NEET* (**Figure 5.12B**)[298]. However, Fe

deficiency signalling reduces bHLH121/URI accumulation in the stele, resulting in preferential formation of the PYE-ILR3 repressive complex. PYE attenuates the expression of Fe storage and distribution genes, including the *FER*, *ZIF1*, *FRO3*, *NAS4* and *NEET*, to promote translocation of Fe to shoots where it is needed most [296, 307]. BTS activity is inhibited in response to Fe deficiency signalling – again, likely mediated through Zn interference with Fe binding – allowing activation of Fe-deficiency responsive gene expression. Overexpression of these genes is prevented through BTS-dependent turnover of IVc and bHLH121/URI targets. An additional negative regulator of FIT, FBP, is also active in the stele under Fe sufficiency conditions and prevents FIT-dependent upregulation of *NAS1*, *NAS2* and *NAS4* [201]. In *bts1x2*, reduced Fe deficiency signalling activates BTS-dependent degradation of IVc bHLH and bHLH121/URI transcription factors, and as such target genes such as *IMA*, *FER* and *NEET* are not as responsive to Fe deficiency or Zn excess (**Table 5.3**). *NAS4* expression is also attenuated in *bts1x2* due to FBP activity in BTS-dependent cells, as well as BTSL2-dependent stele cells where *NAS4* would otherwise be over-expressed. Meanwhile, other stele-expressed genes, such as *ZIF1*, *FRO3* are overexpressed in the epidermis and as such show higher expression in *bts1x2* (**Table 5.3**). Thus, BTSL activity regulates the expression of genes involved in Fe and Zn uptake and distribution likely in response to changes in cellular Fe and Zn balance. As such, it is proposed that BTSL proteins act as regulators of Fe and Zn cross-homeostasis. It is also expected that BTS performs a similar function, but analysis of the *bts-3* mutant Zn phenotype is required to verify this.

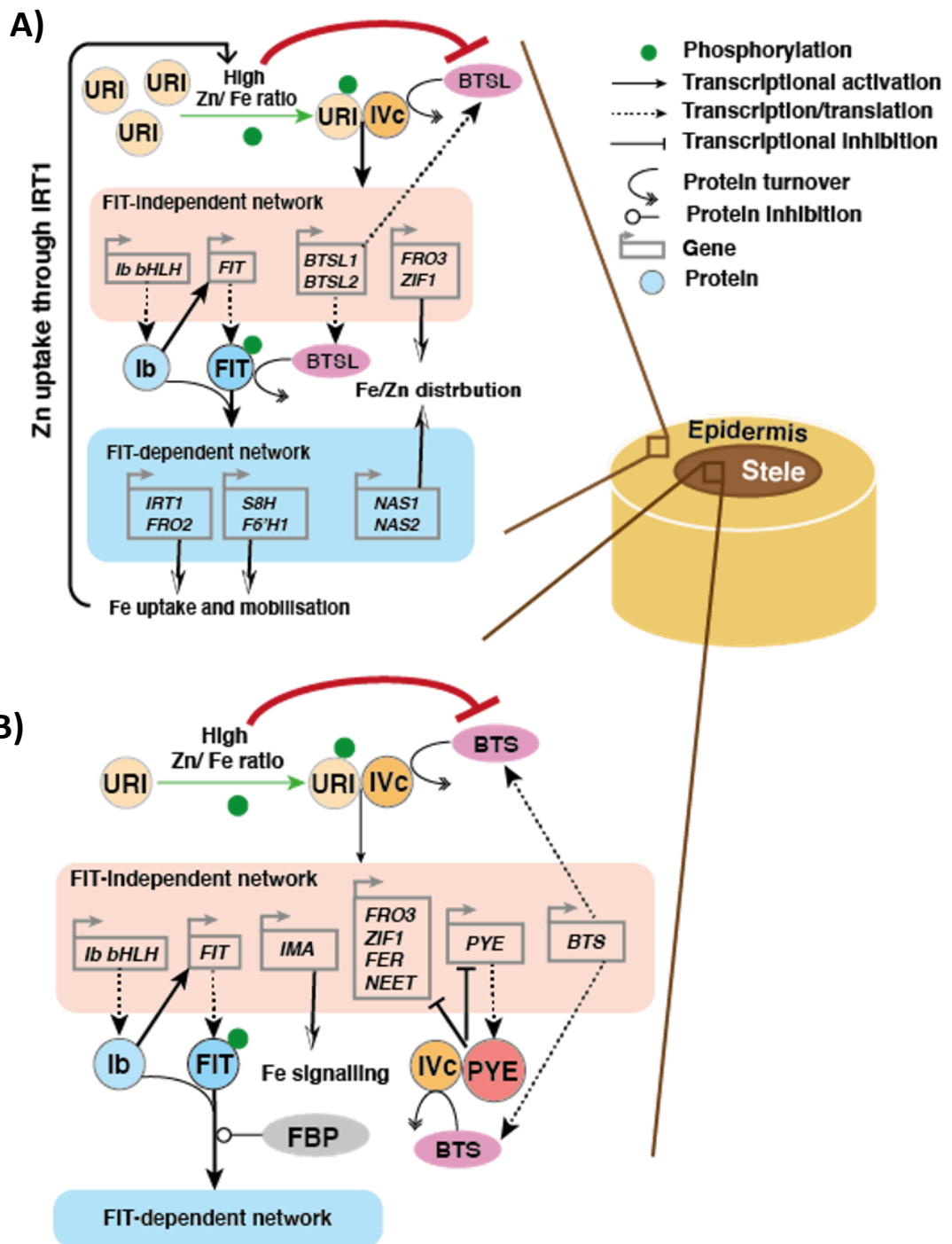


Figure 5.12: Model of proposed new function of BTSL proteins in the root Fe deficiency transcriptional response under Fe deficiency or Zn excess.

Simplified schematic showing the root Fe deficiency transcriptional cascade in the epidermis and stele. Under Fe deficiency or Zn excess the root Zn/Fe ratio increases as a result of low Fe uptake (local signalling) and/or low Fe recirculation from shoots (systemic signal). A) Fe

deficiency signalling leads to the accumulation of phosphorylated bHLH121/URI in epidermal cells, promoting heterodimer formation with IVc bHLH transcription factors (bHLH34, bHLH104, ILR3, bHLH115) [298-300]. This activates the expression of genes such as *Ib bHLH* (*bHLH38*, *bHLH39*, *bHLH100* and *bHLH101*), *FIT*, *BTSL1*, *BTSL2*, *ZIF1* and *FRO3*. *Ib bHLH* transcription factors further upregulate *FIT* expression and then activate FIT-dependent gene expression through stabilising heterodimer formation [301]. FIT is activated by calcium-dependent phosphorylation [321]. FIT-dependent genes include Fe uptake genes *IRT1* and *FRO2* and coumarin biosynthetic genes *S8H* and *F6'H1*, which function together to increase the root Fe uptake capacity. Additional Zn is also able to enter the root through IRT1. BTSL1 and BTSL2-dependent ubiquitination of bHLH121/URI, IVc bHLH and FIT is largely inhibited by high Zn/Fe ratio, but low-level turnover is maintained to keep a small responsive pool of protein. Genes involved in Fe and Zn distribution, such as *FRO3*, *ZIF1*, *NAS1* and *NAS2* are also upregulated. B) bHLH121/URI shows reduced accumulation in the stele under Fe deficiency or Zn excess but still maintains expression of downstream genes, including *Ib bHLH* and *FIT*, *IMA* genes, *FRO3*, *ZIF1*, *FER* genes, *NEET*, *PYE* and *BTS*, through heterodimer formation with IVc bHLH. FIT and *Ib bHLH* upregulate downstream FIT-dependent expression. FBP, which primarily acts under Fe sufficiency, maintains low level inhibition of *NAS* gene expression through binding to FIT [201]. Reduced bHLH121/URI in the stele allows the preferential formation of the PYE-ILR3 repressive complex which downregulates the expression of Fe transport and storage genes. *BTS* maintains low level turnover of bHLH121/URI, bHLH104, ILR3 and bHLH115 [300, 304, 306, 307].

5.3.7 Future outlook for investigation of the BTSL proteins

While transcriptomics of the *bts1x2* mutant has raised some intriguing new possibilities for the role of BTSL proteins in Zn and Fe cross-homeostasis, one of the major limitations of this approach is that it fails to capture post-transcriptional and post-translational regulatory mechanisms, as well as metabolic and biochemical responses. Thus, future experiments are required to verify the proposed model of BTSL1 and BTSL2 protein function under Zn excess, such as bHLH121/URI and IVc bHLH transcription factors as additional BTSL targets and the regulation of BTSL activity by Zn and Fe. For example, protein-protein interaction studies and ubiquitination assays under varying Fe and Zn conditions could show metal-dependent interactions between BTSL proteins and

new candidate targets, and potentially show differences between BTSL1 and BTSL2 target affinity and activity. Experiments looking at bHLH121/URI and IVc bHLH protein accumulation and localisation through the use of GFP-protein fusions in the *bts1x2* mutant background could additionally be used to investigate the effect of BTSL protein activity on Fe deficiency-responsive transcription factors. *In vitro* metal binding assays investigating the role of Zn²⁺ and Fe²⁺ binding to BTSL HHE domains under various concentrations, ratios and redox states could help reveal more about the metal signalling which regulates BTSL function under Fe deficiency and Zn excess. Comparison of BTSL1, BTSL2 and BTS protein metal-binding affinity could also reveal new information about the different functions of these closely-related homologs in responding to Fe signalling at different levels. The BTSL proteins offer an exciting avenue for future investigation and could yield potential candidate targets for crop biofortification, as well as help reveal more about the complicated interplay between plant homeostasis networks.

Chapter 6: General Discussion

6.1 Summary of research findings

This project set out to identify novel genes involved in Zn and Fe cross-homeostasis through forward and reverse genetic approaches. Two luciferase-based mutant screening populations were established, providing resources for future research into Zn homeostasis. Characterisation of the *bts1x2* mutant revealed a novel function for BTSL proteins in Zn and Fe cross-homeostasis, as well as previously unidentified roles in regulation of FIT-independent gene expression and response to systemic Fe signalling. This new information about BTSL proteins (summarised in **Figure 6.1**), and any genes that may be identified from the mutant screens in the future, helps develop and expand the current model for the regulation of Zn and Fe cross-homeostasis, which in turn can inform micronutrient biofortification strategies.

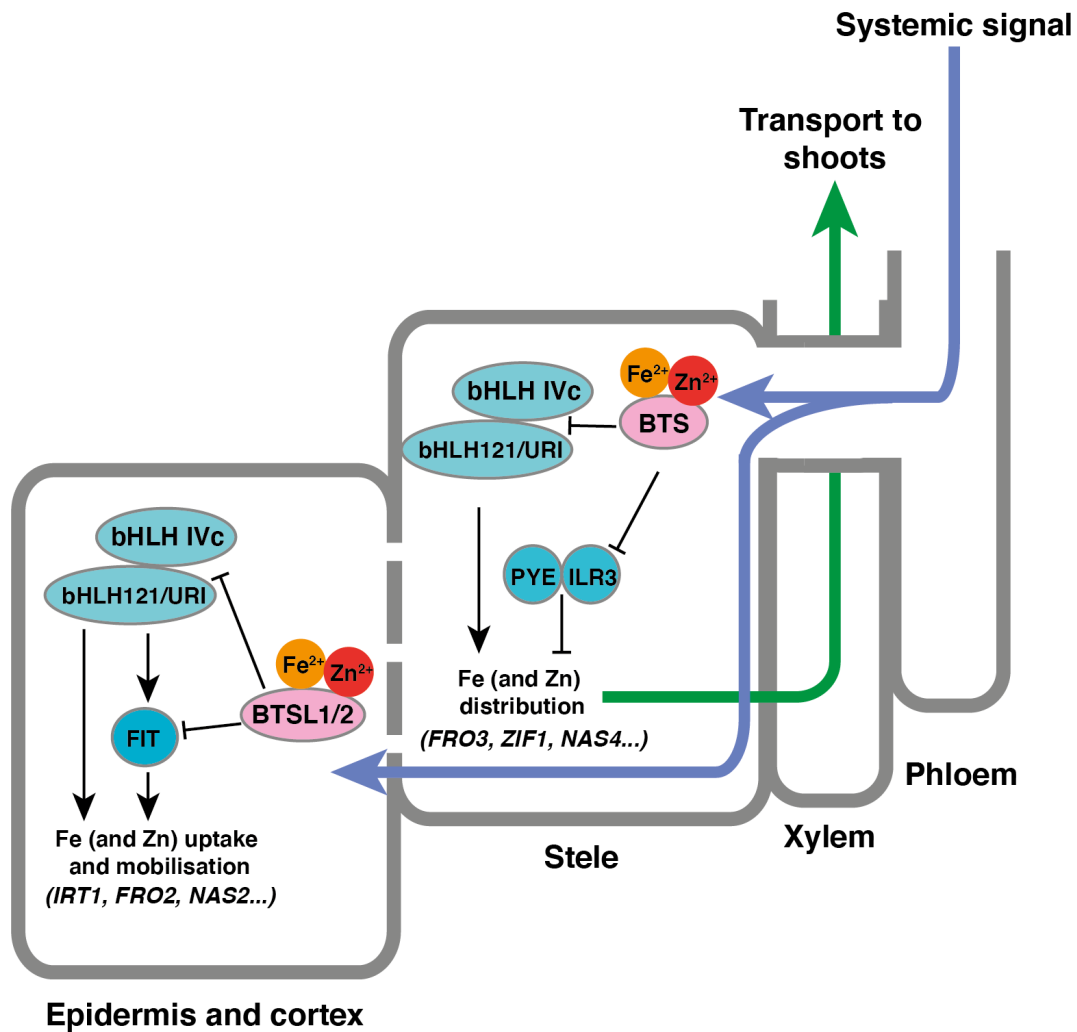


Figure 6.1: Proposed function of BTSL proteins in Zn and Fe cross-homeostasis in *A. thaliana*

Zn²⁺ and Fe²⁺ binding regulates the activity of BTS, BTSL1 and BTSL2 E3, with a high Zn/Fe ratio inhibiting activity. Zn and Fe recirculated in the phloem and acting as a systemic signal from shoots (purple arrow) may partially regulate BTSL, and likely BTS, protein activity. BTSL1 and BTSL2 act in the root epidermis and cortex to negatively regulate FIT protein abundance, and likely IVc bHLH (bHLH34, bHLH104, bHLH105/ILR3 and bHLH115) and bHLH121/URI as well. This activity inhibits Fe and Zn uptake through IRT1 under Fe sufficiency conditions when the cellular Zn/Fe ratio is low (Chapters 4 and 5). BTS acts in the root stele and shoot to negatively regulate bHLH IVc (bHLH104, bHLH105/ILR3 and bHLH115) and bHLH121/URI (only in roots) transcription factor protein abundance to regulate Zn and Fe sequestration and translocation to shoots (green arrow).

6.1.1 Mutant screens utilising *pZIP5:LUC* and *pFRO3:LUC* lines are a useful resource for future Zn homeostasis research

In **Chapter 3**, two luciferase-based mutant screens were established to look for novel genes involved in Zn homeostasis. A reporter-based forward genetic approach was decided on as a result of the previous success of such screens in identifying novel nutrient homeostasis genes and mutant alleles [300, 362, 370, 518, 519]. Based upon their robust upregulation under screening conditions and their position downstream of known gaps in the Zn homeostasis network, the Zn deficiency-responsive *ZIP5* promoter and the Zn excess-responsive *FRO3* promoter were selected for use in the screens. For example, *ZIP5* is upregulated by bZIP19 and bZIP23 under Zn deficiency, however other *ZIP5* transcriptional regulators, possibly bZIP19/23 interacting proteins or Zn-ligand pathways upstream of bZIP19/23 that might deliver Zn²⁺ to the Zinc Sensor Motif, are yet to be identified [159, 520]. *FRO3* is upregulated under Zn excess and Fe deficiency by the Fe deficiency bHLH signalling cascade [307, 469], but as shown through the characterisation of BTL proteins in **Chapters 4 and 5** and FBP [201], Fe regulatory proteins can be important points of Fe and Zn cross-homeostasis. Thus, the *pFRO3:LUC* screening population can identify Zn excess, as well as Zn and Fe cross-homeostasis, regulatory proteins.

Although reporter-based approaches are useful for high throughput seedling analysis, they are not without fault, and this was highlighted by some issues encountered during initial screening of the M₂ populations. For example, silencing of the transgene was observed in some *pZIP5:LUC* lines, potentially due to stress exposure, and a number of false positives and wild-type seed contamination were found in the *pFRO3:LUC* screen. Reliance upon reporter gene expression as a readout for altered homeostasis, as opposed to a physical phenotype such as root length, creates a number of variables during the screening protocol that can exacerbate the problem of false positives. For instance, examples might be mutagenesis of the transgene or genes involved in ATP and Mg homeostasis that affect luciferase activity, as well as uneven application of luciferin substrate or technical errors during bioluminescence imaging. These problems are rarely discussed in published studies, but there are examples where high rates of false positives and the pitfalls of luciferase-based screens have been noted [393, 521, 522].

No candidate mutants were identified during screening of the M₂ populations, however only 2,000 of the pZIP5:LUC and 18,000 of the pFRO3:LUC lines have been imaged to date, and as such there is still scope for finding interesting mutants in the screen. As discussed in **section 3.3**, other comparable screens have required a similar or even higher number of screened individuals to identify mutants of interest [369, 370, 397, 398]. Moreover, expansion of screening conditions to search for mutants with LUC overexpression and LUC expression under standard Zn growth conditions increases the likelihood of identifying interesting mutants that would otherwise be missed. Together, both the pZIP5:LUC and pFRO3:LUC mutant populations are novel resources for future Zn homeostasis, as well as Zn and Fe cross-homeostasis, research.

6.1.2 BTSL proteins regulate Zn and Fe cross-homeostasis

Characterisation of *btsl* mutants in **Chapters 4 and 5** demonstrated that BTSL1 and BTSL2 proteins play partially functionally redundant roles in dampening the expression of genes associated with Fe deficiency and Zn excess tolerance in roots. BTSL activity maintains continual protein turnover of Fe deficiency-responsive transcription factors and rapidly downregulates the root Fe deficiency response in the presence of Fe to prevent excessive Fe uptake [304, 305]. However, the resultant limitation of Fe uptake capacity under Zn excess growth conditions causes shoot Zn accumulation and secondary Fe deficiency (**Chapter 4**). Subsequent shoot-borne systemic signals activate the root Fe deficiency response, which in turn also enhances Zn uptake through IRT1 and further exacerbates competition between Zn and Fe for uptake and translocation. In contrast, constitutive enhanced Fe uptake capacity and insensitivity to systemic Fe signalling in the *btsl1x2* mutant confers increased tolerance to Zn excess, characterised by reduced shoot Zn accumulation and Zn/Fe ratio (**Chapters 4 and 5**). This is similar to the Fe-mediated Zn tolerance phenotype seen upon supplementing plants with Fe under high Zn growth conditions (**Appendix B**)[212], or in plants with enhanced Fe uptake and translocation capacity, such as *fbp* mutants [201], *ZIF1* overexpressing lines [203] and *ZmIRT1* overexpressing *A. thaliana* lines [523].

Under Zn excess, wild type also shows increased root Fe accumulation compared to the *btsl1x2* mutant (**Chapter 4**). Wild type root overaccumulation occurs due to

reduced root-to-shoot Fe transport resulting in Fe-dependent inhibition of FRO2 activity and likely apoplastic Fe³⁺ accumulation, which is commonly observed under Fe excess [524]. Higher resolution Perls'/DAB staining and ICP-MS is required to verify this (**Chapter 4**). Despite high levels of Fe accumulation in roots under Zn excess, overriding shoot-borne Fe deficiency signals maintain activation of the root Fe deficiency transcriptional response (**Chapters 4 and 5**). The nature of the systemic signal is not still fully understood, although BTS and BTSL appear to be the root Fe sensors responsible for altering root homeostasis in response to shoot Fe status (**Chapter 5**)[304-306]. One such possibility is that Zn and Fe binding to BTS and BTSL HHE domains regulates their activity, and as such phloem-mediated recirculation of these micronutrients to roots could act as the shoot-borne signal (**Chapters 4 and 5**). Fe binding to BTSL HHE domains has previously been documented [305], as has Zn and Fe binding to BTS and HRZ HHE domains [306]. Moreover, *IRT1* and *FRO2* show similar levels of upregulation under Fe deficiency and Zn excess, despite very different root Fe concentrations under these two conditions, suggesting that BTSL activity is regulated by the root Zn/Fe ratio rather than absolute Fe concentration (**Chapter 4**). However, the regulatory effect of Zn and Fe binding, as well as oxidative changes that occur during micronutrient stress, on BTS and BTSL protein stability and ubiquitination activity is required to confirm this model.

Thus, the work here implicating BTSL proteins in the regulation of Zn and Fe balance and distribution, and their possible regulation by the Zn/Fe ratio, demonstrates an important new function for BTSL proteins in Zn and Fe cross-homeostasis. Characterisation of the *bts-3* mutant allele Zn excess phenotype is likely to show a similar role for BTS, and could suggest that BTS, BTSL1, BTSL2 and FBP have dual functions as negative regulators of the Fe deficiency response as well as central regulators of the Zn excess response. Further investigation of the Fe-mediated Zn tolerance phenotype for Zn excess-specific responses could help further elucidate whether there are other distinct Zn excess-regulatory proteins, or whether the Zn excess response is a result of its influence on Fe homeostasis.

6.1.3 BTSL proteins regulate FIT-, IVc bHLH- and bHLH121/URI-dependent gene expression

Transcriptomic analysis of the *bts1x2* mutant in **Chapter 5** showed constitutive expression of FIT-dependent and FIT-independent genes in roots. Previous work has shown that the BTSL proteins target FIT for proteasomal degradation [304, 305], while BTS targets bHLH121/URI and three of the IVc bHLH transcription factors (bHLH104, bHLH105/ILR3 and bHLH115) [300, 307]. However, upregulation of FIT-dependent and FIT-independent gene expression in the *bts1x2* mutant cannot be explained by FIT protein accumulation alone [301, 302, 375] and suggests that BTSL proteins likely additionally target IVc bHLH and bHLH121/URI (**Chapter 5**). Fe deficiency activates the phosphorylation and accumulation of bHLH121/URI and FIT, as well as epidermal relocalisation of bHLH121/URI to epidermal cells, which is thought to promote heterodimer formation with partner transcription factors and enhance activation of downstream gene expression [300, 321]. Overaccumulation of these phosphorylated active forms of bHLH121/URI and FIT in the *bts1x2* mutant explains the disproportionate upregulation of Fe deficiency-responsive genes upon exposure to Fe limiting and Zn excess conditions, notably during split root experiments (**Chapters 4 and 5**). Although gene expression analysis of the *bts1* single mutants suggests that BTSL1 and BTSL2 likely have similar protein targets, BTSL2 appears to exert a greater influence on root Fe homeostasis, either due to its expression across more cell types or through differential activity which is yet to be explored (**Chapters 4 and 5**) [304, 305]. Confirmation of BTSL protein interaction with IVc bHLH and bHLH121/URI at the protein level through interaction studies, Western blot analyses as well as analysis of cellular distribution and accumulation of bHLH121/URI in the *bts1x2* mutant could confirm these new proposed BTSL targets.

A small subset of Fe deficiency-responsive genes in roots, such as *NAS4*, *IMA* and *FER* genes, do not show constitutive overexpression in the *bts1x2* mutant and appear responsive to shoot Fe sufficiency signalling (**Chapter 5**). These shoot-responsive genes are largely expressed in the stelar cells where BTS is still active and functional in the *bts1x2* mutant [304, 525]. This cell-specific misregulation of Fe deficiency-responsive genes in the *bts1x2* mutant sharply contrasts with the *bts-3* mutant, which shows

upregulation of BTSL-dependent epidermal genes, such as *IRT1* and *FRO2* [304]. This could suggest an interesting cellular delimitation of Fe signalling in roots, whereby BTSL-regulated systemic signals can override or regulate BTSL activity and downstream Fe deficiency responses. In contrast, BTSL-mediated responses to local Fe signals are restricted to BTSL-expressing cell types. This may be similar to the cell-type specific perception and response to local nitrate signals seen in roots, which is additionally regulated by systemic nitrate signalling [526].

6.2 Open questions

6.2.1 Identification of Zn homeostasis mutants from *pZIP5:LUC* and *pFRO3:LUC* screens

Initial screening of the *pZIP5:LUC* and *pFRO3:LUC* M₂ populations failed to identify any candidate mutants, however further screening of mutant lines and expansion of the growth conditions will likely help identify mutants of interest (**Chapter 3**). For example, the number of M₂ individuals imaged is relatively low compared to comparable *LUC*-based screens [369, 370, 397, 398], and screening for *LUC* overexpressing mutants under altered Zn and standard growth conditions was not carried out. Moreover, the *pFRO3:LUC* lines could also be used to screen for genes and mutant alleles associated with Fe deficiency and Fe-mediated Zn tolerance through screening for high Zn-stressed mutants that fail to be rescued by Fe supplementation.

However, the mutant screens established here are unlikely to identify genes associated with systemic Zn signalling, as *ZIP5* is a known target of local Zn deficiency-responsive bZIP19 and bZIP23, and *FRO3* is regulated by the Fe deficiency bHLH transcriptional cascade [159, 290, 307]. To date only *MTP2* and *HMA2* have been shown to be regulated by systemic Zn signals [162], and as such a genetic mutant screen utilising *MTP2* and *HMA2* promoters, or alternatively a yeast-one-hybrid screen, could provide valuable insight into this unexplored aspect of Zn homeostasis and shoot-to-root signalling. Furthermore, a similar screen looking for components of the systemic Fe deficiency signal could be set up utilising *IMA* genes, or similarly shoot Fe status-regulated genes.

6.2.2 The Zn/Fe-sensing and regulatory mechanism of BTS and BTSL proteins

The work carried out here demonstrates the regulation of BTSL activity by local and systemic Fe signals, however the nature of these signals and the mechanisms which regulate BTS and BTSL activity are not yet fully understood (**Chapters 4 and 5**). The current model suggests that Fe binding to HHE domains regulates BTS and BTSL protein stability [304-306, 525] but the similar degree of Fe deficiency-responsive gene activation under Fe deficiency and Zn excess indicates that Fe is likely sensed as a ratio in relation to Zn or other ions (**Chapters 4 and 5**).

BTS, BTSL and the closely related HRZ proteins have been shown to bind Fe ions at the N-terminal HHE domains, with BTS and HRZ additionally shown to bind Zn [304-306]. Characterisation of the *bts-3* mutant Zn phenotype is first required to see if the Zn binding is physiologically relevant to BTS function. While mammalian FBXL5 is stabilised by Fe and O₂ binding [408, 409, 517], transient expression of BTS-GFP in the presence of an Fe chelator has shown that BTS may be destabilised in the presence of Fe [306]. As such, it will be informative to carry out *in vitro* binding assays of BTS and BTSL proteins with Zn and Fe in different ratios and under different oxidation states to examine the effect on stability and ubiquitination activity. Moreover, it would be interesting to investigate whether BTS, BTSL1 and BTSL2 are responsive to different concentration ranges or oxidation states, and whether this is linked to their different functions and cellular localisation. For example, BTS may be more sensitive to Zn/Fe fluctuations as it is expressed predominantly in shoots where Zn and Fe concentrations are more tightly regulated compared to roots, notably epidermal cells outside of the Casparian strip where *BTSL1* and *BTSL2* are expressed. Investigation into the importance of the Casparian strip as a barrier to regulating BTS and BTSL-dependent Fe signals and Zn/Fe-sensing would be interesting to conduct with endodermal barrier mutants [146]. It would also be of interest to see if natural variation exists across ecotypes and species in BTS and BTSL metal sensing sensitivity, notably in Zn hyperaccumulator species which show altered Fe homeostasis [432]. Furthermore, if a protein crystal structure of BTS and BTSL proteins were to be obtained, modelling could then be used to predict metal and O₂ binding dynamics to natural variant and mutagenised forms of the proteins.

Fully understanding the nature of systemic Fe signalling is necessary in order to build a model for whole plant Fe homeostasis, and to understand where BTS, BTSL and other points of Zn and Fe cross-homeostasis exist. Mismetallation of Fe proteins in shoots is thought to act as the initiator of systemic Fe signalling, with Fe-S cluster containing Cd recently shown to activate shoot Fe deficiency responses through interfering with NEET protein stability and activity [527, 528]. However, full understanding of other sensing proteins, mechanisms and signals involved are yet to be fully understood. The implication of phloem transporters, such as OPT3 [244], in systemic Fe signalling suggests that recirculation of Fe, and likely Zn through other transporters, in the phloem is important for shoot-to-root communication. In addition, other signals, such as the phloem-mobile IMA signalling peptides, have been shown necessary for activation of root Fe deficiency responses [335]. One possibility is that multiple systemic signals exist and these act on different components of the root Fe homeostasis network. For instance, metal binding may regulate BTS and BTSL, while another signal may be responsible for activating phosphorylation of FIT and bHLH121/URI.

6.2.3 The interaction of BTSL proteins with IVc bHLH and bHLH21/URI

Misregulation of FIT-dependent and FIT-independent genes in the *bts1x2* mutant suggests that BTSL1 and BTSL2 negatively regulate IVc bHLH and bHLH121/URI protein accumulation, in addition to the previously known target of FIT (**Chapter 5**). This would give BTSL proteins partially overlapping protein targets with BTS, which negatively regulates IVc bHLH (bHLH104, bHLH105/ILR3 and bHLH115) and bHLH121/URI [300, 306]. However, direct evidence of protein-protein interaction is required to confirm targeting of IVc bHLH and bHLH121/URI, as well as to establish exactly which of the four IVc bHLH transcription factors interact with BTSL proteins.

Evidence of *in vitro* and *in planta* protein-protein interaction, as well as evidence of transcription factor accumulation in the *bts1x2* mutant through use of protein-GFP fusions and Western blot analyses could provide insight into new BTSL targets. Ideally, co-immunoprecipitation of BTS and BTSL proteins with bHLH121/URI could be used to confirm these interactions, as well as evidence for ubiquitination activity *in vitro*.

Investigation of different possible targets or target affinities between BTSL1 and BTSL2 could also give further information on the functional differences between these proteins.

Previous work with BTS and BTSL proteins has shown some difficulties in obtaining stable or long-lived forms of the protein, and has also shown that specific conditions need to be taken into account to prove BTS and BTSL-protein interactions [306]. For example, there is a discrepancy in the literature about BTS targeting of bHLH121/URI, with accumulation of phosphorylated bHLH121/URI observed in the *bts-3* mutant, but yeast two-hybrid studies failing to show BTS or BTSL interaction with bHLH121/URI [298]. However, the yeast-two hybrid fails to take into account the metal-dependent stability of the proteins, as well as the possible requirement of phosphorylation of bHLH121/URI phosphorylation. Thus, greater understanding of metal homeostasis networks can also help inform experimental design and analysis in the future.

6.2.4 BTS and BTSL regulation of other homeostasis networks

The characterisation of the *bts/1x2* mutant demonstrated a new function for BTSL proteins in Zn and Fe cross-homeostasis (**Chapters 4 and 5**), and together with FBP, shows that negative regulators of Fe deficiency are also important regulators of the Zn excess response [201]. Mn homeostasis was also altered in the *bts/1x2* mutant, as well as genes associated with phosphate and sulphur homeostasis being misregulated, which could suggest that BTSL proteins are also important points of cross-homeostasis with other ion regulatory networks (**Chapters 4 and 5**). Phosphate homeostasis regulators, such as PHR1, have been shown to also influence Zn, Fe and sulphur homeostasis, and as such two-way cross-talk between these networks could help maintain nuanced homeostatic balance through incorporating multiple nutrient signalling pathways [328]. Investigation of other metal homeostasis networks in the *bts/1x2* mutant, as well as *bts-3*, could provide valuable insight into the interaction of Fe with other nutrient homeostasis networks.

BTS has recently been shown to regulate cold and drought stress responses positively through targeting Vascular Plant One Zinc Finger 1 (VOZ1) and VOZ2

transcription factors for proteasomal degradation [412]. Thus, BTS and BTSL proteins may have yet still unidentified protein targets involved in signalling pathways unrelated to Fe homeostasis, and in turn also be regulated by non-metal signalling pathways. For instance, hormonal signalling, abiotic and biotic stress and developmental signalling pathways are all influenced by Fe nutrient status, and as such their potential interaction with BTS and BTSL proteins is also worth exploring. Whilst mutant characterisation can be helpful in identifying other signalling pathways affected by loss of BTS and BTSL function, it is worth considering pleiotropic phenotypes that may arise due to mutations or altered Fe homeostasis. Thus, direct evidence for interactions with other regulatory proteins and molecules, such as Zn, is paramount for investigating new physiological roles of BTS and BTSL proteins.

6.3 Implications of research findings

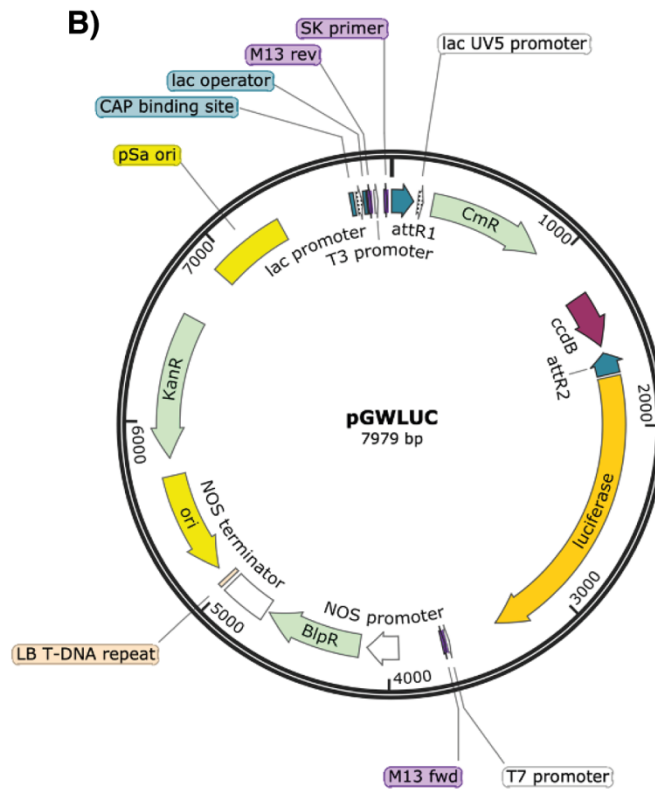
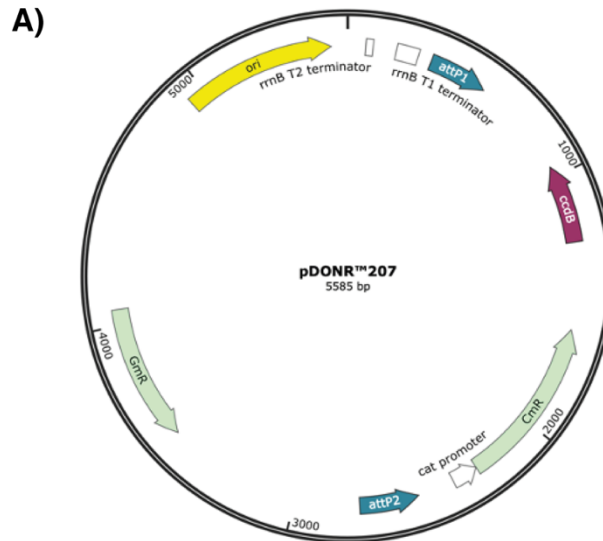
The work presented in this thesis contributes towards our understanding of Zn and Fe cross-homeostasis in plants. Given the strong evidence for interactions between micronutrient homeostasis networks, there is still relatively little known about the proteins which regulate this cross-talk. Prior knowledge of target genes and their effect on micronutrient uptake, distribution and balance is important for increasing the efficiency of biofortification and breeding strategies. The study of *BTSL1* and *BTSL2* shown here, as well as the establishment of two Zn homeostasis mutant screens, assists with developing the current model of Zn and Fe homeostasis and can help inform future biofortification efforts of dicotyledonous crops.

BTSL proteins were identified as negative regulators of the Fe deficiency response, but the work here also shows that they have a role in Zn and Fe cross-homeostasis. Combined with FBP [201], and likely BTS, identification of repressors of Fe deficiency as regulators of the Zn excess response shifts traditional thinking away from viewing Zn and Fe homeostasis as separate signalling pathways. As such, understanding the mechanism of Zn and Fe homeostatic interactions can be exploited to simultaneously improve Zn and Fe nutrition in crops, as well as enhanced tolerance to Zn excess and Fe deficiency.

Together with BTS, BTSL proteins are also proposed to act as cellular Fe sensors, with the work in this thesis supporting previous evidence that Fe is sensed as the cellular concentration ratio between Fe and Zn [27, 407, 529]. Manipulation of BTS and BTSL Zn and Fe binding affinity, or interaction with target proteins, can potentially be used to produce crops with altered micronutrient content and distribution, as well as enhanced tolerance to growth on soils with sub-optimal micronutrient concentrations. It has recently been demonstrated that *bts* mutants are able to accumulate and tolerate high levels of Cd due to the increased Fe levels, and as such it is likely that a similar phytoremediation strategy for Cd and Zn may be achieved through BTSL protein manipulation [69]. Investigation of Zn and Fe sensing mechanisms across species can also give important insight into both recent and historical evolutionary events that have allowed plants to adapt to changing micronutrient availability. Potential natural variation in BTS and BTSL protein functionality between species and cultivars adapted to different micronutrient growth conditions could be a rich source for genetic variation for breeding programmes. For example, cultivars which show enhanced Fe uptake capacity through BTSL variants could be crossed with cultivars or transgenics which show enhanced Zn and Fe partitioning to grains to ensure the bioavailability of enhanced micronutrient content.

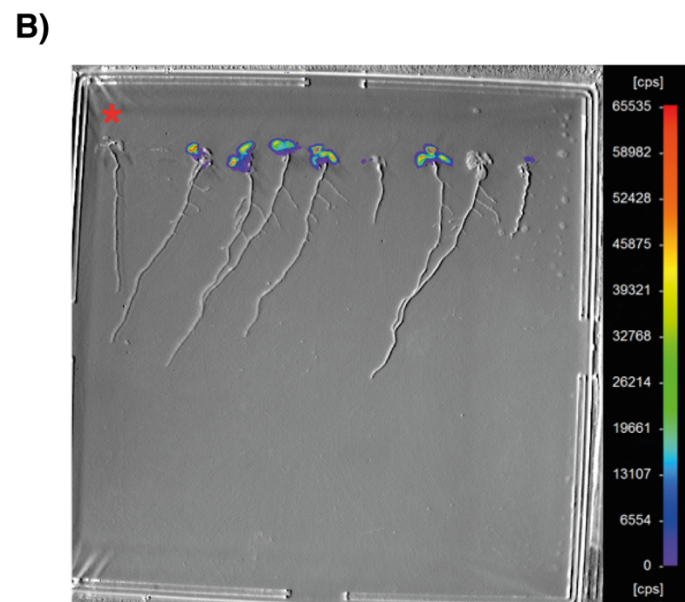
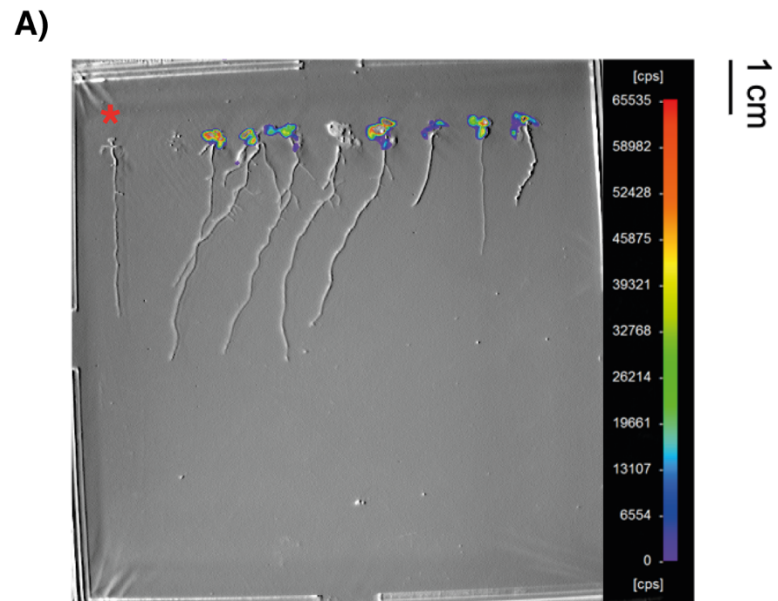
Thus, the research carried out here furthers our model of Zn and Fe homeostasis in plants and offers novel insight into micronutrient interactions, which one day may contribute towards biofortification efforts to tackle malnutrition in agriculture and the human population.

Appendix A: Chapter 3 supplemental figures



Supplementary Figure A1: Plasmid maps of vectors used in Gateway cloning.

A) pDONR207 entry vector and B) pGWLUC destination vector. Maps generated using SnapGene software (available at snappgene.com)



*** = Col-0 control**

Supplementary Figure A2: Luminescence imaging of pDEFL206:LUC T₃ lines.

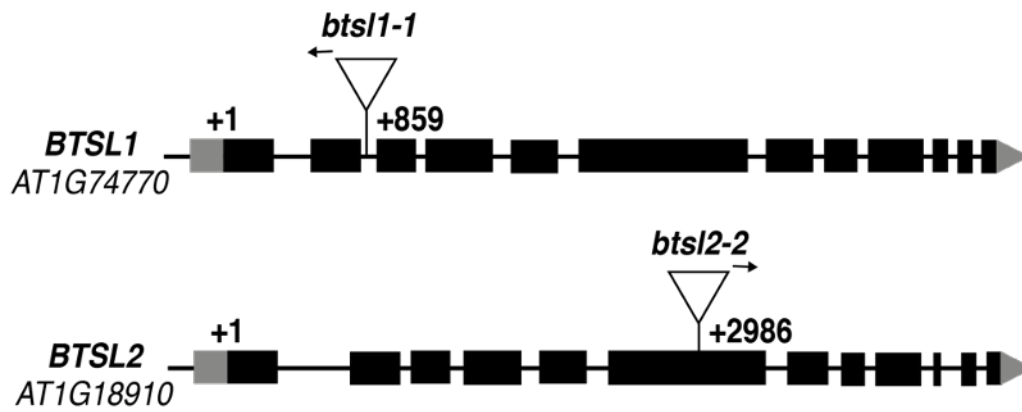
Seedlings were imaged at 10-d-old after 7 d growth on standard media followed by A) transfer to 50 μ M TPEN plates or B) spraying with 50 μ M TPEN solution for 3 d. Seedlings were incubated with luciferin prior to imaging. Red asterisk indicates Col-0 control; cps = counts per second.

	Agar plates (transfer)	96-well plates (liquid media)
Seedlings per plate	12	96
No. of plates imaged at once	1	4
Exposure time	60 s	5 s
Luciferin incubation time	10 min	4 h
Luciferin concentration	1 mM	50 μ M

Supplementary Table A1: Comparison of factors effecting suitability of agar plates and 96-well plate liquid growth systems for high-throughput screening.

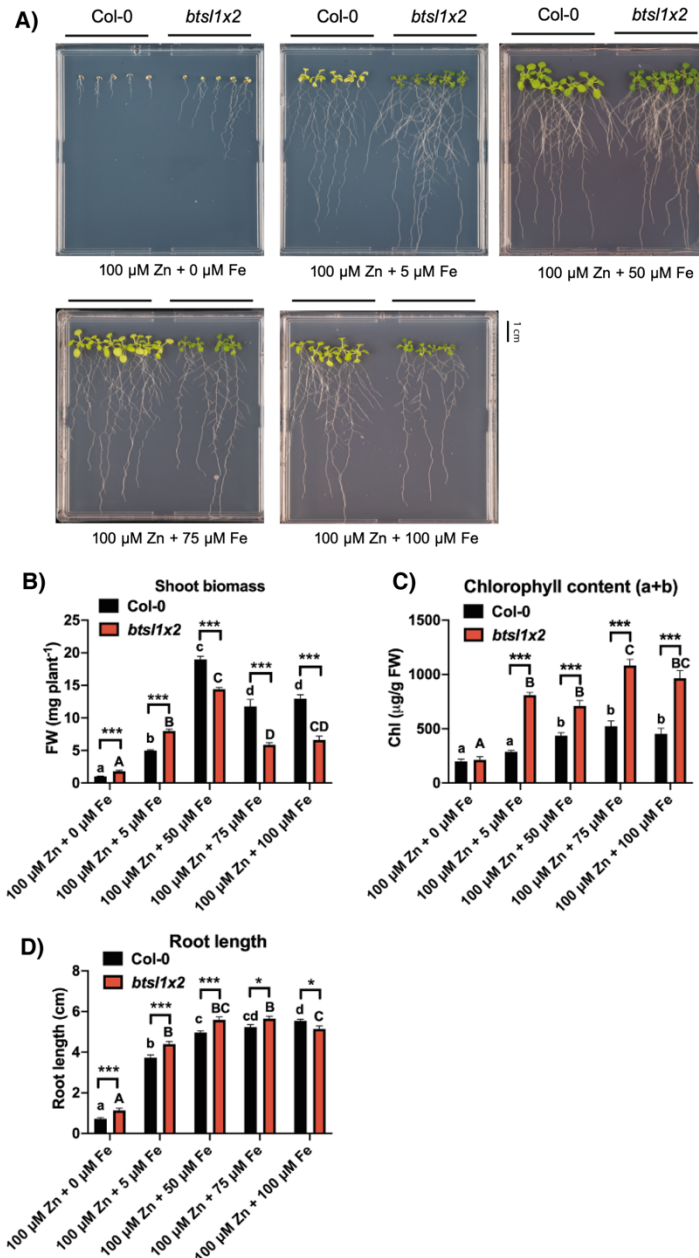
Comparison of parameters that effect the suitability of imaging 12-d-old on agar plates (transferred to TPEN supplemented plates to induce Zn deficiency) or 96-well plates (grown in low Zn liquid media).

Appendix B: Chapter 4 supplementary figures



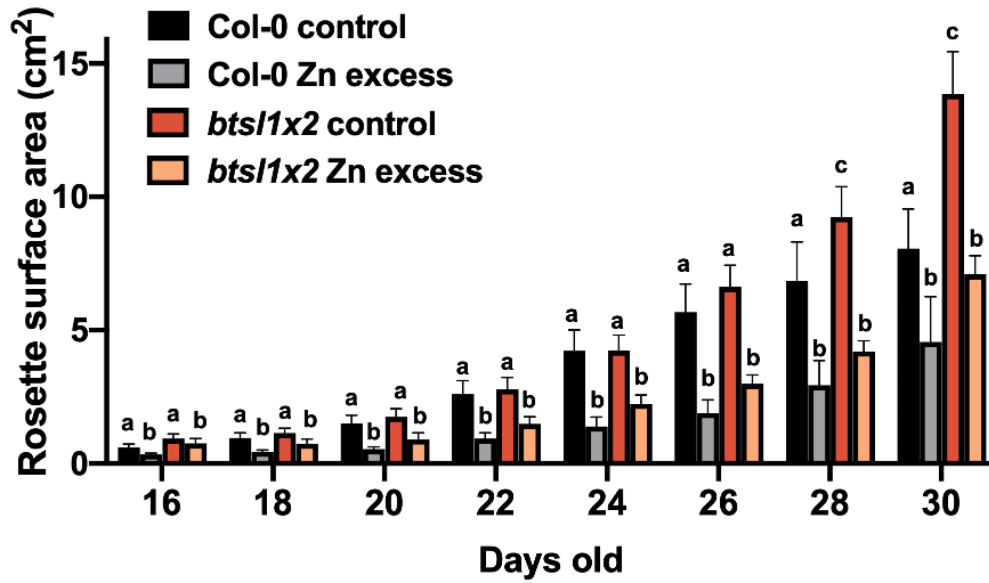
Supplementary Figure B1: Schematic of *BTSL1* and *BTSL2* genes with position of T-DNA insertion shown.

Exons are in black and 5' and 3'-UTRs shown in grey. T-DNA insertions are represented by triangles and arrows indicate the direction of the left border primer used in genotyping. *btsl1-1* = SALK_015054, *btsl2-2* = SALK_048470. Adapted from [305]



Supplementary Figure B2: Fe-mediated Zn tolerance phenotype of Col-0 and *bts1x2*.

A) Representative photographs of Col-0, *bts1*, *bts2* and *bts1x2* 14-d-old, B) shoot fresh weight (FW) and C) total chlorophyll content (chl) of 14-d-old seedlings and D) primary root length of 10-d-old seedlings grown continuously on modified Hoagland medium supplemented with Zn excess (100 μM ZnSO₄) and increasing Fe concentrations (0 μM, 5 μM, 50 μM, 75 μM and 100 μM FeHBED). Data represent mean values (± SEM) from three independent experiments, each comprising six plants per genotype and condition. Statistically significant differences are indicated by asterisks (within conditions, **p* < 0.05, ***p* < 0.01, ****p* < 0.001) or letters (within genotype, *p* < 0.05) as determined by two-way ANOVA followed by Tukey HSD post-hoc test. Non-significant differences are not indicated.



Supplementary Figure B3: Rosette surface area of Col-0 and *bts1x2* grown on Zn excess soil.

Rosette surface area measurements (cm²) taken between 16 and 30-d-old. Data represent mean values (\pm SEM) from three independent experiments, each comprising ten plants per genotype and condition. Statistically significant differences are indicated by letters (within age, $p < 0.05$) as determined by two-way ANOVA followed by Tukey HSD post-hoc test.

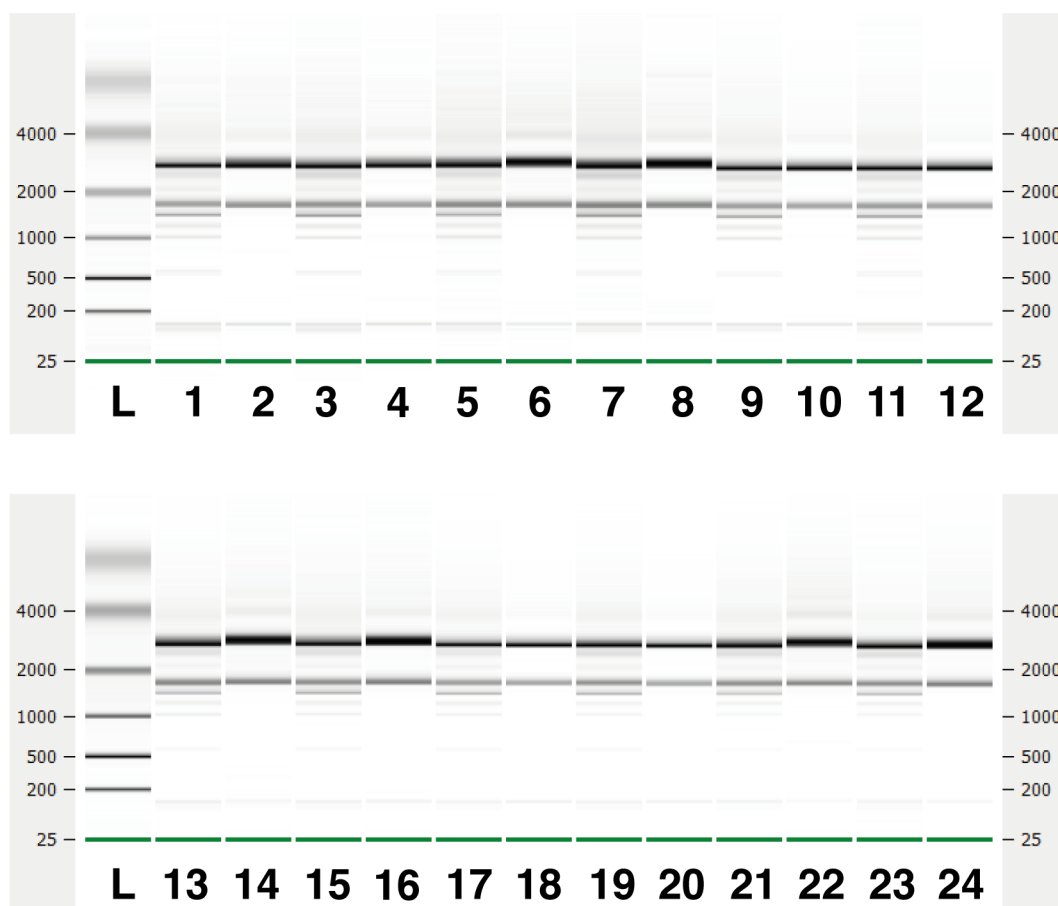
Appendix C: Chapter 5 supplementary figures

Sample no.	Genotype	Tissue	Treatment	Rep	Concentration (ng/ μ L)	Total amount (ng)	rRNA ratio (25s/18s)	RIN
1	Col-0	Shoot	1 μ M Zn	1	100	3000	2.1	8.3
2	Col-0	Root	1 μ M Zn	1	112	3360	2.4	9.7
3	<i>bts1x2</i>	Shoot	1 μ M Zn	1	101	3030	2.3	8.5
4	<i>bts1x2</i>	Root	1 μ M Zn	1	73	2190	2.5	9.4
5	Col-0	Shoot	100 μ M Zn	1	95	2850	2.2	8.6
6	Col-0	Root	100 μ M Zn	1	112	3360	2.5	9.8
7	<i>bts1x2</i>	Shoot	100 μ M Zn	1	119	3570	2.3	8.5
8	<i>bts1x2</i>	Root	100 μ M Zn	1	116	3480	2.5	9.9
9	Col-0	Shoot	1 μ M Zn	2	172	5160	2.5	8.4
10	Col-0	Root	1 μ M Zn	2	115	3450	2.2	9.3
11	<i>bts1x2</i>	Shoot	1 μ M Zn	2	145	4350	2.4	8.3
12	<i>bts1x2</i>	Root	1 μ M Zn	2	128	3840	2.2	9.3
13	Col-0	Shoot	100 μ M Zn	2	135	4050	2.4	8.9
14	Col-0	Root	100 μ M Zn	2	79	2370	2.2	9.8
15	<i>bts1x2</i>	Shoot	100 μ M Zn	N/A	123	3690	2.6	8.8
16	<i>bts1x2</i>	Root	100 μ M Zn	2	71	2130	2.2	9.6
17	Col-0	Shoot	1 μ M Zn	3	138	4140	2.6	8.4
18	Col-0	Root	1 μ M Zn	3	146	4380	2.5	9.3
19	<i>bts1x2</i>	Shoot	1 μ M Zn	3	124	3720	2.1	8.8
20	<i>bts1x2</i>	Root	1 μ M Zn	3	152	4560	2.4	9.1
21	Col-0	Shoot	100 μ M Zn	3	111	3330	2.2	9
22	Col-0	Root	100 μ M Zn	3	94	2820	2.9	9.9

Sample no.	Genotype	Tissue	Treatment	Rep	Concentration (ng/ μ L)	Total amount (ng)	rRNA ratio (25s/18s)	RIN
23	<i>bts1x2</i>	Shoot	100 μ M Zn	2	83	2490	2.2	9
24	<i>bts1x2</i>	Root	100 μ M Zn	3	114	3420	2.6	9.8

Supplementary Table C1: Summary of RNA quality check for RNAseq samples.

rRNA ratio = ribosomal RNA ratio. A rRNA ratio of 2.1 indicates good quality RNA. RIN = RNA Integrity Number. A RIN of >8 indicates good quality RNA with little fragmentation.



Supplementary Figure C1: Gel of RNAseq samples run on Bioanalyzer 2100.

Clear bands indicate high RNA integrity with little degradation. Lane numbers match sample numbers indicated in Supplementary table 1, L = nucleotide ladder.

Genotype	Tissue	Treatment	Rep	Raw reads	Clean reads	Error (%)	Q20 (%)	Q30 (%)	Q score	GC (%)
Col-0	Shoot	1 μ M Zn	1	28753615	28369202	0.02	98.15	94.37	35.56	46.51
Col-0	Shoot	1 μ M Zn	2	32996397	32521849	0.03	97.95	93.88	35.57	46.42
Col-0	Shoot	1 μ M Zn	3	30663868	30289586	0.03	97.97	93.95	35.55	46.31
Col-0	Root	1 μ M Zn	1	30617168	29974012	0.03	97.93	93.95	35.49	44.96
Col-0	Root	1 μ M Zn	2	28515861	27971406	0.03	97.90	93.88	35.49	44.94
Col-0	Root	1 μ M Zn	3	27118347	26619510	0.03	97.89	93.83	35.50	44.90
Col-0	Shoot	100 μ M Zn	1	37145299	36634593	0.03	97.97	93.94	35.56	45.65
Col-0	Shoot	100 μ M Zn	2	30325010	29915877	0.03	97.78	93.47	35.57	45.73
Col-0	Shoot	100 μ M Zn	3	28698744	28325924	0.03	97.92	93.80	35.56	45.59
Col-0	Root	100 μ M Zn	1	30285796	29739425	0.02	98.06	94.20	35.52	44.82
Col-0	Root	100 μ M Zn	2	29986048	29467746	0.03	97.93	93.87	35.55	44.82
Col-0	Root	100 μ M Zn	3	31801542	31209157	0.02	98.09	94.25	35.53	44.80
<i>bts1x2</i>	Shoot	1 μ M Zn	1	31202788	30832325	0.03	97.92	93.82	35.49	46.57
<i>bts1x2</i>	Shoot	1 μ M Zn	2	33591017	33067085	0.02	98.07	94.18	35.57	46.49
<i>bts1x2</i>	Shoot	1 μ M Zn	3	25994973	25174681	0.02	98.23	94.60	35.56	46.37
<i>bts1x2</i>	Root	1 μ M Zn	1	28603626	28055036	0.03	97.79	93.62	35.49	44.95
<i>bts1x2</i>	Root	1 μ M Zn	2	32971800	31942531	0.02	98.05	94.20	35.50	45.07
<i>bts1x2</i>	Root	1 μ M Zn	3	31168763	29980778	0.03	97.66	93.30	35.49	44.99

Genotype	Tissue	Treatment	Rep	Raw reads	Clean reads	Error (%)	Q20 (%)	Q30 (%)	Q score	GC (%)
<i>bts1x2</i>	Shoot	100 μ M Zn	1	33500432	32854903	0.03	98.03	94.10	35.57	46.35
<i>bts1x2</i>	Shoot	100 μ M Zn	2	30008688	29516903	0.02	98.09	94.23	35.56	46.11
<i>bts1x2</i>	Root	100 μ M Zn	1	31093476	30483124	0.03	97.92	93.88	35.50	44.76
<i>bts1x2</i>	Root	100 μ M Zn	2	26910577	26433262	0.02	98.07	94.22	35.53	44.66
<i>bts1x2</i>	Root	100 μ M Zn	3	28345177	27905728	0.03	97.90	93.78	35.54	44.46

Supplementary Table C2: Summary of quality check for RNA-seq raw sequence data.

Error rate (%) is the sequencing per base error rate, Q20 and Q30 are the percentage of base count that have a Phred score > 20 or > 30 respectively. Q score is the average Phred quality score as calculated by FastQC. Phred score is a measure of the quality read of bases with 40 being the highest score possible. GC (%) are the average G and C bases per read.

Principal Component (PC)	Gene ID	Gene name	Gene description
1, 2	AT2G39730	<i>Rubisco Activase (RCA)</i>	Rubisco activase
1, 2	AT1G67090	<i>Ribulose Bisphosphate Carboxylase Small Chain 1A (RBCS1A)</i>	Rubisco small subunit multigene family
1, 2	AT1G29930	<i>Chlorophyll A/B Binding Protein 1 (CAB1/LHCB1.3)</i>	Subunit of light harvesting complex II
1, 2	AT2G08665		Natural antisense transcript overlaps with AT2G34420 (which encodes <i>LHCB1.5</i>)
1	AT1G29920	<i>Chlorophyll A/B Binding Protein 2 (CAB2/LHCB1.1)</i>	Subunit of light harvesting complex IIb
1	AT3G47470	<i>Chlorophyll A/B Binding Protein 4 (CAB4/LHCA4)</i>	Subunit of light harvesting complex I
1	AT5G38410	<i>Rubisco Small Subunit 3B (RBCS3B)</i>	Rubisco small subunit
1, 2	AT3G54890	<i>Chlorophyll A/B Binding Protein 6 (CAB6/LHCA1)</i>	Subunit of light harvesting complex I
1, 2	AT4G10340	<i>Light-Harvesting Complex of PSII (LHCB5)</i>	Subunit of light harvesting complex II
1, 2	AT5G54270	<i>Light-Harvesting Chlorophyll B-Binding Protein 3 (LHCB3)</i>	Subunit of light harvesting complex II
2	AT2G34430	<i>Light-Harvesting Chlorophyll-Protein Complex II Subunit B1 (LHB1B1)</i>	Subunit of light harvesting complex II
2	AT4G33010	<i>Glycine Decarboxylase P-Protein 1 (GLDP1)</i>	Glycine decarboxylase
2	AT4G35090	<i>Cationic Amino Acid Transporter (CAT2)</i>	Tonoplastic cationic amino acid transporter

Supplementary Table C3: Top ten loading transcripts of shoot principal component (PC) 1 and PC2.

Principal Component (PC)	Gene ID	Gene name	Gene description
1, 2	AT3G09260	<i>Beta-glucosidase 23 (BGLU23)</i>	Beta-glucosidase
1, 2	AT1G21310	<i>Extensin 3 (EXT3)</i>	Proline-rich extension-like family protein
1	AT2G43150	<i>Extensin 21 (EXT21)</i>	Proline-rich extension-like family protein
1, 2	AT1G07600	<i>Metallothionein-like Protein 1A (MT1A)</i>	Metallothionein
1	AT5G17920	<i>Methionine Synthesis 1 (MS1)</i>	Methionine synthase
1, 2	AT4G30190	<i>H(+)-ATPase 2 (AHA2)</i>	Plasma membrane P-type ATPase
1	AT1G73330	<i>Drought-Repressed 4 (DR4)</i>	Protease inhibitor-like protein
1	AT4G11320	<i>Cysteine Protease 2 (CP2)</i>	Papain family cysteine protease
1	AT4G05320	<i>Polyubiquitin 10 (UBQ10)</i>	Ubiquitin
1	AT2G05440	<i>Glycine Rich Protein (GRP9)</i>	Glycine rich protein
2	AT1G09560	<i>Germin-like Protein 5 (GLP5)</i>	Plasmodesmal intercellular transport protein
2	AT4G19690	<i>Iron-Regulated Transporter 1 (IRT1)</i>	Fe/Zn/Mn/Co/Cd ZIP family transporter
2	AT1G01580	<i>Ferric Reduction Oxidase 2 (FRO2)</i>	Low-Fe inducible ferric chelate reductase
2	AT1G02500	<i>S-adenosylmethionine Synthetase 1 (SAM1)</i>	S-adenosylmethionine synthetase
2	AT4G31940	<i>Cytochrome P450 82, Subfamily C CYP82C4</i>	Cytochrome P450
2	AT3G53480	<i>ABC Transporter G Family Member 37 (ABCG37/PDR9)</i>	Coumarin efflux transporter

Supplementary Table C4: Top ten loading transcripts of root principal component (PC) 1 and PC2.

	CS1 v BS1 down (13)	CS1 v CS100 up (981)	CS1 v CS100 down (296)	CS1 v BS100 up (54)	CS1 v BS100 down (21)	CS100 v BS100 up (207)	CS100 v BS100 down (564)	BS1 v BS100 up (16)	BS1 v BS100 down (13)
CS1 v BS1 up (2)	0	0	0	2	0	1	0	0	0
CS1 v BS1 down (13)		6	0	0	5	0	11	1	0
CS1 v CS100 up (981)			0	36	1	0	505	14	0
CS1 v CS100 down (296)				0	8	119	1	0	9
CS1 v BS100 up (54)					0	2	9	12	0
CS1 v BS100 down (21)						2	11	0	11
CS100 v BS100 up (207)							0	0	2
CS100 v BS100 down (564)								7	4
BS1 v BS100 up (16)									0

Supplementary Table C5: Overlap of significantly DEGs up- and downregulated in shoots between all pairwise comparisons.

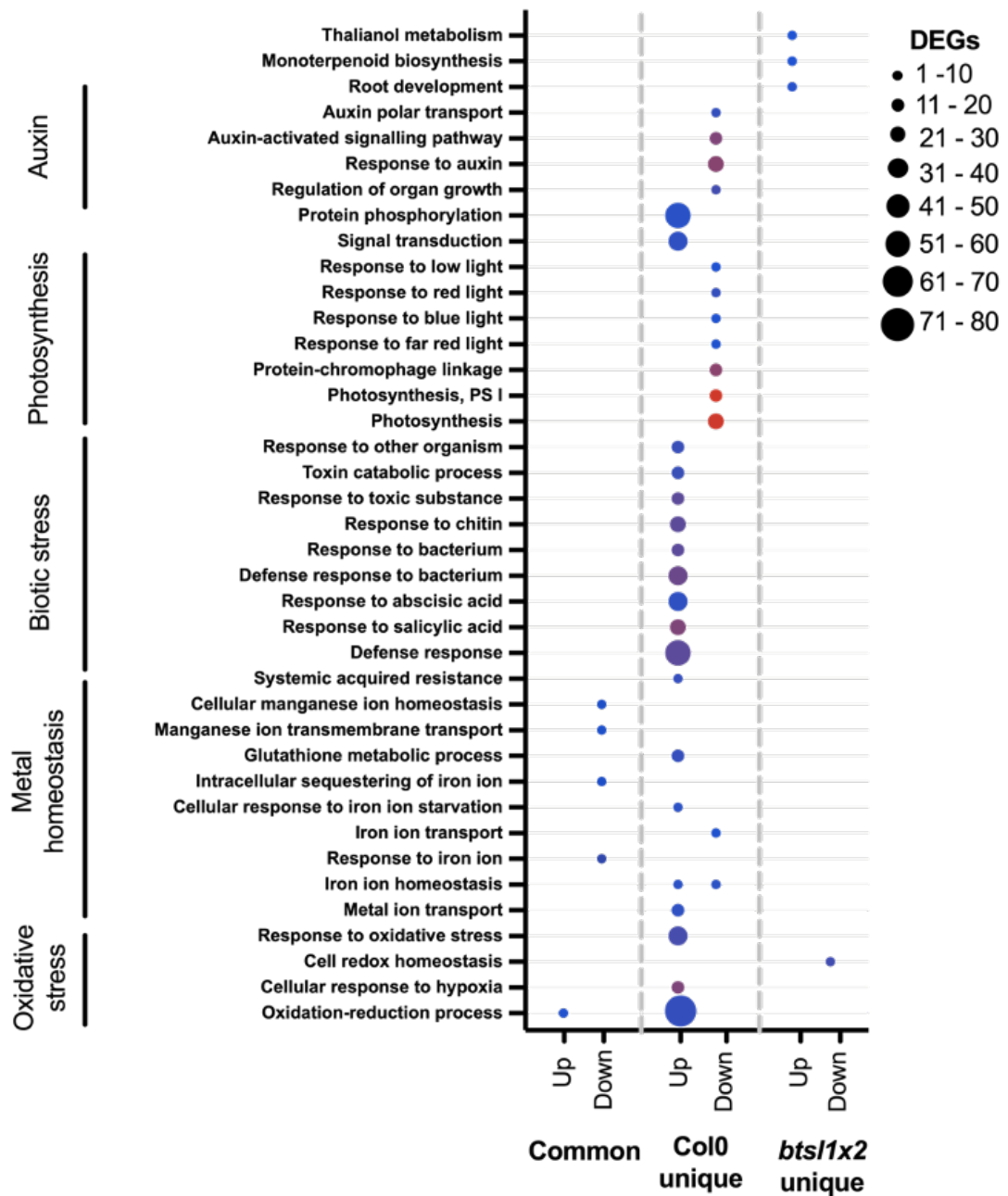
CS1 = Col-0 shoot 1 μ M Zn; CS100 = Col-0 shoot 100 μ M Zn; BS1 = *bts1x2* shoot 1 μ M Zn; BS100 = *bts1x2* shoot 100 μ M Zn

	CR1 v BR1 down (13)	CR1 v CR100 up (168)	CR1 v CR100 down (321)	CR1 v BR100 up (298)	CR1 v BR100 down (162)	CR100 v BR100 up (292)	CR100 v BR100 down (124)	BR1 v BR100 up (189)	BR1 v BR100 down (170)
CR1 v BR1 up (32)	0	21	0	28	0	12	0	20	1
CR1 v BR1 down (13)		0	1	0	8	0	8	0	0
CR1 v CR100 up (168)			0	104	0	16	31	81	0
CR1 v CR100 down (321)				0	80	86	2	0	70
CR1 v BR100 up (298)					0	88	5	167	0
CR1 v BR100 down (162)						14	40	0	104
CR100 v BR100 up (292)							0	72	15
CR100 v BR100 down (124)								5	21
BR1 v BR100 up (189)									0

Supplementary Table C6: Overlap of significantly DEGs up- and downregulated in roots between all pairwise comparisons.

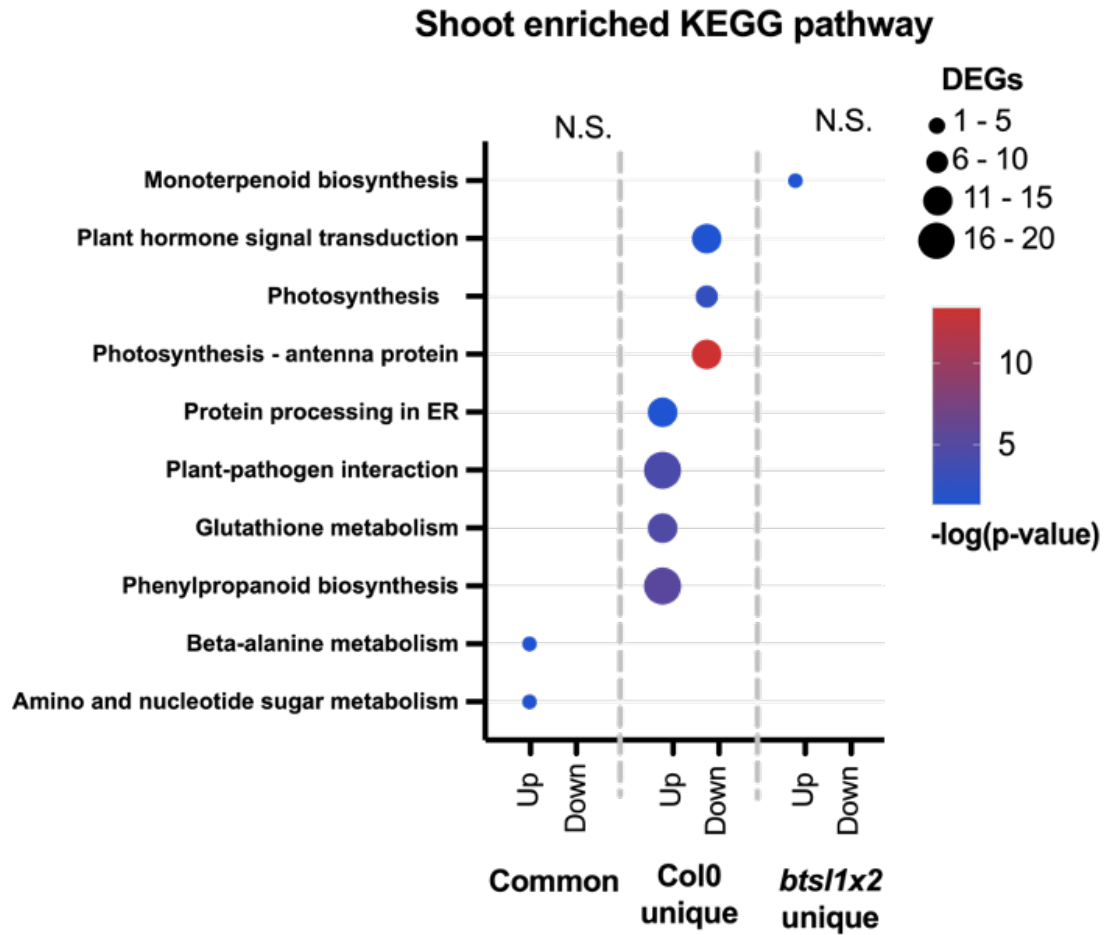
CR1 = Col-0 root 1 μ M Zn; CR100 = Col-0 root 100 μ M Zn; BR1 = *bts1x2* root 1 μ M Zn; BR100 = *bts1x2* root 100 μ M Zn.

Shoot enriched GO



Supplementary Figure C2: GO enrichment analysis of common and unique Zn-responsive DEGs in Col-0 and *bts1x2* shoots.

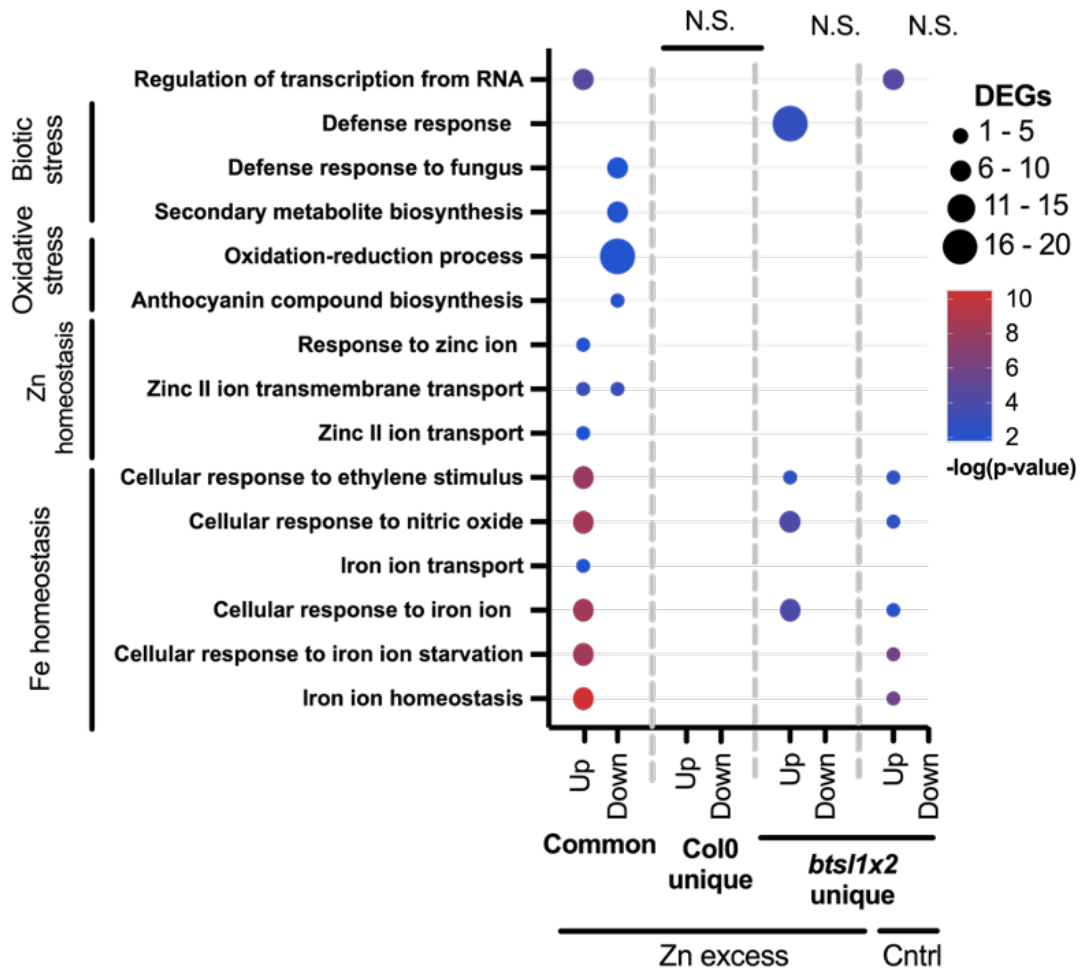
All significant ($\text{padj} < 0.05$) terms are shown on the vertical axis and grouped by similar function. The size of each point represents the number of DEGs associated with each term and the colour shows $-\log(\text{p-value})$.



Supplementary Figure C3: KEGG pathway enrichment analysis of common and unique Zn-responsive DEGs in Col-0 and *bts1x2* shoots.

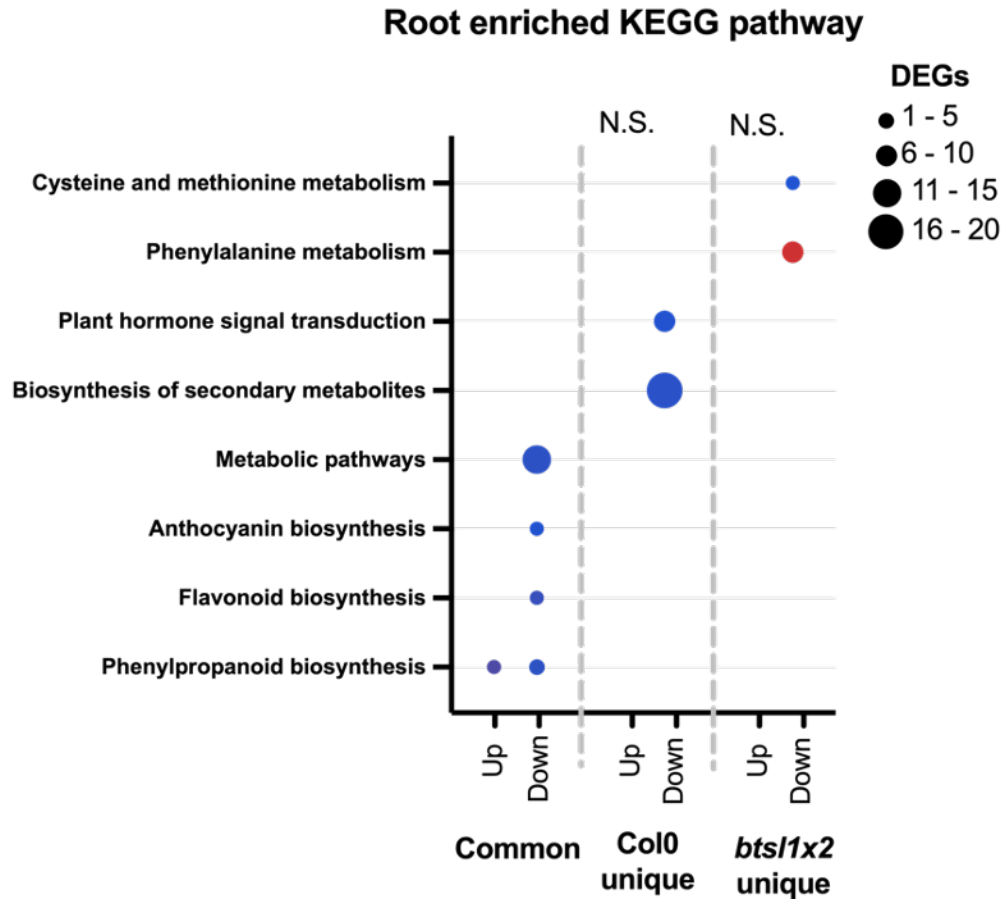
All significant ($\text{padj} < 0.05$) pathways are shown on the vertical axis. The size of each point represents the number of DEGs associated with each pathway and the colour shows $-\log(\text{p-value})$.

Root enriched GO



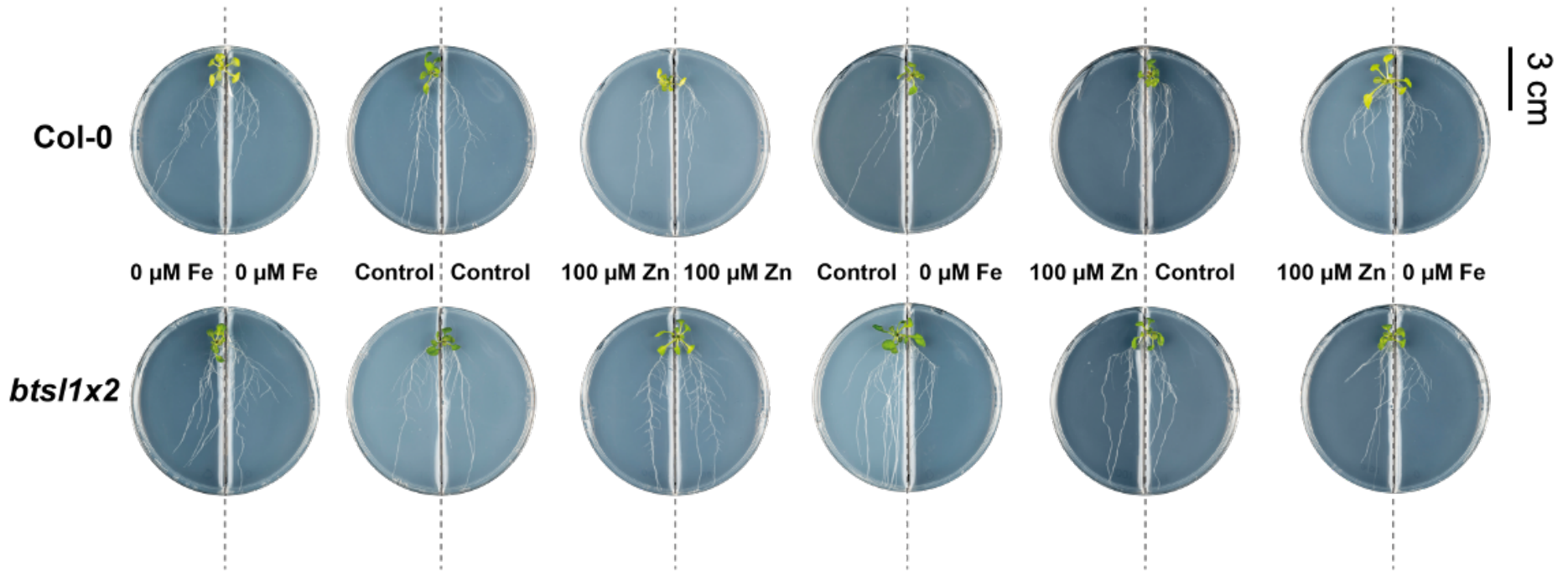
Supplementary Figure C4: GO enrichment analysis of common and unique Zn-responsive DEGs in Col-0 and *bts1x2* roots.

All significant ($p_{adj} < 0.05$) terms are shown on the vertical axis and grouped by similar function. The size of each point represents the number of DEGs associated with each term and the colour shows $-\log(p\text{-value})$.



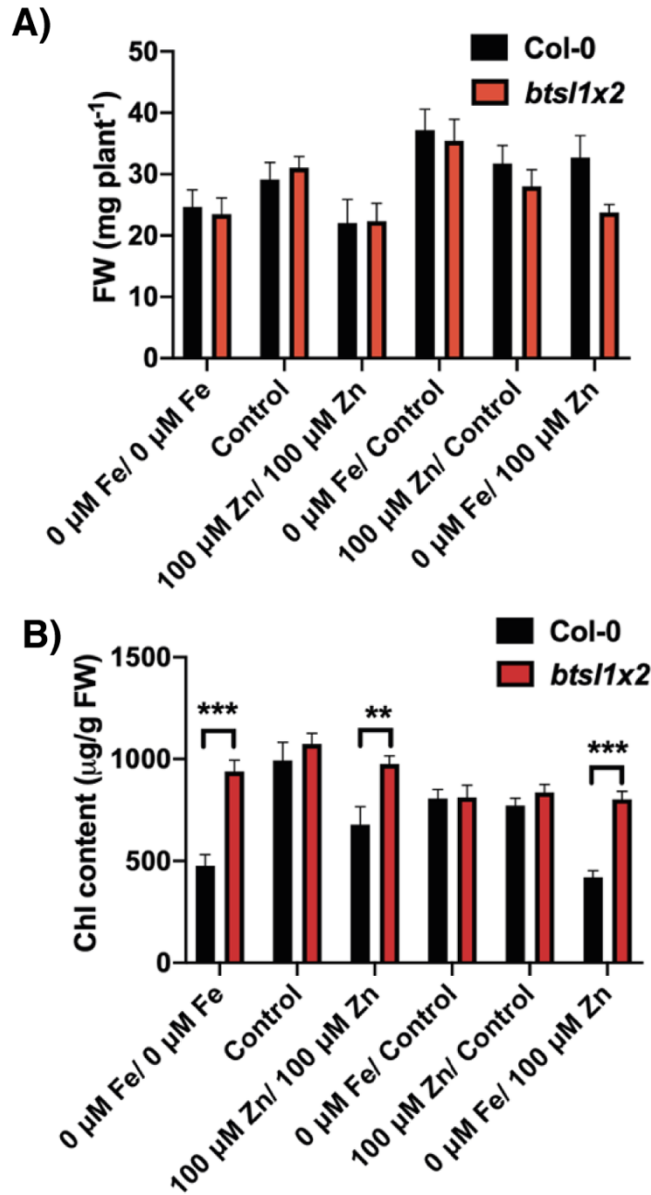
Supplementary Figure C5: KEGG pathway enrichment analysis of common and unique Zn-responsive DEGs in Col-0 and *bts1x2* roots.

All significant ($\text{padj} < 0.05$) pathways are shown on the vertical axis. The size of each point represents the number of DEGs associated with each pathway and the colour shows $-\log(\text{p-value})$.



Supplementary Figure C6: Set up of split root experiment to test local and systemic Fe deficiency signalling in Col-0 and *bts1x2*.

Photographs of Col-0 and *bts1x2* 17-d-old seedlings grown on split root agar plates containing control (5 μM FeHBED, 1 μM ZnSO₄), Fe deficiency (0 μM FeHBED, 1 μM ZnSO₄) or Zn excess (5 μM FeHBED, 100 μM ZnSO₄) modified Hoagland medium in all combinations. Seedlings were germinated on ¼ MS plates, roots excised at 5 days and then transferred to split root plates at 10-d-old.



Supplementary Figure C7: Shoot phenotypes of Col-0 and *bts1x2* seedlings grown in the split-root system.

A) Shoot fresh weight (FW) and B) chlorophyll (chl) content of Col-0 and *bts1x2* 17-d-old seedlings grown on split root agar plates containing control (5 µM FeHBED, 1 µM ZnSO₄), Fe deficiency (0 µM FeHBED, 1 µM ZnSO₄) or Zn excess (5 µM FeHBED, 100 µM ZnSO₄) modified Hoagland medium in all combinations. Seedlings were germinated on ¼ MS plates, roots excised at 5 days and then transferred to split root plates at 10-d-old). Data represent mean values (± SEM) from three independent experiments, each comprising five plants per genotype and condition. Statistically significant differences are indicated by asterisks (within conditions, **p < 0.01, ***p < 0.001) as determined by two-way ANOVA followed by Tukey HSD post-hoc test. Non-significant differences are not indicated.

Bibliography

1. **Marschner, H.**, *9 - Functions of Mineral Nutrients: Micronutrients*, in *Mineral Nutrition of Higher Plants (Second Edition)*. 1995, Academic Press: London. p. 313-404.
2. **Saper, R.B. and R. Rash**, *Zinc: an essential micronutrient*. *American family physician*, 2009. **79**(9): p. 768-772.
3. **Wintz, H., T. Fox, and C. Vulpe**, *Responses of plants to iron, zinc and copper deficiencies*. *Biochemical Society Transactions*, 2002. **30**(4): p. 766-768.
4. **Andreini, C., I. Bertini, and A. Rosato**, *Metalloproteomes: A Bioinformatic Approach*. *Accounts of Chemical Research*, 2009. **42**(10): p. 1471-1479.
5. **Housecroft, C.E., C.M. Thomas, and M.H. Lim**, *The central role of the d-block metals in the periodic table*. *Dalton Transactions*, 2019. **48**(26): p. 9405-9407.
6. **Habashi, F.**, *Zinc, Physical and Chemical Properties*, in *Encyclopedia of Metalloproteins*, R.H. Kretsinger, V.N. Uversky, and E.A. Permyakov, Editors. 2013, Springer New York: New York, NY. p. 2537-2538.
7. **Habashi, F.**, *Iron, Physical and Chemical Properties*, in *Encyclopedia of Metalloproteins*, R.H. Kretsinger, V.N. Uversky, and E.A. Permyakov, Editors. 2013, Springer New York: New York, NY. p. 1033-1034.
8. **Baś, S., M. Szewczyk, and J. Mlynarski**, *Zinc-based Chiral Lewis Acids*. *Chiral Lewis Acids in Organic Synthesis*, 2017: p. 137-181.
9. **Kambe, T., T. Tsuji, A. Hashimoto, and N. Itsumura**, *The Physiological, Biochemical, and Molecular Roles of Zinc Transporters in Zinc Homeostasis and Metabolism*. *Physiological Reviews*, 2015. **95**(3): p. 749-784.
10. **Hoch, F.L. and B.L. Vallee**, *Kinetic studies on the role of zinc and diphosphopyridine nucleotide in the activity of yeast alcohol dehydrogenase*. *J Biol Chem*, 1956. **221**(1): p. 491-500.
11. **Williams, R.J.**, *Binding of zinc in carboxypeptidase*. *Nature*, 1960. **188**: p. 322.
12. **Keilin, D. and T. Mann**, *Carbonic anhydrase. Purification and nature of the enzyme*. *Biochem J*, 1940. **34**(8-9): p. 1163-76.
13. **Huang, C.C., C.A. Lesburg, L.L. Kiefer, C.A. Fierke, and D.W. Christianson**, *Reversal of the hydrogen bond to zinc ligand histidine-119 dramatically*

- diminishes catalysis and enhances metal equilibration kinetics in carbonic anhydrase II. Biochemistry, 1996. 35(11): p. 3439-46.*
14. **Kochanczyk, T., A. Drozd, and A. Krezel**, *Relationship between the architecture of zinc coordination and zinc binding affinity in proteins--insights into zinc regulation. Metallomics, 2015. 7(2): p. 244-57.*
 15. **Laity, J.H., B.M. Lee, and P.E. Wright**, *Zinc finger proteins: new insights into structural and functional diversity. Curr Opin Struct Biol, 2001. 11(1): p. 39-46.*
 16. **Clark-Baldwin, K., D.L. Tierney, N. Govindaswamy, E.S. Gruff, C. Kim, J. Berg, S.A. Koch, and J.E. Penner-Hahn**, *The Limitations of X-ray Absorption Spectroscopy for Determining the Structure of Zinc Sites in Proteins. When Is a Tetrathiolate Not a Tetrathiolate? Journal of the American Chemical Society, 1998. 120(33): p. 8401-8409.*
 17. **Ghafghazi, T., M.L. McDaniel, and P.E. Lacy**, *Zinc-induced inhibition of insulin secretion from isolated rat islets of Langerhans. Diabetes, 1981. 30(4): p. 341-5.*
 18. **Fukada, T., S. Yamasaki, K. Nishida, M. Murakami, and T. Hirano**, *Zinc homeostasis and signaling in health and diseases: Zinc signaling. J Biol Inorg Chem, 2011. 16(7): p. 1123-34.*
 19. **Hirano, T., M. Murakami, T. Fukada, K. Nishida, S. Yamasaki, and T. Suzuki**, *Roles of zinc and zinc signaling in immunity: zinc as an intracellular signaling molecule. Adv Immunol, 2008. 97: p. 149-76.*
 20. **Dupont, C.L., A. Butcher, R.E. Valas, P.E. Bourne, and G. Caetano-Anolles**, *History of biological metal utilization inferred through phylogenomic analysis of protein structures. Proc Natl Acad Sci U S A, 2010. 107(23): p. 10567-72.*
 21. **Li, T., H.L. Bonkovsky, and J.T. Guo**, *Structural analysis of heme proteins: implications for design and prediction. BMC Struct Biol, 2011. 11: p. 13.*
 22. **Jin, Z., M. Heinnickel, C. Krebs, G. Shen, J.H. Golbeck, and D.A. Bryant**, *Biogenesis of iron-sulfur clusters in photosystem I: holo-NfuA from the cyanobacterium Synechococcus sp. PCC 7002 rapidly and efficiently transfers [4Fe-4S] clusters to apo-PsaC in vitro. J Biol Chem, 2008. 283(42): p. 28426-35.*
 23. **Foster, A.W., D. Osman, and N.J. Robinson**, *Metal preferences and metallation. J Biol Chem, 2014. 289(41): p. 28095-103.*
 24. **Irving, H. and R.J.P. Williams**, *Order of stability of metal complexes. Nature, 1948. 162(4123): p. 746-747.*

25. **Solomons, N.W.**, *Competitive Interaction of Iron and Zinc in the Diet: Consequences for Human Nutrition*. The Journal of Nutrition, 1986. **116**(6): p. 927-935.
26. **Kanai, M., M. Hirai, M. Yoshiba, T. Tadano, and K. Higuchi**, *Iron deficiency causes zinc excess in Zea mays*. Soil Science and Plant Nutrition, 2009. **55**(2): p. 271-276.
27. **Leskova, A., R.F.H. Giehl, A. Hartmann, A. Fargasova, and N. von Wiren**, *Heavy Metals Induce Iron Deficiency Responses at Different Hierarchic and Regulatory Levels*. Plant Physiol, 2017. **174**(3): p. 1648-1668.
28. **Smith, K.S. and H.L.O. Huyck**, *An Overview of the Abundance, Relative Mobility, Bioavailability, and Human Toxicity of Metals*, in *The Environmental Geochemistry of Mineral Deposits: Part A: Processes, Techniques, and Health Issues Part B: Case Studies and Research Topics*, G.S. Plumlee, M.J. Logsdon, and L.F. Filipek, Editors. 1997, Society of Economic Geologists. p. 0.
29. **McComish, M.F. and J.H. Ong**, 7 - *TRACE METALS*, in *Environmental Inorganic Chemistry*, I. Bodek, et al., Editors. 1988, Pergamon: Amsterdam. p. 7-1-7.15-11.
30. **Cornell, R.M. and U. Schwertmann**, *Soils. The Iron Oxides*, 2003: p. 433-474.
31. **Barber, S.A.**, *Soil nutrient bioavailability: a mechanistic approach*. 1995: John Wiley & Sons.
32. **Kiekens, L.**, *Zinc in heavy metals*. Soils. London: Blackie Academic and Professional, 1995.
33. **Noulas, C., M. Tziouvalekas, and T. Karyotis**, *Zinc in soils, water and food crops*. J Trace Elem Med Biol, 2018. **49**: p. 252-260.
34. **Colombo, C., G. Palumbo, J.-Z. He, R. Pinton, and S. Cesco**, *Review on iron availability in soil: interaction of Fe minerals, plants, and microbes*. Journal of Soils and Sediments, 2014. **14**(3): p. 538-548.
35. **Sillanpaa, M.**, *Micronutrient assessment at the country level: an international study*. FAO Soils Bulletin, 1990(63).
36. **Cakmak, I. and E. Hoffland**, *Zinc for the improvement of crop production and human health*. Plant and Soil, 2012. **361**(1): p. 1-2.
37. **Alloway, B.J.**, *Soil factors associated with zinc deficiency in crops and humans*. Environ Geochem Health, 2009. **31**(5): p. 537-48.
38. **Alloway, B.J.Z.i.S.a.C.N.**, 2nd Edn. Brussels: IZA and IFA, 23–26., *Zinc in Soils and Crop Nutrition*, I.a. IFA, Editor. 2008: Brussels. p. 23-26.

39. **Dhaliwal, S.S., R.K. Naresh, A. Mandal, R. Singh, and M.K. Dhaliwal**, *Dynamics and transformations of micronutrients in agricultural soils as influenced by organic matter build-up: A review*. Environmental and Sustainability Indicators, 2019. **1-2**: p. 100007.
40. **Loneragan, J.F. and M.J. Webb**, *Interactions Between Zinc and Other Nutrients Affecting the Growth of Plants*, in *Zinc in Soils and Plants: Proceedings of the International Symposium on 'Zinc in Soils and Plants' held at The University of Western Australia, 27–28 September, 1993*, A.D. Robson, Editor. 1993, Springer Netherlands: Dordrecht. p. 119-134.
41. **Kabir, A.H., T. Debnath, U. Das, S.A. Prity, A. Haque, M.M. Rahman, and M.S. Parvez**, *Arbuscular mycorrhizal fungi alleviate Fe-deficiency symptoms in sunflower by increasing iron uptake and its availability along with antioxidant defense*. Plant Physiology and Biochemistry, 2020. **150**: p. 254-262.
42. **Coccina, A., T.R. Cavagnaro, E. Pellegrino, L. Ercoli, M.J. McLaughlin, and S.J. Watts-Williams**, *The mycorrhizal pathway of zinc uptake contributes to zinc accumulation in barley and wheat grain*. BMC Plant Biol, 2019. **19**(1): p. 133.
43. **Manthey, J., D.E. Crowley, and D.G. Luster**, *Biochemistry of metal micronutrients in the rhizosphere*. 1994: CRC Press.
44. **Zuo, Y. and F. Zhang**, *Soil and crop management strategies to prevent iron deficiency in crops*. Plant and Soil, 2011. **339**(1): p. 83-95.
45. **Kihara, J., P. Bolo, M. Kinyua, J. Rurinda, and K. Piikki**, *Micronutrient deficiencies in African soils and the human nutritional nexus: opportunities with staple crops*. Environmental Geochemistry and Health, 2020. **42**(9): p. 3015-3033.
46. **Schulin, R., A. Khoshgoftarmanesh, M. Afyuni, B. Nowack, and E. Frossard**, *Effects of soil management on zinc uptake and its bioavailability in plants*. Development and Uses of Biofortified Agricultural Products. Boca Raton, Florida: CRC Press, Inc, 2008: p. 95-114.
47. **Romheld, V.**, *Mobilization of iron in the rhizosphere of different plant species*. Advances in plant nutrition, 1986. **2**: p. 155-204.
48. **Dobermann, A.**, *Rice: Nutrient disorders & nutrient management*. 2000: Int. Rice Res. Inst.
49. **Shenker, M. and Y. Chen**, *Increasing Iron Availability to Crops: Fertilizers, Organo-Fertilizers, and Biological Approaches*. Soil Science & Plant Nutrition, 2005. **51**(1): p. 1-17.

50. **Cakmak, I.**, *Enrichment of cereal grains with zinc: Agronomic or genetic biofortification?* Plant and Soil, 2008. **302**(1): p. 1-17.
51. **Joy, E.J.M., A.J. Stein, S.D. Young, E.L. Ander, M.J. Watts, and M.R. Broadley**, *Zinc-enriched fertilisers as a potential public health intervention in Africa.* Plant and Soil, 2015. **389**(1): p. 1-24.
52. **Wuana, R.A. and F.E. Okieimen**, *Heavy Metals in Contaminated Soils: A Review of Sources, Chemistry, Risks and Best Available Strategies for Remediation.* ISRN Ecology, 2011. **2011**: p. 402647.
53. **Kashem, M.A., B.R. Singh, S.M.I. Huq, and S. Kawai**, *Fractionation and mobility of cadmium, lead and zinc in some contaminated and non-contaminated soils of Japan.* Journal of Soil Science and Environmental Management, 2011. **2**(9): p. 241-249.
54. **Xiao, H.-Y., S.-Y. Jiang, D.-S. Wu, and W.-B. Zhou**, *Risk element (As, Cd, Cu, Pb, and Zn) contamination of soils and edible vegetables in the vicinity of Guixi Smelter, South China.* Soil and Sediment Contamination: An International Journal, 2011. **20**(5): p. 592-604.
55. **Ray, P., S.P. Datta, and B.S. Dwivedi**, *Long-term irrigation with zinc smelter effluent affects important soil properties and heavy metal content in food crops and soil in Rajasthan, India.* Soil Science and Plant Nutrition, 2017. **63**(6): p. 628-637.
56. **Silveira, V.C.d., A.P.d. Oliveira, R.A. Sperotto, L.S. Espindola, L. Amaral, J.F. Dias, J.B.d. Cunha, and J.P. Fett**, *Influence of iron on mineral status of two rice (Oryza sativa L.) cultivars.* Brazilian Journal of Plant Physiology, 2007. **19**: p. 127-139.
57. **Becker, M. and F. Asch**, *Iron toxicity in rice—conditions and management concepts.* Journal of Plant Nutrition and Soil Science, 2005. **168**(4): p. 558-573.
58. **Mahender, A., B.P. Swamy, A. Anandan, and J. Ali**, *Tolerance of iron-deficient and-toxic soil conditions in rice.* Plants, 2019. **8**(2): p. 31.
59. **Gridley, H.E., A. Efiue, B. Tolou, and T. Bakayako**, *Breeding for tolerance to iron toxicity at WARDA.* Iron toxicity in rice-based systems in West Africa. Africa Rice Center (WARDA), Cotonou, 2006: p. 96-111.
60. **Cao, A., G. Cappai, A. Carucci, and A. Muntoni**, *Selection of plants for zinc and lead phytoremediation.* J Environ Sci Health A Tox Hazard Subst Environ Eng, 2004. **39**(4): p. 1011-24.
61. **Sikirou, M., K. Saito, E.G. Achigan-Dako, K.N. Dramé, A. Adam, and R. Venuprasad**, *Genetic Improvement of Iron Toxicity Tolerance in Rice-Progress,*

- Challenges and Prospects in West Africa*. Plant Production Science, 2015. **18**(4): p. 423-434.
62. **Sidhu, G.P.S., A.S. Bali, H.P. Singh, D.R. Batish, and R.K. Kohli**, *Insights into the tolerance and phytoremediation potential of *Coronopus didymus* L. (Sm) grown under zinc stress*. Chemosphere, 2020. **244**: p. 125350.
63. **Yan, A., Y. Wang, S.N. Tan, M.L. Mohd Yusof, S. Ghosh, and Z. Chen**, *Phytoremediation: A Promising Approach for Revegetation of Heavy Metal-Polluted Land*. Front Plant Sci, 2020. **11**: p. 359.
64. **Li, Y., J. Luo, J. Yu, L. Xia, C. Zhou, L. Cai, and X. Ma**, *Improvement of the phytoremediation efficiency of *Neyraudia reynaudiana* for lead-zinc mine-contaminated soil under the interactive effect of earthworms and EDTA*. Sci Rep, 2018. **8**(1): p. 6417.
65. **Belouchrani, A.S., N. Mameri, N. Abdi, H. Grib, H. Lounici, and N. Drouiche**, *Phytoremediation of soil contaminated with Zn using Canola (*Brassica napus* L.)*. Ecological Engineering, 2016. **95**: p. 43-49.
66. **Dmuchowski, W., D. Gozdowski, P. Brągoszewska, A.H. Baczewska, and I. Suwara**, *Phytoremediation of zinc contaminated soils using silver birch (*Betula pendula* Roth)*. Ecological Engineering, 2014. **71**: p. 32-35.
67. **Chandra, R., W. Cho, and H. Kang**, *Phytoextraction potential of four poplar hybrids under greenhouse conditions*. Forest Science and Technology, 2016. **12**(4): p. 199-206.
68. **Hu, Y., Z. Nan, C. Jin, N. Wang, and H. Luo**, *Phytoextraction potential of poplar (*Populus alba* L. var. *pyramidalis* Bunge) from calcareous agricultural soils contaminated by cadmium*. Int J Phytoremediation, 2014. **16**(5): p. 482-95.
69. **Zhu, Y.X., W.X. Du, X.Z. Fang, L.L. Zhang, and C.W. Jin**, *Knockdown of BTS may provide a new strategy to improve cadmium-phytoremediation efficiency by improving iron status in plants*. J Hazard Mater, 2020. **384**: p. 121473.
70. *Global Soil Data Task*, in *Global Soil Data Products CD-ROM Contents (IGBP-DIS)* Available online: <http://daac.ornl.gov>. 2014: Oak Ridge National Laboratory Distributed Active Archive Centre, Oakridge, Tennessee, USA.
71. **Sillanpää, M.**, *Micronutrients and the nutrient status of soils: a global study*. Vol. 48. 1982: Food & Agriculture Org.
72. **Terry, N. and G. Low**, *Leaf chlorophyll content and its relation to the intracellular localization of iron*. Journal of Plant Nutrition, 1982. **5**(4-7): p. 301-310.

73. **Broadley, M.R., P.J. White, J.P. Hammond, I. Zelko, and A. Lux**, *Zinc in plants*. *New Phytologist*, 2007. **173**(4): p. 677-702.
74. **White, P.J. and M.R. Broadley**, *Physiological limits to zinc biofortification of edible crops*. *Front Plant Sci*, 2011. **2**: p. 80.
75. **Fageria, N.K.**, *The use of nutrients in crop plants*. 2016: CRC press.
76. **Sharma, P.N., C. Chatterjee, S.C. Agarwala, and C.P. Sharma**, *Zinc deficiency and pollen fertility in maize (Zea mays)*. *Plant and Soil*, 1990. **124**(2): p. 221-225.
77. **Balafrej, H., D. Bogusz, Z.A. Triqui, A. Guedira, N. Bendaou, A. Smouni, and M. Fahr**, *Zinc Hyperaccumulation in Plants: A Review*. *Plants (Basel)*, 2020. **9**(5).
78. **Merlot, S., V. Sanchez Garcia de la Torre, and M. Hanikenne**, *Physiology and Molecular Biology of Trace Element Hyperaccumulation*, in *Agromining: Farming for Metals: Extracting Unconventional Resources Using Plants*, A. Van der Ent, et al., Editors. 2018, Springer International Publishing: Cham. p. 93-116.
79. **Vose, P.B.**, *Iron nutrition in plants: A world overview*. *Journal of Plant Nutrition*, 1982. **5**(4-7): p. 233-249.
80. **Abadia, J., S. Vazquez, R. Rellan-Alvarez, H. El-Jendoubi, A. Abadia, A. Alvarez-Fernandez, and A.F. Lopez-Millan**, *Towards a knowledge-based correction of iron chlorosis*. *Plant Physiol Biochem*, 2011. **49**(5): p. 471-82.
81. **Zhang, X., D. Zhang, W. Sun, and T. Wang**, *The Adaptive Mechanism of Plants to Iron Deficiency via Iron Uptake, Transport, and Homeostasis*. *Int J Mol Sci*, 2019. **20**(10).
82. **Connolly, E.L. and M. Guerinot**, *Iron stress in plants*. *Genome Biol*, 2002. **3**(8): p. REVIEWS1024.
83. **Cabot, C., S. Martos, M. Llugany, B. Gallego, R. Tolra, and C. Poschenrieder**, *A Role for Zinc in Plant Defense Against Pathogens and Herbivores*. *Front Plant Sci*, 2019. **10**: p. 1171.
84. **Greenshields, D.L., G. Liu, and Y. Wei**, *Roles of iron in plant defence and fungal virulence*. *Plant Signal Behav*, 2007. **2**(4): p. 300-2.
85. **King, J.C., R.J. Cousins, M.E. Shils, M. Shike, A.C. Ross, and B. Caballero**, *Modern nutrition in health and disease*. *Modern nutrition in health and disease*. Baltimore: Lippincott Williams and Wilkins, 2005: p. 271-85.
86. **Wood, R.J., A. Ronnenberg, J.C. King, R.J. Cousins, J.T. Dunns, R.F. Burk, and O.A. Levander**, *Modern nutrition in health and disease*. *Lippincott's Illustrated Reviews Biochemistry*, Lippincott Williams & Wilkins, 2005: p. 248-270.

87. **Trumbo, P., A.A. Yates, S. Schlicker, and M. Poos**, *Dietary reference intakes: vitamin A, vitamin K, arsenic, boron, chromium, copper, iodine, iron, manganese, molybdenum, nickel, silicon, vanadium, and zinc*. J Am Diet Assoc, 2001. **101**(3): p. 294-301.
88. **Lim, K.H., L.J. Riddell, C.A. Nowson, A.O. Booth, and E.A. Szymlek-Gay**, *Iron and zinc nutrition in the economically-developed world: a review*. Nutrients, 2013. **5**(8): p. 3184-211.
89. **WHO**, *The World Health Report 2010: Health systems financing: the path to universal coverage*. 2010, World Health Organization: Geneva.
90. **Prasad, A.S.**, *Discovery of human zinc deficiency: its impact on human health and disease*. Adv Nutr, 2013. **4**(2): p. 176-90.
91. **Gödecke, T., A.J. Stein, and M. Qaim**, *The global burden of chronic and hidden hunger: Trends and determinants*. Global Food Security, 2018. **17**: p. 21-29.
92. **Kohgo, Y., K. Ikuta, T. Ohtake, Y. Torimoto, and J. Kato**, *Body iron metabolism and pathophysiology of iron overload*. Int J Hematol, 2008. **88**(1): p. 7-15.
93. **Fosmire, G.J.**, *Zinc toxicity*. Am J Clin Nutr, 1990. **51**(2): p. 225-7.
94. **Roohani, N., R. Hurrell, R. Kelishadi, and R. Schulin**, *Zinc and its importance for human health: An integrative review*. Journal of Research in Medical Sciences, 2013. **18**(2): p. 144-157.
95. **Muthayya, S., J.H. Rah, J.D. Sugimoto, F.F. Roos, K. Kraemer, and R.E. Black**, *The global hidden hunger indices and maps: an advocacy tool for action*. PLoS One, 2013. **8**(6): p. e67860.
96. **Gibson, R.S.**, *Principles of nutritional assessment*. 2005: Oxford university press, USA.
97. **Hunt, J.R.**, *Bioavailability of iron, zinc, and other trace minerals from vegetarian diets*. The American Journal of Clinical Nutrition, 2003. **78**(3): p. 633S-639S.
98. **Weaver, C.M. and S. Kannan**, *Food phytates*. Phytate and mineral bioavailability, 2002: p. 215-227.
99. **Gibson, R.S., K.B. Bailey, M. Gibbs, and E.L. Ferguson**, *A review of phytate, iron, zinc, and calcium concentrations in plant-based complementary foods used in low-income countries and implications for bioavailability*. Food and Nutrition Bulletin, 2010. **31**(2): p. S134-S146.

100. **Cheryan, M.**, *Phytic acid interactions in food systems*. Crit Rev Food Sci Nutr, 1980. **13**(4): p. 297-335.
101. **Hallberg, L., M. Brune, and L. Rossander**, *Iron absorption in man: ascorbic acid and dose-dependent inhibition by phytate*. Am J Clin Nutr, 1989. **49**(1): p. 140-4.
102. **Disler, P.B., S.R. Lynch, R.W. Charlton, J.D. Torrance, T.H. Bothwell, R.B. Walker, and F. Mayet**, *The effect of tea on iron absorption*. Gut, 1975. **16**(3): p. 193-200.
103. **Hallberg, L. and L. Rossander**, *Effect of different drinks on the absorption of non-heme iron from composite meals*. Hum Nutr Appl Nutr, 1982. **36**(2): p. 116-23.
104. **Ganji, V. and C.V. Kies**, *Zinc bioavailability and tea consumption. Studies in healthy humans consuming self-selected and laboratory-controlled diets*. Plant Foods Hum Nutr, 1994. **46**(3): p. 267-76.
105. **Hallberg, L. and L. Rossander**, *Effect of soy protein on nonheme iron absorption in man*. Am J Clin Nutr, 1982. **36**(3): p. 514-20.
106. **Davidsson, L., A. Almgren, B. Sandstrom, and R.F. Hurrell**, *Zinc absorption in adult humans: the effect of iron fortification*. Br J Nutr, 1995. **74**(3): p. 417-25.
107. **Wessells, K.R., G.M. Singh, and K.H. Brown**, *Estimating the Global Prevalence of Inadequate Zinc Intake from National Food Balance Sheets: Effects of Methodological Assumptions*. PLOS ONE, 2012. **7**(11): p. e50565.
108. *World Development Indicators*. 2018: World Health Organization, Geneva.
109. **Ritchie, H.** *Micronutrient deficiency*. 2017; Available from: <https://ourworldindata.org/micronutrient-deficiency>.
110. **Siwela, M., K. Pillay, L. Govender, S. Lottering, F.N. Mudau, A.T. Modi, and T. Mabhaudhi**, *Biofortified Crops for Combating Hidden Hunger in South Africa: Availability, Acceptability, Micronutrient Retention and Bioavailability*. Foods (Basel, Switzerland), 2020. **9**(6): p. 815.
111. **Allen, L.H.**, *Interventions for Micronutrient Deficiency Control in Developing Countries: Past, Present and Future*. The Journal of Nutrition, 2003. **133**(11): p. 3875S-3878S.
112. **Bouis, H.E. and A. Saltzman**, *Improving nutrition through biofortification: A review of evidence from HarvestPlus, 2003 through 2016*. Global Food Security, 2017. **12**: p. 49-58.

113. **Saltzman, A., E. Birol, H.E. Bouis, E. Boy, F.F. De Moura, Y. Islam, and W.H. Pfeiffer**, *Biofortification: Progress toward a more nourishing future*. Global Food Security, 2013. **2**(1): p. 9-17.
114. **de Valença, A.W., A. Bake, I.D. Brouwer, and K.E. Giller**, *Agronomic biofortification of crops to fight hidden hunger in sub-Saharan Africa*. Global Food Security, 2017. **12**: p. 8-14.
115. **Borrill, P., J.M. Connorton, J. Balk, A.J. Miller, D. Sanders, and C. Uauy**, *Biofortification of wheat grain with iron and zinc: integrating novel genomic resources and knowledge from model crops*. Front Plant Sci, 2014. **5**: p. 53.
116. **Garg, M., N. Sharma, S. Sharma, P. Kapoor, A. Kumar, V. Chunduri, and P. Arora**, *Biofortified Crops Generated by Breeding, Agronomy, and Transgenic Approaches Are Improving Lives of Millions of People around the World*. Front Nutr, 2018. **5**: p. 12.
117. **Tsai, H., T. Howell, R. Nitcher, V. Missirian, B. Watson, K.J. Ngo, M. Lieberman, J. Fass, C. Uauy, R.K. Tran, A.A. Khan, V. Filkov, T.H. Tai, J. Dubcovsky, and L. Comai**, *Discovery of rare mutations in populations: TILLING by sequencing*. Plant Physiol, 2011. **156**(3): p. 1257-68.
118. **Holme, I.B., P.L. Gregersen, and H. Brinch-Pedersen**, *Induced Genetic Variation in Crop Plants by Random or Targeted Mutagenesis: Convergence and Differences*. Front Plant Sci, 2019. **10**: p. 1468.
119. **Henderson, I.R. and D.E. Salt**, *Natural genetic variation and hybridization in plants*. J Exp Bot, 2017. **68**(20): p. 5415-5417.
120. **Fernie, A.R., Y. Tadmor, and D. Zamir**, *Natural genetic variation for improving crop quality*. Curr Opin Plant Biol, 2006. **9**(2): p. 196-202.
121. **Ludwig, Y. and I.H. Slamet-Loedin**, *Genetic Biofortification to Enrich Rice and Wheat Grain Iron: From Genes to Product*. Frontiers in Plant Science, 2019. **10**: p. 833.
122. **Chattha, M.U., M.U. Hassan, I. Khan, M.B. Chattha, A. Mahmood, M.U. Chattha, M. Nawaz, M.N. Subhani, M. Kharal, and S. Khan**, *Biofortification of Wheat Cultivars to Combat Zinc Deficiency*. Front Plant Sci, 2017. **8**: p. 281.
123. **Gregorio, G.B., D. Senadhira, H. Htut, and R.D. Graham**, *Breeding for trace mineral density in rice*. Food and Nutrition Bulletin, 2000. **21**(4): p. 382-386.
124. **Graham, R.D.**, *Biofortification: a global challenge program*. 2003.
125. **Goto, F., T. Yoshihara, N. Shigemoto, S. Toki, and F. Takaiwa**, *Iron fortification of rice seed by the soybean ferritin gene*. Nat Biotechnol, 1999. **17**(3): p. 282-6.

126. **Paul, S., N. Ali, D. Gayen, S.K. Datta, and K. Datta**, *Molecular breeding of Osfer2 gene to increase iron nutrition in rice grain*. *GM crops & food*, 2012. **3**(4): p. 310-316.
127. **Borg, S., H. Brinch-Pedersen, B. Tauris, L.H. Madsen, B. Darbani, S. Noeparvar, and P.B. Holm**, *Wheat ferritins: improving the iron content of the wheat grain*. *Journal of Cereal Science*, 2012. **56**(2): p. 204-213.
128. **Distelfeld, A., I. Cakmak, Z. Peleg, L. Ozturk, A.M. Yazici, H. Budak, Y. Saranga, and T. Fahima**, *Multiple QTL-effects of wheat Gpc-B1 locus on grain protein and micronutrient concentrations*. *Physiologia Plantarum*, 2007. **129**(3): p. 635-643.
129. **Lee, S., Y.S. Kim, U.S. Jeon, Y.K. Kim, J.K. Schjoerring, and G. An**, *Activation of Rice nicotianamine synthase 2 (OsNAS2) enhances iron availability for biofortification*. *Mol Cells*, 2012. **33**(3): p. 269-75.
130. **Beasley, J.T., J.P. Bonneau, J.T. Sanchez-Palacios, L.T. Moreno-Moyano, D.L. Callahan, E. Tako, R.P. Glahn, E. Lombi, and A.A.T. Johnson**, *Metabolic engineering of bread wheat improves grain iron concentration and bioavailability*. *Plant Biotechnol J*, 2019. **17**(8): p. 1514-1526.
131. **Zheng, L., Z. Cheng, C. Ai, X. Jiang, X. Bei, Y. Zheng, R.P. Glahn, R.M. Welch, D.D. Miller, X.G. Lei, and H. Shou**, *Nicotianamine, a novel enhancer of rice iron bioavailability to humans*. *PLoS One*, 2010. **5**(4): p. e10190.
132. **Masuda, H., M. Suzuki, K.C. Morikawa, T. Kobayashi, H. Nakanishi, M. Takahashi, M. Saigusa, S. Mori, and N.K. Nishizawa**, *Increase in iron and zinc concentrations in rice grains via the introduction of barley genes involved in phytosiderophore synthesis*. *Rice*, 2008. **1**(1): p. 100-108.
133. **Lee, S., J.C. Chiecko, S.A. Kim, E.L. Walker, Y. Lee, M.L. Guerinot, and G. An**, *Disruption of OsYSL15 leads to iron inefficiency in rice plants*. *Plant Physiol*, 2009. **150**(2): p. 786-800.
134. **Ishimaru, Y., H. Masuda, K. Bashir, H. Inoue, T. Tsukamoto, M. Takahashi, H. Nakanishi, N. Aoki, T. Hirose, and R. Ohsugi**, *Rice metal-nicotianamine transporter, OsYSL2, is required for the long-distance transport of iron and manganese*. *The Plant Journal*, 2010. **62**(3): p. 379-390.
135. **Lee, S. and G. An**, *Over-expression of OsIRT1 leads to increased iron and zinc accumulations in rice*. *Plant Cell Environ*, 2009. **32**(4): p. 408-16.
136. **Connorton, J.M., E.R. Jones, I. Rodríguez-Ramiro, S. Fairweather-Tait, C. Uauy, and J. Balk**, *Wheat Vacuolar Iron Transporter TaVIT2 Transports Fe and Mn and Is Effective for Biofortification*. *Plant Physiology*, 2017. **174**(4): p. 2434.

137. **Menguer, P.K., T. Vincent, A.J. Miller, J.K.M. Brown, E. Vincze, S. Borg, P.B. Holm, D. Sanders, and D. Podar**, *Improving zinc accumulation in cereal endosperm using HvMTP1, a transition metal transporter*. Plant biotechnology journal, 2018. **16**(1): p. 63-71.
138. **Brinch-Pedersen, H., A. Olesen, S.K. Rasmussen, and P.B. Holm**, *Generation of transgenic wheat (*Triticum aestivum* L.) for constitutive accumulation of an *Aspergillus phytase**. Molecular Breeding, 2000. **6**(2): p. 195-206.
139. **Bhati, K.K., A. Alok, A. Kumar, J. Kaur, S. Tiwari, and A.K. Pandey**, *Silencing of ABCC13 transporter in wheat reveals its involvement in grain development, phytic acid accumulation and lateral root formation*. J Exp Bot, 2016. **67**(14): p. 4379-89.
140. **Sinclair, S.A. and U. Kramer**, *The zinc homeostasis network of land plants*. Biochimica Et Biophysica Acta-Molecular Cell Research, 2012. **1823**(9): p. 1553-1567.
141. **Claus, J., A. Bohmann, and A. Chavarria-Krauser**, *Zinc uptake and radial transport in roots of *Arabidopsis thaliana*: a modelling approach to understand accumulation*. Ann Bot, 2013. **112**(2): p. 369-80.
142. **Hanikenne, M., I.N. Talke, M.J. Haydon, C. Lanz, A. Nolte, P. Motte, J. Kroymann, D. Weigel, and U. Kramer**, *Evolution of metal hyperaccumulation required cis-regulatory changes and triplication of HMA4*. Nature, 2008. **453**(7193): p. 391-U44.
143. **Steudle, E.**, *Water transport across roots*. Plant and soil, 1994. **167**(1): p. 79-90.
144. **Nagahashi, G., W.W. Thomson, and R.T. Leonard**, *The Casparian strip as a barrier to the movement of lanthanum in corn roots*. 1974, American Association for the Advancement of Science.
145. **Naseer, S., Y. Lee, C. Lapierre, R. Franke, C. Nawrath, and N. Geldner**, *Casparian strip diffusion barrier in *Arabidopsis* is made of a lignin polymer without suberin*. Proc Natl Acad Sci U S A, 2012. **109**(25): p. 10101-6.
146. **Pfister, A., M. Barberon, J. Alassimone, L. Kalmbach, Y. Lee, J.E. Vermeer, M. Yamazaki, G. Li, C. Maurel, J. Takano, T. Kamiya, D.E. Salt, D. Roppolo, and N. Geldner**, *A receptor-like kinase mutant with absent endodermal diffusion barrier displays selective nutrient homeostasis defects*. Elife, 2014. **3**: p. e03115.
147. **Alassimone, J., S. Naseer, and N. Geldner**, *A developmental framework for endodermal differentiation and polarity*. Proc Natl Acad Sci U S A, 2010. **107**(11): p. 5214-9.

148. **Barberon, M., J.E. Vermeer, D. De Bellis, P. Wang, S. Naseer, T.G. Andersen, B.M. Humbel, C. Nawrath, J. Takano, D.E. Salt, and N. Geldner**, *Adaptation of Root Function by Nutrient-Induced Plasticity of Endodermal Differentiation*. *Cell*, 2016. **164**(3): p. 447-59.
149. **Andersen, T.G., M. Barberon, and N. Geldner**, *Suberization - the second life of an endodermal cell*. *Curr Opin Plant Biol*, 2015. **28**: p. 9-15.
150. **Krishnamurthy, P., K. Ranathunge, R. Franke, H.S. Prakash, L. Schreiber, and M.K. Mathew**, *The role of root apoplastic transport barriers in salt tolerance of rice (*Oryza sativa* L.)*. *Planta*, 2009. **230**(1): p. 119-34.
151. **Hacisalihoglu, G. and L.V. Kochian**, *How do some plants tolerate low levels of soil zinc? Mechanisms of zinc efficiency in crop plants*. *New Phytologist*, 2003. **159**(2): p. 341-350.
152. **Ajeesh Krishna, T.P., T. Maharajan, G. Victor Roch, S. Ignacimuthu, and S. Antony Ceasar**, *Structure, Function, Regulation and Phylogenetic Relationship of ZIP Family Transporters of Plants*. *Front Plant Sci*, 2020. **11**: p. 662.
153. **Grotz, N., T. Fox, E. Connolly, W. Park, M.L. Guerinot, and D. Eide**, *Identification of a family of zinc transporter genes from *Arabidopsis* that respond to zinc deficiency*. *Proceedings of the National Academy of Sciences of the United States of America*, 1998. **95**(12): p. 7220-7224.
154. **Guerinot, M.L.**, *The ZIP family of metal transporters*. *Biochim Biophys Acta*, 2000. **1465**(1-2): p. 190-8.
155. **Mäser, P., S. Thomine, J.I. Schroeder, J.M. Ward, K. Hirschi, H. Sze, I.N. Talke, A. Amtmann, F.J.M. Maathuis, and D. Sanders**, *Phylogenetic relationships within cation transporter families of *Arabidopsis**. *Plant Physiology*, 2001. **126**(4): p. 1646-1667.
156. **Milner, M.J., J. Seamon, E. Craft, and L.V. Kochian**, *Transport properties of members of the ZIP family in plants and their role in Zn and Mn homeostasis*. *J Exp Bot*, 2013. **64**(1): p. 369-81.
157. **Lin, Y.F., H.M. Liang, S.Y. Yang, A. Boch, S. Clemens, C.C. Chen, J.F. Wu, J.L. Huang, and K.C. Yeh**, **Arabidopsis* IRT3 is a zinc-regulated and plasma membrane localized zinc/iron transporter*. *New Phytologist*, 2009. **182**(2): p. 392-404.
158. **Kramer, U., I.N. Talke, and M. Hanikenne**, *Transition metal transport*. *FEBS Letters*, 2007. **581**.
159. **Assuncao, A.G.L., E. Herrero, Y.F. Lin, B. Huettel, S. Talukdar, C. Smaczniak, R.G.H. Immink, M. van Eldik, M. Fiers, H. Schat, and M.G.M. Aarts**, **Arabidopsis**

- thaliana* transcription factors *bZIP19* and *bZIP23* regulate the adaptation to zinc deficiency. Proceedings of the National Academy of Sciences of the United States of America, 2010. **107**(22): p. 10296-10301.
160. **Ricachenevsky, F.K., P.K. Menguer, R.A. Sperotto, L.E. Williams, and J.P. Fett**, Roles of plant metal tolerance proteins (MTP) in metal storage and potential use in biofortification strategies. *Frontiers in plant science*, 2013. **4**: p. 144-144.
 161. **Gustin, J.L., M.J. Zanis, and D.E. Salt**, Structure and evolution of the plant cation diffusion facilitator family of ion transporters. *BMC Evolutionary Biology*, 2011. **11**(1): p. 76.
 162. **Sinclair, S.A., T. Senger, I.N. Talke, C.S. Cobbett, M.J. Haydon, and U. Kraemer**, Systemic upregulation of MTP2- and HMA2-mediated Zn partitioning to the shoot supplements local Zn deficiency responses of *Arabidopsis*. *Plant Cell*, 2018.
 163. **Marschner, H.**, 2 - Ion Uptake Mechanisms of Individual Cells and Roots: Short-Distance Transport, in *Mineral Nutrition of Higher Plants (Second Edition)*. 1995, Academic Press: London. p. 6-78.
 164. **Robinson, N.J., C.M. Procter, E.L. Connolly, and M.L. Guerinot**, A ferric-chelate reductase for iron uptake from soils. *Nature*, 1999. **397**(6721): p. 694-7.
 165. **Eide, D., M. Broderius, J. Fett, and M.L. Guerinot**, A novel iron-regulated metal transporter from plants identified by functional expression in yeast. Proceedings of the National Academy of Sciences of the United States of America, 1996. **93**(11): p. 5624-5628.
 166. **Kobayashi, T. and N.K. Nishizawa**, Iron Uptake, Translocation, and Regulation in Higher Plants. *Annual Review of Plant Biology*, 2012. **63**(1): p. 131-152.
 167. **Varotto, C., D. Maiwald, P. Pesaresi, P. Jahns, F. Salamini, and D. Leister**, The metal ion transporter *IRT1* is necessary for iron homeostasis and efficient photosynthesis in *Arabidopsis thaliana*. *Plant J*, 2002. **31**(5): p. 589-99.
 168. **Vert, G.A., J.F. Briat, and C. Curie**, Dual regulation of the *Arabidopsis* high-affinity root iron uptake system by local and long-distance signals. *Plant Physiol*, 2003. **132**(2): p. 796-804.
 169. **Santi, S. and W. Schmidt**, Dissecting iron deficiency-induced proton extrusion in *Arabidopsis* roots. *New Phytol*, 2009. **183**(4): p. 1072-84.
 170. **Korshunova, Y.O., D. Eide, W.G. Clark, M.L. Guerinot, and H.B. Pakrasi**, The *IRT1* protein from *Arabidopsis thaliana* is a metal transporter with a broad substrate range. *Plant Mol Biol*, 1999. **40**(1): p. 37-44.

171. **Connolly, E.L., J.P. Fett, and M.L. Guerinot**, *Expression of the IRT1 metal transporter is controlled by metals at the levels of transcript and protein accumulation*. *Plant Cell*, 2002. **14**(6): p. 1347-57.
172. **Dubeaux, G., J. Neveu, E. Zelazny, and G. Vert**, *Metal Sensing by the IRT1 Transporter-Receptor Orchestrates Its Own Degradation and Plant Metal Nutrition*. *Mol Cell*, 2018. **69**(6): p. 953-964 e5.
173. **Connolly, E.L., N.H. Campbell, N. Grotz, C.L. Prichard, and M.L. Guerinot**, *Overexpression of the FRO2 ferric chelate reductase confers tolerance to growth on low iron and uncovers posttranscriptional control*. *Plant physiology*, 2003. **133**(3): p. 1102-1110.
174. **Pan, I.C., H.H. Tsai, Y.T. Cheng, T.N. Wen, T.J. Buckhout, and W. Schmidt**, *Post-Transcriptional Coordination of the Arabidopsis Iron Deficiency Response is Partially Dependent on the E3 Ligases RING DOMAIN LIGASE1 (RGLG1) and RING DOMAIN LIGASE2 (RGLG2)*. *Mol Cell Proteomics*, 2015. **14**(10): p. 2733-52.
175. **Martin-Barranco, A., J. Spielmann, G. Dubeaux, G. Vert, and E. Zelazny**, *Dynamic Control of the High-Affinity Iron Uptake Complex in Root Epidermal Cells*. *Plant Physiol*, 2020. **184**(3): p. 1236-1250.
176. **Romheld, V. and H. Marschner**, *Mechanism of iron uptake by peanut plants : I. Fe reduction, chelate splitting, and release of phenolics*. *Plant Physiol*, 1983. **71**(4): p. 949-54.
177. **Bienfait, H.F., W. van den Briel, and N.T. Mesland-Mul**, *Free space iron pools in roots: generation and mobilization*. *Plant Physiol*, 1985. **78**(3): p. 596-600.
178. **Rodriguez-Celma, J. and W. Schmidt**, *Reduction-based iron uptake revisited: on the role of secreted iron-binding compounds*. *Plant Signal Behav*, 2013. **8**(11): p. e26116.
179. **Schmidt, H., C. Gunther, M. Weber, C. Sporlein, S. Loscher, C. Bottcher, R. Schobert, and S. Clemens**, *Metabolome analysis of Arabidopsis thaliana roots identifies a key metabolic pathway for iron acquisition*. *PLoS One*, 2014. **9**(7): p. e102444.
180. **Schmid, N.B., R.F. Giehl, S. Doll, H.P. Mock, N. Strehmel, D. Scheel, X. Kong, R.C. Hider, and N. von Wiren**, *Feruloyl-CoA 6'-Hydroxylase1-dependent coumarins mediate iron acquisition from alkaline substrates in Arabidopsis*. *Plant Physiol*, 2014. **164**(1): p. 160-72.
181. **Tsai, H.H., J. Rodriguez-Celma, P. Lan, Y.C. Wu, I.C. Velez-Bermudez, and W. Schmidt**, *Scopoletin 8-Hydroxylase-Mediated Fraxetin Production Is Crucial for Iron Mobilization*. *Plant Physiol*, 2018. **177**(1): p. 194-207.

182. **Rajniak, J., R.F.H. Giehl, E. Chang, I. Murgia, N. von Wirén, and E.S. Sattely**, *Biosynthesis of redox-active metabolites in response to iron deficiency in plants*. *Nat Chem Biol*, 2018. **14**(5): p. 442-450.
183. **Sisó-Terraza, P., A. Luis-Villarroya, P. Fourcroy, J.-F. Briat, A. Abadía, F. Gaymard, J. Abadía, and A. Álvarez-Fernández**, *Accumulation and Secretion of Coumarinolignans and other Coumarins in Arabidopsis thaliana Roots in Response to Iron Deficiency at High pH*. *Frontiers in Plant Science*, 2016. **7**: p. 1711.
184. **Fourcroy, P., P. Siso-Terraza, D. Sudre, M. Saviron, G. Reyt, F. Gaymard, A. Abadia, J. Abadia, A. Alvarez-Fernandez, and J.F. Briat**, *Involvement of the ABCG37 transporter in secretion of scopoletin and derivatives by Arabidopsis roots in response to iron deficiency*. *New Phytol*, 2014. **201**(1): p. 155-67.
185. **Zamioudis, C., J. Hanson, and C.M.J. Pieterse**, *β -Glucosidase BGLU42 is a MYB72-dependent key regulator of rhizobacteria-induced systemic resistance and modulates iron deficiency responses in Arabidopsis roots*. *New Phytologist*, 2014. **204**(2): p. 368-379.
186. **Rodriguez-Celma, J., W.D. Lin, G.M. Fu, J. Abadia, A.F. Lopez-Millan, and W. Schmidt**, *Mutually exclusive alterations in secondary metabolism are critical for the uptake of insoluble iron compounds by Arabidopsis and Medicago truncatula*. *Plant Physiol*, 2013. **162**(3): p. 1473-85.
187. **Robe, K., G. Conejero, F. Gao, L. Lefebvre-Legendre, E. Sylvestre-Gonon, V. Rofidal, S. Hem, N. Rouhier, M. Barberon, A. Hecker, F. Gaymard, E. Izquierdo, and C. Dubos**, *Coumarin accumulation and trafficking in Arabidopsis thaliana: a complex and dynamic process*. *New Phytol*, 2020.
188. **Voges, M., Y. Bai, P. Schulze-Lefert, and E.S. Sattely**, *Plant-derived coumarins shape the composition of an Arabidopsis synthetic root microbiome*. *Proc Natl Acad Sci U S A*, 2019. **116**(25): p. 12558-12565.
189. **Williams, L.E., J.K. Pittman, and J.L. Hall**, *Emerging mechanisms for heavy metal transport in plants*. *Biochimica et Biophysica Acta (BBA)-Biomembranes*, 2000. **1465**(1-2): p. 104-126.
190. **Thomine, S., R. Wang, J.M. Ward, N.M. Crawford, and J.I. Schroeder**, *Cadmium and iron transport by members of a plant metal transporter family in Arabidopsis with homology to Nramp genes*. *Proc Natl Acad Sci U S A*, 2000. **97**(9): p. 4991-6.
191. **Cailliatte, R., A. Schikora, J.F. Briat, S. Mari, and C. Curie**, *High-affinity manganese uptake by the metal transporter NRAMP1 is essential for Arabidopsis growth in low manganese conditions*. *Plant Cell*, 2010. **22**(3): p. 904-17.

192. **Castaigns, L., A. Caquot, S. Loubet, and C. Curie**, *The high-affinity metal Transporters NRAMP1 and IRT1 Team up to Take up Iron under Sufficient Metal Provision*. *Sci Rep*, 2016. **6**: p. 37222.
193. **Wang, N., W. Qiu, J. Dai, X. Guo, Q. Lu, T. Wang, S. Li, T. Liu, and Y. Zuo**, *AhNRAMP1 Enhances Manganese and Zinc Uptake in Plants*. *Front Plant Sci*, 2019. **10**: p. 415.
194. **Maret, W.**, *Analyzing free zinc(II) ion concentrations in cell biology with fluorescent chelating molecules*. *Metallomics*, 2015. **7**(2): p. 202-11.
195. **Olsen, L.I. and M.G. Palmgren**, *Many rivers to cross: the journey of zinc from soil to seed*. *Front Plant Sci*, 2014. **5**: p. 30.
196. **Curie, C., G. Cassin, D. Couch, F. Divol, K. Higuchi, M. Le Jean, J. Misson, A. Schikora, P. Czernic, and S. Mari**, *Metal movement within the plant: contribution of nicotianamine and yellow stripe 1-like transporters*. *Ann Bot*, 2009. **103**(1): p. 1-11.
197. **Scholz, G., R. Becker, A. Pich, and U.W. Stephan**, *Nicotianamine—a common constituent of strategies I and II of iron acquisition by plants: A review*. *Journal of Plant Nutrition*, 1992. **15**(10): p. 1647-1665.
198. **Bauer, P. and M. Schuler**, *Heavy metals need assistance: the contribution of nicotianamine to metal circulation throughout the plant and the Arabidopsis NAS gene family*. *Frontiers in plant science*, 2011. **2**: p. 69.
199. **von Wiren, N., S. Klair, S. Bansal, J.F. Briat, H. Khodr, T. Shioiri, R.A. Leigh, and R.C. Hider**, *Nicotianamine chelates both FeIII and FeII. Implications for metal transport in plants*. *Plant Physiol*, 1999. **119**(3): p. 1107-14.
200. **Klatte, M., M. Schuler, M. Wirtz, C. Fink-Straube, R. Hell, and P. Bauer**, *The analysis of Arabidopsis nicotianamine synthase mutants reveals functions for nicotianamine in seed iron loading and iron deficiency responses*. *Plant Physiol*, 2009. **150**(1): p. 257-71.
201. **Chen, C.L., Y. Cui, M. Cui, W.J. Zhou, H.L. Wu, and H.Q. Ling**, *A FIT-binding protein is involved in modulating iron and zinc homeostasis in Arabidopsis*. *Plant Cell and Environment*, 2018. **41**(7): p. 1698-1714.
202. **Koen, E., A. Besson-Bard, C. Duc, J. Astier, A. Gravot, P. Richaud, O. Lamotte, J. Boucherez, F. Gaymard, and D. Wendehenne**, *Arabidopsis thaliana nicotianamine synthase 4 is required for proper response to iron deficiency and to cadmium exposure*. *Plant Science*, 2013. **209**: p. 1-11.

203. **Haydon, M.J., M. Kawachi, M. Wirtz, S. Hillmer, R. Hell, and U. Kramer,** *Vacuolar Nicotianamine Has Critical and Distinct Roles under Iron Deficiency and for Zinc Sequestration in Arabidopsis.* *Plant Cell*, 2012. **24**(2): p. 724-737.
204. **Weber, M., E. Harada, C. Vess, E. Roepenack-Lahaye, and S. Clemens,** *Comparative microarray analysis of Arabidopsis thaliana and Arabidopsis halleri roots identifies nicotianamine synthase, a ZIP transporter and other genes as potential metal hyperaccumulation factors.* *Plant J*, 2004. **37**(2): p. 269-81.
205. **Uraguchi, S., M. Weber, and S. Clemens,** *Elevated root nicotianamine concentrations are critical for Zn hyperaccumulation across diverse edaphic environments.* *Plant Cell Environ*, 2019. **42**(6): p. 2003-2014.
206. **Tsednee, M., S.-C. Yang, D.-C. Lee, and K.-C. Yeh,** *Root-Secreted Nicotianamine from Arabidopsis halleri Facilitates Zinc Hypertolerance by Regulating Zinc Bioavailability.* *Plant Physiology*, 2014. **166**(2): p. 839-852.
207. **Xiang, C., B.L. Werner, E.M. Christensen, and D.J. Oliver,** *The biological functions of glutathione revisited in arabidopsis transgenic plants with altered glutathione levels.* *Plant Physiol*, 2001. **126**(2): p. 564-74.
208. **Wongkaew, A., S.I. Nakamura, N. Suzui, Y.G. Yin, S. Ishii, N. Kawachi, K. Kojima, H. Sekimoto, T. Yokoyama, and N. Ohkama-Ohtsu,** *Elevated glutathione synthesis in leaves contributes to zinc transport from roots to shoots in Arabidopsis.* *Plant Sci*, 2019. **283**: p. 416-423.
209. **Wachter, A., S. Wolf, H. Steininger, J. Bogs, and T. Rausch,** *Differential targeting of GSH1 and GSH2 is achieved by multiple transcription initiation: implications for the compartmentation of glutathione biosynthesis in the Brassicaceae.* *The Plant Journal*, 2005. **41**(1): p. 15-30.
210. **Zlobin, I.E., A.V. Kartashov, and G.V. Shpakovski,** *Different roles of glutathione in copper and zinc chelation in Brassica napus roots.* *Plant Physiol Biochem*, 2017. **118**: p. 333-341.
211. **Wójcik, M., E. Skórzyńska-Polit, and A. Tukiendorf,** *Organic acids accumulation and antioxidant enzyme activities in Thlaspi caerulescens under Zn and Cd stress.* *Plant Growth Regulation*, 2006. **48**(2): p. 145-155.
212. **Shanmugam, V., M. Tsednee, and K.C. Yeh,** *ZINC TOLERANCE INDUCED BY IRON 1 reveals the importance of glutathione in the cross-homeostasis between zinc and iron in Arabidopsis thaliana.* *Plant J*, 2012. **69**(6): p. 1006-17.
213. **Shanmugam, V., Y.W. Wang, M. Tsednee, K. Karunakaran, and K.C. Yeh,** *Glutathione plays an essential role in nitric oxide-mediated iron-deficiency signaling and iron-deficiency tolerance in Arabidopsis.* *Plant J*, 2015. **84**(3): p. 464-77.

214. **Rea, P.A.**, *Phytochelatin synthase: of a protease a peptide polymerase made*. *Physiol Plant*, 2012. **145**(1): p. 154-64.
215. **Garcia-Garcia, J.D., L. Girard, G. Hernandez, E. Saavedra, J.P. Pardo, J.S. Rodriguez-Zavala, R. Encalada, A. Reyes-Prieto, D.G. Mendoza-Cozatl, and R. Moreno-Sanchez**, *Zn-bis-glutathionate is the best co-substrate of the monomeric phytochelatin synthase from the photosynthetic heavy metal-hyperaccumulator Euglena gracilis*. *Metallomics*, 2014. **6**(3): p. 604-16.
216. **Tennstedt, P., D. Peisker, C. Böttcher, A. Trampczynska, and S. Clemens**, *Phytochelatin Synthesis Is Essential for the Detoxification of Excess Zinc and Contributes Significantly to the Accumulation of Zinc*. *Plant Physiology*, 2009. **149**(2): p. 938-948.
217. **Kühnlentz, T., C. Hofmann, S. Uraguchi, H. Schmidt, S. Schempp, M. Weber, B. Lahner, D.E. Salt, and S. Clemens**, *Phytochelatin Synthesis Promotes Leaf Zn Accumulation of Arabidopsis thaliana Plants Grown in Soil with Adequate Zn Supply and is Essential for Survival on Zn-Contaminated Soil*. *Plant and Cell Physiology*, 2016. **57**(11): p. 2342-2352.
218. **Kühnlentz, T., H. Schmidt, S. Uraguchi, and S. Clemens**, *Arabidopsis thaliana phytochelatin synthase 2 is constitutively active in vivo and can rescue the growth defect of the PCS1-deficient cad1-3 mutant on Cd-contaminated soil*. *J Exp Bot*, 2014. **65**(15): p. 4241-53.
219. **Robinson, N.J., A.M. Tommey, C. Kuske, and P.J. Jackson**, *Plant metallothioneins*. *Biochem J*, 1993. **295 (Pt 1)**: p. 1-10.
220. **Cobbett, C. and P. Goldsbrough**, *Phytochelatin and metallothioneins: roles in heavy metal detoxification and homeostasis*. *Annu Rev Plant Biol*, 2002. **53**: p. 159-82.
221. **Pan, Y., M. Zhu, S. Wang, G. Ma, X. Huang, C. Qiao, R. Wang, X. Xu, Y. Liang, K. Lu, J. Li, and C. Qu**, *Genome-Wide Characterization and Analysis of Metallothionein Family Genes That Function in Metal Stress Tolerance in Brassica napus L*. *International journal of molecular sciences*, 2018. **19**(8): p. 2181.
222. **Benatti, M.R., N. Yookongkaew, M. Meetam, W.J. Guo, N. Punyasuk, S. AbuQamar, and P. Goldsbrough**, *Metallothionein deficiency impacts copper accumulation and redistribution in leaves and seeds of Arabidopsis*. *New Phytol*, 2014. **202**(3): p. 940-51.
223. **Ren, Y., Y. Liu, H. Chen, G. Li, X. Zhang, and J. Zhao**, *Type 4 metallothionein genes are involved in regulating Zn ion accumulation in late embryo and in*

- controlling early seedling growth in Arabidopsis*. Plant Cell Environ, 2012. **35**(4): p. 770-89.
224. **Imam, H.T. and C.A. Blindauer**, *Differential reactivity of closely related zinc(II)-binding metallothioneins from the plant Arabidopsis thaliana*. J Biol Inorg Chem, 2018. **23**(1): p. 137-154.
225. **Hussain, D., M.J. Haydon, Y. Wang, E. Wong, S.M. Sherson, J. Young, J. Camakaris, J.F. Harper, and C.S. Cobbett**, *P-type ATPase heavy metal transporters with roles in essential zinc homeostasis in Arabidopsis*. Plant Cell, 2004. **16**(5): p. 1327-1339.
226. **Axelsen, K.B. and M.G. Palmgren**, *Inventory of the superfamily of P-type ion pumps in Arabidopsis*. Plant Physiol, 2001. **126**(2): p. 696-706.
227. **Baekgaard, L., M.D. Mikkelsen, D.M. Sorensen, J.N. Hegelund, D.P. Persson, R.F. Mills, Z. Yang, S. Husted, J.P. Andersen, M.J. Buch-Pedersen, J.K. Schjoerring, L.E. Williams, and M.G. Palmgren**, *A combined zinc/cadmium sensor and zinc/cadmium export regulator in a heavy metal pump*. J Biol Chem, 2010. **285**(41): p. 31243-52.
228. **van de Mortel, J.E., L. Almar Villanueva, H. Schat, J. Kwekkeboom, S. Coughlan, P.D. Moerland, E. Ver Loren van Themaat, M. Koornneef, and M.G. Aarts**, *Large expression differences in genes for iron and zinc homeostasis, stress response, and lignin biosynthesis distinguish roots of Arabidopsis thaliana and the related metal hyperaccumulator Thlaspi caerulescens*. Plant Physiol, 2006. **142**(3): p. 1127-47.
229. **Song, W.-Y., K.S. Choi, D.Y. Kim, M. Geisler, J. Park, V. Vincenzetti, M. Schellenberg, S.H. Kim, Y.P. Lim, E.W. Noh, Y. Lee, and E. Martinoia**, *Arabidopsis PCR2 Is a Zinc Exporter Involved in Both Zinc Extrusion and Long-Distance Zinc Transport*. The Plant Cell, 2010. **22**(7): p. 2237-2252.
230. **Cornu, J.Y., U. Deinlein, S. Horeth, M. Braun, H. Schmidt, M. Weber, D.P. Persson, S. Husted, J.K. Schjoerring, and S. Clemens**, *Contrasting effects of nicotianamine synthase knockdown on zinc and nickel tolerance and accumulation in the zinc/cadmium hyperaccumulator Arabidopsis halleri*. New Phytol, 2015. **206**(2): p. 738-50.
231. **Kozhevnikova, A.D., I.V. Seregin, N.T. Erlikh, T.A. Shevyreva, I.M. Andreev, R. Verweij, and H. Schat**, *Histidine-mediated xylem loading of zinc is a species-wide character in Noccaea caerulescens*. New Phytol, 2014. **203**(2): p. 508-19.
232. **McKie, A.T., P. Marciani, A. Rolfs, K. Brennan, K. Wehr, D. Barrow, S. Miret, A. Bomford, T.J. Peters, F. Farzaneh, M.A. Hediger, M.W. Hentze, and R.J. Simpson**, *A novel duodenal iron-regulated transporter, IREG1, implicated in the basolateral transfer of iron to the circulation*. Mol Cell, 2000. **5**(2): p. 299-309.

233. **Morrissey, J., I.R. Baxter, J. Lee, L. Li, B. Lahner, N. Grotz, J. Kaplan, D.E. Salt, and M.L. Guerinot**, *The Ferroportin Metal Efflux Proteins Function in Iron and Cobalt Homeostasis in Arabidopsis*. *The Plant Cell*, 2009. **21**(10): p. 3326.
234. **Kim, L.J., K.M. Tsuyuki, F. Hu, E.Y. Park, J. Zhang, J.G. Iraheta, J.-C. Chia, R. Huang, A.E. Tucker, M. Clyne, C. Castellano, A. Kim, D.D. Chung, C.T. DaVeiga, E.M. Parsons, O.K. Vatamaniuk, and J. Jeong**, *Ferroportin 3 is a dual-targeted mitochondrial/chloroplast iron exporter necessary for iron homeostasis in Arabidopsis*. *bioRxiv*, 2020: p. 2020.07.15.203646.
235. **Lopez-Millan, A.F., F. Morales, A. Abadia, and J. Abadia**, *Effects of iron deficiency on the composition of the leaf apoplastic fluid and xylem sap in sugar beet. Implications for iron and carbon transport*. *Plant Physiol*, 2000. **124**(2): p. 873-84.
236. **Rellan-Alvarez, R., J. Giner-Martinez-Sierra, J. Orduna, I. Orera, J.A. Rodriguez-Castrillon, J.I. Garcia-Alonso, J. Abadia, and A. Alvarez-Fernandez**, *Identification of a tri-iron(III), tri-citrate complex in the xylem sap of iron-deficient tomato resupplied with iron: new insights into plant iron long-distance transport*. *Plant Cell Physiol*, 2010. **51**(1): p. 91-102.
237. **Rogers, E.E. and M.L. Guerinot**, *FRD3, a member of the multidrug and toxin efflux family, controls iron deficiency responses in Arabidopsis*. *The Plant cell*, 2002. **14**(8): p. 1787-1799.
238. **Durrett, T.P., W. Gassmann, and E.E. Rogers**, *The FRD3-mediated efflux of citrate into the root vasculature is necessary for efficient iron translocation*. *Plant physiology*, 2007. **144**(1): p. 197-205.
239. **Pineau, C., S. Loubet, C. Lefoulon, C. Chabies, C. Fizames, B. Lacombe, M. Ferrand, O. Loudet, P. Berthomieu, and O. Richard**, *Natural variation at the FRD3 MATE transporter locus reveals cross-talk between Fe homeostasis and Zn tolerance in Arabidopsis thaliana*. *PLoS Genet*, 2012. **8**(12): p. e1003120.
240. **DiDonato Jr, R.J., L.A. Roberts, T. Sanderson, R.B. Easley, and E.L. Walker**, *Arabidopsis Yellow Stripe-Like2 (YSL2): a metal-regulated gene encoding a plasma membrane transporter of nicotianamine-metal complexes*. *The Plant Journal*, 2004. **39**(3): p. 403-414.
241. **Waters, B.M., H.H. Chu, R.J. DiDonato, L.A. Roberts, R.B. Easley, B. Lahner, D.E. Salt, and E.L. Walker**, *Mutations in Arabidopsis Yellow Stripe-Like1 and Yellow Stripe-Like3 reveal their roles in metal ion homeostasis and loading of metal ions in seeds*. *Plant Physiology*, 2006. **141**(4): p. 1446-1458.

242. **Stacey, M.G., A. Patel, W.E. McClain, M. Mathieu, M. Remley, E.E. Rogers, W. Gassmann, D.G. Blevins, and G. Stacey**, *The Arabidopsis AtOPT3 protein functions in metal homeostasis and movement of iron to developing seeds*. *Plant physiology*, 2008. **146**(2): p. 589-601.
243. **Mendoza-Cozatl, D.G., Q. Xie, G.Z. Akmakjian, T.O. Jobe, A. Patel, M.G. Stacey, L. Song, D.W. Demoin, S.S. Jurisson, G. Stacey, and J.I. Schroeder**, *OPT3 is a component of the iron-signaling network between leaves and roots and misregulation of OPT3 leads to an over-accumulation of cadmium in seeds*. *Mol Plant*, 2014. **7**(9): p. 1455-1469.
244. **Zhai, Z., S.R. Gayomba, H.I. Jung, N.K. Vimalakumari, M. Pineros, E. Craft, M.A. Rutzke, J. Danku, B. Lahner, T. Punshon, M.L. Guerinot, D.E. Salt, L.V. Kochian, and O.K. Vatamaniuk**, *OPT3 Is a Phloem-Specific Iron Transporter That Is Essential for Systemic Iron Signaling and Redistribution of Iron and Cadmium in Arabidopsis*. *Plant Cell*, 2014. **26**(5): p. 2249-2264.
245. **Jain, A., G.T. Wilson, and E.L. Connolly**, *The diverse roles of FRO family metalloreductases in iron and copper homeostasis*. *Frontiers in plant science*, 2014. **5**: p. 100-100.
246. **Gayomba, S.R., Z. Zhai, H.I. Jung, and O.K. Vatamaniuk**, *Local and systemic signaling of iron status and its interactions with homeostasis of other essential elements*. *Front Plant Sci*, 2015. **6**: p. 716.
247. **Lanquar, V., M.S. Ramos, F. Lelievre, H. Barbier-Brygoo, A. Krieger-Liszkay, U. Kramer, and S. Thomine**, *Export of vacuolar manganese by AtNRAMP3 and AtNRAMP4 is required for optimal photosynthesis and growth under manganese deficiency*. *Plant Physiol*, 2010. **152**(4): p. 1986-99.
248. **Ricachenevsky, F.K., T. Punshon, D.E. Salt, J.P. Fett, and M.L. Guerinot**, *Arabidopsis thaliana zinc accumulation in leaf trichomes is correlated with zinc concentration in leaves*. *bioRxiv*, 2020: p. 2020.09.10.291880.
249. **Arrivault, S., T. Senger, and U. Kramer**, *The Arabidopsis metal tolerance protein AtMTP3 maintains metal homeostasis by mediating Zn exclusion from the shoot under Fe deficiency and Zn oversupply*. *Plant J*, 2006. **46**.
250. **Desbrosses-Fonrouge, A.G., K. Voigt, A. Schroder, S. Arrivault, S. Thomine, and U. Kramer**, *Arabidopsis thaliana MTP1 is a Zn transporter in the vacuolar membrane which mediates Zn detoxification and drives leaf Zn accumulation*. *FEBS Lett*, 2005. **579**.
251. **Fujiwara, T., M. Kawachi, Y. Sato, H. Mori, N. Kutsuna, S. Hasezawa, and M. Maeshima**, *A high molecular mass zinc transporter MTP12 forms a functional heteromeric complex with MTP5 in the Golgi in Arabidopsis thaliana*. *FEBS J*, 2015. **282**(10): p. 1965-79.

252. **Wang, Y., J. Yang, R. Miao, Y. Kang, and Z. Qi**, *A novel zinc transporter essential for Arabidopsis zinc and iron-dependent growth*. J Plant Physiol, 2020. **256**: p. 153296.
253. **Kim, Y.-Y., H. Choi, S. Segami, H.-T. Cho, E. Martinoia, M. Maeshima, and Y. Lee**, *AtHMA1 contributes to the detoxification of excess Zn(II) in Arabidopsis*. The Plant Journal, 2009. **58**(5): p. 737-753.
254. **Morel, M., J. Crouzet, A. Gravot, P. Auroy, N. Leonhardt, A. Vavasseur, and P. Richaud**, *AtHMA3, a P1B-ATPase allowing Cd/Zn/Co/Pb vacuolar storage in Arabidopsis*. Plant Physiol, 2009. **149**(2): p. 894-904.
255. **Park, W. and S.-J. Ahn**, *HMA3 is a key factor for differences in Cd- and Zn-related phenotype between Arabidopsis Ws and Col-0 ecotypes*. Plant Biotechnology Reports, 2017. **11**(4): p. 209-218.
256. **Haydon, M.J. and C.S. Cobbett**, *A novel major facilitator superfamily protein at the tonoplast influences zinc tolerance and accumulation in Arabidopsis*. Plant Physiol, 2007. **143**(4): p. 1705-19.
257. **Remy, E., T.R. Cabrito, R.A. Batista, M.A. Hussein, M.C. Teixeira, A. Athanasiadis, I. Sa-Correia, and P. Duque**, *Intron retention in the 5'UTR of the novel ZIF2 transporter enhances translation to promote zinc tolerance in arabidopsis*. PLoS Genet, 2014. **10**(5): p. e1004375.
258. **Pao, S.S., I.T. Paulsen, and M.H. Saier, Jr.**, *Major facilitator superfamily*. Microbiol Mol Biol Rev, 1998. **62**(1): p. 1-34.
259. **Ren, Q. and I.T. Paulsen**, *Comparative analyses of fundamental differences in membrane transport capabilities in prokaryotes and eukaryotes*. PLoS Comput Biol, 2005. **1**(3): p. e27.
260. **Cao, J.**, *Molecular Evolution of the Vacuolar Iron Transporter (VIT) Family Genes in 14 Plant Species*. Genes, 2019. **10**(2): p. 144.
261. **Denance, N., B. Szurek, and L.D. Noel**, *Emerging functions of nodulin-like proteins in non-nodulating plant species*. Plant Cell Physiol, 2014. **55**(3): p. 469-74.
262. **Li, L., O.S. Chen, D.M. Ward, and J. Kaplan**, *CCC1 is a transporter that mediates vacuolar iron storage in yeast*. Journal of Biological Chemistry, 2001. **276**(31): p. 29515-29519.
263. **Kim, S.A., T. Punshon, A. Lanzirotti, L. Li, J.M. Alonso, J.R. Ecker, J. Kaplan, and M.L. Guerinot**, *Localization of iron in Arabidopsis seed requires the vacuolar membrane transporter VIT1*. Science, 2006. **314**(5803): p. 1295-8.

264. **Gollhofer, J., R. Timofeev, P. Lan, W. Schmidt, and T.J. Buckhout**, *Vacuolar-Iron-Transporter1-Like proteins mediate iron homeostasis in Arabidopsis*. PLoS one, 2014. **9**(10): p. e110468-e110468.
265. **Gollhofer, J., C. Schlawicke, N. Jungnick, W. Schmidt, and T.J. Buckhout**, *Members of a small family of nodulin-like genes are regulated under iron deficiency in roots of Arabidopsis thaliana*. Plant Physiol Biochem, 2011. **49**(5): p. 557-64.
266. **Yamada, K., A.J. Nagano, M. Nishina, I. Hara-Nishimura, and M. Nishimura**, *Identification of two novel endoplasmic reticulum body-specific integral membrane proteins*. Plant Physiol, 2013. **161**(1): p. 108-20.
267. **Lanquar, V., F. Lelièvre, H. Barbier-Brygoo, and S. Thomine**, *Regulation and function of AtNRAMP4 metal transporter protein*. Soil Science and Plant Nutrition, 2004. **50**(7): p. 1141-1150.
268. **Thomine, S., F. Lelievre, E. Debarbieux, J.I. Schroeder, and H. Barbier-Brygoo**, *AtNRAMP3, a multispecific vacuolar metal transporter involved in plant responses to iron deficiency*. Plant J, 2003. **34**(5): p. 685-95.
269. **Kim, S.A. and M.L. Guerinot**, *Mining iron: iron uptake and transport in plants*. FEBS Lett, 2007. **581**(12): p. 2273-80.
270. **Lanquar, V., F. Lelièvre, S. Bolte, C. Hamès, C. Alcon, D. Neumann, G. Vansuyt, C. Curie, A. Schröder, U. Krämer, H. Barbier-Brygoo, and S. Thomine**, *Mobilization of vacuolar iron by AtNRAMP3 and AtNRAMP4 is essential for seed germination on low iron*. The EMBO journal, 2005. **24**(23): p. 4041-4051.
271. **Oomen, R.J.F.J., J. Wu, F. Lelièvre, S. Blanchet, P. Richaud, H. Barbier-Brygoo, M.G.M. Aarts, and S. Thomine**, *Functional characterization of NRAMP3 and NRAMP4 from the metal hyperaccumulator Thlaspi caerulescens*. New Phytologist, 2009. **181**(3): p. 637-650.
272. **Li, J., Y. Wang, L. Zheng, Y. Li, X. Zhou, J. Li, D. Gu, E. Xu, Y. Lu, X. Chen, and W. Zhang**, *The Intracellular Transporter AtNRAMP6 Is Involved in Fe Homeostasis in Arabidopsis*. Front Plant Sci, 2019. **10**: p. 1124.
273. **Vert, G., M. Barberon, E. Zelazny, M. Seguela, J.F. Briat, and C. Curie**, *Arabidopsis IRT2 cooperates with the high-affinity iron uptake system to maintain iron homeostasis in root epidermal cells*. Planta, 2009. **229**(6): p. 1171-9.
274. **Vert, G., J.F. Briat, and C. Curie**, *Arabidopsis IRT2 gene encodes a root-periphery iron transporter*. Plant J, 2001. **26**(2): p. 181-9.

275. **Briat, J.F., C. Duc, K. Ravet, and F. Gaymard**, *Ferritins and iron storage in plants*. *Biochim Biophys Acta*, 2010. **1800**(8): p. 806-14.
276. **Petit, J.M., J.F. Briat, and S. Lobreaux**, *Structure and differential expression of the four members of the Arabidopsis thaliana ferritin gene family*. *Biochem J*, 2001. **359**(Pt 3): p. 575-82.
277. **Tarantino, D., F. Casagrande, C. Soave, and I. Murgia**, *Knocking out of the mitochondrial AtFer4 ferritin does not alter response of Arabidopsis plants to abiotic stresses*. *Journal of Plant Physiology*, 2010. **167**(6): p. 453-460.
278. **Lopez-Millan, A.F., D. Duy, and K. Philippar**, *Chloroplast Iron Transport Proteins - Function and Impact on Plant Physiology*. *Front Plant Sci*, 2016. **7**: p. 178.
279. **Duy, D., G. Wanner, A.R. Meda, N. von Wiren, J. Soll, and K. Philippar**, *PIC1, an ancient permease in Arabidopsis chloroplasts, mediates iron transport*. *Plant Cell*, 2007. **19**(3): p. 986-1006.
280. **Duy, D., R. Stube, G. Wanner, and K. Philippar**, *The chloroplast permease PIC1 regulates plant growth and development by directing homeostasis and transport of iron*. *Plant Physiol*, 2011. **155**(4): p. 1709-22.
281. **Jeong, J., C. Cohu, L. Kerkeb, M. Pilon, E.L. Connolly, and M.L. Guerinot**, *Chloroplast Fe(III) chelate reductase activity is essential for seedling viability under iron limiting conditions*. *Proc Natl Acad Sci U S A*, 2008. **105**(30): p. 10619-24.
282. **Tarantino, D., P. Morandini, L. Ramirez, C. Soave, and I. Murgia**, *Identification of an Arabidopsis mitoferrinlike carrier protein involved in Fe metabolism*. *Plant Physiology and Biochemistry*, 2011. **49**(5): p. 520-529.
283. **Voith von Voithenberg, L., J. Park, R. Stube, C. Lux, Y. Lee, and K. Philippar**, *A Novel Prokaryote-Type ECF/ABC Transporter Module in Chloroplast Metal Homeostasis*. *Front Plant Sci*, 2019. **10**: p. 1264.
284. **Shimoni-Shor, E., M. Hassidim, N. Yuval-Naeh, and N. Keren**, *Disruption of Nap14, a plastid-localized non-intrinsic ABC protein in Arabidopsis thaliana results in the over-accumulation of transition metals and in aberrant chloroplast structures*. *Plant Cell Environ*, 2010. **33**(6): p. 1029-38.
285. **Jain, A., Z.S. Dashner, and E.L. Connolly**, *Mitochondrial Iron Transporters (MIT1 and MIT2) Are Essential for Iron Homeostasis and Embryogenesis in Arabidopsis thaliana*. *Front Plant Sci*, 2019. **10**: p. 1449.
286. **Divol, F., D. Couch, G. Conéjéro, H. Roschttardt, S. Mari, and C. Curie**, *The Arabidopsis YELLOW STRIPE LIKE4 and 6 transporters control iron release from the chloroplast*. *The Plant Cell*, 2013. **25**(3): p. 1040-1055.

287. **Conte, S.S., H.H. Chu, D.C. Rodriguez, T. Punshon, K.A. Vasques, D.E. Salt, and E.L. Walker**, *Arabidopsis thaliana Yellow Stripe1-Like4 and Yellow Stripe1-Like6 localize to internal cellular membranes and are involved in metal ion homeostasis*. *Front Plant Sci*, 2013. **4**: p. 283.
288. **Inaba, S., R. Kurata, M. Kobayashi, Y. Yamagishi, I. Mori, Y. Ogata, and Y. Fukao**, *Identification of putative target genes of bZIP19, a transcription factor essential for Arabidopsis adaptation to Zn deficiency in roots*. *Plant Journal*, 2015. **84**(2): p. 323-334.
289. **Lilay, G.H., P.H. Castro, A. Campilho, and A.G.L. Assuncao**, *The Arabidopsis bZIP19 and bZIP23 Activity Requires Zinc Deficiency - Insight on Regulation From Complementation Lines*. *Front Plant Sci*, 2018. **9**: p. 1955.
290. **Lilay, G.H., D.P. Persson, P.H. Castro, F. Liao, R.D. Alexander, M.G.M. Aarts, and A.G.L. Assunção**, *The Arabidopsis bZIP19 and bZIP23 transcription factors act as zinc-sensors to control plant zinc status*. *bioRxiv*, 2020: p. 2020.06.29.177287.
291. **Gustin, J.L., M.E. Loureiro, D. Kim, G. Na, M. Tikhonova, and D.E. Salt**, *MTP1-dependent Zn sequestration into shoot vacuoles suggests dual roles in Zn tolerance and accumulation in Zn-hyperaccumulating plants*. *Plant J*, 2009. **57**(6): p. 1116-27.
292. **Lasswell, J., L.E. Rogg, D.C. Nelson, C. Rongey, and B. Bartel**, *Cloning and characterization of IAR1, a gene required for auxin conjugate sensitivity in Arabidopsis*. *Plant Cell*, 2000. **12**(12): p. 2395-2408.
293. **Sofo, A., R. Bochicchio, M. Amato, N. Rendina, A. Vitti, M. Nuzzaci, M.M. Altamura, G. Falasca, F.D. Rovere, and A. Scopa**, *Plant architecture, auxin homeostasis and phenol content in Arabidopsis thaliana grown in cadmium- and zinc-enriched media*. *J Plant Physiol*, 2017. **216**: p. 174-180.
294. **Escudero, V., Á. Castro-León, D.F. Sánchez, I. Abreu, M. Bernal, U. Krämer, D. Grolimund, M. González-Guerrero, and L. Jordá**, *Arabidopsis thaliana Zn²⁺-efflux ATPases HMA2 and HMA4 are required for resistance to the necrotrophic fungus Plectosphaerella cucumerina BMM*. *bioRxiv*, 2020: p. 2020.08.10.243014.
295. **Gao, F., K. Robe, F. Gaymard, E. Izquierdo, and C. Dubos**, *The Transcriptional Control of Iron Homeostasis in Plants: A Tale of bHLH Transcription Factors?* *Front Plant Sci*, 2019. **10**: p. 6.
296. **Liang, G., H. Zhang, X. Li, Q. Ai, and D. Yu**, *bHLH transcription factor bHLH115 regulates iron homeostasis in Arabidopsis thaliana*. *J Exp Bot*, 2017. **68**(7): p. 1743-1755.

297. **Zhang, J., B. Liu, M. Li, D. Feng, H. Jin, P. Wang, J. Liu, F. Xiong, J. Wang, and H.B. Wang**, *The bHLH transcription factor bHLH104 interacts with IAA-LEUCINE RESISTANT3 and modulates iron homeostasis in Arabidopsis*. *Plant Cell*, 2015. **27**(3): p. 787-805.
298. **Gao, F., K. Robe, M. Bettembourg, N. Navarro, V. Rofidal, V. Santoni, F. Gaymard, F. Vignols, H. Roschzttardtz, E. Izquierdo, and C. Dubos**, *The Transcription Factor bHLH121 Interacts with bHLH105 (ILR3) and Its Closest Homologs to Regulate Iron Homeostasis in Arabidopsis*. *Plant Cell*, 2020. **32**(2): p. 508-524.
299. **Lei, R., Y. Li, Y. Cai, C. Li, M. Pu, C. Lu, Y. Yang, and G. Liang**, *bHLH121 Functions as a Direct Link that Facilitates the Activation of FIT by bHLH IVc Transcription Factors for Maintaining Fe Homeostasis in Arabidopsis*. *Mol Plant*, 2020. **13**(4): p. 634-649.
300. **Kim, S.A., I.S. LaCroix, S.A. Gerber, and M.L. Guerinot**, *The iron deficiency response in Arabidopsis thaliana requires the phosphorylated transcription factor URI*. *Proc Natl Acad Sci U S A*, 2019. **116**(50): p. 24933-24942.
301. **Wang, N., Y. Cui, Y. Liu, H. Fan, J. Du, Z. Huang, Y. Yuan, H. Wu, and H.Q. Ling**, *Requirement and functional redundancy of Ib subgroup bHLH proteins for iron deficiency responses and uptake in Arabidopsis thaliana*. *Mol Plant*, 2013. **6**(2): p. 503-13.
302. **Yuan, Y., H. Wu, N. Wang, J. Li, W. Zhao, J. Du, D. Wang, and H.Q. Ling**, *FIT interacts with AtbHLH38 and AtbHLH39 in regulating iron uptake gene expression for iron homeostasis in Arabidopsis*. *Cell Res*, 2008. **18**(3): p. 385-97.
303. **Colangelo, E.P. and M.L. Guerinot**, *The essential basic helix-loop-helix protein FIT1 is required for the iron deficiency response*. *Plant Cell*, 2004. **16**(12): p. 3400-12.
304. **Hindt, M.N., G.Z. Akmajian, K.L. Pivarski, T. Punshon, I. Baxter, D.E. Salt, and M.L. Guerinot**, *BRUTUS and its paralogs, BTS LIKE1 and BTS LIKE2, encode important negative regulators of the iron deficiency response in Arabidopsis thaliana*. *Metallomics*, 2017. **9**(7): p. 876-890.
305. **Rodriguez-Celma, J., J.M. Connorton, I. Kruse, R.T. Green, M. Franceschetti, Y.T. Chen, Y. Cui, H.Q. Ling, K.C. Yeh, and J. Balk**, *Arabidopsis BRUTUS-LIKE E3 ligases negatively regulate iron uptake by targeting transcription factor FIT for recycling*. *Proc Natl Acad Sci U S A*, 2019. **116**(35): p. 17584-17591.
306. **Selote, D., R. Samira, A. Matthiadis, J.W. Gillikin, and T.A. Long**, *Iron-binding E3 ligase mediates iron response in plants by targeting basic helix-loop-helix transcription factors*. *Plant Physiol*, 2015. **167**(1): p. 273-86.

307. **Long, T.A., H. Tsukagoshi, W. Busch, B. Lahner, D.E. Salt, and P.N. Benfey,** *The bHLH transcription factor POPEYE regulates response to iron deficiency in Arabidopsis roots.* Plant Cell, 2010. **22**(7): p. 2219-36.
308. **Schwarz, B. and P. Bauer,** *FIT, a regulatory hub for iron deficiency and stress signaling in roots, and FIT-dependent and -independent gene signatures.* J Exp Bot, 2020. **71**(5): p. 1694-1705.
309. **Lucena, C., F.J. Romera, M.J. Garcia, E. Alcantara, and R. Perez-Vicente,** *Ethylene Participates in the Regulation of Fe Deficiency Responses in Strategy I Plants and in Rice.* Front Plant Sci, 2015. **6**: p. 1056.
310. **Wu, H. and H.-Q. Ling,** *FIT-Binding Proteins and Their Functions in the Regulation of Fe Homeostasis.* Frontiers in Plant Science, 2019. **10**: p. 844.
311. **Lingam, S., J. Mohrbacher, T. Brumbarova, T. Potuschak, C. Fink-Straube, E. Blondet, P. Genschik, and P. Bauer,** *Interaction between the bHLH transcription factor FIT and ETHYLENE INSENSITIVE3/ETHYLENE INSENSITIVE3-LIKE1 reveals molecular linkage between the regulation of iron acquisition and ethylene signaling in Arabidopsis.* Plant Cell, 2011. **23**(5): p. 1815-29.
312. **Yang, Y., B. Ou, J. Zhang, W. Si, H. Gu, G. Qin, and L.J. Qu,** *The Arabidopsis Mediator subunit MED16 regulates iron homeostasis by associating with EIN3/EIL1 through subunit MED25.* Plant J, 2014. **77**(6): p. 838-51.
313. **Zhang, Y., H. Wu, N. Wang, H. Fan, C. Chen, Y. Cui, H. Liu, and H.Q. Ling,** *Mediator subunit 16 functions in the regulation of iron uptake gene expression in Arabidopsis.* New Phytol, 2014. **203**(3): p. 770-83.
314. **Liu, W., N.J.U. Karemera, T. Wu, Y. Yang, X. Zhang, X. Xu, Y. Wang, and Z. Han,** *The ethylene response factor AtERF4 negatively regulates the iron deficiency response in Arabidopsis thaliana.* PLoS One, 2017. **12**(10): p. e0186580.
315. **Liu, W., Q. Li, Y. Wang, T. Wu, Y. Yang, X. Zhang, Z. Han, and X. Xu,** *Ethylene response factor AtERF72 negatively regulates Arabidopsis thaliana response to iron deficiency.* Biochem Biophys Res Commun, 2017. **491**(3): p. 862-868.
316. **Hindt, M.N. and M.L. Guerinot,** *Getting a sense for signals: regulation of the plant iron deficiency response.* Biochim Biophys Acta, 2012. **1823**(9): p. 1521-30.
317. **Chen, W.W., J.L. Yang, C. Qin, C.W. Jin, J.H. Mo, T. Ye, and S.J. Zheng,** *Nitric oxide acts downstream of auxin to trigger root ferric-chelate reductase activity in response to iron deficiency in Arabidopsis.* Plant Physiol, 2010. **154**(2): p. 810-9.

318. **Romera, F.J., M.J. García, E. Alcántara, and R. Pérez-Vicente**, *Latest findings about the interplay of auxin, ethylene and nitric oxide in the regulation of Fe deficiency responses by Strategy I plants*. *Plant signaling & behavior*, 2011. **6**(1): p. 167-170.
319. **Garcia, M.J., C. Lucena, F.J. Romera, E. Alcantara, and R. Perez-Vicente**, *Ethylene and nitric oxide involvement in the up-regulation of key genes related to iron acquisition and homeostasis in Arabidopsis*. *J Exp Bot*, 2010. **61**(14): p. 3885-99.
320. **Yang, J.L., W.W. Chen, L.Q. Chen, C. Qin, C.W. Jin, Y.Z. Shi, and S.J. Zheng**, *The 14-3-3 protein GENERAL REGULATORY FACTOR11 (GRF11) acts downstream of nitric oxide to regulate iron acquisition in Arabidopsis thaliana*. *New Phytologist*, 2013. **197**(3): p. 815-824.
321. **Gratz, R., P. Manishankar, R. Ivanov, P. Köster, I. Mohr, K. Trofimov, L. Steinhorst, J. Meiser, H.-J. Mai, M. Drerup, S. Arendt, M. Holtkamp, U. Karst, J. Kudla, P. Bauer, and T. Brumbarova**, *CIPK11-Dependent Phosphorylation Modulates FIT Activity to Promote Arabidopsis Iron Acquisition in Response to Calcium Signaling*. *Developmental Cell*, 2019. **48**(5): p. 726-740.e10.
322. **Cui, Y., C.L. Chen, M. Cui, W.J. Zhou, H.L. Wu, and H.Q. Ling**, *Four IVa bHLH Transcription Factors Are Novel Interactors of FIT and Mediate JA Inhibition of Iron Uptake in Arabidopsis*. *Mol Plant*, 2018. **11**(9): p. 1166-1183.
323. **Seguela, M., J.F. Briat, G. Vert, and C. Curie**, *Cytokinins negatively regulate the root iron uptake machinery in Arabidopsis through a growth-dependent pathway*. *Plant J*, 2008. **55**(2): p. 289-300.
324. **Wild, M., J.-M. Davière, T. Regnault, L. Sakvarelidze-Achard, E. Carrera, I.L. Diaz, A. Cayrel, G. Dubeaux, G. Vert, and P. Achard**, *Tissue-specific regulation of gibberellin signaling fine-tunes Arabidopsis iron-deficiency responses*. *Developmental Cell*, 2016. **37**(2): p. 190-200.
325. **Le, C.T.T., T. Brumbarova, R. Ivanov, C. Stoof, E. Weber, J. Mohrbacher, C. Fink-Straube, and P. Bauer**, *Zinc finger of Arabidopsis thaliana12 (ZAT12) interacts with FER-like iron deficiency-induced transcription factor (FIT) linking iron deficiency and oxidative stress responses*. *Plant Physiology*, 2016. **170**(1): p. 540-557.
326. **Yan, J.Y., C.X. Li, L. Sun, J.Y. Ren, G.X. Li, Z.J. Ding, and S.J. Zheng**, *A WRKY Transcription Factor Regulates Fe Translocation under Fe Deficiency*. *Plant Physiol*, 2016. **171**(3): p. 2017-27.
327. **Bournier, M., N. Tissot, S. Mari, J. Boucherez, E. Lacombe, J.F. Briat, and F. Gaymard**, *Arabidopsis ferritin 1 (AtFer1) gene regulation by the phosphate starvation response 1 (AtPHR1) transcription factor reveals a direct molecular*

- link between iron and phosphate homeostasis. J Biol Chem, 2013. 288(31): p. 22670-80.*
328. **Briat, J.F., H. Rouached, N. Tissot, F. Gaymard, and C. Dubos**, *Integration of P, S, Fe, and Zn nutrition signals in Arabidopsis thaliana: potential involvement of PHOSPHATE STARVATION RESPONSE 1 (PHR1)*. *Front Plant Sci*, 2015. **6**: p. 290.
 329. **Oliva, M.**, *Identification and functional characterization of novel genes contributing to iron homeostasis in Arabidopsis thaliana*, in *Faculty of Natural Sciences and Mathematics*. 2013, PhD Thesis, Ruperto-Carola University of Heidelberg, Germany.
 330. **Brown, R.**, *Lectures on the Inorganic Nutrition of Plants*. *Nature*, 1944. **154(3916)**: p. 624-624.
 331. **Becher, M., I.N. Talke, L. Krall, and U. Kramer**, *Cross-species microarray transcript profiling reveals high constitutive expression of metal homeostasis genes in shoots of the zinc hyperaccumulator Arabidopsis halleri*. *Plant J*, 2004. **37(2)**: p. 251-68.
 332. **Boyes, D.C., A.M. Zayed, R. Ascenzi, A.J. McCaskill, N.E. Hoffman, K.R. Davis, and J. Gorchach**, *Growth stage-based phenotypic analysis of Arabidopsis: a model for high throughput functional genomics in plants*. *Plant Cell*, 2001. **13(7)**: p. 1499-510.
 333. **Pfaffl, M.W.**, *A new mathematical model for relative quantification in real-time RT-PCR*. *Nucleic Acids Res*, 2001. **29(9)**: p. e45.
 334. **Czechowski, T., M. Stitt, T. Altmann, M.K. Udvardi, and W.R. Scheible**, *Genome-wide identification and testing of superior reference genes for transcript normalization in Arabidopsis*. *Plant Physiol*, 2005. **139(1)**: p. 5-17.
 335. **Grillet, L., P. Lan, W. Li, G. Mokkaapati, and W. Schmidt**, *IRON MAN is a ubiquitous family of peptides that control iron transport in plants*. *Nat Plants*, 2018. **4(11)**: p. 953-963.
 336. **Hanahan, D.**, *Studies on transformation of Escherichia coli with plasmids*. *J Mol Biol*, 1983. **166(4)**: p. 557-80.
 337. **Bertani, G.**, *Studies on lysogeny. I. The mode of phage liberation by lysogenic Escherichia coli*. *J Bacteriol*, 1951. **62(3)**: p. 293-300.
 338. **Emre Aksoy, E. and H. Koiwa**, *Determination of Ferric Chelate Reductase Activity in the Arabidopsis thaliana Root*. *Bio-protocol*, 2013. **3(15)**: p. e843.
 339. **Brumbarova, T. and R. Ivanov**, *Perls Staining for Histochemical Detection of Iron in Plant Samples*. *Bio-protocol*, 2014. **4(18)**: p. e1245.

340. **Andrew, S.** *FastQC: A Quality Control Tool for High Throughput Sequence Data [Online]*. 2010 20/11/2019; Available from: <http://www.bioinformatics.babraham.ac.uk/projects/fastqc/>.
341. **Bray, N.L., H. Pimentel, P. Melsted, and L. Pachter,** *Near-optimal probabilistic RNA-seq quantification*. *Nat Biotechnol*, 2016. **34**(5): p. 525-7.
342. **Pimentel, H., N.L. Bray, S. Puente, P. Melsted, and L. Pachter,** *Differential analysis of RNA-seq incorporating quantification uncertainty*. *Nat Methods*, 2017. **14**(7): p. 687-690.
343. **Powell, D.** *Degust: interactive RNA-seq analysis*. 2015 13/11/2019; Available from: <https://degust.erc.monash.edu/>.
344. **Cermak, V.** *Multiple List Comparator [Online]*. 2020; Available from: <http://www.molbiotools.com/listcompare.html>.
345. *Morpheus*. Available from: <https://software.broadinstitute.org/morpheus/>.
346. **Mi, H., A. Muruganujan, D. Ebert, X. Huang, and P.D. Thomas,** *PANTHER version 14: more genomes, a new PANTHER GO-slim and improvements in enrichment analysis tools*. *Nucleic Acids Res*, 2019. **47**(D1): p. D419-D426.
347. **Kanehisa, M. and S. Goto,** *KEGG: kyoto encyclopedia of genes and genomes*. *Nucleic Acids Res*, 2000. **28**(1): p. 27-30.
348. **Kanehisa, M., Y. Sato, M. Furumichi, K. Morishima, and M. Tanabe,** *New approach for understanding genome variations in KEGG*. *Nucleic Acids Res*, 2019. **47**(D1): p. D590-D595.
349. **Kanehisa, M.,** *Toward understanding the origin and evolution of cellular organisms*. *Protein Sci*, 2019. **28**(11): p. 1947-1951.
350. **Huang da, W., B.T. Sherman, and R.A. Lempicki,** *Bioinformatics enrichment tools: paths toward the comprehensive functional analysis of large gene lists*. *Nucleic Acids Res*, 2009. **37**(1): p. 1-13.
351. **Huang da, W., B.T. Sherman, and R.A. Lempicki,** *Systematic and integrative analysis of large gene lists using DAVID bioinformatics resources*. *Nat Protoc*, 2009. **4**(1): p. 44-57.
352. **Morgan, T.H.,** *The Origin of Five Mutations in Eye Color in Drosophila and Their Modes of Inheritance*. *Science*, 1911. **33**(849): p. 534-537.
353. **Morgan, T.H.,** *THE ORIGIN OF NINE WING MUTATIONS IN DROSOPHILA*. *Science*, 1911. **33**(848): p. 496.

354. **Nguyen, B.D. and R.H. Valdivia**, *Forward genetic approaches in Chlamydia trachomatis*. J Vis Exp, 2013(80): p. e50636.
355. **St Onge, R., U. Schlecht, C. Scharfe, and M. Evangelista**, *Forward chemical genetics in yeast for discovery of chemical probes targeting metabolism*. Molecules, 2012. **17**(11): p. 13098-115.
356. **Nurse, P., P. Thuriaux, and K. Nasmyth**, *Genetic control of the cell division cycle in the fission yeast Schizosaccharomyces pombe*. Molecular and General Genetics MGG, 1976. **146**(2): p. 167-178.
357. **Moresco, E.M., X. Li, and B. Beutler**, *Going forward with genetics: recent technological advances and forward genetics in mice*. Am J Pathol, 2013. **182**(5): p. 1462-73.
358. **Takahashi, J.S., L.H. Pinto, and M.H. Vitaterna**, *Forward and reverse genetic approaches to behavior in the mouse*. Science, 1994. **264**(5166): p. 1724.
359. **Jankowicz-Cieslak, J. and B.J. Till**, *Forward and Reverse Genetics in Crop Breeding*, in *Advances in Plant Breeding Strategies: Breeding, Biotechnology and Molecular Tools*, J.M. Al-Khayri, S.M. Jain, and D.V. Johnson, Editors. 2015, Springer International Publishing: Cham. p. 215-240.
360. **Pareek, A., A. Arora, and O.P. Dhankher**, *Stepping forward and taking reverse as we move ahead in genetics*. Indian Journal of Plant Physiology, 2018. **23**(4): p. 609-611.
361. **Bolle, C., A. Schneider, and D. Leister**, *Perspectives on Systematic Analyses of Gene Function in Arabidopsis thaliana: New Tools, Topics and Trends*. Curr Genomics, 2011. **12**(1): p. 1-14.
362. **Kim, M.J., D. Ruzicka, R. Shin, and D.P. Schachtman**, *The Arabidopsis AP2/ERF transcription factor RAP2.11 modulates plant response to low-potassium conditions*. Mol Plant, 2012. **5**(5): p. 1042-57.
363. **Huang, X.Y., D.Y. Chao, A. Koprivova, J. Danku, M. Wirtz, S. Muller, F.J. Sandoval, H. Bauwe, S. Roje, B. Dilkes, R. Hell, S. Kopriva, and D.E. Salt**, *Nuclear Localised MORE SULPHUR ACCUMULATION1 Epigenetically Regulates Sulphur Homeostasis in Arabidopsis thaliana*. PLoS Genet, 2016. **12**(9): p. e1006298.
364. **Wu, Y., Q. Zhao, L. Gao, X.M. Yu, P. Fang, D.J. Oliver, and C.B. Xiang**, *Isolation and characterization of low-sulphur-tolerant mutants of Arabidopsis*. J Exp Bot, 2010. **61**(12): p. 3407-22.

365. **Ohkama-Ohtsu, N., I. Kasajima, T. Fujiwara, and S. Naito**, *Isolation and Characterization of an Arabidopsis Mutant That Overaccumulates γ -Acetyl-Ser*. *Plant Physiology*, 2004. **136**(2): p. 3209.
366. **Oda, K., T. Kamiya, Y. Shikanai, S. Shigenobu, K. Yamaguchi, and T. Fujiwara**, *The Arabidopsis Mg Transporter, MRS2-4, is Essential for Mg Homeostasis Under Both Low and High Mg Conditions*. *Plant and Cell Physiology*, 2016. **57**(4): p. 754-763.
367. **Poirier, Y., S. Thoma, C. Somerville, and J. Schiefelbein**, *Mutant of Arabidopsis deficient in xylem loading of phosphate*. *Plant Physiol*, 1991. **97**(3): p. 1087-93.
368. **Wang, L., J. Dong, Z. Gao, and D. Liu**, *The Arabidopsis gene HYPERSENSITIVE TO PHOSPHATE STARVATION 3 encodes ETHYLENE OVERPRODUCTION 1*. *Plant and Cell Physiology*, 2012. **53**(6): p. 1093-1105.
369. **Bian, B., S. Kageshima, K. Yano, T. Fujiwara, and T. Kamiya**, *Screening Arabidopsis thaliana mutants for low sensitivity to manganese identifies novel alleles of NRAMP1 and PGSIP6*. *J Exp Bot*, 2018. **69**(7): p. 1795-1803.
370. **Sharma, R. and K.C. Yeh**, *The dual benefit of a dominant mutation in Arabidopsis IRON DEFICIENCY TOLERANT1 for iron biofortification and heavy metal phytoremediation*. *Plant Biotechnol J*, 2020. **18**(5): p. 1200-1210.
371. **Duc, C., F. Cellier, S. Lobreaux, J.F. Briat, and F. Gaymard**, *Regulation of iron homeostasis in Arabidopsis thaliana by the clock regulator time for coffee*. *J Biol Chem*, 2009. **284**(52): p. 36271-81.
372. **Catarecha, P., M.D. Segura, J.M. Franco-Zorrilla, B. Garcia-Ponce, M. Lanza, R. Solano, J. Paz-Ares, and A. Leyva**, *A mutant of the Arabidopsis phosphate transporter PHT1;1 displays enhanced arsenic accumulation*. *Plant Cell*, 2007. **19**(3): p. 1123-33.
373. **Dong, J., M.A. Piñeros, X. Li, H. Yang, Y. Liu, A.S. Murphy, L.V. Kochian, and D. Liu**, *An Arabidopsis ABC Transporter Mediates Phosphate Deficiency-Induced Remodeling of Root Architecture by Modulating Iron Homeostasis in Roots*. *Molecular Plant*, 2017. **10**(2): p. 244-259.
374. **Wild, M., J.M. Daviere, T. Regnault, L. Sakvarelidze-Achard, E. Carrera, I. Lopez Diaz, A. Cayrel, G. Dubeaux, G. Vert, and P. Achard**, *Tissue-Specific Regulation of Gibberellin Signaling Fine-Tunes Arabidopsis Iron-Deficiency Responses*. *Dev Cell*, 2016. **37**(2): p. 190-200.

375. **Li, X., H. Zhang, Q. Ai, G. Liang, and D. Yu**, *Two bHLH Transcription Factors, bHLH34 and bHLH104, Regulate Iron Homeostasis in Arabidopsis thaliana*. *Plant Physiol*, 2016. **170**(4): p. 2478-93.
376. **Ogo, Y., T. Kobayashi, R. Nakanishi Itai, H. Nakanishi, Y. Kakei, M. Takahashi, S. Toki, S. Mori, and N.K. Nishizawa**, *A novel NAC transcription factor, IDEF2, that recognizes the iron deficiency-responsive element 2 regulates the genes involved in iron homeostasis in plants*. *J Biol Chem*, 2008. **283**(19): p. 13407-17.
377. **Kim, Y., K.S. Schumaker, and J.-K. Zhu**, *EMS Mutagenesis of Arabidopsis*, in *Arabidopsis Protocols*, J. Salinas and J.J. Sanchez-Serrano, Editors. 2006, Humana Press: Totowa, NJ. p. 101-103.
378. **Kumawat, S., N. Rana, R. Bansal, G. Vishwakarma, S.T. Mehetre, B.K. Das, M. Kumar, S. Kumar Yadav, H. Sonah, T.R. Sharma, and R. Deshmukh**, *Expanding Avenue of Fast Neutron Mediated Mutagenesis for Crop Improvement*. *Plants (Basel)*, 2019. **8**(6).
379. **Gou, X. and J. Li**, *Activation Tagging*, in *Plant Signalling Networks: Methods and Protocols*, Z.-Y. Wang and Z. Yang, Editors. 2012, Humana Press: Totowa, NJ. p. 117-133.
380. **Krysan, P.J., J.C. Young, and M.R. Sussman**, *T-DNA as an Insertional Mutagen in Arabidopsis*. *The Plant Cell*, 1999. **11**(12): p. 2283.
381. **Khursheed, S., A. Raina, R.A. Laskar, and S. Khan**, *Effect of gamma radiation and EMS on mutation rate: their effectiveness and efficiency in faba bean (Vicia faba L.)*. *Caryologia*, 2018. **71**(4): p. 397-404.
382. **Peters, J.L., F. Cnudde, and T. Gerats**, *Forward genetics and map-based cloning approaches*. *Trends Plant Sci*, 2003. **8**(10): p. 484-91.
383. **Sun, H. and K. Schneeberger**, *SHOREmap v3.0: fast and accurate identification of causal mutations from forward genetic screens*. *Methods Mol Biol*, 2015. **1284**: p. 381-95.
384. **Dinh, T.T., E. Luscher, S. Li, X. Liu, S.Y. Won, and X. Chen**, *Genetic screens for floral mutants in Arabidopsis thaliana: enhancers and suppressors*. *Methods in molecular biology (Clifton, N.J.)*, 2014. **1110**: p. 127-156.
385. **DeLuca, M. and W.D. McElroy**, *Kinetics of the firefly luciferase catalyzed reactions*. *Biochemistry*, 1974. **13**(5): p. 921-925.
386. **Aflalo, C.**, *Biologically Localized Firefly Luciferase: A Tool to Study Cellular Processes*, in *International Review of Cytology*, K.W. Jeon and M. Friedlander, Editors. 1991, Academic Press. p. 269-323.

387. **Denburg, J.L., R.T. Lee, and W.D. McElroy**, *Substrate-binding properties of firefly luciferase: I. Luciferin-binding site*. Archives of Biochemistry and Biophysics, 1969. **134**(2): p. 381-394.
388. **Kailasam, S., Y. Wang, J.C. Lo, H.F. Chang, and K.C. Yeh**, *S-Nitrosoglutathione works downstream of nitric oxide to mediate iron-deficiency signaling in Arabidopsis*. Plant J, 2018. **94**(1): p. 157-168.
389. **Zlobin, I.E., P.P. Pashkovskiy, A.V. Kartashov, A.V. Nosov, A.A. Fomenkov, and V.V. Kuznetsov**, *The relationship between cellular Zn status and regulation of Zn homeostasis genes in plant cells*. Environmental and Experimental Botany, 2020. **176**: p. 104104.
390. **Azevedo, H., S.G. Azinheiro, A. Munoz-Merida, P.H. Castro, B. Huettel, M.G. Aarts, and A.G. Assuncao**, *Transcriptomic profiling of Arabidopsis gene expression in response to varying micronutrient zinc supply*. Genom Data, 2016. **7**: p. 256-8.
391. **Talke, I.N., M. Hanikenne, and U. Kramer**, *Zinc-dependent global transcriptional control, transcriptional deregulation, and higher gene copy number for genes in metal homeostasis of the hyperaccumulator Arabidopsis halleri*. Plant Physiology, 2006. **142**(1): p. 148-167.
392. **Wintz, H., T. Fox, Y.Y. Wu, V. Feng, W.Q. Chen, H.S. Chang, T. Zhu, and C. Vulpe**, *Expression profiles of Arabidopsis thaliana in mineral deficiencies reveal novel transporters involved in metal homeostasis*. Journal of Biological Chemistry, 2003. **278**(48): p. 47644-47653.
393. **Littlejohn, G.**, *Isolation and characterisation of Arabidopsis mutants altered in the regulation of flavonoid biosynthetic genes by UV-B and blue light*. 2005, PhD Thesis, University of Glasgow.
394. **McCallum, C.M., L. Comai, E.A. Greene, and S. Henikoff**, *Targeted screening for induced mutations*. Nat Biotechnol, 2000. **18**(4): p. 455-7.
395. **Anderson, P.**, *Chapter 2 Mutagenesis*, in *Methods in Cell Biology*, H.F. Epstein and D.C. Shakes, Editors. 1995, Academic Press. p. 31-58.
396. **Jander, G., S.R. Baerson, J.A. Hudak, K.A. Gonzalez, K.J. Gruys, and R.L. Last**, *Ethylmethanesulfonate saturation mutagenesis in Arabidopsis to determine frequency of herbicide resistance*. Plant Physiol, 2003. **131**(1): p. 139-46.
397. **Jobe, T.O., D.Y. Sung, G. Akmakjian, A. Pham, E.A. Komives, D.G. Mendoza-Cozatl, and J.I. Schroeder**, *Feedback inhibition by thiols outranks glutathione depletion: a luciferase-based screen reveals glutathione-deficient gamma-ECS and glutathione synthetase mutants impaired in cadmium-induced sulfate assimilation*. Plant J, 2012. **70**(5): p. 783-95.

398. **Feike, D.**, *The control of starch degradation in Arabidopsis thaliana leaves at night*, in *School of Biological Sciences*. 2013, PhD Thesis, University of East Anglia.
399. **Matzke, M.A., W. Aufsatz, T. Kanno, M.F. Mette, and A.J.M. Matzke**, 8 - *Homology-Dependent Gene Silencing and Host Defense in Plants*, in *Advances in Genetics*, J.C. Dunlap and C.t. Wu, Editors. 2002, Academic Press. p. 235-275.
400. **Schubert, D., B. Lechtenberg, A. Forsbach, M. Gils, S. Bahadur, and R. Schmidt**, *Silencing in Arabidopsis T-DNA transformants: the predominant role of a gene-specific RNA sensing mechanism versus position effects*. *The Plant cell*, 2004. **16**(10): p. 2561-2572.
401. **Mlotshwa, S., G.J. Pruss, Z. Gao, N.L. Mgutshini, J. Li, X. Chen, L.H. Bowman, and V. Vance**, *Transcriptional silencing induced by Arabidopsis T-DNA mutants is associated with 35S promoter siRNAs and requires genes involved in siRNA-mediated chromatin silencing*. *The Plant Journal* 2010. **64**(4): p. 699-704.
402. **F. de Felippes, F., M. McHale, R.L. Doran, S. Roden, A.L. Eamens, E.J. Finnegan, and P.M. Waterhouse**, *The key role of terminators on the expression and post-transcriptional gene silencing of transgenes*. *The Plant Journal*, 2020. **104**(1): p. 96-112.
403. **Meza, T.J., D. Kamfjord, A.-M. Håkelién, I. Evans, L.H. Godager, A. Mandal, K.S. Jakobsen, and R.B. Aalen**, *The Frequency of Silencing in Arabidopsis Thaliana Varies Highly Between Progeny of Siblings and can be Influenced by Environmental Factors*. *Transgenic Research*, 2001. **10**(1): p. 53-67.
404. **Chou, T.C. and R.L. Moyle**, *Synthetic versions of firefly luciferase and Renilla luciferase reporter genes that resist transgene silencing in sugarcane*. *BMC Plant Biol*, 2014. **14**: p. 92.
405. **Hsiao, P.Y., C.P. Cheng, K.W. Koh, and M.T. Chan**, *The Arabidopsis defensin gene, AtPDF1.1, mediates defence against Pectobacterium carotovorum subsp. carotovorum via an iron-withholding defence system*. *Sci Rep*, 2017. **7**(1): p. 9175.
406. **Mirouze, M., J. Sels, O. Richard, P. Czernic, S. Loubet, A. Jacquier, I.E. Francois, B.P. Cammue, M. Lebrun, P. Berthomieu, and L. Marques**, *A putative novel role for plant defensins: a defensin from the zinc hyper-accumulating plant, Arabidopsis halleri, confers zinc tolerance*. *Plant J*, 2006. **47**(3): p. 329-42.
407. **Kobayashi, T., S. Nagasaka, T. Senoura, R.N. Itai, H. Nakanishi, and N.K. Nishizawa**, *Iron-binding haemerythrin RING ubiquitin ligases regulate plant iron responses and accumulation*. *Nat Commun*, 2013. **4**: p. 2792.

408. **Vashisht, A.A., K.B. Zumbrennen, X. Huang, D.N. Powers, A. Durazo, D. Sun, N. Bhaskaran, A. Persson, M. Uhlen, O. Sangfelt, C. Spruck, E.A. Leibold, and J.A. Wohlschlegel**, *Control of iron homeostasis by an iron-regulated ubiquitin ligase*. Science, 2009. **326**(5953): p. 718-21.
409. **Salahudeen, A.A., J.W. Thompson, J.C. Ruiz, H.W. Ma, L.N. Kinch, Q. Li, N.V. Grishin, and R.K. Bruick**, *An E3 ligase possessing an iron-responsive hemerythrin domain is a regulator of iron homeostasis*. Science, 2009. **326**(5953): p. 722-6.
410. **Outten, C.E.**, *Checks and balances for the iron bank*. J Biol Chem, 2017. **292**(38): p. 15990-15991.
411. **Matthiadis, A. and T.A. Long**, *Further insight into BRUTUS domain composition and functionality*. Plant Signaling & Behavior, 2016. **11**(8).
412. **Selote, D., A. Matthiadis, J.W. Gillikin, M.H. Sato, and T.A. Long**, *The E3 ligase BRUTUS facilitates degradation of VOZ1/2 transcription factors*. Plant Cell and Environment, 2018. **41**(10): p. 2463-2474.
413. **Tissot, N., K. Robe, F. Gao, S. Grant-Grant, J. Boucherez, F. Bellegarde, A. Maghiaoui, R. Marcelin, E. Izquierdo, M. Benhamed, A. Martin, F. Vignols, H. Roschttardt, F. Gaymard, J.-F. Briat, and C. Dubos**, *Transcriptional integration of the responses to iron availability in Arabidopsis by the bHLH factor ILR3*. New Phytologist, 2019. **223**(3): p. 1433-1446.
414. **Kumar, S., A. Palve, C. Joshi, R.K. Srivastava, and Rukhsar**, *Crop biofortification for iron (Fe), zinc (Zn) and vitamin A with transgenic approaches*. Heliyon, 2019. **5**(6): p. e01914.
415. **Bernier, G., A. Havelange, C. Houssa, A. Petitjean, and P. Lejeune**, *Physiological Signals That Induce Flowering*. Plant Cell, 1993. **5**(10): p. 1147-1155.
416. **Wada, K.C. and K. Takeno**, *Stress-induced flowering*. Plant Signaling & Behavior, 2010. **5**(8): p. 944-947.
417. **Cho, L.H., J. Yoon, and G. An**, *The control of flowering time by environmental factors*. Plant J, 2017. **90**(4): p. 708-719.
418. **Kolár, J. and J. Senková**, *Reduction of mineral nutrient availability accelerates flowering of Arabidopsis thaliana*. J Plant Physiol, 2008. **165**(15): p. 1601-9.
419. **Lin, Y.L. and Y.F. Tsay**, *Influence of differing nitrate and nitrogen availability on flowering control in Arabidopsis*. J Exp Bot, 2017. **68**(10): p. 2603-2609.

420. **Castro Marín, I., I. Loef, L. Bartetzko, I. Searle, G. Coupland, M. Stitt, and D. Osuna**, Nitrate regulates floral induction in *Arabidopsis*, acting independently of light, gibberellin and autonomous pathways. *Planta*, 2011. **233**(3): p. 539-52.
421. **Pigliucci, M. and C.D. Schlichting**, Reaction norms of *Arabidopsis* (*Brassicaceae*). III. Response to nutrients in 26 populations from a worldwide collection. *American Journal of Botany*, 1995. **82**(9): p. 1117-1125.
422. **Atanassova, B. and N. Zapryanova**, Influence of Heavy Metal Stress on Growth and Flowering of *Salvia Splendens* Ker.- Gawl. *Biotechnology & Biotechnological Equipment*, 2009. **23**(sup1): p. 173-176.
423. **Przedpelska-Wasowicz, E. and P. Wasowicz**, Does zinc concentration in the substrate influence the onset of flowering in *Arabidopsis arenosa* (*Brassicaceae*)? *Plant Growth Regulation*, 2013. **69**(1): p. 87-97.
424. **Chen, X. and U. Ludewig**, Biomass increase under zinc deficiency caused by delay of early flowering in *Arabidopsis*. *J Exp Bot*, 2018.
425. **Hong, S., S.A. Kim, M.L. Guerinot, and C.R. McClung**, Reciprocal interaction of the circadian clock with the iron homeostasis network in *Arabidopsis*. *Plant physiology*, 2013. **161**(2): p. 893-903.
426. **Sudre, D., E. Gutierrez-Carbonell, G. Lattanzio, R. Rellán-Álvarez, F. Gaymard, G. Wohlgemuth, O. Fiehn, A. Alvarez-Fernández, A.M. Zamarreño, E. Bacaicoa, D. Duy, J.M. García-Mina, J. Abadía, K. Philippar, A.F. López-Millán, and J.F. Briat**, Iron-dependent modifications of the flower transcriptome, proteome, metabolome, and hormonal content in an *Arabidopsis* ferritin mutant. *J Exp Bot*, 2013. **64**(10): p. 2665-88.
427. **Chen, Y.-Y., Y. Wang, L.-J. Shin, J.-F. Wu, V. Shanmugam, M. Tsednee, J.-C. Lo, C.-C. Chen, S.-H. Wu, and K.-C. Yeh**, Iron Is Involved in the Maintenance of Circadian Period Length in *Arabidopsis*. *Plant Physiology*, 2013. **161**(3): p. 1409.
428. **Sivitz, A.B., V. Hermand, C. Curie, and G. Vert**, *Arabidopsis* bHLH100 and bHLH101 control iron homeostasis via a FIT-independent pathway. *PLoS One*, 2012. **7**(9): p. e44843.
429. **Jakoby, M., H.-Y. Wang, W. Reidt, B. Weisshaar, and P. Bauer**, FRU (*BHLH029*) is required for induction of iron mobilization genes in *Arabidopsis thaliana*. *FEBS Letters*, 2004. **577**(3): p. 528-534.
430. **Vert, G., N. Grotz, F. Dedaldechamp, F. Gaymard, M.L. Guerinot, J.F. Briat, and C. Curie**, IRT1, an *Arabidopsis* transporter essential for iron uptake from the soil and for plant growth. *Plant Cell*, 2002. **14**(6): p. 1223-33.

431. **Bashir, K., S. Rasheed, T. Kobayashi, M. Seki, and N.K. Nishizawa**, *Regulating Subcellular Metal Homeostasis: The Key to Crop Improvement*. *Frontiers in Plant Science*, 2016. **7**: p. 1192.
432. **Shanmugam, V., J.C. Lo, C.L. Wu, S.L. Wang, C.C. Lai, E.L. Connolly, J.L. Huang, and K.C. Yeh**, *Differential expression and regulation of iron-regulated metal transporters in Arabidopsis halleri and Arabidopsis thaliana--the role in zinc tolerance*. *New Phytol*, 2011. **190**(1): p. 125-37.
433. **Rai, V., R. Sanagala, B. Sinilal, S. Yadav, A.K. Sarkar, P.K. Dantu, and A. Jain**, *Iron Availability Affects Phosphate Deficiency-Mediated Responses, and Evidence of Cross-Talk with Auxin and Zinc in Arabidopsis*. *Plant and Cell Physiology*, 2015. **56**(6): p. 1107-1123.
434. **Twyman, E.S.**, *The Iron-Manganese Balance and its Effect on the Growth and Development of Plants*. *The New Phytologist*, 1946. **45**(1): p. 18-24.
435. **Ward, J.T., B. Lahner, E. Yakubova, D.E. Salt, and K.G. Raghothama**, *The effect of iron on the primary root elongation of Arabidopsis during phosphate deficiency*. *Plant Physiol*, 2008. **147**(3): p. 1181-91.
436. **Xie, X., W. Hu, X. Fan, H. Chen, and M. Tang**, *Interactions Between Phosphorus, Zinc, and Iron Homeostasis in Nonmycorrhizal and Mycorrhizal Plants*. *Frontiers in plant science*, 2019. **10**: p. 1172-1172.
437. **Kajala, K., K.L. Walker, G.S. Mitchell, U. Krämer, S.R. Cherry, and S.M. Brady**, *Real-time whole-plant dynamics of heavy metal transport in Arabidopsis halleri and Arabidopsis thaliana by gamma-ray imaging*. *Plant Direct*, 2019. **3**(4): p. e00131.
438. **Sugita, R., N.I. Kobayashi, A. Hirose, T. Saito, R. Iwata, K. Tanoi, and T.M. Nakanishi**, *Visualization of Uptake of Mineral Elements and the Dynamics of Photosynthates in Arabidopsis by a Newly Developed Real-Time Radioisotope Imaging System (RRIS)*. *Plant and Cell Physiology*, 2016. **57**(4): p. 743-753.
439. **Kanno, S., M. Yamawaki, H. Ishibashi, N.I. Kobayashi, A. Hirose, K. Tanoi, L. Nussaume, and T.M. Nakanishi**, *Development of real-time radioisotope imaging systems for plant nutrient uptake studies*. *Philosophical transactions of the Royal Society of London. Series B, Biological sciences*, 2012. **367**(1595): p. 1501-1508.
440. **Lanquar, V., G. Grossmann, J.L. Vinkenborg, M. Merx, S. Thomine, and W.B. Frommer**, *Dynamic imaging of cytosolic zinc in Arabidopsis roots combining FRET sensors and RootChip technology*. *New Phytologist*, 2014. **202**(1): p. 198-208.

441. **Sivitz, A., C. Grinvalds, M. Barberon, C. Curie, and G. Vert**, *Proteasome-mediated turnover of the transcriptional activator FIT is required for plant iron-deficiency responses*. *Plant J*, 2011. **66**(6): p. 1044-52.
442. **Meiser, J., S. Lingam, and P. Bauer**, *Posttranslational regulation of the iron deficiency basic helix-loop-helix transcription factor FIT is affected by iron and nitric oxide*. *Plant physiology*, 2011. **157**(4): p. 2154-2166.
443. **Wang, X., Z. Wang, Z. Zheng, J. Dong, L. Song, L. Sui, L. Nussaume, T. Desnos, and D. Liu**, *Genetic Dissection of Fe-Dependent Signaling in Root Developmental Responses to Phosphate Deficiency*. *Plant physiology*, 2019. **179**(1): p. 300-316.
444. **Meguro, R., Y. Asano, S. Odagiri, C. Li, H. Iwatsuki, and K. Shoumura**, *Nonheme-iron histochemistry for light and electron microscopy: a historical, theoretical and technical review*. *Arch Histol Cytol*, 2007. **70**(1): p. 1-19.
445. **Daudi, A. and J.A. O'Brien**, *Detection of Hydrogen Peroxide by DAB Staining in Arabidopsis Leaves*. *Bio-protocol*, 2012. **2**(18): p. e263.
446. **Fukuda, N., N. Kitajima, Y. Terada, T. Abe, I. Nakai, and A. Hokura**, *Visible cellular distribution of cadmium and zinc in the hyperaccumulator Arabidopsis halleri ssp. gemmifera determined by 2-D X-ray fluorescence imaging using high-energy synchrotron radiation*. *Metallomics*, 2020. **12**(2): p. 193-203.
447. **Spolaor, A., P. Vallelonga, J. Gabrieli, G. Cozzi, C. Boutron, and C. Barbante**, *Determination of Fe²⁺ and Fe³⁺ species by FIA-CRC-ICP-MS in Antarctic ice samples*. *Journal of Analytical Atomic Spectrometry*, 2012. **27**(2): p. 310-317.
448. **Ravet, K., B. Touraine, J. Boucherez, J.F. Briat, F. Gaymard, and F. Cellier**, *Ferritins control interaction between iron homeostasis and oxidative stress in Arabidopsis*. *Plant J*, 2009. **57**(3): p. 400-12.
449. **Mai, H.J., S. Pateyron, and P. Bauer**, *Iron homeostasis in Arabidopsis thaliana: transcriptomic analyses reveal novel FIT-regulated genes, iron deficiency marker genes and functional gene networks*. *BMC Plant Biol*, 2016. **16**(1): p. 211.
450. **Hindt, M.N., G.Z. Akmakjian, K.L. Pivarski, T. Punshon, I. Baxter, D.E. Salt, and M.L. Guerinot**, *BRUTUS and its paralogs, BTS LIKE1 and BTS LIKE2, encode important negative regulators of the iron deficiency response in Arabidopsis thaliana*. *Metallomics*, 2017.
451. **Naranjo-Arcos, M.A., F. Maurer, J. Meiser, S. Pateyron, C. Fink-Straube, and P. Bauer**, *Dissection of iron signaling and iron accumulation by overexpression of subgroup Ib bHLH039 protein*. *Sci Rep*, 2017. **7**(1): p. 10911.
452. **Kastoori Ramamurthy, R., Q. Xiang, E.-J. Hsieh, K. Liu, C. Zhang, and B.M. Waters**, *New aspects of iron-copper crosstalk uncovered by transcriptomic*

characterization of Col-0 and the copper uptake mutant spl7 in Arabidopsis thaliana. Metallomics, 2018. **10**(12): p. 1824-1840.

453. **Peng, M., Y.M. Bi, T. Zhu, and S.J. Rothstein**, *Genome-wide analysis of Arabidopsis responsive transcriptome to nitrogen limitation and its regulation by the ubiquitin ligase gene NLA*. Plant Mol Biol, 2007. **65**(6): p. 775-97.
454. **Cloonan, N., A.R. Forrest, G. Kolle, B.B. Gardiner, G.J. Faulkner, M.K. Brown, D.F. Taylor, A.L. Steptoe, S. Wani, G. Bethel, A.J. Robertson, A.C. Perkins, S.J. Bruce, C.C. Lee, S.S. Ranade, H.E. Peckham, J.M. Manning, K.J. McKernan, and S.M. Grimmond**, *Stem cell transcriptome profiling via massive-scale mRNA sequencing*. Nat Methods, 2008. **5**(7): p. 613-9.
455. **Lister, R., R.C. O'Malley, J. Tonti-Filippini, B.D. Gregory, C.C. Berry, A.H. Millar, and J.R. Ecker**, *Highly integrated single-base resolution maps of the epigenome in Arabidopsis*. Cell, 2008. **133**(3): p. 523-36.
456. **Mortazavi, A., B.A. Williams, K. McCue, L. Schaeffer, and B. Wold**, *Mapping and quantifying mammalian transcriptomes by RNA-Seq*. Nat Methods, 2008. **5**(7): p. 621-8.
457. **Nagalakshmi, U., Z. Wang, K. Waern, C. Shou, D. Raha, M. Gerstein, and M. Snyder**, *The transcriptional landscape of the yeast genome defined by RNA sequencing*. Science, 2008. **320**(5881): p. 1344-9.
458. **Wilhelm, B.T., S. Marguerat, S. Watt, F. Schubert, V. Wood, I. Goodhead, C.J. Penkett, J. Rogers, and J. Bahler**, *Dynamic repertoire of a eukaryotic transcriptome surveyed at single-nucleotide resolution*. Nature, 2008. **453**(7199): p. 1239-43.
459. **Wang, Z., M. Gerstein, and M. Snyder**, *RNA-Seq: a revolutionary tool for transcriptomics*. Nat Rev Genet, 2009. **10**(1): p. 57-63.
460. **Stark, R., M. Grzelak, and J. Hadfield**, *RNA sequencing: the teenage years*. Nat Rev Genet, 2019. **20**(11): p. 631-656.
461. **Li, W.V. and J.J. Li**, *Modeling and analysis of RNA-seq data: a review from a statistical perspective*. Quant Biol, 2018. **6**(3): p. 195-209.
462. **Rodriguez-Celma, J., I.C. Pan, W. Li, P. Lan, T.J. Buckhout, and W. Schmidt**, *The transcriptional response of Arabidopsis leaves to Fe deficiency*. Front Plant Sci, 2013. **4**: p. 276.
463. **Tsai, H.-H. and W. Schmidt**, *pH-dependent transcriptional profile changes in iron-deficient Arabidopsis roots*. BMC Genomics, 2020. **21**(1): p. 694.

464. **Park, E.Y., K.M. Tsuyuki, E.M. Parsons, and J. Jeong**, *PRC2-mediated H3K27me3 modulates shoot iron homeostasis in*. *Plant Signal Behav*, 2020. **15**(9): p. 1784549.
465. **Mai, H.-J., S. Pateyron, and P. Bauer**, *Iron homeostasis in Arabidopsis thaliana: transcriptomic analyses reveal novel FIT-regulated genes, iron deficiency marker genes and functional gene networks*. *BMC plant biology*, 2016. **16**(1): p. 211-211.
466. **Buckhout, T.J., T.J. Yang, and W. Schmidt**, *Early iron-deficiency-induced transcriptional changes in Arabidopsis roots as revealed by microarray analyses*. *BMC Genomics*, 2009. **10**: p. 147.
467. **Yang, T.J.W., W.-D. Lin, and W. Schmidt**, *Transcriptional profiling of the Arabidopsis iron deficiency response reveals conserved transition metal homeostasis networks*. *Plant physiology*, 2010. **152**(4): p. 2130-2141.
468. **Brumbarova, T. and R. Ivanov**, *The Nutrient Response Transcriptional Regulome of Arabidopsis*. *iScience*, 2019. **19**: p. 358-368.
469. **Dinneny, J.R., T.A. Long, J.Y. Wang, J.W. Jung, D. Mace, S. Pointer, C. Barron, S.M. Brady, J. Schiefelbein, and P.N. Benfey**, *Cell identity mediates the response of Arabidopsis roots to abiotic stress*. *Science*, 2008. **320**(5878): p. 942-5.
470. **Siwinska, J., K. Siatkowska, A. Olry, J. Grosjean, A. Hehn, F. Bourgaud, A.A. Meharg, M. Carey, E. Lojkowska, and A. Ilnatowicz**, *Scopoletin 8-hydroxylase: a novel enzyme involved in coumarin biosynthesis and iron-deficiency responses in Arabidopsis*. *J Exp Bot*, 2018. **69**(7): p. 1735-1748.
471. **Schuler, M., R. Rellán-Álvarez, C. Fink-Straube, J. Abadía, and P. Bauer**, *Nicotianamine functions in the Phloem-based transport of iron to sink organs, in pollen development and pollen tube growth in Arabidopsis*. *The Plant cell*, 2012. **24**(6): p. 2380-2400.
472. **Palmer, C.M., M.N. Hindt, H. Schmidt, S. Clemens, and M.L. Guerinot**, *MYB10 and MYB72 are required for growth under iron-limiting conditions*. *PLoS Genet*, 2013. **9**(11): p. e1003953.
473. **Schaaf, G., A. Honsbein, A.R. Meda, S. Kirchner, D. Wipf, and N. von Wirén**, *AtIREG2 encodes a tonoplast transport protein involved in iron-dependent nickel detoxification in Arabidopsis thaliana roots*. *J Biol Chem*, 2006. **281**(35): p. 25532-40.
474. **Tiwari, M., P. Venkatachalam, L. Penarrubia, and S.V. Sahi**, *COPT2, a plasma membrane located copper transporter, is involved in the uptake of Au in Arabidopsis*. *Sci Rep*, 2017. **7**(1): p. 11430.

475. **Müller, M. and W. Schmidt**, *Environmentally Induced Plasticity of Root Hair Development in Arabidopsis*. Plant Physiology, 2004. **134**(1): p. 409.
476. **Tanaka, N., H. Uno, S. Okuda, S. Gunji, A. Ferjani, T. Aoyama, and M. Maeshima**, *SRPP, a Cell Wall Protein is Involved in Development and Protection of Seeds and Root Hairs in Arabidopsis thaliana*. Plant Cell Physiol, 2017. **58**(4): p. 760-769.
477. **ZhiMing, Y., K. Bo, H. XiaoWei, L. ShaoLei, B. YouHuang, D. WoNa, C. Ming, C. Hyung-Taeg, and W. Ping**, *Root hair-specific expansins modulate root hair elongation in rice*. The Plant Journal, 2011. **66**(5): p. 725-734.
478. **Bruex, A., R.M. Kainkaryam, Y. Wieckowski, Y.H. Kang, C. Bernhardt, Y. Xia, X. Zheng, J.Y. Wang, M.M. Lee, P. Benfey, P.J. Woolf, and J. Schiefelbein**, *A Gene Regulatory Network for Root Epidermis Cell Differentiation in Arabidopsis*. PLOS Genetics, 2012. **8**(1): p. e1002446.
479. **Manzano, C., M. Pallero-Baena, I. Casimiro, B. De Rybel, B. Orman-Ligeza, G. Van Isterdael, T. Beeckman, X. Draye, P. Casero, and J.C. Del Pozo**, *The Emerging Role of Reactive Oxygen Species Signaling during Lateral Root Development*. Plant Physiol, 2014. **165**(3): p. 1105-1119.
480. **Maris, A., N. Kaewthai, J.M. Eklöf, J.G. Miller, H. Brumer, S.C. Fry, J.-P. Verbelen, and K. Vissenberg**, *Differences in enzymic properties of five recombinant xyloglucan endotransglucosylase/hydrolase (XTH) proteins of Arabidopsis thaliana*. Journal of Experimental Botany, 2011. **62**(1): p. 261-271.
481. **Li, Y., R. Lei, M. Pu, Y. Cai, C. Lu, Z. Li, and G. Liang**, *bHLH11 negatively regulates Fe homeostasis by its EAR motifs recruiting corepressors in Arabidopsis*. bioRxiv, 2020: p. 2020.04.09.035097.
482. **Hirayama, T., G.J. Lei, N. Yamaji, N. Nakagawa, and J.F. Ma**, *The Putative Peptide Gene FEP1 Regulates Iron Deficiency Response in Arabidopsis*. Plant Cell Physiol, 2018. **59**(9): p. 1739-1752.
483. **Kroh, G.E. and M. Pilon**, *Connecting the negatives and positives of plant iron homeostasis*. New Phytologist, 2019. **223**(3): p. 1052-1055.
484. **Nechushtai, R., A.R. Conlan, Y. Harir, L. Song, O. Yogev, Y. Eisenberg-Domovich, O. Livnah, D. Michaeli, R. Rosen, V. Ma, Y. Luo, J.A. Zuris, M.L. Paddock, Z.I. Cabantchik, P.A. Jennings, and R. Mittler**, *Characterization of Arabidopsis NEET Reveals an Ancient Role for NEET Proteins in Iron Metabolism*. The Plant Cell, 2012. **24**(5): p. 2139.

485. **Gao, F., K. Robe, and C. Dubos**, *Further insights into the role of bHLH121 in the regulation of iron homeostasis in Arabidopsis thaliana*. *Plant Signaling & Behavior*, 2020. **15**(10): p. 1795582.
486. **Samira, R., B. Li, D. Kliebenstein, C. Li, E. Davis, J.W. Gillikin, and T.A. Long**, *The bHLH transcription factor ILR3 modulates multiple stress responses in Arabidopsis*. *Plant Molecular Biology*, 2018. **97**(4): p. 297-309.
487. **Kobayashi, T. and N.K. Nishizawa**, *Iron sensors and signals in response to iron deficiency*. *Plant Sci*, 2014. **224**: p. 36-43.
488. **Giehl, R.F., J.E. Lima, and N. von Wiren**, *Localized iron supply triggers lateral root elongation in Arabidopsis by altering the AUX1-mediated auxin distribution*. *Plant Cell*, 2012. **24**(1): p. 33-49.
489. **Matsuoka, K., J. Furukawa, H. Bidadi, M. Asahina, S. Yamaguchi, and S. Satoh**, *Gibberellin-induced expression of Fe uptake-related genes in Arabidopsis*. *Plant Cell Physiol*, 2014. **55**(1): p. 87-98.
490. **Lei, G.J., X.F. Zhu, Z.W. Wang, F. Dong, N.Y. Dong, and S.J. Zheng**, *Abscisic acid alleviates iron deficiency by promoting root iron reutilization and transport from root to shoot in Arabidopsis*. *Plant Cell Environ*, 2014. **37**(4): p. 852-63.
491. **Maurer, F., S. Müller, and P. Bauer**, *Suppression of Fe deficiency gene expression by jasmonate*. *Plant Physiology and Biochemistry*, 2011. **49**(5): p. 530-536.
492. **Hofmann, N.R.**, *Nicotianamine in zinc and iron homeostasis*. *Plant Cell*, 2012. **24**(2): p. 373.
493. **Sun, H., F. Feng, J. Liu, and Q. Zhao**, *The Interaction between Auxin and Nitric Oxide Regulates Root Growth in Response to Iron Deficiency in Rice*. *Frontiers in Plant Science*, 2017. **8**: p. 2169.
494. **Liu, K., R. Yue, C. Yuan, J. Liu, L. Zhang, T. Sun, Y. Yang, S. Tie, and C. Shen**, *Auxin signaling is involved in iron deficiency-induced photosynthetic inhibition and shoot growth defect in rice (Oryza sativa L.)*. *Journal of Plant Biology*, 2015. **58**(6): p. 391-401.
495. **He, M. and N.Z. Ding**, *Plant Unsaturated Fatty Acids: Multiple Roles in Stress Response*. *Front Plant Sci*, 2020. **11**: p. 562785.
496. **Kobayashi, T., R.N. Itai, T. Senoura, T. Oikawa, Y. Ishimaru, M. Ueda, H. Nakanishi, and N.K. Nishizawa**, *Jasmonate signaling is activated in the very early stages of iron deficiency responses in rice roots*. *Plant Mol Biol*, 2016. **91**(4-5): p. 533-47.

497. **Wang, J., L. Song, X. Gong, J. Xu, and M. Li**, *Functions of Jasmonic Acid in Plant Regulation and Response to Abiotic Stress*. *Int J Mol Sci*, 2020. **21**(4).
498. **Romera, F.J., M.J. García, C. Lucena, A. Martínez-Medina, M.A. Aparicio, J. Ramos, E. Alcántara, M. Angulo, and R. Pérez-Vicente**, *Induced Systemic Resistance (ISR) and Fe Deficiency Responses in Dicot Plants*. *Frontiers in plant science*, 2019. **10**: p. 287-287.
499. **Waters, B.M. and L.C. Armbrust**, *Optimal copper supply is required for normal plant iron deficiency responses*. *Plant Signaling & Behavior*, 2013. **8**(12): p. e26611.
500. **Perea-Garcia, A., A. Garcia-Molina, N. Andres-Colas, F. Vera-Sirera, M.A. Perez-Amador, S. Puig, and L. Penarrubia**, *Arabidopsis copper transport protein COPT2 participates in the cross talk between iron deficiency responses and low-phosphate signaling*. *Plant Physiol*, 2013. **162**(1): p. 180-94.
501. **Zhang, M., X. Hu, M. Zhu, M. Xu, and L. Wang**, *Transcription factors NF-YA2 and NF-YA10 regulate leaf growth via auxin signaling in Arabidopsis*. *Scientific Reports*, 2017. **7**(1): p. 1395.
502. **Rouhier, N., J. Couturier, M.K. Johnson, and J.P. Jacquot**, *Glutaredoxins: roles in iron homeostasis*. *Trends Biochem Sci*, 2010. **35**(1): p. 43-52.
503. **Walters, L.A. and M.A. Escobar**, *The AtGRXS3/4/5/7/8 glutaredoxin gene cluster on Arabidopsis thaliana chromosome 4 is coordinately regulated by nitrate and appears to control primary root growth*. *Plant signaling & behavior*, 2016. **11**(4): p. e1171450-e1171450.
504. **To, J.P.C., G. Haberer, F.J. Ferreira, J. Deruère, M.G. Mason, G.E. Schaller, J.M. Alonso, J.R. Ecker, and J.J. Kieber**, *Type-A Arabidopsis response regulators are partially redundant negative regulators of cytokinin signaling*. *The Plant cell*, 2004. **16**(3): p. 658-671.
505. **Böhme, K., Y. Li, F. Charlot, C. Grierson, K. Marrocco, K. Okada, M. Laloue, and F. Nogué**, *The Arabidopsis COW1 gene encodes a phosphatidylinositol transfer protein essential for root hair tip growth*. *The Plant Journal*, 2004. **40**(5): p. 686-698.
506. **Fukao, Y., A. Ferjani, R. Tomioka, N. Nagasaki, R. Kurata, Y. Nishimori, M. Fujiwara, and M. Maeshima**, *iTRAQ Analysis Reveals Mechanisms of Growth Defects Due to Excess Zinc in Arabidopsis*. *Plant Physiology*, 2011. **155**(4): p. 1893.
507. **Paniagua, C., A. Bilkova, P. Jackson, S. Dabravolski, W. Riber, V. Didi, J. Houser, N. Gigli-Bisceglia, M. Wimmerova, E. Budinska, T. Hamann, and J.**

- Hejatko**, *Dirigent proteins in plants: modulating cell wall metabolism during abiotic and biotic stress exposure*. J Exp Bot, 2017. **68**(13): p. 3287-3301.
508. **Takahashi, H., A. Watanabe-Takahashi, F.W. Smith, M. Blake-Kalff, M.J. Hawkesford, and K. Saito**, *The roles of three functional sulphate transporters involved in uptake and translocation of sulphate in Arabidopsis thaliana*. The Plant Journal, 2000. **23**(2): p. 171-182.
509. **Shin, H., H.S. Shin, G.R. Dewbre, and M.J. Harrison**, *Phosphate transport in Arabidopsis: Pht1;1 and Pht1;4 play a major role in phosphate acquisition from both low- and high-phosphate environments*. Plant J, 2004. **39**(4): p. 629-42.
510. **Ivanov, R., T. Brumbarova, and P. Bauer**, *Fitting into the Harsh Reality: Regulation of Iron-deficiency Responses in Dicotyledonous Plants*. Molecular Plant, 2012. **5**(1): p. 27-42.
511. **Uraguchi, S., Y. Sone, Y. Ohta, N. Ohkama-Ohtsu, C. Hofmann, N. Hess, R. Nakamura, Y. Takanezawa, S. Clemens, and M. Kiyono**, *Identification of C-terminal Regions in Arabidopsis thaliana Phytochelatase 1 Specifically Involved in Activation by Arsenite*. Plant Cell Physiol, 2018. **59**(3): p. 500-509.
512. **Eroglu, S., B. Meier, N. von Wiren, and E. Peiter**, *The Vacuolar Manganese Transporter MTP8 Determines Tolerance to Iron Deficiency-Induced Chlorosis in Arabidopsis*. Plant Physiol, 2016. **170**(2): p. 1030-45.
513. **Kumar, R.K., H.H. Chu, C. Abundis, K. Vasques, D.C. Rodriguez, J.C. Chia, R. Huang, O.K. Vatamaniuk, and E.L. Walker**, *Iron-Nicotianamine Transporters Are Required for Proper Long Distance Iron Signaling*. Plant Physiol, 2017. **175**(3): p. 1254-1268.
514. **Ravet, K., B. Touraine, J. Boucherez, J.-F. Briat, F. Gaymard, and F. Cellier**, *Ferritins control interaction between iron homeostasis and oxidative stress in Arabidopsis*. The Plant Journal, 2009. **57**(3): p. 400-412.
515. **Mukherjee, I., N.H. Campbell, J.S. Ash, and E.L. Connolly**, *Expression profiling of the Arabidopsis ferric chelate reductase (FRO) gene family reveals differential regulation by iron and copper*. Planta, 2006. **223**(6): p. 1178-1190.
516. **Stenkamp, R.E.**, *Dioxygen and Hemerythrin*. Chemical Reviews, 1994. **94**(3): p. 715-726.
517. **Ruiz, J.C. and R.K. Bruick**, *F-box and leucine-rich repeat protein 5 (FBXL5): sensing intracellular iron and oxygen*. J Inorg Biochem, 2014. **133**: p. 73-7.
518. **Girin, T., S. El-Kafafi el, T. Widiez, A. Erban, H.M. Hubberten, J. Kopka, R. Hoefgen, A. Gojon, and M. Lepetit**, *Identification of Arabidopsis mutants*

impaired in the systemic regulation of root nitrate uptake by the nitrogen status of the plant. Plant Physiol, 2010. **153**(3): p. 1250-60.

519. **Wang, R., X. Xing, Y. Wang, A. Tran, and N.M. Crawford,** *A genetic screen for nitrate regulatory mutants captures the nitrate transporter gene NRT1.1.* Plant Physiol, 2009. **151**(1): p. 472-8.
520. **Assuncao, A.G.L., D.P. Persson, S. Husted, J.K. Schjorring, R.D. Alexander, and M.G.M. Aarts,** *Model of how plants sense zinc deficiency.* Metallomics, 2013. **5**(9): p. 1110-1116.
521. **Bjornson, M., X. Song, A. Dandekar, A. Franz, G. Drakakaki, and K. Dehesh,** *A Chemical Genetic Screening Procedure for Arabidopsis thaliana Seedlings.* Bio-protocol, 2015. **5**(13): p. e1519.
522. **Heitman, L.H., J.P.D. van Veldhoven, A.M. Zweemer, K. Ye, J. Brussee, and A.P. Ijzerman,** *False Positives in a Reporter Gene Assay: Identification and Synthesis of Substituted N-Pyridin-2-ylbenzamides as Competitive Inhibitors of Firefly Luciferase.* Journal of Medicinal Chemistry, 2008. **51**(15): p. 4724-4729.
523. **Li, S., X. Zhou, H. Li, Y. Liu, L. Zhu, J. Guo, X. Liu, Y. Fan, J. Chen, and R. Chen,** *Overexpression of ZmIRT1 and ZmZIP3 Enhances Iron and Zinc Accumulation in Transgenic Arabidopsis.* PLoS One, 2015. **10**(8): p. e0136647.
524. **Müller, J., T. Toev, M. Heisters, J. Teller, Katie L. Moore, G. Hause, Dhurvas C. Dinesh, K. Bürstenbinder, and S. Abel,** *Iron-Dependent Callose Deposition Adjusts Root Meristem Maintenance to Phosphate Availability.* Developmental Cell, 2015. **33**(2): p. 216-230.
525. **Rodriguez-Celma, J., H. Chou, T. Kobayashi, T.A. Long, and J. Balk,** *Hemerythrin E3 Ubiquitin Ligases as Negative Regulators of Iron Homeostasis in Plants.* Front Plant Sci, 2019. **10**: p. 98.
526. **Alvarez, J.M., E.A. Vidal, and R.A. Gutierrez,** *Integration of local and systemic signaling pathways for plant N responses.* Curr Opin Plant Biol, 2012. **15**(2): p. 185-91.
527. **McInturf, S.A., M.A. Khan, A. Gokul, N.A. Castro-Guerrero, R. Hoehner, J. Li, H. Margault, H.H. Kunz, F.L. Goggin, M. Keyster, R. Nechushtai, R. Mittler, and D.G. Mendoza-Cózatl,** *Cadmium interference with iron sensing reveals transcriptional programs sensitive and insensitive to reactive oxygen species.* bioRxiv, 2020: p. 2020.07.05.188649.
528. **Zandalinas, S.I., L. Song, S. Sengupta, S.A. McInturf, D.G. Grant, H.B. Marjault, N.A. Castro-Guerrero, D. Burks, R.K. Azad, D.G. Mendoza-Cozatl, R. Nechushtai, and R. Mittler,** *Expression of a dominant-negative AtNEET-H89C*

protein disrupts iron-sulfur metabolism and iron homeostasis in Arabidopsis.
Plant J, 2020. **101**(5): p. 1152-1169.

529. **Kobayashi, T., R.N. Itai, M.S. Aung, T. Senoura, H. Nakanishi, and N.K. Nishizawa**, *The rice transcription factor IDEF1 directly binds to iron and other divalent metals for sensing cellular iron status.* Plant J, 2012. **69**(1): p. 81-91.